

Spider Silk Scaffolds as a Material for new Biomedical Applications

DISSERTATION

zur Erlangung des akademischen Grades einer Doktorin/eines
Doktors der Naturwissenschaften

(Dr. rer. nat.)

in der Bayreuther Graduiertenschule für Mathematik und Naturwissenschaften
(BayNAT)

der Universität Bayreuth

vorgelegt von

Tamara Bernadette Aigner

aus Linz, Österreich

Bayreuth, 2020

This doctoral thesis was prepared at the department of Biomaterials at the University of Bayreuth from August 2014 until January 2019 and was supervised by Prof. Dr. Thomas Scheibel.

This is a full reprint of the dissertation submitted to obtain the academic degree of Doctor of Natural Sciences (Dr. rer. nat.) and approved by the Bayreuth Graduate School of Mathematical and Natural Sciences (BayNAT) of the University of Bayreuth.

Date of submission: 29.03.2019, resubmission 28.10.2019

Date of defence: 12.03.2020

Acting director: Prof. Dr. Markus Lippitz

Doctoral committee:

Prof. Dr. Thomas Scheibel	(reviewer)
Prof. Dr. Hans-Werner Schmidt	(reviewer)
Prof. Dr. Georg Papastavrou	(chairman)
Prof. Dr. Stefan Geimer	

*A scientist in his laboratory is not a mere technician:
He is also a child confronting natural phenomena that impress him
as though they were fairy tales.*

(Marie Curie)

Table of Contents

Summary	1
Zusammenfassung	3
1 Introduction.....	7
1.1 Biomedical engineering	7
1.2 Biomaterials	9
1.2.1 Polymers.....	9
1.2.2 Silk.....	11
1.3 Tissue engineering	18
1.3.1 Bioactive agents in tissue engineering	19
1.3.2 Silk and bioactive agents.....	22
1.3.3 Heart muscle regeneration.....	23
1.3.4 Silk in heart muscle regeneration	27
1.3.5 Nerve regeneration	29
1.3.6 Silk in nerve regeneration.....	35
1.4 Bioinstrumentation.....	36
1.4.1 Enzyme confinement.....	36
1.4.2 Silk in enzyme confinements.....	39
2 Aim of the work.....	41
3 Synopsis	43
3.1 Scaffold with bioactive substance.....	45
3.2 Particles as antibacterial agent	47
3.3 Heart muscle regeneration	48
3.4 Nerve regeneration.....	51
3.5 Enzyme containers	53

4	Literature.....	57
5	Publications and Manuscripts	71
6	Individual contributions to joint publications and manuscripts	73
	Publications and Manuscripts.....	77
	Part 1. Biomedical applications of recombinant silk.....	77
	Part 2. Aqueous electrospinning of recombinant spider silk proteins.....	107
	Part 3. Enhanced antibacterial activity of Se nanoparticles upon coating with recombinant spider silk protein eADF4(κ 16)	121
	Part 4. Surface Features of Recombinant Spider Silk Protein eADF4(κ 16)-Made Materials are Well-Suited for Cardiac Tissue Engineering	155
	Part 5. Nerve Guidance Conduit Design based on Self-rolling Tubes.....	173
	Part 6. Self-rolling Tubular Structures made of Spider Silk and Chitosan as Enzyme Containers	189
	Acknowledgement.....	207
	Eidesstattliche Versicherungen und Erklärungen.....	209

Summary

Biomedical engineering arose out of the collaboration of medical doctors, biologists and engineers and substantially accelerated advances in medicine. Researchers in this field strive to improve medical care through the development of diagnostic tools and devices, prosthetics, surgical tools and robots, and tissue engineering. The latter one seeks regeneration or restoration of a damaged or diseased tissue.

Materials used on or in human body must fulfill several divergent requirements. Firstly, they should provide mechanical support by offering sufficient mechanical strength, on a scale commonly found in synthetic polymers. Secondly, they should be biologically compatible and for instance trigger cell recognition usually attributed to natural polymers. One material type that captures both requirements are spider silk-based materials. Their unique chemistry and structure give spider silk fibers extraordinary mechanical properties and no immune response is induced in the body. Inherent cell recognition (eukaryotic and prokaryotic) of most native spider silks is poor, but if required, cell binding motives can be added using a biotechnological approach to produce recombinant spider silk proteins, which can further be processed into various morphologies.

The objective of this dissertation was to exploit the beneficial properties of coatings, films, nonwovens and self-rolling bilayers made of recombinant spider silk proteins to widen the scope of their use in biomedical engineering. Spider silk scaffolds were investigated for loading with bioactive agents, use in heart muscle and nerve regeneration and as enzyme container.

Accurate delivery of sensitive biological substances can improve cell behavior on scaffolds for tissue engineering. In the first project electrospun nanofibers with their inherent advantages of high porosity and surface-to-volume ratio were loaded with green fluorescent protein (GFP) as a bioactive agent model. Its fluorescence is structure dependent and common solvents used for electrospinning and post-treatment of silk destroyed GFP's structure. Therefore, an aqueous electrospinning and post-treatment process was developed, which allowed a mild encapsulation and kept the structural integrity of GFP. The fast release of GFP could be inhibited or slowed down by genetic modification giving the system a broader application window.

Post-surgical infections are a life-threatening risk and the increase in antibiotic resistant bacteria prove the need for alternatives. The second project investigated the antibacterial properties of spider silk coated selenium nanoparticles alone and encapsulated in silk films. Selenium nanoparticles are effective against gram-positive bacteria. By applying a coating of spider silk, the scope could be widened to gram-negative bacteria. Low doses of the coated nanoparticles killed *Escherichia coli* without impairing eukaryotic cell viability.

The body's capability of cardiac repair after a myocardial infarct is poor and materials to assist cardiac regeneration are desperately needed. Thus, in the third project, the behavior of primary cardiac cells on spider silk films was investigated. The secondary structure content and the water contact angle of these films was found to be in a suitable range. Cell studies showed that silk films are non-toxic and provoke no pharmacologic effect. Furthermore, cardiac cells grown on these silk films showed required cell-to-cell communication and responded properly to extracellular stimuli, thus, laying the foundation for use of silk in cardiac tissue engineering.

Injuries of the peripheral nerve system still show an unacceptable recovery rate. Thus, in the fourth project, bilayers of spider silk and chitosan were self-rolled into tubular structures to act as nerve guidance conduits. The tubes were either lined with a silk film containing a cell-recognition motif or aligned silk nanofibers, or an anisotropic collagen cryogel was encapsulated filling out the luminal space. The mechanical properties of the collagen cryogel are in the range of healthy peripheral nerves. Nerve cells could be entrapped by the gentle rolling process and their differentiation was achieved inside of the tubes, allowing the formation of neurite outgrowths. The aligned structures even triggered orientation of these neurite outgrowths in longitudinal direction, as is required in nerve repair.

In the fifth project, these self-rolling tubular structures were optimized to encapsulate enzymes. They were shown to be stable in relevant organic and aqueous solutions and to possess a molecular weight cut-off above 20 kDa. Hence, these enzyme containers allowed the entrapment of enzymes, while substrates, intermediates and/or products can diffuse freely through the tube wall. This allowed to exchange the surrounding media without removing the enzymes, thereby saving often costly enzymes and enabling the design of a flow-through system. Reaction rates were slowed down, but longer reaction times were observed. Thus, this system can protect enzymes and may be useful for applications in biodiagnostics.

Through this work, we showed that recombinant spider silk-based materials have a high potential in several fields of biomedical engineering. The processability into various morphologies and the precise control over the protein sequence makes it an interesting option for diverse applications. This thesis only gives a small glimpse at the scope of possibilities and more is yet to come.

Zusammenfassung

Die Biomedizintechnik entstand durch die Zusammenarbeit von Ärzten, Biologen und Ingenieuren und beschleunigte so signifikant die Weiterentwicklung der modernen Medizin. Wissenschaftler in diesem Bereich streben eine Verbesserung des Gesundheitssystems durch die Entwicklung von Diagnoseinstrumenten, Prothesen, chirurgischen Werkzeugen/Robotern und Geweberegeneration an, welche auf eine komplette Regeneration oder Wiederherstellung von geschädigtem oder erkranktem Gewebe abzielt.

Materialien, welche am und im Körper eingesetzt werden, müssen viele divergente Anforderungen erfüllen. Einerseits sollten sie mechanische Stabilität in einem Bereich bieten, der üblicherweise bei synthetischen Polymeren zu finden ist. Andererseits sollten die Polymere biokompatibel sein und zum Beispiel von Zellen erkannt werden, ein Attribut, das üblicherweise natürlichen Polymeren zugeschrieben wird. Bei einer Materialart verschwimmen diese Grenzen, da es die Vorteile von beiden Seiten vereint – spinnenseidenbasierte Materialien. Die einzigartige Chemie und Struktur verleiht Spinnenseidenfasern außergewöhnliche mechanische Eigenschaften und zusätzlich lösen sie keine Immunantwort aus. Die meisten natürlichen Spinnenseiden werden weder von eukaryotischen noch von prokaryotischen Zellen erkannt. Durch die Entwicklung eines biotechnologischen Prozesses zur Herstellung rekombinanter Seidenproteine, können, wenn gewünscht, zellbindende Motive genetisch hinzugefügt werden. Auch können rekombinante Seidenproteine in verschiedene Morphologien prozessiert werden.

Ziel dieser Arbeit war es, die vorteilhaften Eigenschaften von Beschichtungen, Filmen, Vliesen und selbstrollenden Röhrchen basierend auf rekombinant hergestellten Spinnenseidenproteinen zu nutzen, um deren Anwendungsmöglichkeiten in der Biomedizintechnik auszuweiten. Spinnenseidengerüste wurden mit bioaktiven Substanzen beladen, für die Anwendung in der Herzmuskelregeneration, als Nervenleitstruktur, sowie als Enzymcontainer untersucht.

Präzise Positionierung sensibler bioaktiver Substanzen kann das Zellverhalten an Gerüststrukturen für die Geweberekonstruktion verbessern. Im ersten Projekt wurden elektrogewobene Nanofasern, welche nicht nur eine vorteilhafte hohe Porosität, sondern auch ein hohes Oberflächen-Volumen-Verhältnis aufweisen, mit grün fluoreszierendem Protein (GFP) als Modell für bioaktive Moleküle beladen. Die GFP Fluoreszenz ist strukturabhängig und gängige Lösungsmittel fürs Elektrogeweben und die Nachbehandlung von Seidennanofasern zerstören diese. Deshalb wurde ein wässriges Spinn- und Nachbehandlungsverfahren entwickelt, welches eine sanfte Verkapselung und somit die Erhaltung der GFP Struktur ermöglichte. Die rasche Freisetzung des GFP konnte mit Hilfe genetischer Modifikation verhindert oder deutlich verlangsamt werden und ermöglicht somit dem System einen breiteren Anwendungsbereich.

Postoperative Infektionen sind ein lebensbedrohendes Risiko und die rapide Vermehrung antibiotikaresistenter Keime erfordern die Entwicklung von Alternativen. Das zweite Projekt untersuchte die antibakteriellen Eigenschaften von seidenbeschichteten Selen-Nanopartikeln allein und eingebettet in Seidenfilmen. Die Wirkung gegen gram-positive Bakterien der Selen-Nanopartikel konnte durch die Beschichtung mit Spinnenseide auch auf gram-negative Bakterien ausgeweitet werden. Schon kleinste Dosen der beschichteten Nanopartikel töteten erfolgreich *Escherichia coli*, ohne einen schädlichen Einfluss auf eukaryotische Zellen aufzuweisen.

Die Fähigkeit des menschlichen Körpers, den Herzmuskel nach einem Herzinfarkt zu regenerieren, ist nicht vorhanden und es werden händeringend neue Materialien zur Förderung der Regeneration gesucht. Darum wurde im dritten Projekt das Zellverhalten von primären Herzmuskelzellen auf unterschiedlichen Seidenfilmen untersucht. Die Zusammensetzung der Sekundärstruktur sowie der Wasserkontaktwinkel waren in einem geeigneten Bereich. Es konnte gezeigt werden, dass Seidenfilme weder giftig sind noch pharmakologische Effekte hervorrufen. Zusätzlich zeigten die auf den Filmen wachsenden Herzmuskelzellen für das Herz notwendige Zell-Zell-Kommunikation und reagierten angemessen auf extrazelluläre Stimulation, wodurch die Grundlage für die Verwendung von rekombinanten Spinnenseidenmaterialien in der Herzmuskelgeweberegeneration gelegt werden konnte.

Verletzungen peripherer Nerven zeigen noch immer einen inakzeptablen Genesungsgrad. Im vierten Projekt wurden daher Röhren durch einen selbstrollenden Mechanismus von einer Doppelschicht aus Spinnenseide und Chitosan hergestellt, um als Nervenleitstruktur zu agieren. Dafür wurden die Röhren entweder mit einem Seidenfilm mit zellbindendem Peptid oder mit ausgerichteten elektrogewebenen Nanofasern ausgekleidet, oder ein anisotropes Kollagen Cryogel wurde umrollt, wodurch der gesamte Hohlraum ausgefüllt wurde. Die mechanischen Eigenschaften von Kollagen Cryogelen lagen im Bereich von gesunden peripheren Nerven. Durch den sanften Roll-Prozess konnten Nervenzellen behutsam eingefangen und direkt in den Röhren differenziert werden. Die ausgerichteten Nanofasern und die Cryogele ermöglichten sogar die Ausbildung von gerichtetem Neuriten-Auswuchs, welcher in der Nervenregeneration nötig ist.

Im fünften Projekt wurden diese selbstrollenden Röhren optimiert, um Enzyme darin einzuschließen. Es konnte gezeigt werden, dass die Röhren stabil sind gegenüber relevanten organischen und wässrigen Lösungen und die Diffusion von Molekülen über 20 kDa verhindern. Daher konnten Enzyme eingeschlossen werden, wobei deren Substrate, Intermediate und/oder Produkte durch die Wand der Röhren diffundieren konnten. Die Enzymkontainer ermöglichten den Austausch des umgebenden Mediums, ohne das Enzyme zu entfernen, wodurch nicht nur oft teure Enzyme gespart werden, sondern auch Durchflusssysteme generiert werden könnten. Die

Reaktionsraten wurden durch die doppelte Diffusion verlangsamt, dafür konnten längere Reaktionszeiten beobachtet werden. Somit kann dieses System eingesetzt werden, um Enzyme zu schützen. Weitere Anwendungen im Bereich der Biodiagnose wären denkbar.

In dieser Dissertation konnte gezeigt werden, dass Materialien aus rekombinanten Spinnenseidenproteinen hohes Potential in verschiedenen Bereichen der Biomedizintechnik aufweisen. Die Möglichkeit, Spinnenseide in verschiedenste Morphologien zu verarbeiten, kombiniert mit der Fähigkeit, die Sequenz der Spinnenseide präzise kontrollieren zu können, macht Spinnenseide zu einem interessanten Material für unterschiedliche Anwendungen. Diese Arbeit gibt nur einen kleinen Einblick in die Vielfalt an Anwendungsmöglichkeiten, und viele weitere spannende Entwicklungen werden erwartet.

1 Introduction

1.1 Biomedical engineering

In the 17th century the power relationship of science and church was shifted in favor of science paving the way for modern medicine. First steps included preventative medicine by for example increasing hygiene standards.¹ Later, by the end of the 19th century, also curative medicine came into play by beginning with medication and surgery. As the knowledge requirement for all fields grew, different specialty fields were found – one of them being biomedical engineering (BME).



Figure 1: Research focuses of biomedical engineering (BME): BME is an interdisciplinary field containing 14 subfields as defined by the Biomedical Engineering Society (BMES).²

Scientists working in BME use engineering principles and try to adapt them for medical applications. As a result, the application window is very broad and includes fourteen subfields as depicted in Figure 1.² Exemplarily, scientists in BME developed medical electronic devices like smart wearable sensors for health monitoring³, cardiac pacemakers⁴, hearing aids, X-ray machines,

ultrasound or positron emission tomography. Other devices are concerned with measuring and administering substances in blood as for example blood chemistry sensors, infusion pumps or automated delivery of insulin.²

Challenges currently tackled by BME are the ageing population, accidental injuries and monetary restrictions. The ageing population is associated with problems like arthritis in joints⁵, cardiovascular diseases⁶, organ failure⁷, or neurological diseases like Alzheimer's disease⁸. The success of the treatments varies for example, joints can be replaced by hard, inorganic materials, which are unable to restore the or integrate with the host tissue. Thus, the ailment is eased, but not treated. Organs can be replaced by autografts (e.g. nerve repair) or allografts (e.g. liver, heart or kidney), whereby an autograft can result in the loss of function at the donor site and allografts usually result in foreign body response, and the immune-system must be suppressed to avoid implant rejection. Here, tissue engineering (TE) another big field in BME comes into play, which reflects the repair, restoration and regeneration of living tissue by using biomaterials, cells and factors.⁹ One development in TE is biofabrication, which uses emerging technologies like 3D bioprinting. Thereby, 3D tissue-like structures are prepared *in vitro* by precisely depositing biomaterials and cells to control cell-material and cell-cell interaction.¹⁰ Hereby, the aim is not only to develop technologies for *in vivo* use, but also for *in vitro* modelling for example to screen new pharmaceutical drugs for their safety.

Accidental injuries are age-independent and include peripheral nerve damage, bone fracture, ligament tear, skeletal muscle damage or burns.¹¹ The success of the treatment depends on the severity of the ailment as well as on the age of the patient. Some of these injuries can even be cured completely for example in bone fracture the fractured parts are aligned and immobilized by a plaster cast allowing the bone to heal. A further issue worth mentioning is the increase in costs of superior and often personalized medical treatments. When we take peripheral nerve repair as an example, it takes a very skilled surgeon to introduce the conduit and then later, the patient requires physical therapy to help restore complete function. It is obvious, that only a small fraction of the population worldwide is in the privileged position to be able to afford such a treatment. In third world countries the focus still lies on disease prevention by for instance improving water quality, providing education and developing vaccines for e.g. vector-borne diseases like malaria.¹² This is a first step into the right direction, but more needs to be done.

In summary, BME is a rapidly growing field showing many advances, which not only help to prolong, but also to increase the quality of a patient's life. Many inventions entered the public health care system already. Several new developments are still in an early phase, and translation to

clinics is awaited. Clearly, the monetary issue has to be solved, to ensure high quality treatment for a wide mass of patients.

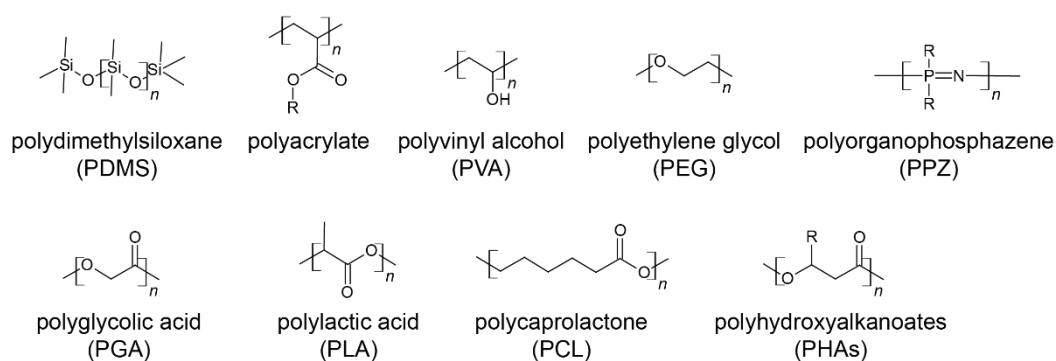
1.2 Biomaterials

A biomaterial is “defined as any substance (other than a drug) or combination of substances, synthetic or natural in origin, which can be used for any period of time, as a whole or as a part of a system which treats, augments, or replaces any tissue, organ, or function of the body” according to the National Institutes of Health (1980s).¹³ This includes metals e.g. titanium alloys used for joint replacement¹⁴, ceramics e.g. calcium orthophosphates used in dental applications¹⁵ and polymers.

1.2.1 Polymers

Polymers are often used in biomedical applications as they not only offer a wide variety of physico-chemical properties, but in addition can be transferred into several morphologies ranging from thin polymer sheets to complex 3D constructs to suit applications in all branches of BME. In order to be used in or on human body, the polymers must be biocompatible and nonimmunogenic. Synthetic polymers in general provide good mechanical properties and frequently allow for control of the molecular weight. Polymers like silicone, poly(acrylate), poly(vinyl alcohol) (PVA) or poly(ethylene glycol) (PEG) can be used for applications, where no to slow degradation is required.^{9,16} Aliphatic polyesters as for example poly(glycolic acid) (PGA), poly(lactic acid) (PLA; poly(L-lactic acid) (PLLA) and poly(D-lactic acid) (PLDA)), polycaprolactone (PCL) or poly(hydroxyalkanoates) (PHAs) (Figure 2) gained interest especially in the field of tissue engineering, as they show reasonable biodegradability. Problematic hereby is, that they commonly show bulk degradation kinetics instead of surface erosion, thus, the body has no chance to slowly replace the scaffold. Further, these polyesters degrade into acidic products not only reducing the pH in the surrounding tissue, but also accelerating the degradation of the scaffold.¹⁷⁻²⁰ To avoid this, polymers such as poly(phosphazenes) have been developed, which degrade into pH neutral products.²¹ Synthetic polymers also lack inherent cell-binding motifs. Thus, cell-recognition sites must either be added during synthesis or the polymer must be coated with natural biopolymers like fibronectin²². Another option is to use them for applications, where cell-binding is not required for example PCL has been used as a dermal filler in form of microcapsules embedded in a carboxymethylcellulose matrix (Ellansé[®]²³), as a root canal filling (Resilon[®]²⁴) or blended with PGA as a surgical suture material (Stratafix Spiral from Ethicon[®]²⁵). PLLA has been used as medical implants in form of pins, screws, suture anchors, rods or miniplates²⁶.

synthetic polymers



natural polymers

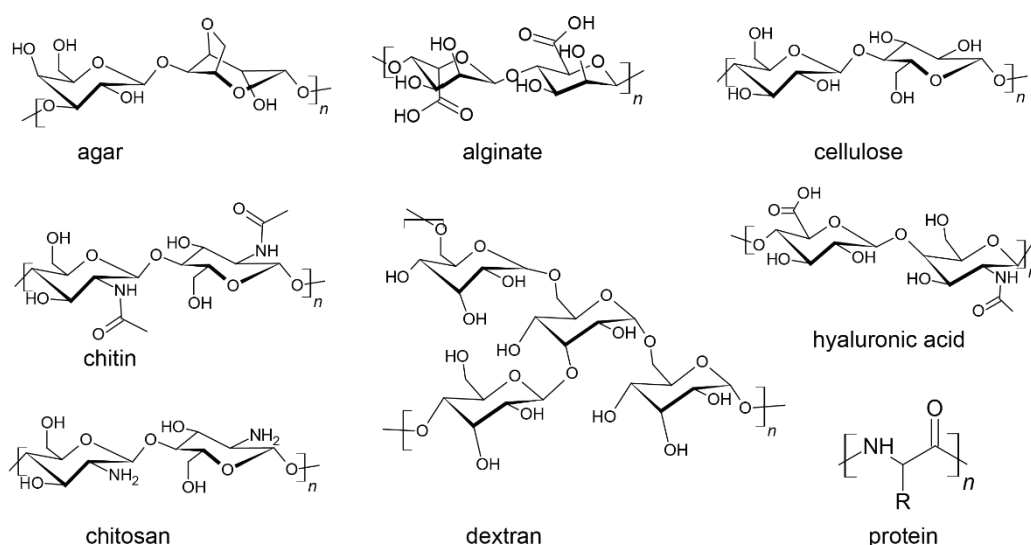


Figure 2: Synthetic and natural polymers. Chemical structures of several polymers investigated for biomedical applications are shown. Polydimethylsiloxane, polyacrylate and polyvinyl alcohol are not biodegradable, polyethylene glycol is degradable if $n < 1500$ and poly(organophosphazene) backbone degrades into pH neutral ammonia and phosphate, “R” is commonly an *O*- or *N*-linked organic rest. The polyesters depicted are examples of the most commonly used ones in biomedical applications (PGA, PLA, PCL and PHAs), the “R” in poly(hydroxyalkanoates) refers to an aliphatic rest. Polysaccharides shown here are naturally derived polymers and made of sugar units connected via *O*-glycosidic bonds. They can be linear as agar, alginate, cellulose, chitin, chitosan and hyaluronic acid or branched like dextran. Proteins are made of amino acid chains connected via amide bonds. The “R” here varies between the different amino acids.

In order to overcome the limitations of synthetic polymers, biopolymers of natural origin are heavily investigated. These can be divided into three main groups, namely proteins, polysaccharides and deoxyribonucleic acids (DNAs).²⁷ Examples of commonly used natural polymers are hyaluronic acid, starch, cellulose, alginate, dextran, chitin, chitosan, agar, fibronectin,

collagen, gelatin, soy and silk (Figure 2).^{16, 18, 28, 29} These natural polymers show advantages in terms of biocompatibility and biodegradability, as the degradation products – amino acids and sugars are commonly found in our body. In addition, these biopolymers often present recognition sites for cells e.g. RGD sequence in fibronectin.³⁰ The major problem of natural biopolymers is that they suffer from poor mechanical properties (compared to synthetic polymers), limited control over physicochemical properties, batch-to-batch variations, scale-up difficulties and problems in sterilization.^{17, 18, 29, 31, 32} Collagen from natural sources is already used in patients for wound dressing e.g. BioPad™ made of native equine collagen³³ or collagen sheets and particles from Maiden Biosciences made of bovine collagen³⁴. Materials that combine extraordinary mechanically properties with biocompatibility and biodegradability are based on spider silk and will be discussed in more detail in the following chapter.

To date, only a few commercial applications using a single biopolymer were developed. Especially, in case of bigger constructs and more complicated structures, a single material seldom fulfills all necessary requirements. Hence, the development of a multi-component system comprising several polymers, factors (e.g. growth factors) and/or helping cells (e.g. Schwann cells in nerve regeneration³⁵) will be necessary.²⁹

1.2.2 Silk

1.2.2.1 *Natural silk*

Silk was recognized early on, well before the 18th century, to be a viable material to be used as surgical thread or wound dressings.³⁶⁻³⁸ At the time, the people recognized that there is no abnormal secretion (pus), swelling or redness. Today it is known that silk is biocompatible and hypoallergenic, and it continues to be highly regarded as biomaterial.

Silks are described by Craig³⁹ as “fibrous proteins containing highly repetitive sequences of amino acids”, which “are stored in the animal as a liquid and configure into fibers when sheared or ‘spun’ at secretion”. The remarkable part here is, that the fibrous silk proteins are processed out of highly concentrated solutions, usually typical for glues and unusual for other fibrous proteins like collagen.³⁹ Silks evolved independently in different organisms possessing different structural characteristics designed for the desired purpose, probably evoked due to variable evolutionary pressures.^{40, 41} The driving mechanism behind the properties of different silks is the secondary structure. The secondary structure depends on the primary amino acid sequence, which is in silk proteins rich in glycine, alanine and/or serine. Commonly, silk materials show either a high α -helical or β -sheet content. Insect silk proteins can adopt five protein structures, namely extended β -

sheet, cross β -sheet, coiled-coil, collagen triple helix and polyglycine II and can be produced in dermal or labial glands or Malpighian tubules.⁴² So for example, lacewings use silk for production of egg stalks to protect the eggs from predators. This silk consists of cross β -sheets giving the egg stalk incredible bending stiffness. Honeybees on the other hand use silk for lining the nests and cocoons. These silks are not meant to withstand high forces and are therefore rich in α -helices. Silkworms produce silk as a cocoon to protect themselves during metamorphosis. This protection-silk is made of crystalline patches embedded in an amorphous matrix.⁴²

Spiders are the only known animals producing up to seven different types of silks for various applications i.e. aggregate silk is used as glue for prey capturing and is very sticky, cylindrical silk is used to prepare egg cocoons and is very stiff, and major-ampullate silk also known as the “lifeline” of the spider, is strong as steel, but possesses a high toughness.⁴³ Spiders possess different glands for all the silk types they produce and depending on the amino acid composition and the spinning process, the different functions of the silks are realized.^{41,44} The most investigated spider silk is major ampullate silk consisting primarily of two protein classes, namely major ampullate spidroin 1 and 2 (MaSp1 and 2). The MaSp proteins consist of a repetitive core domain flanked by non-repetitive terminal domains. The repetitive unit of the core domain exhibits an amphiphilic nature comparable to block-*co*-polymers consisting of a GGX and GPGXX (only in MaSp2) rich part and a poly(A) sequence. The latter one forms β -sheets and β -crystals, which are embedded in an amorphous but still strongly orientated region formed by the GGX/GPGXX-part.^{40,45} This structural arrangement is the reason that silk is not brittle like other structures with high crystallinity, but possesses extraordinary mechanical properties. The amorphous regions enable elastic deformations, whereby the crystalline parts give the fiber the necessary strength resulting in very high toughness.^{46,47}

1.2.2.2 Recombinant silk

Bombyx mori (*B. mori*) silk can be obtained by large scale farming, but for spiders or insects, harvesting natural silk is tedious work. Generally farming suffers from batch-to-batch variations and the possibility of impurities.⁴⁸ Especially problematic with farming of spiders is that they are territorial, cannibalistic and male spiders are often consumed after mating. Further, silk quality depends on the spider’s nutrition, age and well-being.⁴⁹⁻⁵¹ Still, it has been shown that natural silk from *Nephila* spiders can be used in combination with decellularized porcine veins to prepare nerve guidance conduits.⁵² Farming of lacewing flies or bees would be more convenient, but the amounts of silk produced by these animals are minuscule that harvesting in reasonable amounts is not feasible.⁵³ Therefore, biotechnological approaches have been developed, which allow for protein

production in large amounts with consistent quality and biological safety. Within the last 15 years recombinant silk production was established in *Escherichia coli* (*E.coli*) and yeast, and certain variants are mass-produced and can be purchased.⁵⁴

Recombinant silk production can be divided into the following steps: (I) Determination of the natural DNA sequence; (II) Design of recombinant DNA; (III) Cloning of the vector; (IV) Transformation of the host organism; (V) Fermentation and/or protein production; (VI) Purification of the protein.⁵⁵ Different host organisms from unicellular pro- or eukaryotes to multicellular plants or animals can be used, whereby the size of the protein, its necessity for post-translational modifications as well as their folding play a role.^{56, 57} Several groups developed recombinant silk proteins and variants thereof (Figure 3) e.g. 4RepCT^{58, 59}, 6mer and 15mer⁶⁰⁻⁶², rMaSp1/2 or 1F9 and rS1/9⁶³⁻⁶⁶; recombinant insect silk proteins e.g. moth silk EAEFN_{5/10}⁶⁷, honey bee silk AmelF1-4^{68, 69}, hornet silk Vssilk1-4^{70, 71} or lacewing silk N[AS]₈C^{72, 73}. Further, transgenic silkworm silk was developed like for example L-RGDSx2 fibroin^{74, 75}, SELP-47K and SLEP-815K⁷⁶⁻⁷⁸ or [(AGSGAG)₄E₈AS]₄^{79, 80}.

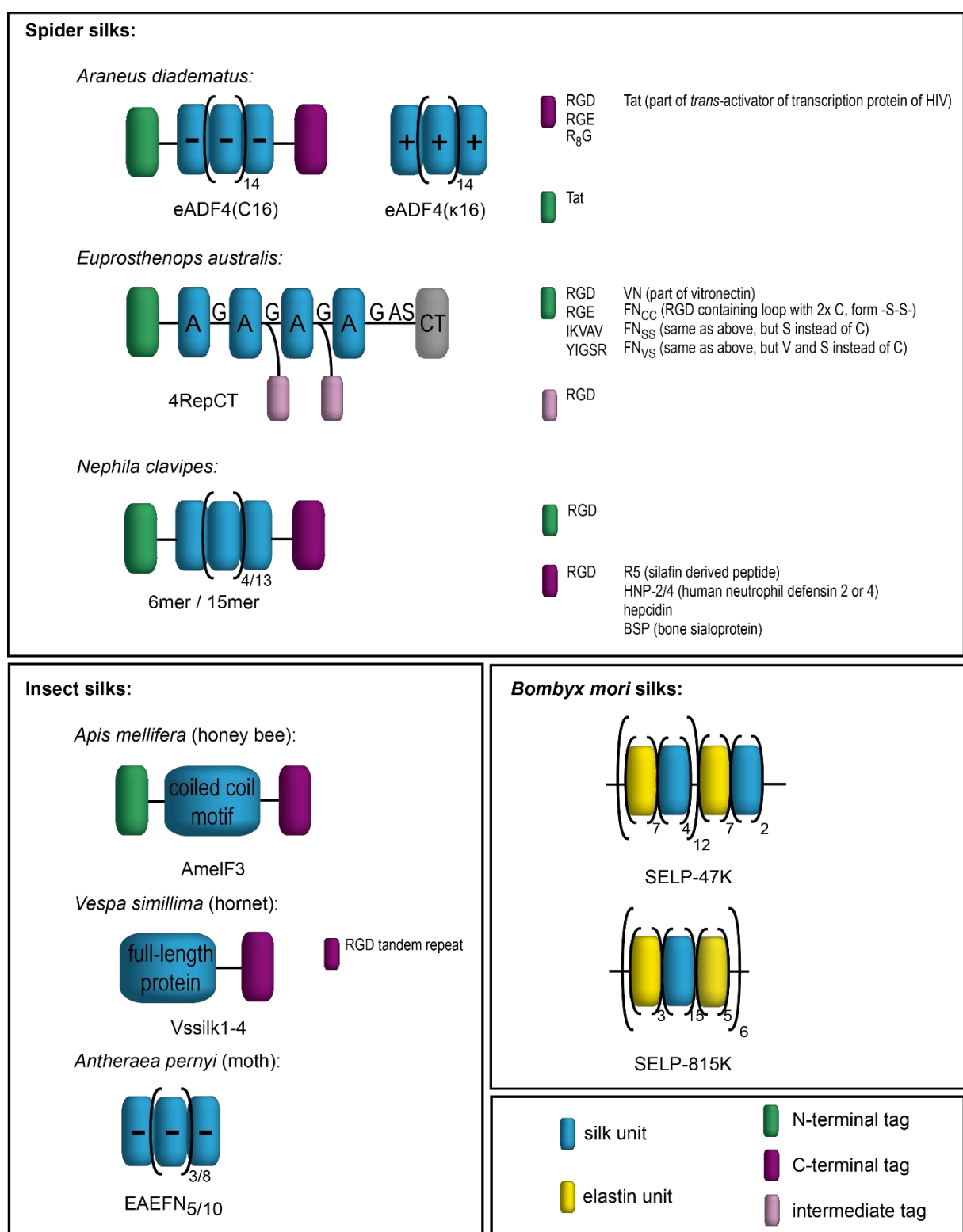


Figure 3: Schematic summary of various recombinantly produced spider and insect silks. Several of these silks show variations by the addition of N-, C- or intermediate tags, mainly used to trigger certain cell interactions like for instance the addition of an RGD-, IKVAV-, YGSR-, VN-, FN-tag to improve cell attachment.

In this work, the focus was on the *Araneus diadematus*' MaSp2 derivative eADF4(C16) (engineered *Araneus diadematus* fibroin 4) and variations thereof. The repetitive unit of the core domain of MaSp2 was used as a template for the C-module. This C-module was then repeated 16 times to obtain the artificial silk protein eADF4(C16) (Figure 4). Each C-module holds a glutamic acid residue, giving the whole protein an overall negative charge.⁸¹ In order to increase cell adhesion, an integrin binding RGD-tag was added to create eADF4(C16)-RGD.⁸² Further, the glutamic acid was exchanged by lysine rendering it into the positively charged eADF4(κ 16).⁸³

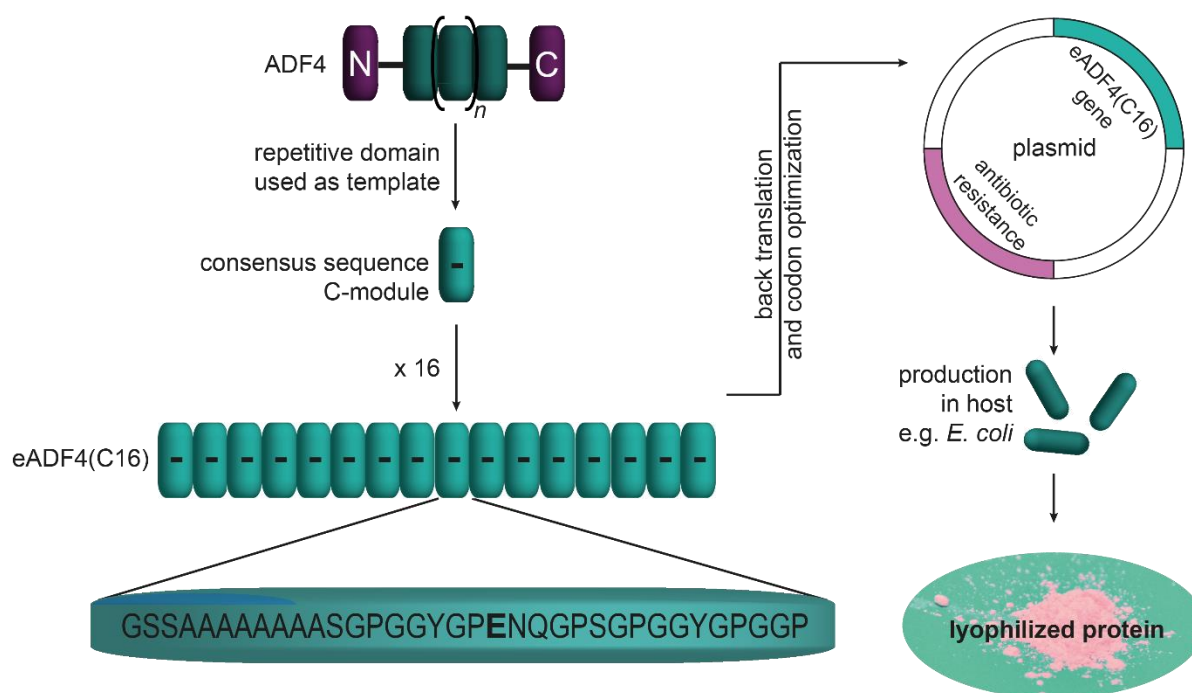


Figure 4: Scheme of recombinant eADF4(C16) production. The repetitive core domain of *Araneus diadematus* fibroin 4 (ADF4) was used as a template to obtain the C-module. The engineered ADF4 (eADF4(C16)) was created by repeating this C-module 16 times. After back translation of the amino acid sequence and codon optimization for use in *E. coli* it was inserted into a plasmid containing also a gene for antibiotic resistance for selection. Then the host was transfected, and protein production induced. Several purification steps are necessary to obtain the pure protein powder, which can be processed into several morphologies. Reproduced with permission.⁸⁴ Copyright 2018, WILEY-VHC Verlag GmbH & Co.

1.2.2.3 Morphologies of recombinant silk and their applicability in BME

Recombinant silk is usually obtained in form of a lyophilized powder in case of biotechnological produced silk proteins or fibers in case of transgenic silkworms. Recombinant silk

proteins can further be processed into different morphologies, namely films, micro- and nanofibers, foams, hydrogels, capsules and particles as shown in Figure 5.⁸⁴ By far the most studied morphology are flat films as they are convenient for screening for biochemical features, cytocompatibility and physical characterization of the designed silk. Only a small amount of material is required to cast, dip- or spray-coat the required substrate and allow for high-throughput experiments. Especially, the effect of incorporation of cell binding peptides like RGD, IKVAV, YIGSR or other sequences from vitronectin (VN), vascular endothelial growth factor (VEGF), silaffin-derived R5 tag or antibiotics were studied in films using cell lines, primary cells, stem cells and subcutaneous pockets *in vivo*.^{82, 85-91} Furthermore, implants were successfully coated with silk films e.g. coating of silicone implants^{92, 93} or catheters^{94, 95} to reduce the negative side effects of the foreign body response or thrombotic fouling.

Micrometer fibers of recombinant silk protein were prepared either by wet or biomimetic spinning^{96, 97} and self-assembly⁹⁸. Fibers produced by self-assembly could be arranged into fiber meshes and compared to other morphologies in terms of fibroblast growth and maintenance of differentiation state.⁹⁹ *In vivo* test of these fibers showed no toxicity and low immunogenicity.¹⁰⁰ Another source of micrometer sized fibers is *B. mori* silk. The cocoons from silkworms consist of one thread and after “degumming” plain silk fiber, also referred to as regenerated silk fibroin (RSF), is obtained and can be used in various forms (single strands, yarn, woven). Such transgenic RSFs were investigated as vascular grafts.^{86, 101, 102} Sub-micrometer and nanofibers are commonly produced by electrospinning, whereby a nonwoven fiber mat is produced. It was found that the fiber diameter plays a crucial role in cell attachment, whereby increasing fiber diameter increases cell attachment.¹⁰³ Further, mixing with collagen was shown to be beneficial for stem cell differentiation.¹⁰⁴ In general nonwoven fiber mats can be seen as the bridge between 2D films and 3D networks.

Characteristic for 3D foams are thin-walled pores. The pore diameter plays a crucial role in terms of nutrient/waste diffusion and vascularization.^{18, 105} In combination with recombinant silk proteins salt-leaching,^{63, 66, 79, 106} freeze-drying⁷⁴ and an unknown mechanism⁹⁹ were used for foam preparation. Next to *in vitro* tests with cell lines^{63, 66, 106}, primary cells^{74, 99} or stem cells^{87, 107}, studies on pancreatic island engineering^{88, 108} and femoral defects^{66, 79} were conducted. In order to closer resemble the natural extracellular matrix (ECM) hydrogels composed of >90 % water are gaining more and more interest. Here the polymer, i.e., silk protein can be physically or chemically crosslinked in solution. It was shown that cells could be encapsulated into self-assembling spider silk hydrogels, which could further be used as bioink in 3D printing.^{109, 110}

A further approach are silk capsules and particles designed as mobile drug or gene delivery systems. Silk capsules enable the encapsulation of larger molecules and are formed by an emulsion process.¹¹¹ Silk particles are commonly produced by salting-out in phosphate buffer, whereby the concentration of the silk and buffer solution as well as the mixing time play an important role in particle size.¹¹² Particle loading was achieved by co-precipitation of the (model) drug with silk or by diffusion of the (model) drug into the particles. The desired cellular uptake was found to be increased using positively charged silk¹¹³ or specific cell binding peptides¹¹⁴. Herewith, cancer cells could be exclusively killed by delivery of doxorubicin.¹¹⁵ Additionally, several studies in terms of gene delivery were conducted showing for instance that Luciferase production was successfully induced in tumorous tissue in mice.¹¹⁶

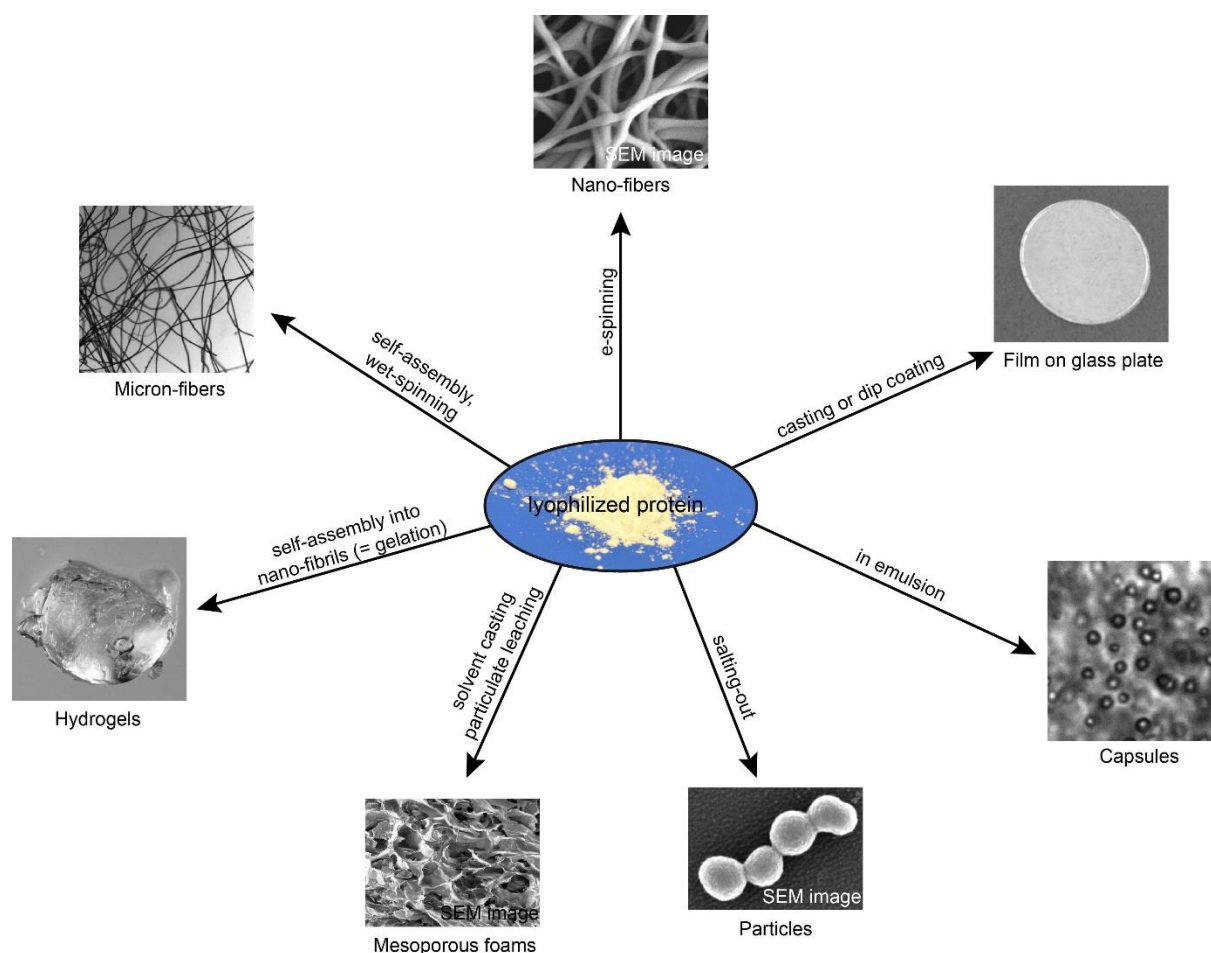


Figure 5: Processing routes of recombinant silk proteins. Different morphologies can be prepared from the lyophilized silk powder by using various techniques. Reproduced with permission.⁸⁴ Copyright 2018, WILEY-VHC Verlag GmbH & Co.

1.3 Tissue engineering

“Tissue engineering is an interdisciplinary field that applies the principles of engineering and life sciences toward the development of biological substitutes that restore, maintain, or improve tissue function” according to Langer and Vacanti.¹⁷ The native physiological niche of cells entails complex physical and biochemical stimuli i.e. external and intrinsic cues determine cell fate. Physical cues include external forces, topography and substrate mechanics, whereby biochemical cues consist of the composition of the substrate and soluble molecules.¹¹⁷ Mimicking this environment is the goal of artificial tissue creation. Two approaches exist for their creation: (I) Bottom-up approach: Cells or cell clusters are allowed to assemble and mature into 3D structures by the aid of stimulation of chemical or mechanical nature. Thereby, the cells build extracellular matrix (ECM) as a scaffold for the tissue. An example for this approach is the assembly of cell spheroids to build organ like structures e.g. vessels¹¹⁸ (II) Bottom-down approach: A biomaterial scaffold is seeded with cells and the combination is allowed to mature by providing chemical or mechanical stimulation. Here, the biomaterial predetermines the structure and while slowly degrading, cells form their own ECM scaffold. An example for this second approach is the seeding of pancreatic beta cells into a mesoporous foam scaffolds for insulin production.¹⁰⁸ For heart muscle tissue engineering both approaches are holding promises for example, cell-sheet patches created to cover the infarct-region and couple with the host tissue and also decellularized animal hearts seeded with cardiac cells were investigated. In nerve tissue engineering, the bottom-down approach seems straight-forward by creating a tubular structure to aid nerve regrowth. The addition of bioactive agents can further increase the success of artificial tissue formation in both approaches. Antibacterial agents decrease the risk of bacterial infections after implantation.¹¹⁹ Stimulating agents like growth factors can further promote cell growth, proliferation and differentiation and thereby for instance assist in healing processes.¹²⁰ Figure 6 below depicts the TE triad composed of biomaterials, cells and signals.

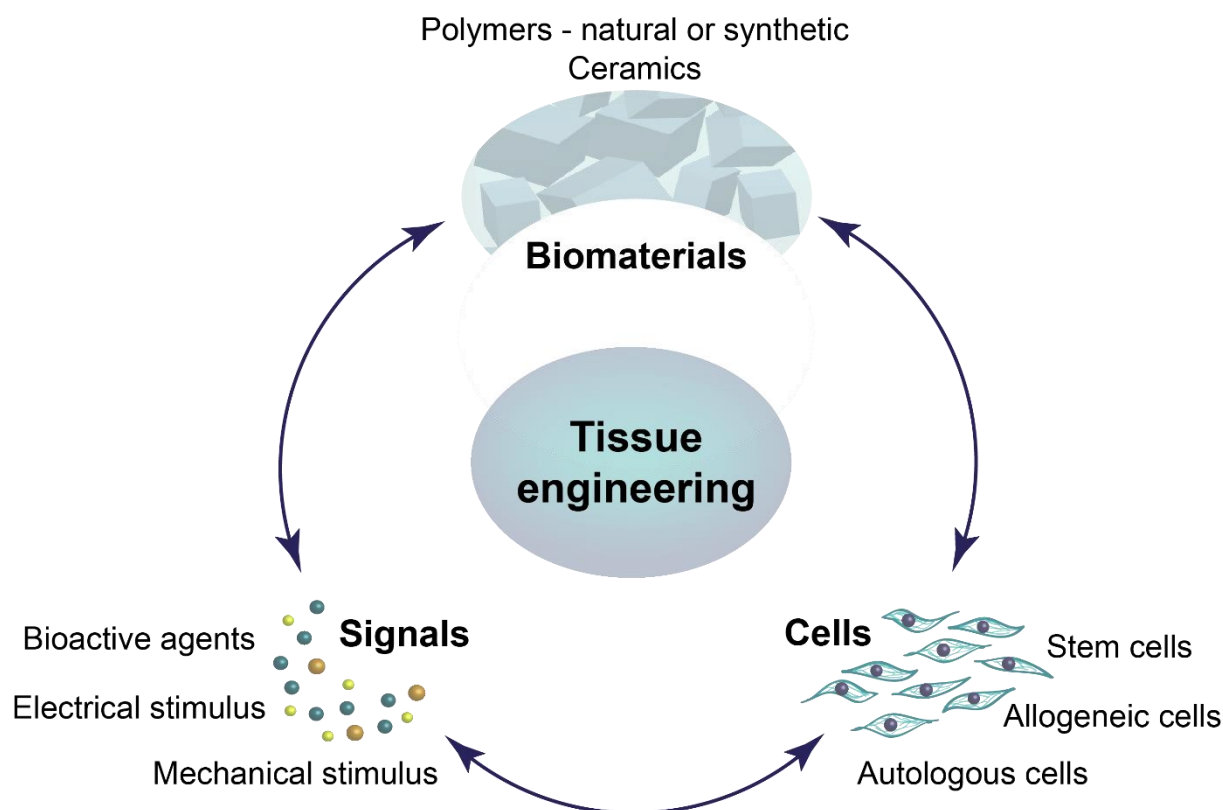


Figure 6: Tissue engineering triad. The combination of the three pillars of tissue engineering – cells, signals and biomaterials – are pivotal for the success of a tissue engineering application. Biomaterials usually form the scaffold of the tissue engineering construct and can be of natural or synthetic origin. Cells are inevitably part of a tissue engineering construct, they can be the patient’s (autologous), a donor’s (allogeneic) or stem cells. Signals include mechanical and/or electrical stimulation as well as bioactive agents like growth factors and help bringing cells into the desired niche.

1.3.1 Bioactive agents in tissue engineering

Bioactive agents are compounds showing an effect on a living cell, tissue and/or organism.¹²¹ They comprise antibacterial agents e.g. antibiotics, silver or zinc nanoparticles (NPs) or antimicrobial peptides as well as molecules able to enhance healing processes like growth factors, cytokines, vitamins or anti-inflammatory molecules. Growth factors (GFs) and cytokines are signaling peptides acting via binding to specific transmembrane receptors i.e. do not cross cell membrane. This binding event starts a signaling cascade inside of the cell guiding cell fate. A GF for instance has effects on cell proliferation, intercellular signaling, chemotaxis, angiogenesis and ECM formation¹²², hence, could significantly promote artificial tissue formation. To induce their effect, GFs can be added directly in the cell suspension or applied in a bioreactor, which provides a hydrodynamic shear stress allowing to continuously refresh the GFs. Here the bioreactor approach seemed more efficient for instance allowing to build glossy and smooth cartilage-like tissue from

chondrocytes in PLA nanofibers in contrast to the rough tissue obtained by drop-seeding.¹²³ However, short half-lives in the range of minutes to few hours¹²⁴, temperature instability¹²⁵ and degradation caused by fragmentation via oxidation or pH change¹²⁶ as well as severe effects of concentration i.e. too little leads to the formation of non-homogeneous tissue¹²⁷ and too much can cause abnormal tissue and inflammation¹²⁸, hamper the direct application of GFs. Therefore, to protect and preserve the native structure of the bioactive molecule and allow for its steady release, several strategies were developed.

In scaffold immobilization the GF is either physically or chemically entrapped within a scaffold. In physical entrapment like for instance in hydrogels, the GF is captured in a porous mesh and can be released by diffusion, swelling, erosion or osmotic effects, hence, usually useful for short term release.¹²¹ Chemical entrapment involves either affinity interactions or covalent bonds for example, heparin coating of a PCL structure allowed for entrapment of vascular endothelial GF (VEGF) leading to improved neovascularization compared to control without heparin.¹²⁹ Another approach is programmed delivery using self-regulated systems for spatiotemporal release as for example pH triggered release, where a pH change in certain tissue areas induces release of the GF; molecular recognition, where the release is induced by biomolecule-recognition e.g. aptamer binding; or triggered delivery systems. The latter one uses external stimuli like for instance the application of magnetic fields on magnetic particles coated with the GF or light for release of photocleavable GF e.g. bone morphogenetic protein was photocleavable coupled to PEG and was shown to induce higher cellular metabolic activity in mesenchymal stem cells.^{121, 130} In a third approach bioactive molecules are entrapped within carriers like microtubes, crystals or more common in microspheres, nanoparticles (NPs) and micelles. These particulate systems can either be applied directly at the target site or integrated in a scaffold allowing for release via diffusion or bulk degradation e.g. PLGA NPs were loaded with VEGF and glial cell line-derived neurotrophic factor and used for treatment of Parkinson's disease in rat brains showing a significant enhancement of neurons.¹³¹

Another group of bioactive reagents improving the performance of TE constructs are antibacterial substances. Post implantation infections are one of the most common problems for instance infections were the cause of revisions in 20.4 % of total knee arthroplasty in US between 2009 and 2013.¹³² The patient's susceptibility to infections is increased as the immune system is hampered by the presence of a foreign body. Problematic hereby is that bacteria tend to form biofilms – an organized community of several bacterial strains enclosed in a self-made polymer matrix. A biofilm is the most successful form of life and hence is highly resistant to conventional drugs and the immune system.¹³³ Therefore, conventional medication with antibiotics often give poor results as the antibiotic's penetration ability to the infected site and further inside of the biofilm

is reduced not being able to kill it. Another point adding up to the problem is the increase in bacteria resistances to antibiotics by development of e.g. efflux-pumps, metabolic inactivation or restriction in uptake.¹³⁴

An efficient way to avoid bacterial infections can be achieved by hindering bacterial attachment onto implants. This can be done by applying an antibacterial coating. A passive coating can work as antiadhesive e.g. using PEG¹³⁵ or nanotopographies thereby preventing the attachment of cells and proteins. Unfortunately, this coating also prevents attachment of eukaryotic cells, hence requires the addition of eukaryotic cell binding sequences.¹³⁶ Active coatings kill bacteria via incorporation of bactericidal substances like antibiotics, silver, zinc or selenium NPs, quaternary ammonium salts (QAS), positively charged polymers like chitosan, or antimicrobial peptides.¹³⁶ The positive charge of the latter three leads to bacterial membrane permeabilization and cell lysis.^{117, 137} Antibiotics either kill bacteria or hinder their growth by interaction with cell wall synthesis, protein synthesis, interference with nucleic acid synthesis, inhibiting metabolic pathways or disrupting their membrane.¹³⁸ The mode of action of NPs depends on the material they are made of and range from cell wall damage via growth inhibition by generation of reactive oxygen species to effects on protein synthesis.¹³⁹ These bactericidal substances can be physically adsorbed or entrapped, or covalently attached within the active coating.

As previously described in GF encapsulation, bactericidal substances can also be incorporated directly into the TE scaffold e.g. the synthetic peptide Tet213 or zinc oxide could be encapsulated in hydrogels of gelatin methacryloyl – tropoelastin and thereby decreased colonization by *E.coli* and *Staphylococcus aureus* (*S. aureus*).¹⁴⁰ Another way to deliver antimicrobial substances can be achieved via polymeric particles, which protect their payload, are able to overcome cellular tissue barriers and promise a slow and sustained release to improve biodistribution and pharmacokinetics.¹⁴¹ Hence, they are more effective against biofilms as a high dose of antibacterial molecules can be delivered directly at the place of need e.g. formulation of liposomal antibiotics were shown to fuse with bacterial outer membrane delivering their contents directly inside of *Pseudomonas aeruginosa* cells¹⁴²; or chitosan NPs loaded with vancomycin and decorated with folic acid showed enhanced uptake and efficiency against vancomycin resistant *S. aureus*.¹⁴³

All the described strategies depend on the interplay between the bioactive molecule, the encapsulating material and the cells involved. Due to the fact, that the stability of the bioactive agents as well as the cell requirements differ, not a single material or strategy will be able to fit all applications. Further, during tissue formation commonly several bioactive molecules are required in a time and dose dependent manner, which is far from what can be technically be realized up to

now. Thus, it is still a long way until such a complex system delivering the right molecule at the right time in the perfect concentration can be realized. However, more and more is learned about how materials can be modified and how pro- and eukaryotic cells react to certain stimuli pathing the way for generating optimized constructs for each application.

1.3.2 Silk and bioactive agents

Many studies focus on the incorporation of bioactive molecules into silk matrices. An easy approach is to immerse a silk matrix in a solution containing the bioactive molecule triggering their absorption into silk matrix. Transforming GF beta 3 (TGF β -3) and bone morphogenetic protein-2 (BMP-2) were absorbed on multi-layer *B. mori* and *A. mylitta* silk scaffold. Implantation into knee joints of Wistar rats yielded the formation of neo-matrix with glycosaminoglycans and collagen after 8 weeks.¹⁴⁴ Another possibility is to blend silk proteins with the desired agent and subsequently process the mixture into the desired morphology. Using this approach RSF was blended with nerve growth factor (NGF) and subsequently cast into a film conduit. In vitro tests proved a significant outgrowth of neurites due to the slow release of the NGF over 3 weeks.¹⁴⁵ Another study analyzed aligned electrospun fibers of RSF blended with brain-derived neurotrophic factor and VEGF. The constructs were implanted subcutaneously in adult mice and showed a release of the bioactive molecules over two weeks leading to de-novo innervation and vascularization without inducing a chronic inflammatory response.¹⁴⁶ Further, injectable silk hydrogels were loaded with BMP-2 and VEGF. A minimal invasive approach was used to implant the GF loaded scaffold into rabbit maxillary sinus, where new bone was formed and angiogenesis was promoted.¹⁴⁷ These two techniques – immersion and blending – can be rather easily realized, but often lead to an undesired quick release.

In order to slow down the release, bioactive agents can first be encapsulated in spherical structures and then embedded in a matrix e.g. the antibiotic gentamycin sulfate was loaded onto gelatin microspheres, which were embedded into a silk matrix. This composite material exhibited slower release kinetics and stronger antibacterial effects against *E. coli*, *S. aureus* and *Pseudomonas aeruginosa* compared to the materials alone loaded with the antibiotic and was able to reduce burn infection in rats.¹⁴⁸ In another interesting approach silver NPs with antibacterial properties were directly synthesized on a RSF matrix. Thereby the negatively charged amino acid residues acted as nucleation sites for positively charged silver ions and silver NPs were formed via UV-irradiation.¹⁴⁹

Covalent attachment of quaternary ammonium compounds onto silk fibroin was realized with the formation of 3-(trimethoxysilyl)-propyldimethyloctadecyl ammonium chloride. The antimicrobial function was not inhibited by the binding and the long chains allowed the interaction

of the compound with the bacterial cell wall eventually killing the cell.¹⁵⁰ Further, covalent bonds can be introduced by creating genetic fusion proteins, which was done by genetically adding human neutrophil defensin 2 and 4 as well as hepcidin to recombinant spider silk protein 6mer. The self-assembling features of silk were maintained and additionally antibacterial properties against *E. coli* and *S. aureus* without harming proliferation in mammalian cells were proven.⁶¹ The covalently attached antimicrobial peptide Cys-KR12 to electrospun RSF not only showed a reduction of several bacteria strains, but in addition showed an enhancement in proliferation of dermal fibroblasts and keratinocytes as well as immune-modulating properties assisting in wound healing.¹⁵¹ In a different study a non-natural azide bearing amino acid was incorporated into the recombinant 4RepCT spider silk protein. This azide group was used for copper catalyzed azide-alkyne cycloaddition to add the antibiotic levofloxacin. With the acid-labile glycerol-ester linker a slow and steady antibiotic release could be achieved being effective against *E. coli*.⁸⁹

Silk matrices were successfully modified with diverse bioactive agents and underwent *in vitro* and *in vivo* studies. All studies incorporating GFs resulted in an improvement in cell behavior and/or tissue generation and the studies dealing with the addition of antibacterial agents illustrated bactericidal effects. It could be shown that dependent on the loading strategy, the agents were released either fast or slow providing adaptable systems for different requirements in TE. Hence, silk can be considered a promising material for bioactive agent delivery.

1.3.3 Heart muscle regeneration

The heart is a muscular, hollow organ enclosed by a protective sac, the pericardium. The heart walls are made of myocardium and endocardium. The heart is responsible for pumping blood through the circulatory system. This pivotal process supplies cells with oxygen and nutrients and removes metabolic wastes. In mammals the heart is built of four chambers, left and right atria (upper chambers) and ventricles (lower chambers). The left heart is responsible for pumping the oxygen enriched blood via arteries to all parts of the body (systemic circulation). The oxygen depleted blood from the systemic circulation reaches the right heart from where it is pumped to the lungs (pulmonary circulation) for gas exchange.¹⁵² The blood then enters the left heart again and the cycle restarts in healthy individuals.

Heart failure is one of the main causes of death in industrialized nations usually resulting from a deficiency of cardiac cells.¹⁵³ The different classes, characteristics and their impact on physical activity are shown in Table 1. According to the American Heart Association heart failures are categorized into left-sided, right-sided and congestive heart failure. In the left-sided heart failure insufficient blood is pumped through the system circulation. This can have two causes: (I) he left

ventricle cannot contract normally (reduced ejection fraction) or (II) the left ventricle is too stiff to relax normally and thus proper filling with blood is impeded (preserved ejection fraction). In the right-sided heart failure blood backs up in the veins due to reduced pumping power of the right ventricle. In the congestive heart failure fluid builds up in the body due to a reduced blood flow out of the heart.¹⁵⁴

Table 1: Classification of heart failure adapted from Baliga *et al.*^{155, 156}

NYHA Class	Characteristics	Impact on physical activity	2-year Mortality (%) on ACE-I*
I	No heart failure - no rales or S ₃ §	Asymptomatic – no limitation, no shortness of breath, fatigue or palpitations during physical activity	10
II	Heart failure – rales (<50 % lungs), S ₃ and venous hypertension	Slight limitations – shortness of breath, fatigue or palpitations during physical activity	20
III	Severe heart failure – frank pulmonary edema, rales (>50 % lungs)	Marked limitations – shortness of breath, fatigue or palpitations during activities of daily living	30-40
IV	Cardiogenic shock – signs include hypotension and peripheral vasoconstriction Heart failure – often with pulmonary edema	Symptoms at rest – shortness of breath, fatigue or palpitations	40-50

New York Heart Association

* angiotensin-converting enzyme inhibitors

§ third heart sound – associated with heart failure

The human left ventricle is made of 2-4 billion cardiomyocytes, and a single myocardial infarction can kill up to 25 % of these cells within a few hours.¹⁵⁷ Other reasons for loss of cardiac cells are disorders of cardiac load e.g. hypertension or valvar heart disease, which lead to a cellular reduction over many years¹⁵⁸. Further, ageing in general is already accompanied by a reduction by 1 gram of myocardium per year even in the absence of a disease.¹⁵⁹ The problem is that the heart is one of the organs showing least regenerative capacity¹⁵³ with annual cardiomyocyte turnover rates of 1.9 % in adolescent, 1 % in middle aged and 0.45 % in old aged humans.¹⁶⁰ Interestingly, human

cardiomyocytes react to pathological workloads like hypertension, valvar disease and post-infarction overload by reinitiating DNA synthesis without a nuclear division and therefore, most possess polyploid nuclei.^{161, 162} A potential reason for their post-mitotic state in adult mammals is that the centrosomes of cardiac cells disassemble shortly after birth and thus, sending cardiomyocytes into a cell-cycle arrest.¹⁶³ Another possible route for cardiomyocyte production, next to proliferation, is differentiation of cardiac progenitor cells (CPC). Although it was shown, that CPC are activated for instance in the case of an infarction and prompted to divide, migrate, experience lineage commitment and mitigate pathological damage,¹⁶⁴ the rate is too slow with the additional issue of a severe reduction of cardiac progenitor cells during ageing.¹⁶⁵ In summary, several studies offer a strong evidence for plasticity in human heart, but the processes of cardiomyocyte production are too slow to compensate for their loss. Therefore, strategies dealing with cellular reprogramming, stem cell therapy and tissue engineering are investigated (Figure 7).¹⁵³

Cellular reprogramming means that for instance the scar forming fibroblasts at the infarct site are reprogrammed and become cardiomyocytes. The idea seems very appealing, but an efficient and transgenic-free process as well as information on how normal these cardiomyocytes behave are still missing.¹⁵³ Due to the insufficient cardiac cell regeneration in the body, stem cell (SC) therapy is a promising route for cardiac engineering. Extensive research went into analysis of the potential of pluripotent SCs like embryonic SCs (ESC) and human induced pluripotent SCs (hiPSC), which have the capability to differentiate into nearly all cell types, hence also cardiomyocytes. Problematic hereby is, that often these cells are immature and lack not only expression profile, but also morphology and function of ventricular cardiac cells.¹⁵³ Another important point is that ESC therapies would be allogenic, thus, requiring immunosuppression.¹⁵³ On the other hand, every hiPSC, which could be obtained by reprogramming of the patient's somatic cells, is officially a new product that needs to undergo all safety studies before usage. The alternative could be a well-characterized bank of several SC lines that can be matched according to human leukocyte antigen to reduce immune suppression to a minimum.¹⁶⁶ A further issue that must be clarified before using PSCs is their chromosomal instability and the possibility of introduction of mutations that could cause a malignant transformation.¹⁶⁶ Several clinical trials tested the treatment of heart failure patients with bone marrow derived SCs proposing the safety of the method. Unfortunately, only little improvement in myocardial structure and function was observed.¹⁶⁵ Thus, using SC alone might not be the holy grail to cardiac repair, but the combination with a scaffold like in cardiac tissue engineering (TE) it might lead to a breakthrough in the field.

One of the major objectives of cardiac TE is to produce functional heart muscle tissue, which is further transplanted on malformed or injured hearts to regain normal function.¹⁶⁶ The expected advantages are a higher cell retention than in cell therapy¹⁶⁷ and the possibility of quality

control before implantation¹⁶⁶. Cardiomyocytes tend to beat spontaneously and possess the intrinsic capacity of forming 3D functional syncytia¹⁶⁶ –promising features for TE. Further, it was found, that constructs containing mixtures of cardiomyocytes with nonmyocytes were able to develop three times higher forces than with cardiomyocytes alone.¹⁶⁸ This might be due to an ECM mediated mechanism, as ventricular rat cardiac cells showed enhanced growth on ECM produced by fibroblasts.¹⁶⁹ Thus, one approach to prepare an artificial heart is to decellularize a whole heart (here rat) by extended Langendorff perfusion leading to an almost complete removal of heart cells and leaving the connective tissue. This tissue possesses the right shape and can further be perfused, but a high mechanical stiffness was observed and repopulation with cells to regain full function remains a challenge.¹⁷⁰

Other approaches aim at the preparation of tissue patches – either based on a scaffold e.g. composite hydrogel from collagen and Matrigel with cardiac cells,¹⁷¹ stacked cell sheets e.g. by co-culturing endothelial with cardiac cells and stacking three of these sheets¹⁷² or scaffold-free aggregates obtained e.g. by gyratory shaking in 6-well dish¹⁷³. These patches are theoretically not limited in width or length, but – as in all tissue engineering applications – the thickness possesses a critical limit of about 80 µm if no vascularization is present.¹⁷⁴ Although spontaneous vascularization of 3D cardiac constructs was observed with^{172, 173} and without^{168, 175} the addition of endothelial cells, pre-vascularization is required to obtain a reasonable thick construct of several millimeters. Another important factor in cardiac patches is the need for electric coupling with the host so that synchronized beating following the lead of pacemaker cells can be achieved. Therefore, often bigger implants are investigated to enable contact with healthy myocardium.¹⁷⁶ Still, this is not an easy task as the heart's epicardium, the epithelial cell layer on the graft's surface and/or the formation of a cell-free ECM layer between host and implant can inhibit contacting of cardiomyocytes.¹⁷¹

Another open question is the time point of transplantation. Electrical¹⁷⁷ and mechanical¹⁷⁸ stimulation *in vitro* showed an enhancement in longitudinal orientation and alignment, hypertrophy and electromechanical function, thus, resulted in more mature constructs. Important here, even in good 3D constructs, cardiomyocytes are not showing a fully mature phenotype i.e. lacking densely packed contractile machinery¹⁷⁵ and possessing unusual length/width ratio.¹⁷⁹ However, greater cell differentiation leads to worse survival rates after transplantation.¹⁸⁰ Thus, there is an ongoing search for optimal constructs that allow to fully regenerate heart function.

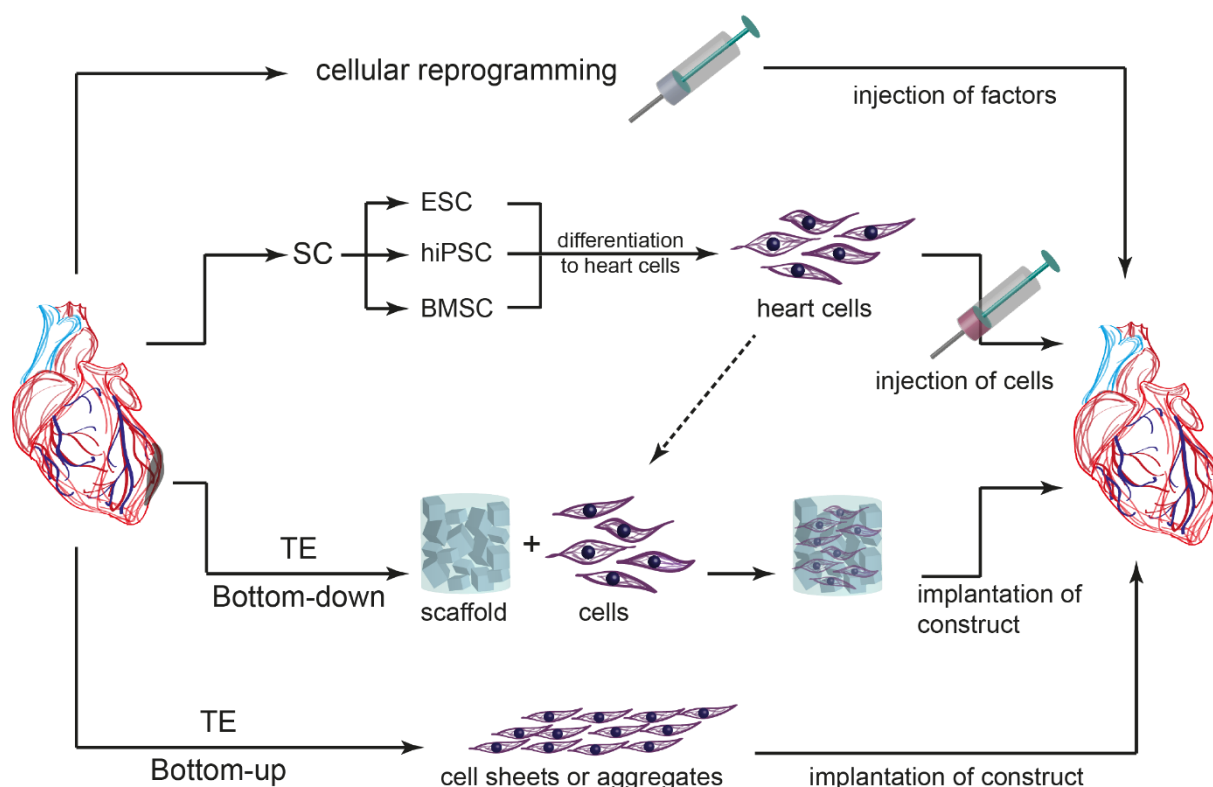


Figure 7: Routes investigated for heart muscle regeneration after myocardial infarct (grey patch on heart). First row: cellular reprogramming – fibroblasts in the scar tissue of the myocardial infarct should be reprogrammed to cardiac cells. Second row: stem cell (SC) therapy – stem cells are differentiated into heart cells and then injected into the scar tissue. Third row: tissue engineering (TE) – bottom-down approach: A scaffold is combined with heart cells (probably provided from SC differentiation) and the construct is implanted into the infarct site. Fourth row: TE – bottom-up approach: Cell sheets or aggregates are prepared and implanted onto the infarct site.

1.3.4 Silk in heart muscle regeneration

Lately, several studies using moth, silkworm and recombinant spider silk investigated their suitability for cardiac regeneration. In one of the first studies, *B. mori* silk fibroin was mixed with chitosan and/or hyaluronic acid. Sprayed microparticles were pressed and crosslinked with genipin. The cardiac patches were seeded with ratMSCs, and it was shown that growth rate and differentiation were superior on the hybrid patches.¹⁸¹ In the first follow up study patches from silk with hyaluronic acid pre-seeded with or without BMSC were implanted in rats onto induced myocardial infarcts. Especially the cell loaded constructs showed improvement of left ventricular modeling, low to no cytotoxic response, prevented apoptosis of cardiomyocytes, restored contractile proteins and stimulated the secretion of growth factors for cardiac repair.¹⁸² Further, silk and chitosan-hyaluronan patches without cells were implanted in rats onto myocardial infarcts showing

similar promising results than the previous study suggesting the suitability of hybrid silk constructs in cardiac regeneration.¹⁸³

Stoppel *et al.*¹⁸⁴ examined anisotropic and isotropic *B. mori* sponges blended with cardiac tissue-derived ECM or collagen using atrial cardiomyocytes and hESCs derived cardiomyocytes and additional *in vivo* tests. The aligned structures in combination with ECM cues supported cell infiltration and vascularization *in vivo* as well as a functional phenotype *in vitro*.¹⁸⁴ Castellano *et al.*¹⁸⁵ compared electrospun silkworm silk with PCL, PLA, polyamide, poly(3-hydroxybutyrate) and non-crosslinked collagen membrane in terms of cell compatibility using cardiac cells and MSC. Although cell attachment was comparable to controls, *in vivo* studies showed an encapsulation due to foreign body response and no prevention of negative remodeling after the myocardial infarct was observed.¹⁸⁵ In another study, BMSC and menstrual blood derived SCs were seeded onto sponges from *B. mori* silk. They could show that the SCs attached and distributed well in the scaffold and in addition proliferation and the level of cardiac differentiation marker was higher than in 2D controls.¹⁸⁶ Another group showed that cardiac progenitor cells seeded into anisotropic *B. mori* silk sponges distributed uniformly and synthesized a great quantity of ECM. Analysis with qPCR revealed similar protein expression levels than in cardiac tissue, proving the possibility of resembling a stem cell niche driving efficiently cardiac progenitor cell commitment.¹⁸⁷

Antheraea mylitta silk coated on glass coverslips and in form of a foam was investigated using primary cardiomyocytes from postnatal rats. Cardiomyocytes efficiently attached, responded to extracellular stimuli, expressed connexin 43 (cell communication), exhibited aligned sarcomers (basic unit responsible for contraction) and coupled electrically with each other resulting in synchronous beating. Due to the inherent RGD domain in *Antheraea mylitta* silk, it outperformed *B. mori* silk in this study.¹⁸⁸ In another study *Antheraea assama* silk was compared to *B. mori* silk by investigating neonatal cardiomyocytes on micro-grooved films. In general, *Antheraea assama* silk outperformed silkworm silk in terms of mechanical robustness, elasticity, cell compatibility and lower immunogenicity *in vivo*. The grooved structure allowed the production of aligned cell monolayers with an upregulation in several factors i.e. connexin 43, myosin heavy chain alpha and troponin I (maturation and functionality). Additionally, these layers could be stacked to form a 3D construct.¹⁸⁹

On the foam of the recombinant spider silk protein VN-4RepCT – an analog of *Euprosthrops australis* MaSp1 with a vitronectin tag – hESC could be successfully differentiated into cardiomyocytes. Under xeno-free conditions, markers for cardiac lineage were expressed.⁸⁷ In another study materials made of the recombinant spidroins rS1/9, rS2/12 and the RGD variant of the latter one – all originating from *Nephila* species – were compared to silkworm silk. The

electrospun mats, especially the variants containing RGD, showed promising results when seeded with neonatal rat cardiomyocytes. The cells attached, grew and formed confluent layers, but also formed a cardiac syncytium and were shown to be fully functional, thus, capable of coordinated contraction.⁶⁴

In general, the low to no immune response, the slow biodegradation and the possibility to form various morphologies make silk a very interesting material in cardiac TE applications. The results using *B. mori* silk are slightly diverse, being not very persuading. The reason could be the missing cell binding motifs, as blends with other materials like collagen offering these binding moieties indicated positive results. Hereby, recombinant spider silk provides the advantage to genetically add such cell binding peptides like in rS2/12-RGDS triggering cell behavior. Further, recombinant silk can be produced in big amounts and in constant quality. Especially, the xeno-free preparation of 4RepCT and its variants seems promising.

1.3.5 Nerve regeneration

The nervous system is responsible for transmission of signals throughout the body by detecting environmental changes and responding to them. In higher developed organisms, it can be divided into two parts, namely the central nervous system (CNS) and the peripheral nervous system (PNS). The CNS consists of the brain and spinal cord and the PNS includes all nerve bundles connecting the CNS with the rest of the body. The PNS can be divided into sensory and motor division responsible for transport of information in form of chemical signals and electrical impulses from a receptor to the CNS or the CNS to effectors (muscle and glands), respectively.

A peripheral nerve consists of several layers, whereby the smallest unit are neurons (Figure 8). A neuronal cell consists of a cell body and different extensions – the short ones are called dendrites and are responsible for sensing signals, the long ones can grow up to a meter, are called axon and are responsible for signal transmission.¹⁹⁰ The axons can be covered by a myelin sheath as a protection as well as for faster signal transduction. These nerve fibers are enclosed by the endoneurium, a loose connective tissue. Numerous of these form a nerve bundle/fascicle, which in turn is covered by the perineurium. Several fascicles and blood vessels are bundled together by the epineurium forming a peripheral nerve.¹⁹¹

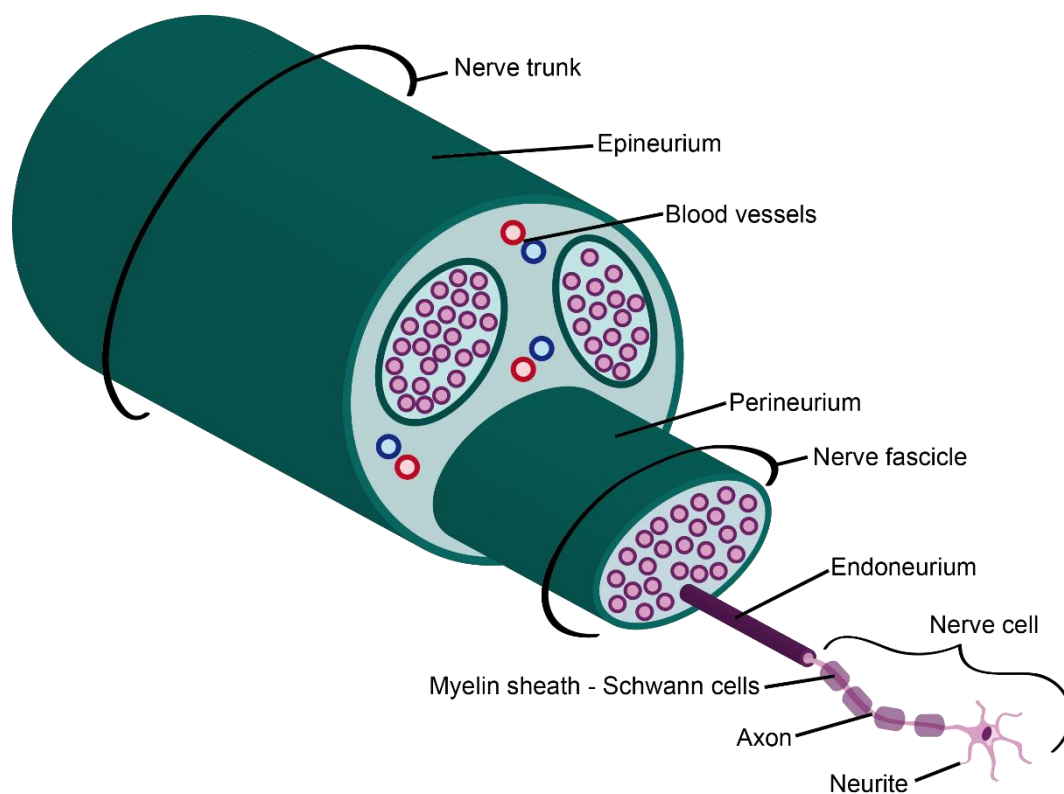


Figure 8: Peripheral nerve: Neuronal cells are composed of a cell body with two types of extensions: neurites (short extension for sensing signals) and axons (long extensions for signal transduction). In higher developed organisms, axons are often covered by a myelin sheath for protection and faster signal transduction. Such nerve fibers are enclosed by the endoneurium and several of these are then collected into fascicles surrounded by the perineurium. The fascicles, blood vessels and fibroblasts form the nerve trunk and are surrounded by the epineurium.

Injuries at the peripheral nerve system can occur from vehicle or industrial accidents, penetrating trauma or falls and can lead to muscle paralysis or a complete or partial loss of motor functionality. Estimates assume approximately five million cases of peripheral nerve injuries every year.¹⁹² Robinson¹⁹³ summarized in a Table the classifications of nerve injuries as described by Seddon¹⁹⁴ and Sunderland¹⁹⁵ including the pathology as well as the prognosis - this table is shown as Table 2.¹⁹³

Table 2: Classification systems of nerve injuries as present by Robinson¹⁹³

Seddon classification	Sunderland classification	Pathology	Prognosis
Neurapraxia	First degree	Myelin injury or ischemia	Excellent recovery in weeks to months
Axonotmesis	First degree	Axon loss, variable stromal disruption	Good to poor, depending upon integrity of supporting structures and distance to muscle
	Second degree	Axon loss, endoneurial tubes, perineurium and epineurium intact	Good, depending upon distance to muscle
	Third degree	Axon loss, endoneurial tubes disrupted, perineurium and epineurium intact	Poor, axonal misdirection, surgery may be required
	Fourth degree	Axon loss, endoneurial tubes and perineurium disrupted, epineurium intact	Poor, axonal misdirection, surgery usually required
Neurotmesis	Fifth degree	Axon loss, endoneurial tubes, perineurium and epineurium severed	No spontaneous recovery, surgery required, prognosis after surgery not guaranteed

The PNS reacts to an injury – crush or section – by active de- and regeneration. It begins with the Wallerian degeneration of the distal axon part.¹⁹⁶ Hereby, first the axonal skeleton and then the myelin sheath degenerate. Macrophages infiltrate and clear the debris, promoting vascularization¹⁹⁷ and axonal regeneration¹⁹⁸. Schwann cells dedifferentiate into a pro-regenerative, nonmyelinating phenotype and start to proliferate and migrate. They express surface proteins, secrete neurotrophic factors and deposit basal lamina proteins e.g. laminin and fibronectin, to form bands of Büngner. This bands guide the way for reinnervation of the proximal part activated by certain signaling pathways.^{199, 200} If the gap between the distal and proximal part is too wide, fibrin deposition and scar tissue formation occurs in its way, limiting reinnervation. Thus, the nerve will not gain back its original function.²⁰⁰ In such cases, surgery can help, whereby a tension-free end-to-end suture is favored for gap sizes smaller than one centimeter. For bigger gap sizes (20-80 mm) nerve autografts e.g. from the patient's sural nerve, are the current gold standard.²⁰¹ Hereby, the axons within in the autograft degenerate and leave a 3D network of ECM with aligned structures

that gives physical guidance and allows the ingrowth of the proximal nerve stump. In addition to this physical guidance, the autograft provides chemical and cellular signals i.e. neurotrophic factors and Schwann cells. Unfortunately, this treatment shows limitations in supply of donor nerve, results in donor morbidity, shows limited restoration function to the acceptor site, induces the risk of neuroma formation and needs time consuming surgery.¹⁹² The success rate, getting back good to excellent motor or sensory function, is below 50 percent.²⁰² An attractive alternative are nerve guidance conduits (NGCs), which should provide a guidance similar to autografts along which the nerve stumps can regrow towards each other.²⁰³

The ideal NGC is depicted in Figure 9. It is biocompatible, immunologically inert and biodegrades slowly to avoid foreign body reactions and scar tissue formation. The materials used should be flexible and soft and at the same time possess a high tensile strength mimicking the natural model – the ECM with its basal lamina.¹⁹² The tube should be semi-permeable. On the one hand, it should avoid infiltration of inflammatory cells and myofibroblasts, which would impede nerve regeneration by for instance depositing axon repulsive proteoglycans. On the other hand, they should allow diffusion of gases, vital nutrients and factors and permit revascularization to provide a good regenerative environment.²⁰⁴ Furthermore, the material should provide a physical guidance cue to lead the way for Schwann cells and growing axons, termed contact guidance theory.¹⁹² Moreover, studies claimed beneficial effects on reinnervation upon the addition of bioactive molecules, ECM-like matrix, supporting cells and electrical conductivity. Bioactive molecules like neurotrophic factors assist the survival, growth and differentiation of neural cells. Ideally, these factors are released in controlled doses over an extended period of time to allow for long term repair.²⁰⁵ In order to resemble the natural environment of a peripheral nerve, ECM-like matrices containing for example collagen²⁰⁶, laminin or fibronectin²⁰⁷ were introduced. Cellular assistance can be provided by the introduction of Schwann cells. Autologous Schwann cells and stem cells, with the capability to differentiate into Schwann cells, gave promising results.¹⁹² Additionally, technical requirements concerning production, sterilization, long-term storage and surgical handling need to be met.^{35, 201}

Up to now, most FDA approved NGCs consist of a hollow tube and are made of synthetic polymers like for example PGA (Neurotube), PVA (SaluBridge/SaluTunnel), polyhydroxybutyrate (AxonScaff/Cellscaff/StemScaff), poly(DL-lactic-*co*- ϵ -caprolactone) (NeuroLac). Furthermore, collagen I was used as a tube forming material (NeuraGen, NeuroMend, NeuraWrap, NeuroMatrix/Neuroflex).²⁰⁸ These tubes fail in treatment of larger nerve gaps, probably due to the missing filling. In an attempt to solve this problem, NeuraGen 3D was developed. Here, the NeuraGen tube was filled with a collagen-glycosaminoglycan matrix.²⁰⁹ Another approach uses processed human nerve allograft (Avance® Nerve Graft) to provide a naturally derived NGC.²¹⁰

However, current clinical data suggests that NGC show a similar performance than autologous nerve grafts for short gaps, but are still outperformed in large gaps (> 20 mm).²⁰⁰ A possible explanation could be the missing chemical and cellular signals, which did not yet obtain regulatory approval.¹⁹²

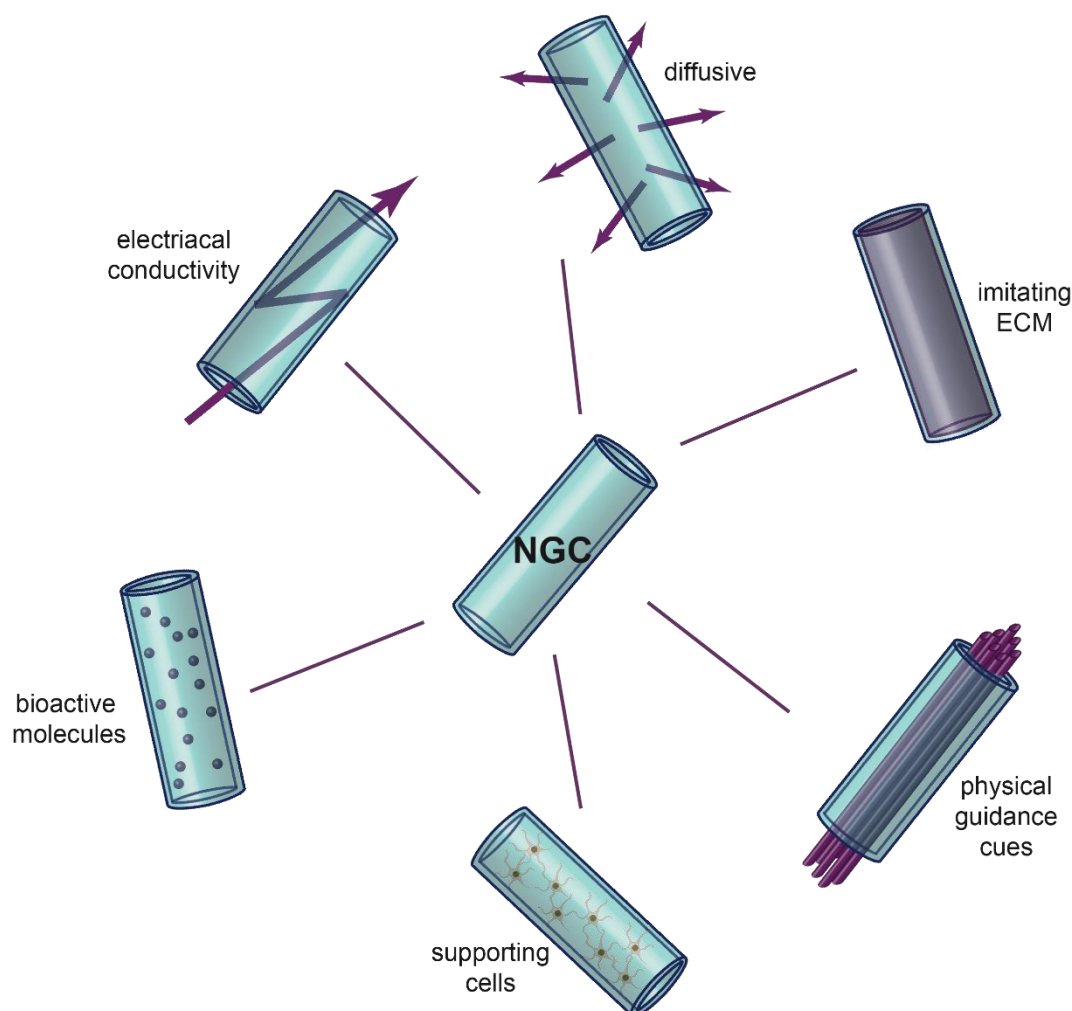


Figure 9: The optimal nerve guidance conduit (NGC). NGCs should provide a semi-permeable membrane, an ECM-like filling, physical guidance cues, support cells, bioactive molecules and electrical stimulation.

1.3.5.1 Self-rolling tubular structures

The fundamental part of an NGC is a tubular structure, which can be further equipped with the beforementioned bioactive molecules, supporting cells, guidance cues and ECM like filling. Post-preparational filling of tubes with these additives can be tricky. Therefore, a self-rolling approach, where the additives can be applied onto a film and rolling can be induced afterwards, would be beneficial.

Self-assembling mechanisms are a major driving principle of structure formation in nature and hence the concept of intelligent materials.^{211, 212} The idea is to mimic mechanisms observed in organ development, fruit growth and plant movement as for instance the closing mechanism in a Venus fly trap. A transition from concave to convex structure evoked by hydration allows the trap to close its “jaws” in only 100 ms.^{213, 214} The principle behind this natural mechanism is an inhomogeneous reaction of an either inherent inhomogeneous material or of the different layers of a multi-layer system in response to environmental stimuli like a change in pH, temperature, solvent, light, electric field or enzyme concentration.^{213, 215} In multi-layer systems the layers are termed as active and passive. The active layer responds to the environmental stimulus by swelling and thus, induces a change in the passive one. If the passive layer is hard, wrinkles and creases are formed, whereas if the passive layer is soft curling and rolling occurs to release the internal stress.^{216, 217}

Imitating this principle can be used to produce self-folding microconstructs, often referred to as microorigami. Advantages are not only the quick and reproducible fabrication but also the possibility to render the chemical properties as well as the morphology of the interior and exterior of the constructs.^{215, 217, 218} Pioneering work in the field of self-folding materials was performed by Jager *et al.*²¹⁹ and Smela *et al.*²²⁰. They were the first working with metal-polymer films, which responded to an electric signal. Several more self-rolling approaches comprising metals were performed.^{221, 222} These are mainly interesting as microelectronic devices, though inapplicable in the field of biomedical engineering, as they show a limited biocompatibility and are non-biodegradable. Thus, stimuli-responsive polymers were gaining more and more interest in this field. They respond to mild changes in their environment by undergoing dramatic changes in physico-chemical properties as for instance a volumetric change due to swelling.²²³ Common intelligent polymers used in this field are pH-, thermo- or solvent responsive.²¹⁵ Sometimes they are even multi-responsive, hence reacting to several stimuli like poly(*N*-isopropylacrylamide-*co*-acrylic acid) responding to temperature and pH.²²⁴ Poly(*N*-isopropylacrylamide) derivatives were often used and show an excellent performance as active polymer, but are not biodegradable.^{217, 224-227} Therefore, biodegradable polymers like gelatin²²⁸, polysuccinimide²¹⁸ or silk²²⁹ were investigated as self-rolling tubes also for the use with cells.

1.3.6 Silk in nerve regeneration

Several studies using silk fibroin or spider silk in combination with nerve and/or Schwann cells gave promising results. Schwann cells were cultured in the presence of silk fibroin extract fluid and no difference was observed compared to plain medium in terms of morphology, viability, proliferation and factor secretion suggesting very good biocompatibility of silk fibroin-based materials.²³⁰ Further, Schwann cells seeded onto electrospun silk fibroin non-woven mats exhibited more ordered and longer outgrowths as well as more extensive and more complex interconnections compared to polylysine.²³¹ In another study, *B. mori* silk tubes were filled with Spidrex® fibers and implanted to bridge an 8 mm gap in rat sciatic nerve. After 12 weeks, the number of myelinated axons, gastrocnemius muscle interaction and hind paw stance (catwalk food print analysis) were comparable to that of animals with the autologous nerve graft control.²³² Further, several studies investigated silk fibroin blends with natural or synthetic polymers like chitosan, collagen, tropoelastin, PLLA, poly(lactide-*co*-glycolide) (PLGA), poly(lactide-*co*-caprolactone) (PLCL), polyacrylamide or poly(*p*-dioxanone) as reviewed in²⁰⁰. An interesting study here used a lysine-doped poly(pyrrole)/regenerated spider silk protein/PLLA/nerve growth factor (NGF) composite scaffold prepared by co-axial electro-spraying and -spinning. First tests with PC-12 cells were already successful in terms of biocompatibility, cell adhesion and stable conductivity and successive *in vivo* tests bridging a 2 cm sciatic nerve gap in rat showed a promotion in Schwann cell migration and axonal regrowth within 10 months.²³³

Other studies investigated natural fibers from *Nephila* spiders as nerve guidance cues embedded with Schwann cells in Matrigel inside of acellularized veins.²³⁴ After this first successful study a 2 cm sciatic nerve defect in rats was bridged with and without Schwann cells and Matrigel. It was shown that all constructs lead to nerve regeneration within 6 months by guiding Schwann cell migration and proliferation and axonal re-growth.²³⁵ In a later study, a 6 cm tibial nerve defect in sheep was bridged with an acellularized pig vein construct filled with *Nephila* fibers and compared to autologous nerve grafts. No significant difference was observed in Schwann cell migration, axonal regrowth and remyelination including electrophysiological recovery.⁵² In an *in vitro* study, it was even suggested that these constructs are able to bridge a 15 cm gap.²³⁶

Recombinant silk is scarcely used in peripheral nerve repair, and mainly *in vitro* studies are available. Neural stem cells were investigated on films of the *Euprosthenois australis* derived 4RepCT protein and showed successful proliferation as well as maturation into neurons at the presence of bone morphogenetic protein.²³⁷ Films of the *Nephila clavipes* derived rMaSp1 protein supported growth of primary rat cortical neurons in terms of axon extension and network connectivity, and in addition, an increase in neural cell adhesion molecule expression was

observed.²³⁸ Foams of another *Nephila clavipes* derived protein rS1/9 film was implanted into midline dorsal subcutaneous areas in mice and promoted the ingrowth of nerve fibers and vascularized connective tissue elements.⁶³

Thus, silk seems to be a promising material for nerve regeneration not least because of its outstanding mechanical properties combined with biocompatibility. Especially, in terms of recombinant silk more investigations are necessary, to finally confirm its suitability in bridging nerve gaps.

1.4 Bioinstrumentation

According to Berkley Bioengineering, “Bioinstrumentation is the development of technologies for the measurement and manipulation of parameters within biological systems, focusing on the application of engineering tools for scientific discovery and for the diagnosis and treatment of disease”.²³⁹ Bioinstrumentation spans a wide field of commonly computer-assisted devices, biosensors being one of them. The basic principle of a biosensor is the transformation of a chemical information like the concentration of a certain analyte in the sample into an analytically useful signal. Hence, the two basic elements are the biological recognition system and a physicochemical transducer²⁴⁰ connected to a computer to produce a user-friendly read-out. The biological recognition element should be sensitive to the desired analyte and measure it with a high degree of selectivity,²⁴¹ a feature often attributed to enzymes.

1.4.1 Enzyme confinement

Catalysts decrease the activation energy needed for a chemical reaction and thereby increase the reaction rate without being used up themselves. Thus, a catalyst changes the kinetics, but not the thermodynamics of a reaction, i.e., the equilibrium is achieved faster with a catalyst than without, but the equilibrium is not changed. A catalyst influences the reaction mechanism by forming an often otherwise instable intermediate with the reactant and thereby it lowers the potential energy. Nature is an expert in using biocatalysts, called enzymes, to perform enantiopure, site- and substrate-specific reactions in an all-aqueous system at body-friendly reaction conditions. Another essential part of nature’s ingenuity is its ability to run all reactions in a crowded environment i.e., synthetic reactions occur mainly in cells in our body, often in specific compartments thereof. This compartmentalization helps to organize reaction processes as well as it enhances efficiency thereof.²⁴²

In an attempt to use this natural principle, enzymes are immobilized by either adsorbing or binding them to a surface, physically entrapping them in a matrix or encapsulating them in a container.²⁴³ Enzymes can be fixed onto a surface by adsorption to the surface via non-covalent interactions either directly with the surface or via affinity tags e.g. biotin coupled to the surface interacting with streptavidin bound to the enzyme. Further, enzymes can be bound covalently to a surface via an organic linker either directly connected to the surface using for instance crosslinkers like glutaraldehyde or to a soft coating like an amphiphilic bilayer.²⁴⁴ These methods commonly also allow to immobilize more enzymes to enable cascade reactions. Special systems were developed, to even precisely control the spatial arrangement of the enzymes e.g. a DNA origami nanotube was used to precisely position glucose oxidase (GOX) and horseradish peroxidase (HRP).²⁴⁵ For physically entrapment of enzymes in a matrix, the components are often mixed in liquid form and then processed into the matrix e.g. bioactive glasses were prepared by a sol-gel method encapsulating HRP in (alkylated) silica.²⁴⁶ In all these approaches care must be taken to not block the active site of the enzyme as this would cause a decrease or complete suppression of the catalytic activity. An advantage of immobilized enzymes is the ease in separating the product from the enzyme.

Another approach are volume confined containers to encapsulate enzymes. Hereby, enzymes in solution are encapsulated in distinct compartments. The substrate can either be supplied by placing it directly with the enzyme into the container, by fusing two compartments like vesicles one filled with the enzyme and the other with the substrate, or by diffusion in semi-permeable containers.²⁴³ The membrane can protect the cargo from harmful, like for instance hydrolytically active substances in surrounding media. Realizations of such a system are depicted in Figure 10: (I) vesicles like liposomes from biological bilayers^{247, 248} or polymerosomes consisting of amphiphilic block copolymers²⁴⁹; (II) protein cages with proteinous boundaries like in prokaryotic microcompartments or virus capsids²⁵⁰; (III) reverse micelles for example formed by emulsions from ionic liquids or surfactants²⁵¹; (IV) water-in-oil droplets forming semi-permeable capsules from amphiphilic molecules²⁵²; (V) polymer capsules like polyelectrolytes using a layer-by-layer approach to form a capsule around a removable template²⁵³; (VI) arrays of small reaction vessels prepared for instance by chemical etching²⁵⁴.

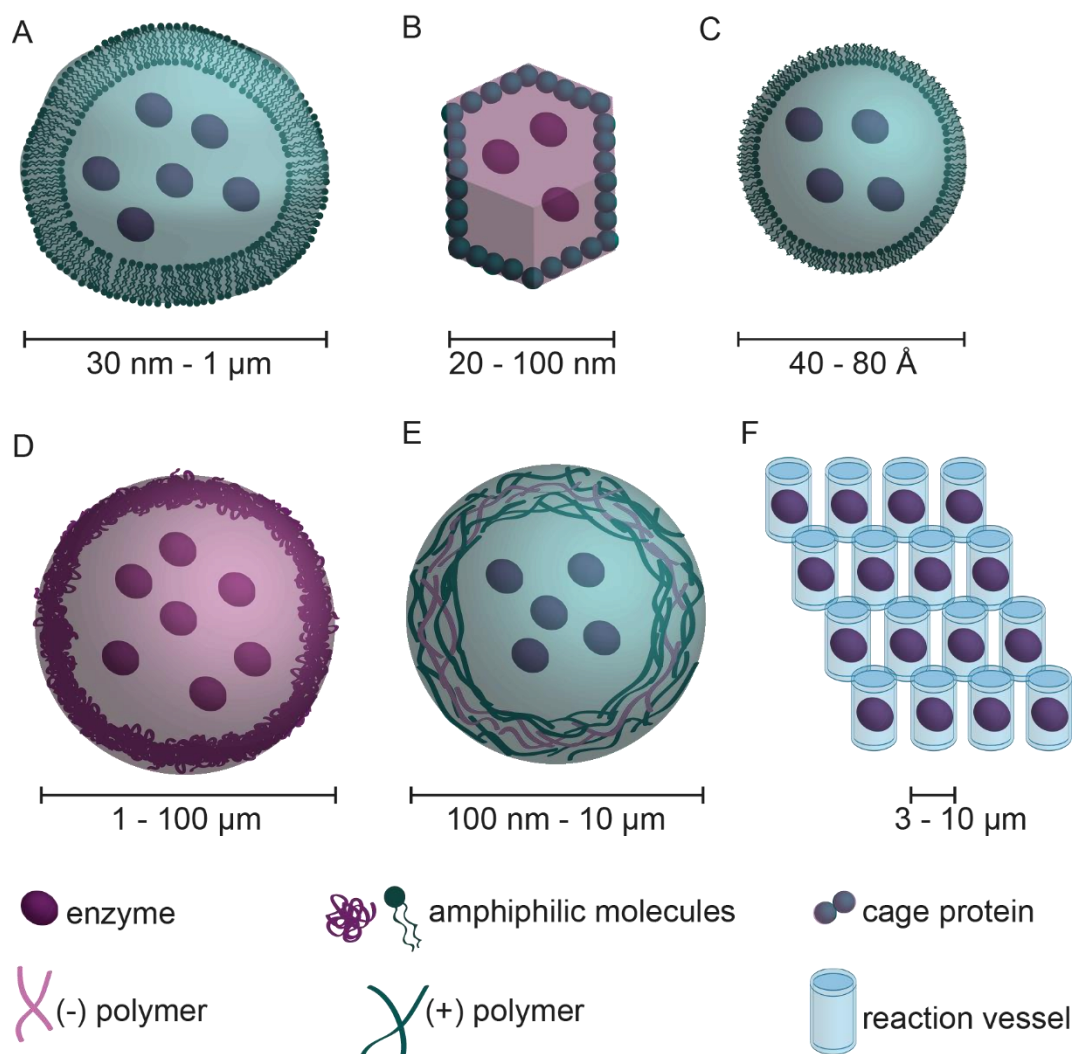


Figure 10: Schematic drawing of enzyme containers: liposome from an amphiphilic molecule e.g. (A) small unilamellar vesicle (diameter in tens of nanometer range) or polymerosome (diameter up to a few micrometers); (B) protein cage formed by proteinous boundaries e.g. virus capsid (diameter in the tens to hundreds nanometer range); (C) reverse micelle formed from an amphiphilic molecule e.g. phospholipid monolayer (diameter in tens of Ångström range); (D) semi-permeable capsule formed from amphiphilic molecules in a water-in-oil system e.g. spider silk as described in the following chapter (diameter varies between systems from several up to hundreds of micrometer); (E) polymer capsuled formed by a layer-by-layer approach after template removal, usually a positively and negatively charged polymer are used consecutively e.g. poly(styrene sulfonate) (-) in combination with poly(allylamine hydrochloride) (+) (diameter varies from hundreds of nanometer to several micrometer); (F) array of small reactions vessels obtained by e.g. chemical etching containing usually one enzyme only (vessel diameter are a few micrometers and height from several hundred nanometers to a few micrometers)

1.4.2 Silk in enzyme confinements

Matrices from silk fibroin were found to stabilize enzymes in liquid and solid form in terms of temperature, pH, electro dialysis, proteolysis, UV light, detergents and/or organic solvents. Mainly, bulk-loaded silk films were investigated, where silk and enzyme were simply mixed in liquid state and cast. This approach was often applied in the field of biosensors using redox enzymes. Hereby, an electrode was coated with a silk film containing the desired enzyme e.g. GOX, to monitor the amount of the substrate in a given analyte e.g. glucose level in blood.²⁵⁵ Further, porous silk fibroin membranes, sponges, microparticles, powders, fibers, woven fabrics and mats and even inks²⁵⁶ were prepared. These *B. mori* silk scaffolds were either kept as they are, if a water-soluble system was required or rendered water insoluble by either alcohol treatment, water annealing, glutaraldehyde crosslinking or physical treatment. Several studies dealt with HRP and GOX but also other enzymes like lipase, cholesterol oxidase, tyrosinase, ribonuclease, alkaline phosphatase, uricase, L-asparaginase, heme proteins, phenylalanine ammonia-lyase, invertase, organophosphorus hydrolase and β -glucosidase were examined for industrial, diagnostic, medical and biosensor applications. Especially in terms of biosensors, the matrix permeability plays a crucial role and could be controlled via the secondary structure i.e. β -sheet content or addition of porogens e.g. PEG.²⁵⁷ All these systems have in common, that the enzymes are encapsulated within the silk network. The glassy dynamics suppresses enzyme's mobility via β -relaxation processes, which prevents unfolding and mass transport of reactive species that would be necessary for degradation.²⁵⁸ Hence, a long storage life can be provided as well as a greater reusability.²⁵⁷

In order to protect biologicals in solution, layer-by-layer silk fibroin capsules were used as a cage. Here two strategies were investigated: (I) pre-loading strategy, where a porous template like silica was loaded with the biological and after silk capsule formation, the core was removed²⁵⁹ and (II) post-loading strategy, where layer-by-layer microcapsule was formed from silk fibroin modified with either poly(lysine) (+) or poly(glutamic acid) (-), which allowed pH triggered permeability that could be used for encapsulation and release of the biosensing system²⁶⁰. Another approach used spider silk capsules for enzyme entrapment. Hereby, the amphiphilic silk protein self-assembled at an oil/water interface, thereby forming a nanometer-thin film, which was either immediately water insoluble, when toluene was used^{261, 262} or had to be post-treated in an ethanol/water bath, when silicon oil was used as an organic phase. This film protected the encapsulated β -galactosidase even against proteases, whereby the substrates as well as the products could diffuse freely. Additionally, α -complementation was used to control the activation of β -galactosidase. Therefore, the inactive enzyme precursor EA22 was encapsulated. Then the peptide ED28 could be added to the surrounding medium, which was able to diffuse through the capsule wall to activate the enzyme by

inducing dimerization.¹¹¹ In another approach using recombinant spider silk esterase-2 was genetically coupled to the silk protein. This modified silk protein could then be self-assembled into nanofibrils or particles, retaining enzyme activity.²⁶³

2 Aim of the work

Silk is a promising material for biomedical applications. Within this work the suitability of engineered *Araneus diadematus* fibroin 4 (eADF4(C16)) and variants thereof was investigated for use in the field of biomedical engineering.

The first study aimed the development of an all aqueous electrospinning process for spider silk proteins. The morphology, secondary structure content and thermal behavior of the resulting nonwoven silk mat should be characterized and compared to nonwoven mats produced by previously established methods. Further, a model for a sensitive bioactive compound should be incorporated to investigate the ability of the process to preserve the molecules activity.

The aim of the second study was to expand the bactericidal effect of selenium nanoparticles towards gram-negative bacteria. This should be realized by applying a silk coating. The morphology of coated nanoparticles as well as the secondary structure content of the silk coating should be characterized. The coated particles should be tested for their effect against gram-negative bacteria and on eukaryotic cells.

The aim of the third study was to determine the potential of eADF4(κ 16) films for heart muscle regeneration. The films should be characterized in terms of secondary structure content and water contact angle. Then cardiac cell response to these films should be investigated applying different conditions in order to determine their ability to attach, communicate, contract and their reaction to external stimuli.

The fourth study aimed the characterization and development of a tubular structure for use as a nerve guidance conduit (NGC) in nerve regeneration. In order to assist re-growing peripheral nerves, it is beneficial, if the inside of the tube wall as well as its filling is adjustable. Therefore, a biodegradable self-rolling tubular structure should be developed, which allows for modifications of the inside tube wall with different silk types and morphologies as well as the addition of filler material. After optimization the tubes should undergo cell viability and differentiation studies to determine, if the designed NGC is able to guide neural outgrowths.

The aim of the fifth study was the optimization and characterization of the beforementioned tubular structures for use as enzyme containers. The tubes should be analyzed in terms of swelling, chemical stability and molecular weight cut-off. The containers should be filled easily with various enzyme solutions and retain these enzymes inside, while still allowing the diffusion of their substrates, intermediates and products. The system should be established by using a single enzyme reaction. Later, an enzyme cascade should be mimicked by using two enzymes, each in a separate tube.

3 Synopsis

This dissertation entails five publications and one manuscript showing a variety of applications using spider silk scaffolds in the field of biomedical engineering. It starts with a review about the use of the biomaterial ‘recombinant silk proteins’ in biomedical applications. The four following papers investigate the usability of spider silk scaffolds in tissue engineering. Two papers study the addition of possible additives to silk scaffolds to introduce either a sensitive biological substance or an antibacterial substance. The next two papers deal with the use of spider silk scaffolds for *in vitro* cell seeding. 2D spider silk films were investigated for cardiac tissue engineering and self-rolling bilayer structures for nerve regeneration. The last paper moves towards *in vitro* diagnostic tools and investigates the self-rolling bilayers as an enzyme container. A schematic overview is given in Figure 11.

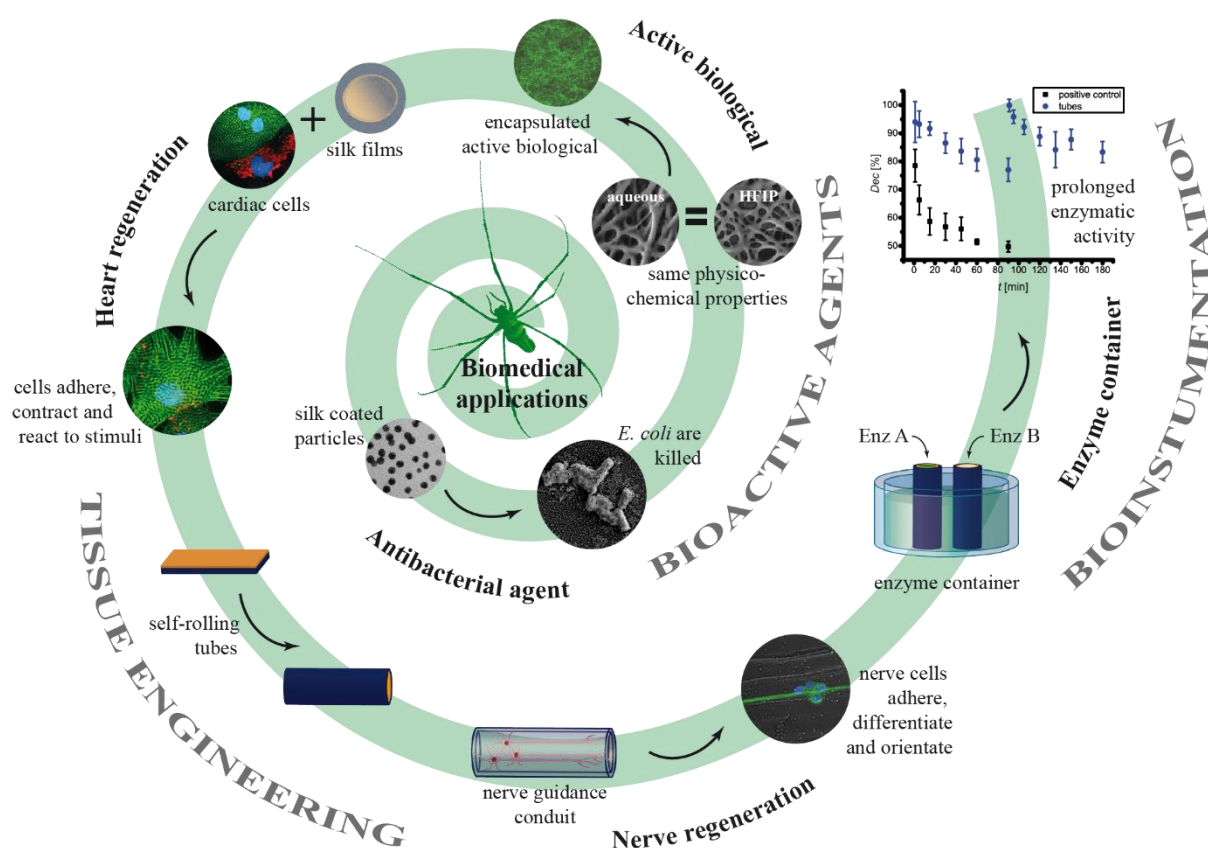


Figure 11: The dissertation starts in the middle of the spiral with a review about biomedical applications of recombinant silk proteins. The path goes on to silk with bioactive agents improving its usability in tissue engineering, namely active biological substances and antibacterial agents. Then the interaction of cells with spider silk scaffolds was investigated. Films underwent tests for heart muscle regeneration and self-rolling bilayers for nerve regeneration. These self-rolling bilayers were further analyzed for use as enzyme containers.

The first part of this dissertation is a review article (chapter 7, publication I, Biomedical Applications of Recombinant Silk-Based Materials). It provides a broad overview of the state of the art of recombinant silk-based materials in biomedical applications. Silk proteins have been transformed into various morphologies for use in regenerative medicine i.e. fibers, films, foams and hydrogels. Moreover, implant coatings seem a promising near-future application, whereas several drug delivery approaches using hydrogels, films, capsules and particles did not yet made the translation into clinics.

The second part is a publication (chapter 7, publication III, Aqueous electrospinning of recombinant spider silk proteins). A completely aqueous process for electrospinning and post-treatment of spider silk nonwoven mats was developed. The nonwoven mats were compared to conventional spun nonwoven mats in terms of morphology, secondary structure content and thermal behavior. The structural sensitive green fluorescent protein (GFP) and eADF4(C16) genetically modified with GFP were successfully encapsulated. Both kept their activity and the release could be studied.

The third part is a manuscript (chapter 7, manuscript I, Enhanced antibacterial activity of Se nanoparticles upon coating with recombinant spider silk protein eADF4(κ 16)) dealing with the coating of antibacterial selenium nanoparticles with eADF4(κ 16) to increase the nanoparticle's antibacterial effects against Gram-negative bacteria. The size, charge and coating of the nanoparticles was characterized, before their effect on eukaryotic and prokaryotic cells was investigated.

The fourth part consists of a publication (chapter 7, publication II, Surface Features of Recombinant Spider Silk Protein eADF4(κ 16)-Made Materials are Well-Suited for Cardiac Tissue Engineering) dealing with the interaction of cardiac cells on eADF4(κ 16) films. The water contact angle and the secondary structure content were determined. Then, cardiomyocytes were seeded and their response to the material under different external stimuli was examined to determine the materials suitability for cardiac TE.

The fifth part of this work is a paper (chapter 7, publication V, Nerve Guidance Conduit Design based on Self-rolling Tubes). It analyses the suitability of self-rolled tubular structures filled with a silk film, aligned silk nonwoven mats and an anisotropic collagen cryogel as a nerve guidance conduit. The mechanical properties of the materials, their morphology and the response of a nerve cell line were analyzed.

The sixth part is a publication (chapter 7, publication IV, Self-Rolling Refillable Tubular Enzyme Containers Made of Recombinant Spider Silk and Chitosan). Self-rolling tubular structures were prepared, the swelling degree, the stability towards aqueous and organic solvents (SEM + gravimetric analysis) and the molecular weight cut-off (photometric) were determined. Then one- or two-tubes systems were created allowing the addition of one/two enzymes and analyzing their reactions.

3.1 Scaffold with bioactive substance

Here, an all-aqueous process was developed to prepare electrospun nonwoven meshes for mild encapsulation of active biological substances. Therefore, an aqueous solution of the recombinant silk protein eADF4(C16) was prepared at a high concentration and mixed with PEO to obtain the desired viscosity for spinning. A standard nonwoven mat prepared from HFIP solution was used as control. For this electrospinning process the silk polymer solution was transferred into a syringe connected to a pump. The needle was conducted with the collector plate, so that the droplet at the needle forms a Taylor cone by applying a high voltage. From this Taylor cone a liquid jet was accelerated towards the collector plate. The solvent evaporated in air and whipping instabilities lead to a random deposition of spider silk nanofibers onto the collector.²⁶⁴ After the spinning process the samples were subjected to different post-treatment methods using ethanol vapor or water annealing at different temperatures. Analysis of the materials using Fourier transform infrared spectroscopy (FTIR) with subsequent Fourier self-deconvolution (FSD) for secondary structure determination, differential scanning calorimetry (DSC) as well as scanning electron microscopy (SEM, Figure 12) showed no difference in secondary structure content (35.9 ± 1.3 % in all aqueous system and 38.6 ± 1.2 % in all organic system), the successful removal of PEG with post-treatment and a slight melting of the nonwovens in all aqueous processes, respectively.

Green fluorescence protein (GFP) was used as a model for an active biological substance. It only fluoresces when its tertiary structure arranging the fluorophore is intact, allowing to easily analyze the destructive power of every step in the process. It could be shown that only an all aqueous system was able to retain its activity. GFP could be released from the nonwoven mat with a recovery rate of about 90 % within about 30 minutes. In order to avoid this burst release, a spider silk variant with genetically coupled GFP was incorporated into the nonwovens. This sample also showed a high activity after aqueous spinning and post-treatment, but no release of GFP was observed. Thus, the eADF4(C16) part of GFP-eADF4(C16) is fully integrated in the eADF4(C16) scaffold, whereby the structure of GFP was preserved. In future genetic modification of eADF4(C16) with different

signaling biologicals with an enzymatically cleavable linker could be imagined, enhancing the formation of new tissue.

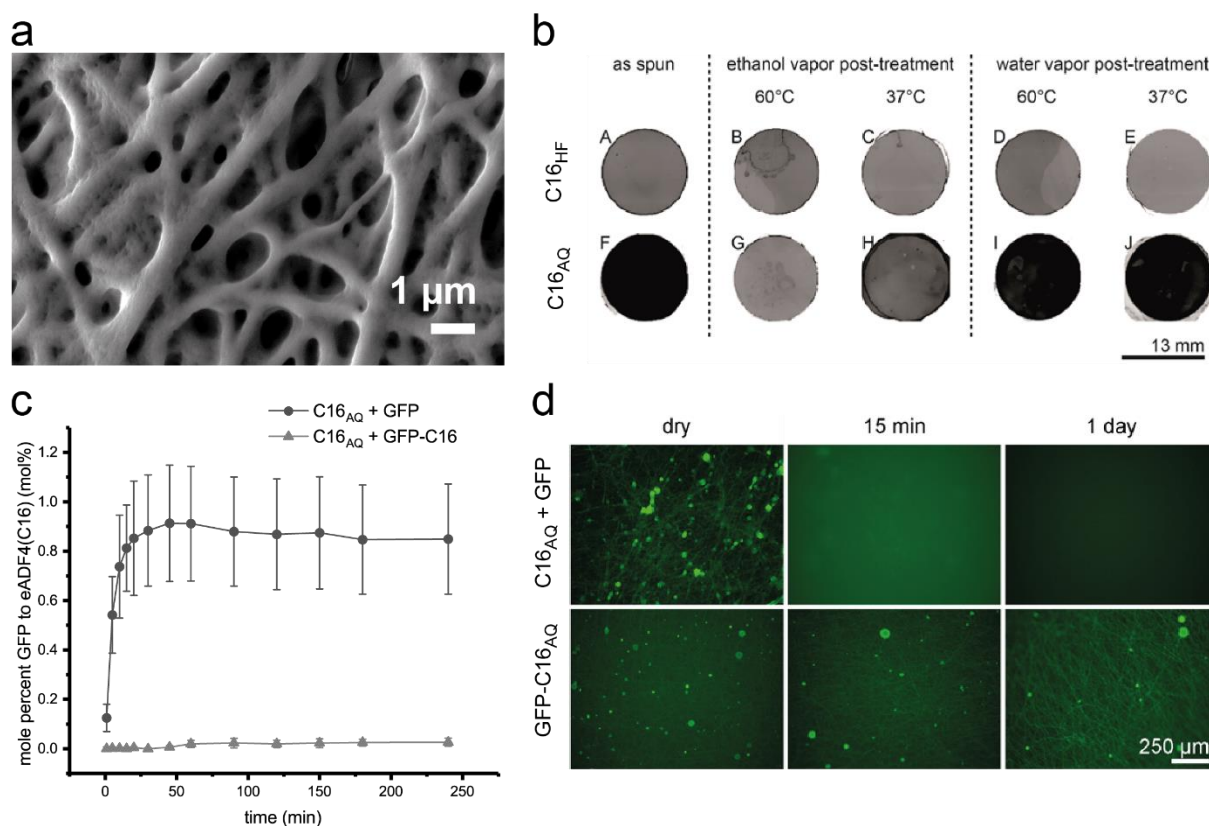


Figure 12: Electrospun nonwoven spider silk mat from aqueous solution with GFP. (a) SEM image of eADF4(C16) nonwoven mat spun from an aqueous solution and post-treated by water annealing at 37 °C. The fibers slightly melted together, but can still be clearly distinguished from each other. (b) Inverted fluorescence scanner images of eADF4(C16) nonwovens with GFP electrospun from HFIP or aqueous solution after different post-treatment procedures. GFP was only active in all aqueous processes. (c) Cumulative GFP release over time of unbound GFP (C16_{AQ} + GFP) as well as genetically coupled GFP (C16_{AQ} + GFP-C16) from eADF4(C16) nonwoven mats. The unbound GFP was released within 30 minutes, no release was observed from the genetically coupled GFP over 250 minutes. (d) Fluorescence microscope images of GFP release from unbound GFP (C16_{AQ} + GFP) as well as genetically coupled GFP (C16_{AQ} + GFP-C16). In the case of unbound GFP the picture was blurry already after 15 minutes proving a substantial release. After one day the GFP in the genetically coupled version was still active and clearly associated with the nonwoven mat. Reproduced (adapted) with permission.²⁶⁵ Copyright 2019, Elsevier GmbH.

3.2 Particles as antibacterial agent

This study was performed to extend the scope of selenium nanoparticles (NPs) showing antibacterial properties against gram-positive bacteria towards gram-negative bacteria by applying a spider silk coating. The NPs were coated by mixing them into an aqueous eADF4(κ 16) solution and subsequent washing (Figure 13). As a control, the NPs were coated with poly(vinyl alcohol) (PVA) in a similar fashion. TEM imaging proved a quite homogeneous size distribution of about 46 nm in both cases. Energy dispersive spectroscopy (EDS) analysis as well as FTIR measurements proved the presence of silk. Further FSD analysis of the FTIR data proved to be in the desired β -sheet rich secondary silk structure with 40.7 ± 0.8 %. The zeta potential of the NPs was determined to be positive in case of the silk coating (46.0 ± 0.6 mV) and slightly negative in case of the PVA coating (-7.3 ± 0.1 mV).

Antibacterial tests using *E. coli* as a model for gram-negative bacteria showed, that the minimum bactericidal concentration of the silk coated NPs was 50 times lower than the that of the PVA coated NPs. The morphologies of *E. coli* after treatment determined by SEM explained this effect. The negatively charged cell wall of *E. coli* seemed to repel the negatively charged PVA NPs, whereby the silk coated NPs were attached to the bacterial cell wall. The silk coated NPs were further incorporated into eADF4(C16) and eADF4(κ 16) films to avoid aggregation in nutrient-rich medium. Only the particles in the positively charged eADF4(κ 16) film showed an antibacterial activity using colony forming units assay (Figure 13). This can presumably be attributed to the release of the silk coated NPs from the positive film due to electrostatic repulsion, which was confirmed by analyzing the supernatant with inductive coupled plasma-optical emission spectrometry (ICP-OES).

The viability of Balb/3T3 fibroblasts and HaCaT keratinocytes in the presence of the NPs was investigated. PVA coated NPs showed no negative effect on fibroblasts, whereby silk coated NPs showed cytotoxic effects at four times the bactericidal dose. A cytotoxic effect in HaCaT was observed in both cases at the same concentration. This concentration corresponds to eight times the bactericidal dose in silk coated NPs, but to one eighth of the bactericidal dose in PVA coated NPs. This study presents an alternative to antibiotics with the advantage, that up to now no prove was found, that bacteria can develop resistance against NPs. Especially hospitals are a hot spot for infections, so called healthcare associated infections with a considerable part of them being surgical-site infections.²⁶⁶ The silk coated NPs could be encapsulated in various scaffolds protecting the TE construct from bacterial infections avoiding after surgical complications.

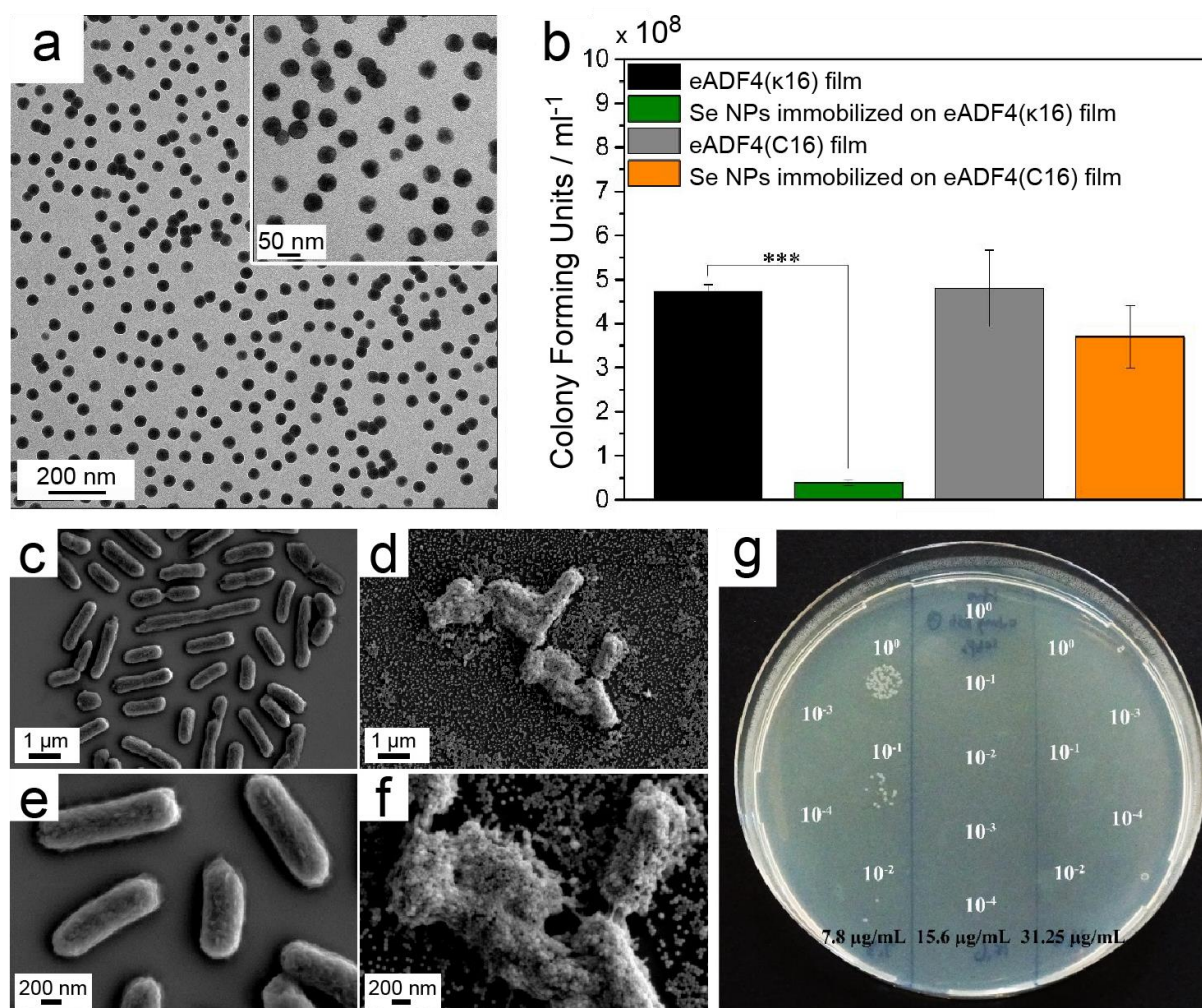


Figure 13: Spider silk coated Se NPs. (a) TEM images of eADF4(κ 16) coated Se NPs show a homogeneous size distribution. (b) Colony Forming unit (CFU) of *E. coli* of eADF4(κ 16) coated Se NPs encapsulated in eADF4(κ 16) and eADF4(C16) films compared to the films without NPs. Only the eADF4(κ 16) film with coated NPs reduced the CFU. (c-f) SEM images of *E. coli* without (c & e) and treated with (d & f) silk coated Se NPs clearly attacking the bacteria. (g) Agar plate of CFU tests with *E. coli* incubated with different amounts of silk coated Se NPs. At 15.6 μ g/ml no colonies were found at any *E. coli* concentration applied.

3.3 Heart muscle regeneration

The third study was devoted to heart muscle regeneration. The cellular behavior of primary cardiac cells from 3-days-old Sprague-Dawley rats on eADF4(κ 16) films was investigated and compared to fibronectin (positive control) and gelatin (neutral control) coating. The silk films were prepared by a dip-coating process. For the positively charged eADF4(κ 16), cleaned glass coverslips were dipped into an eADF4(κ 16) solution in formic acid and dried on parafilm to enable a complete coverage of the coverslips avoiding delamination during cell culture.

The films were characterized using water contact angle measurements and secondary structure determination via FTIR with FSD. The water contact angle of the eADF4(κ 16) film was $38 \pm 9^\circ$. Thus, the silk rendered glass more hydrophilic and lay in a similar range than gelatin ($29 \pm 7^\circ$). The β -sheet content is an important measure of crystallinity of the silk and hence, the physicochemical properties like water solubility. The β -sheet content commonly lies between 10 % and 45 % and mainly depends on the preparation method. A value below 20 % leads to water soluble structures (data not shown). The silk film possessed a β -sheet content of $33.6 \pm 0.6\%$, hence clearly above 20 % and was water-insoluble.

Cell studies showed that spider silk films are nontoxic and cardiomyocytes as well as endothelial cells and fibroblasts attached to them. On eADF4(κ 16) films cardiomyocytes adhered better than the other cell types investigated. This could be beneficial in artificial constructs, as compared to cardiomyocytes all other cell types are proliferating. Cardiomyocyte proliferation could be stimulated by the addition of fetal bovine serum (FBS) or fibroblast growth factor 1 (FGF1)/p38 inhibitor (p38i). An interesting feature of silk films was that they, in comparison with fibronectin, did not induce hypertrophy, which was only observed under the addition of stimulating factors like FBS or phenylephrine (PE). Hypertrophy is the increase of cell size and in the heart commonly induced by hormones like in pregnancy. Hypertrophy induced without stimulating factors can lead to pathological hypertrophy.²⁶⁷

In order to provide proper contractility, well-differentiated as well as aligned sarcomers are important, which could be seen on silk and fibronectin films. Contractility analysis demonstrated that cardiomyocytes beat with a comparable frequency and possessed a similar amplitude on silk and on fibronectin films. Cardiomyocytes on eADF4(κ 16) films were further analyzed in terms of cell-to-cell communication and electric coupling. Connexin 43 is a gap-junction protein associated with cell-to-cell communication and staining proved its presence in cardiomyocytes cultured on eADF4(κ 16) and fibronectin. Calcium homeostasis gives an important hint about electric coupling of cardiomyocytes, what is an important factor for proper host integration. Calcium imaging of eADF4(κ 16) and fibronectin films showed excitation waves going through the samples with a comparable rate and amplitude. (Figure 14)

Spider silk films proved to be non-toxic, showed no pharmacological effect and cardiomyocytes grown on these films exhibited proper excitation propagation and responded properly to extracellular stimuli. Future tests should aim at testing these primary cells in 3D environment like encapsulated in hydrogels, a morphology that cannot be formed with fibronectin. Moreover, stem cell behavior on silk materials could be investigated, before first *in vivo* studies are planned. The addition of the beforementioned additives could further increase the success of silk

scaffolds in cardiac regeneration. Another possible route for such tissue mimicking materials is drug screening, which could allow a reduction of patients in clinical studies.

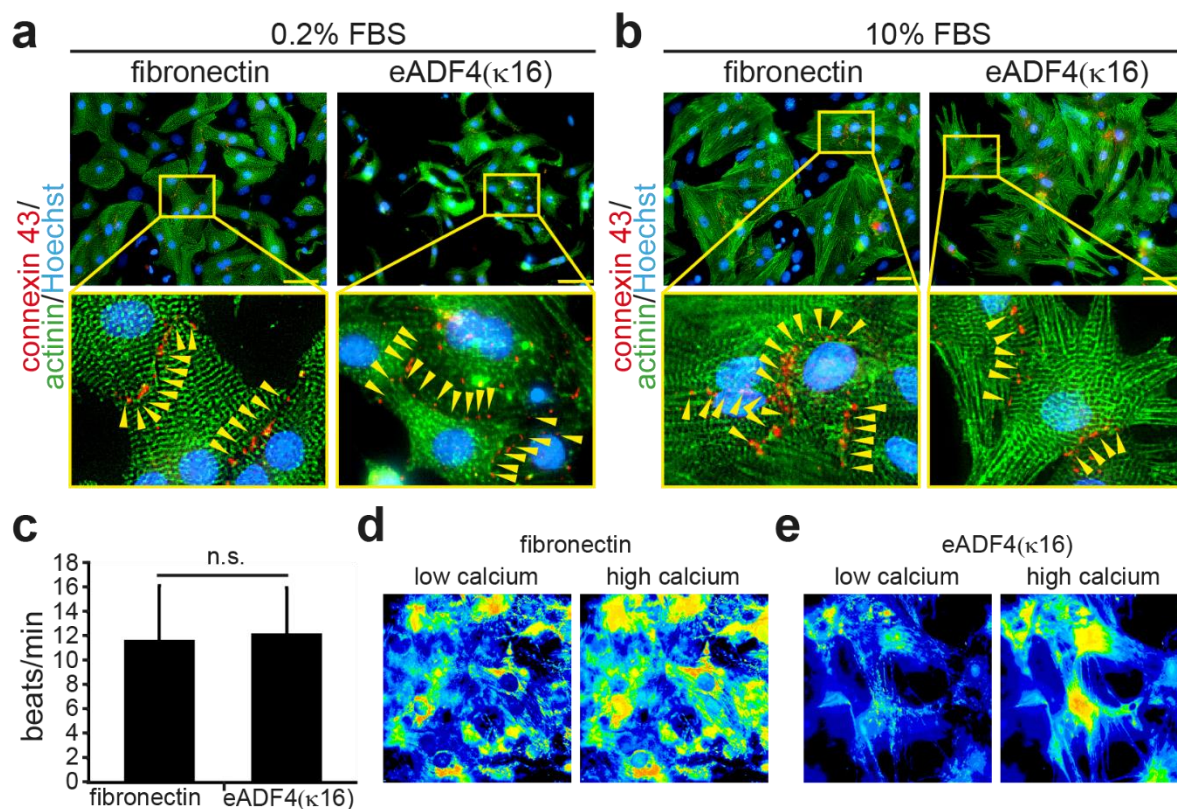


Figure 14: Cardiomyocytes cultured on eADF4(κ 16) and fibronectin films. (a, b) Cardiac cells seeded on eADF4(κ 16) and fibronectin films with 0.2 % (a) and 10 % (b) stimulation with fetal bovine serum (FBS). The cells were stained for sarcomeric- α -actinin (green), showing well-differentiated sarcomeres, whose alignment is beneficial in contraction. The staining of the gap junction protein connexin-43 (red) proposes cell-to-cell communication (yellow arrows) and nuclei were stained with Hoechst (blue). Fibronectin induces hypertrophy, therefore, the cells look similar in size in low and high FBS, whereby the silk allowed for stimulation of hypertrophy upon the addition of stimulating factors like FBS. Thus, the cells showed an increase in size in the high FBS compared to low FBS concentrations. (c) Beats per minute were comparable in both samples. (d, e) Calcium imaging records the change in calcium concentration in cardiac cells during contraction. The number of contractions as well as the frequency thereof was the same on both materials. Reproduced (adapted) with permission.²⁶⁸ Copyright 2017, WILEY-VCH Verlag GmbH & Co.

3.4 Nerve regeneration

An adaptable tubular system for use as nerve guidance conduit (NGC) made of biodegradable self-rolling tubes was developed. The self-rolling mechanism allows to not only modify the inner surface, but in addition provides a gentle way to encapsulate sensitive substances. Here, this advantage was taken to line chitosan tubes with an eADF4(C16)-RGD film or aligned eADF4(C16) fibers-mat and to encapsulate anisotropic cryogels. The PC-12 nerve cell line was gently encapsulated by the rolling process and allowed to grow and differentiate in these three different types of tubes (Figure 15).

The tubes lined with an eADF4(C16)-RGD film were prepared by successive casting of the silk and chitosan. For the other two constructs a chitosan film was cast. The aligned eADF4(C16) fiber-mat was electrospun directly onto the chitosan film. The anisotropic collagen cryogel was simply applied on the film before rolling was induced. The self-rolling process was initiated by the addition of any aqueous solution and took a few seconds only. This simple preparation of these tubes did not require the addition of possible harmful crosslinkers.

An anisotropic collagen cryogel offers a longitudinal porous structure in which nerve cells are guided to the posterior end. The cryogel is produced by unidirectional cryogelation. Here, an acidic aqueous collagen solution was mixed with the crosslinker glutaraldehyde. Then the solution was transferred to an insulated tube and placed on top of a copper plate and put into a freezer. Ice crystals started to grow from the copper plate to the top of the tube. This caused the collagen and crosslinker solution to concentrate, enabling the reaction of the two materials. The ice crystals acted as a porogen, which could be removed by thawing and the excess of glutaraldehyde could be removed by washing with glycine, leaving a crosslinked collagen network with longitudinal-oriented structures (Figure 15).

Mechanical testing was performed and the tensile stress, maximum strain and Young's modulus of the moisturized chitosan film were determined to be 47 ± 17 MPa, 101 ± 24 % and 30 ± 13 MPa and of the moist collagen cryogels (longitudinal) 0.15 ± 0.035 MPa, 65 ± 11 % and 0.2 ± 0.055 MPa. Both materials showed long ranging linear elastic deformations. The chitosan film had a sharp rupture point, whereby the collagen cryogels illustrated a gradual deformation continuing up to 300 % strain. Worth to mention here, the mechanical properties of the collagen cryogels were in the range of healthy peripheral nerves.¹⁹²

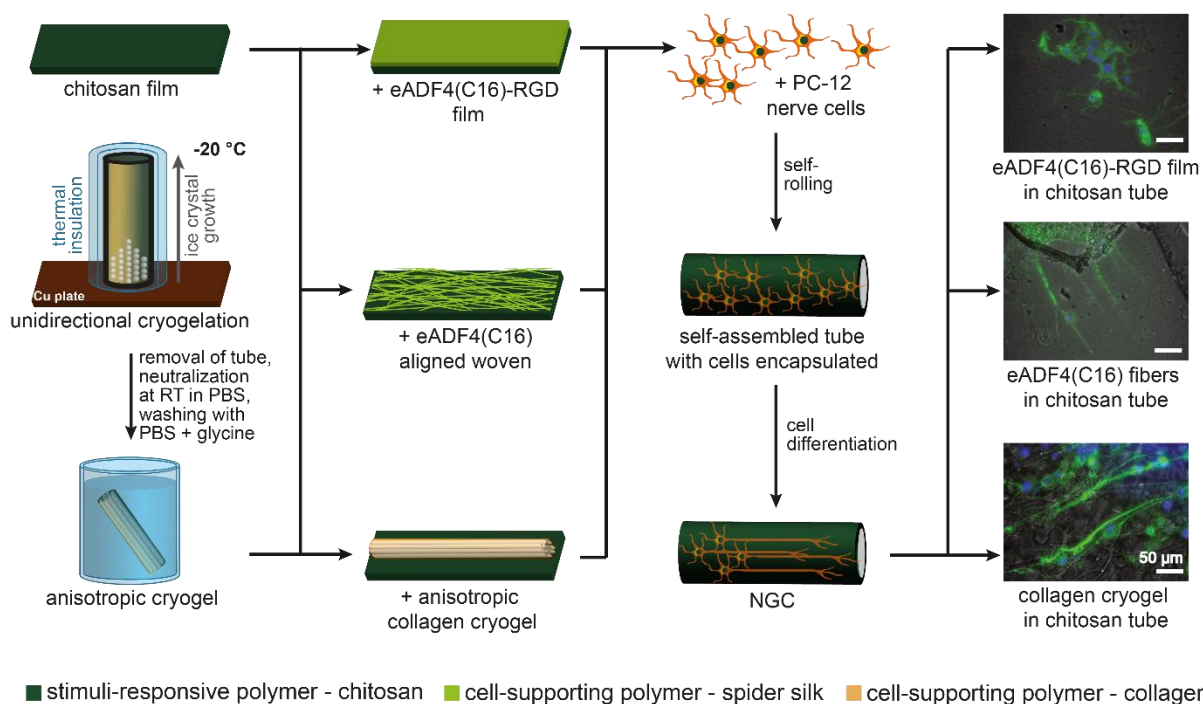


Figure 15: Nerve guidance conduit (NGC) preparation: Chitosan film is modified with either an eADF4(C16)-RGD film, an eADF4(C16) aligned nonwoven or with an anisotropic collagen cryogel. The cryogel is prepared using directional freezing combined with glutaraldehyde crosslinking. The tubes are allowed to roll in nerve cell suspension, thereby encapsulating the PC-12 cells. The cells are then differentiated in the tubes. The pictures on the right side show examples of immunostained PC-12 cells after differentiation in the respective NGCs – cells were stained for β -III tubulin, a microtubule forming protein, which is present in differentiated cells only (green) and nuclei with Hoechst (blue). Reproduced (adapted) with permission.²⁶⁹ Copyright 2020, Elsevier GmbH.

The interaction of PC-12 nerve cells was investigated on all materials used. The cells adhered and proliferated on eADF4(C16)-RGD films, eADF4(C16) nonwoven mats as well as on collagen cryogel. Then the differentiation potential was tested on these promising materials and it was found, that the cells could be differentiated directly on them. In a last step, NGCs were prepared by allowing the tubes to self-roll in a PC-12 cell suspension for encapsulation. In the case of the cryogel, the cell suspension was soaked up and then chitosan was allowed to roll around it. Cells were able to attach to the provided inner surface and differentiate upon the addition of differentiation media. Neurite like outgrowths were formed, which could be detected by immunostaining. It could further be shown, that the neurites accepted the internal structure, as they grew in all directions in the case of eADF4(C16)-RGD films but followed the structure of aligned eADF4(C16) nonwovens or anisotropic collagen cryogels (Figure 15). Surprisingly, the outgrowths in collagen cryogels formed even bundle like structures.

For future experiments one could imagine testing of primary or stem cells or even first *in vivo* tests, bridging artificial nerve defects like sciatic nerve in rats. Also adding the beforementioned additives could help improving the performance of the NGCs. Especially a gradual addition of nerve growth factor could trigger the outgrowth of the axons at the proximal stump into the NGC.

3.5 Enzyme containers

Self-rolling tubular structures can be further applied as enzyme containers using a bilayer made of recombinant spider silk protein eADF4(C16) and chitosan. Silk films showed only little swelling by AFM analysis (9.9 ± 8.3 %), whereas chitosan absorbed 250 ± 20 % of its dry weight in water. The tubes were prepared by allowing the bilayer to roll around a needle in PBS for five seconds. After drying, the needle was removed, and a stable tube was obtained. The dimension of the container could be adjusted by e.g. using needles with various diameters. The tubes were shown to be stable in biologically relevant organic solvents and in aqueous buffers with pH ranging from 3 to 11. Scanning electron microscopy (SEM) showed no delamination of the layers upon rolling.

The tubes were glued into tissue culture plates to create biodegradable containers for one-pot enzymes reactions. The enzymes could be pipetted inside of the tubes, hence neither genetical modification nor immobilization on solid carriers was required avoiding hampered enzyme activity. With a molecular weight cut-off above 20,000 g/mol the semi-permeable tube wall retained the enzymes inside of the tube and allowed substrates and/or products to diffuse. Thus, the surrounding reaction media could be exchanged, or the product harvested, without the need to change or remove the often costly enzyme. The suitability of the system was shown with esterase-2 using *p*-nitrophenyl acetate as a substrate. Therefore, the tube was loaded with enzyme solution and the reaction mixture was added to the surrounding. Product was detected in the surrounding medium, thus, the substrate was able to diffuse in and the product to diffuse out of the tube. The reaction rate and enzyme activity were lower than in the positive control (free enzyme in solution) presumably due to the required double diffusion.

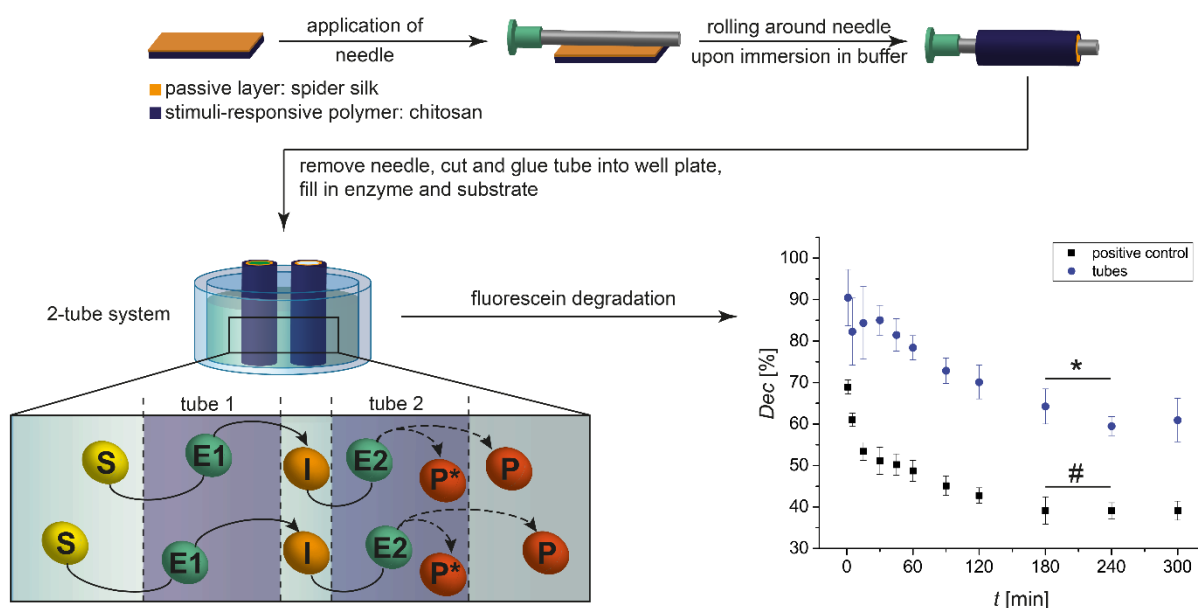


Figure 16: Two-tube system. A stimuli responsive bilayer made of chitosan (active polymer) and eADF4(C16) (passive polymer) was allowed to roll around a needle in PBS. After drying, the needle was removed, the tube cut to desired length and two of these tubes glued into one well of a tissue culture well plate. Each tube was then filled with an enzyme (E1 and E2) and the solution containing the substrate (S) for E1 was added to the surrounding. This substrate then diffused into tube 1, where it reacted with E1 forming an intermediate = substrate (I) for E2. In tube 2 I was then converted by E2 into the product, which then either stayed in the tube or diffused outside. Exemplarily a graph of c-fluorescein degradation by glucose oxidase (GOX) and horseradish peroxidase (HRP) is shown. The positive control showed a faster degradation than in the two-tube system, probably due to the diffusion time. But the reaction stopped after 180 min in the positive control, whereby the degradation continued up to 240 min in the two-tube system (* significantly different, # not significantly different, t-test: $p < 0.05$). Reproduced (adapted) with permission.²⁷⁰ Copyright 2019, ACS Publications.

Further, an enzyme cascade was mimicked using a two-tube system with the coupled reaction of glucose oxidase (GOX) and horseradish peroxidase (HRP) using either 2,2'-azino-bis(3-ethylbenzothiazoline-6-sulphonic acid) (ABTS) or carboxy-fluorescein as a substrate (Figure 16). In the case of ABTS, the product was captured inside of the HRP-tube. Thus, the substrate and intermediate were able to diffuse through the tube walls, but the product was hindered. The product is a radical cation and therefore, is prone to react with or stick to the tube. Such a system could be beneficial, if such species should be removed from a solution. Carboxy-fluorescein was successfully degraded by GOX and HRP in the two-tube system. Due to the necessity of diffusion of substrates, intermediates and products, the reaction rate was slowed down as already observed in the one-tube system. Nevertheless, the two-tube system enabled a longer reaction time than the control (240 min

vs. 180 min), presumably due to protection of the enzyme from H₂O₂. Furthermore, the surrounding media could be exchanged without decrease in enzyme activity. This system could be imagined as a biological recognition element of a biosensor. Moreover, cells could be encapsulated to analyze their metabolic products in changeable environments.

4 Literature

1. Kligour, F. G., *Modern Medicine in Historical Perspective*. Yale Medical Library: New Haven, Connecticut, USA, 1962; p 15.
2. BMES, BMES - FAQs about BME. <http://www.bmes.org/content.asp?contentid=140> (accessed 08, 2017).
3. Rodgers, M. M.; Pai, V. M.; Conroy, R. S., Recent Advances in Wearable Sensors for Health Monitoring. *Ieee Sens J* **2015**, *15* (6), 3119-3126.
4. NIH Pacemaker,. <https://www.nhlbi.nih.gov/health-topics/pacemakers> (accessed 03, 2019).
5. Quintana, J. M.; Arostegui, I.; Escobar, A.; Azkarate, J.; Goenaga, J. I.; Lafuente, I., Prevalence of knee and hip osteoarthritis and the appropriateness of joint replacement in an older population. *Arch Intern Med* **2008**, *168* (14), 1576-1584.
6. Mozaffarian, D.; Benjamin, E. J.; Go, A. S.; Arnett, D. K.; Blaha, M. J.; Cushman, M.; Das, S. R.; de Ferranti, S.; Despres, J. P.; Fullerton, H. J.; Howard, V. J.; Huffman, M. D.; Isasi, C. R.; Jimenez, M. C.; Judd, S. E.; Kissela, B. M.; Lichtman, J. H.; Lisabeth, L. D.; Liu, S. M.; Mackey, R. H.; Magid, D. J.; McGuire, D. K.; Mohler, E. R.; Moy, C. S.; Muntner, P.; Mussolino, M. E.; Nasir, K.; Neumar, R. W.; Nichol, G.; Palaniappan, L.; Pandey, D. K.; Reeves, M. J.; Rodriguez, C. J.; Rosamond, W.; Sorlie, P. D.; Stein, J.; Towfighi, A.; Turan, T. N.; Virani, S. S.; Woo, D.; Yeh, R. W.; Turner, M. B.; Comm, A. H. A. S.; Subcomm, S. S., Heart Disease and Stroke Statistics-2016 Update A Report From the American Heart Association. *Circulation* **2016**, *133* (4), E38-E360.
7. Lysaght, M. J.; O'Loughlin, J. A., Demographic scope and economic magnitude of contemporary organ replacement therapies. *Asaio J* **2000**, *46* (5), 515-21.
8. Alzheimer's association, *2016 Alzheimer's Disease Facts and Figures*. Chicago, Washington, **2016**.
9. Laurencin, C. T.; Ambrosio, A. M. A.; Borden, M. D.; Cooper, J. A., Tissue engineering: Orthopedic applications. *Annu Rev Biomed Eng* **1999**, *1*, 19-46.
10. Moroni, L.; Burdick, J. A.; Highley, C.; Lee, S. J.; Morimoto, Y.; Takeuchi, S.; Yoo, J. J., Biofabrication strategies for 3D in vitro models and regenerative medicine. *Nat Rev Mater* **2018**, *3* (5), 21-37.
11. Warburton, D., Stem Cells, Tissue Engineering and Regenerative Medicine. In *Stem Cells, Tissue Engineering and Regenerative Medicine*, Warburton, D., Ed. World Scientific Publishing Co. Pte. Ltd.: Singapore, Singapore, **2015**.
12. HELI – Health and Environment Linkages Initiative. <http://www.who.int/heli/en/> (accessed 03, 2019).
13. NIH, Clinical Applications of Biomaterials *NIH Consens Statement Online* **1982**, *4* (5), 19.
14. Long, M.; Rack, H. J., Titanium alloys in total joint replacement—a materials science perspective. *Biomaterials* **1998**, *19* (18), 1621-1639.
15. Dorozhkin, S. V., Biphasic, triphasic and multiphasic calcium orthophosphates. *Acta Biomater* **2012**, *8* (3), 963-977.
16. Mayet, N.; Choonara, Y. E.; Kumar, P.; Tomar, L. K.; Tyagi, C.; Du Toit, L. C.; Pillay, V., A Comprehensive Review of Advanced Biopolymeric Wound Healing Systems. *J Pharm Sci-US* **2014**, *103* (8), 2211-2230.
17. Langer, R.; Vacanti, J. P., Tissue Engineering. *Science* **1993**, *260* (5110), 920-926.
18. Naderi, H.; Matin, M. M.; Bahrami, A. R., Review paper: Critical Issues in Tissue Engineering: Biomaterials, Cell Sources, Angiogenesis, and Drug Delivery Systems. *J Biomater Appl* **2011**, *26* (4), 383-417.
19. Vert, M.; Mauduit, J.; Li, S. M., Biodegradation of Pla/Ga Polymers - Increasing Complexity. *Biomaterials* **1994**, *15* (15), 1209-1213.
20. Wang, Y.; Ameer, G. A.; Sheppard, B. J.; Langer, R., A tough biodegradable elastomer. *Nat Biotechnol* **2002**, *20* (6), 602-6.

21. Rothmund, S.; Aigner, T. B.; Iturmendi, A.; Rigau, M.; Husar, B.; Hildner, F.; Oberbauer, E.; Prambauer, M.; Olawale, G.; Forstner, R.; Liska, R.; Schroder, K. R.; Bruggemann, O.; Teasdale, I., Degradable Glycine-Based Photo-Polymerizable Polyphosphazenes for Use as Scaffolds for Tissue Regeneration. *Macromolecular Bioscience* **2015**, *15* (3), 351-363.
22. Pankov, R.; Yamada, K. M., Fibronectin at a glance. **2002**, *115* (20), 3861-3863.
23. Ellansé Ellansé. <https://ellanse.com/de/physician-landing/> (accessed 03, 2019).
24. Lotfi, M.; Ghasemi, N.; Rahimi, S.; Vosoughhosseini, S.; Saghiri, M. A.; Shahidi, A., Resilon: a comprehensive literature review. *J Dent Res Dent Clin Dent Prospects* **2013**, *7* (3), 119-30.
25. Johnson & Johnson Medical GmbH STRATAFIX SPIRAL Selbstsichernde Nahtsysteme. <http://de.ethicon.com/healthcare-professionals/Unsere-Produkte/Nahtmaterial/Spezialit%C3%A4ten/STRATAFIX-SPIRAL> (accessed 03, 2019).
26. Auras, R.; Lim, L.-T.; Selke, S. E. M.; Tsuji, H., *Poly(Lactic Acid): Synthesis, Structures, Properties, Processing, and Applications*. Wiley, New Jersey, USA: **2010**.
27. Berg, J. M.; Tymoczko, J. L.; Gatto Jr., G. J.; Stryer, L., *Stryer Biochemie*. 8. Edition ed.; Springer Spektrum: Berlin, Germany, **2018**.
28. Agrawal, P.; Soni, S.; Mittal, G.; Bhatnagar, A., Role of Polymeric Biomaterials as Wound Healing Agents. *Int J Low Extr Wound* **2014**, *13* (3), 180-190.
29. Armentano, I.; Dottori, M.; Fortunati, E.; Mattioli, S.; Kenny, J. M., Biodegradable polymer matrix nanocomposites for tissue engineering: A review. *Polym Degrad Stabil* **2010**, *95* (11), 2126-2146.
30. Hersel, U.; Dahmen, C.; Kessler, H., RGD modified polymers: biomaterials for stimulated cell adhesion and beyond. *Biomaterials* **2003**, *24* (24), 4385-415.
31. Arem, A., Collagen modifications. *Clin Plast Surg* **1985**, *12* (2), 209-20.
32. Shi, C.; Zhu, Y.; Ran, X.; Wang, M.; Su, Y.; Cheng, T., Therapeutic potential of chitosan and its derivatives in regenerative medicine. *J Surg Res* **2006**, *133* (2), 185-92.
33. Angelini PharmaInc. BioPad™ Wound Dressing with Collagen. <http://angelini-us.com/biopad/> (accessed 03, 2019).
34. Maiden Biosciences Collagen for Advanced Wound Care. <https://maidenbio.com/products/> (accessed 03, 2019).
35. Kehoe, S.; Zhang, X. F.; Boyd, D., FDA approved guidance conduits and wraps for peripheral nerve injury: A review of materials and efficacy. *Injury* **2012**, *43* (5), 553-572.
36. Bon, M., A Discourse upon the Usefulness of Silk of Spiders. *Philos T R Soc B* **1710**, *27*, 2-16.
37. Altman, G. H.; Diaz, F.; Jakuba, C.; Calabro, T.; Horan, R. L.; Chen, J. S.; Lu, H.; Richmond, J.; Kaplan, D. L., Silk-based biomaterials. *Biomaterials* **2003**, *24* (3), 401-416.
38. Santin, M.; Motta, A.; Freddi, G.; Cannas, M., In vitro evaluation of the inflammatory potential of the silk fibroin. *J Biomed Mater Res* **1999**, *46* (3), 382-389.
39. Craig, C. L., Evolution of arthropod silks. *Annu Rev Entomol* **1997**, *42*, 231-267.
40. van Beek, J. D.; Hess, S.; Vollrath, F.; Meier, B. H., The molecular structure of spider dragline silk: Folding and orientation of the protein backbone. *P Natl Acad Sci USA* **2002**, *99* (16), 10266-10271.
41. Gatesy, J.; Hayashi, C.; Motriuk, D.; Woods, J.; Lewis, R., Extreme diversity, conservation, and convergence of spider silk fibroin sequences. *Science* **2001**, *291* (5513), 2603-2605.
42. Sutherland, T. D.; Young, J. H.; Weisman, S.; Hayashi, C. Y.; Merritt, D. J., Insect Silk: One Name, Many Materials. *Annu Rev Entomol* **2010**, *55*, 171-188.
43. Foelix, R., *Biology of Spiders*. 3 ed.; Oxford University Press: Oxford, UK, 2011; p 432.
44. Vollrath, F.; Madsen, B.; Shao, Z. Z., The effect of spinning conditions on the mechanics of a spider's dragline silk. *P Roy Soc B-Biol Sci* **2001**, *268* (1483), 2339-2346.
45. Thamm, C.; Scheibel, T., Recombinant Production, Characterization, and Fiber Spinning of an Engineered Short Major Ampullate Spidroin (MaSp1s). *Biomacromolecules* **2017**, *18* (4), 1365-1372.

46. Simmons, A. H.; Michal, C. A.; Jelinski, L. W., Molecular orientation and two-component nature of the crystalline fraction of spider dragline silk. *Science* **1996**, *271* (5245), 84-87.
47. Anton, A. M.; Heidebrecht, A.; Mahmood, N.; Beiner, M.; Scheibel, T.; Kremer, F., Foundation of the Outstanding Toughness in Biomimetic and Natural Spider Silk. *Biomacromolecules* **2017**, *18* (12), 3954-3962.
48. Aamodt, J. M.; Grainger, D. W., Extracellular matrix-based biomaterial scaffolds and the host response. *Biomaterials* **2016**, *86*, 68-82.
49. Vollrath, F., Biology of spider silk. *Int J Biol Macromol* **1999**, *24* (2-3), 81-88.
50. Madsen, B.; Shao, Z. Z.; Vollrath, F., Variability in the mechanical properties of spider silks on three levels: interspecific, intraspecific and intraindividual. *Int J Biol Macromol* **1999**, *24* (2-3), 301-306.
51. Guehrs, K. H.; Schlott, B.; Grosse, F.; Weisshart, K., Environmental conditions impinge on dragline silk protein composition. *Insect Mol Biol* **2008**, *17* (5), 553-564.
52. Radtke, C.; Allmeling, C.; Waldmann, K. H.; Reimers, K.; Thies, K.; Schenk, H. C.; Hillmer, A.; Guggenheim, M.; Brandes, G.; Vogt, P. M., Spider Silk Constructs Enhance Axonal Regeneration and Remyelination in Long Nerve Defects in Sheep. *Plos One* **2011**, *6* (2), e16990.
53. Neuenfeldt, M.; Scheibel, T., Sequence Identification, Recombinant Production, and Analysis of the Self-Assembly of Egg Stalk Silk Proteins from Lacewing *Chrysoperla carnea*. *Biomolecules* **2017**, *7* (2), 43.
54. DeFrancesco, L., Hanging on a thread. *Nat Biotechnol* **2017**, *35* (6), 496-499.
55. Rosano, G. L.; Ceccarelli, E. A., Recombinant protein expression in *Escherichia coli*: advances and challenges. *Front Microbiol* **2014**, *5*, 172.
56. Kaplan, D. L.; Scheibel, T., *Recombinant Silk Production in Bacteria*. Elsevier Inc.: Amsterdam, Netherlands, **2017**.
57. Heidebrecht, A.; Scheibel, T., Recombinant Production of Spider Silk Proteins. In *Advances in Applied Microbiology*, Gadd, G.; Sariaslani, S., Eds. Elsevir Inc.: Amsterdam, Netherlands, **2013**; Vol. 82, pp 115-153.
58. Hedhammar, M.; Rising, A.; Grip, S.; Martinez, A. S.; Nordling, K.; Casals, C.; Stark, M.; Johansson, J., Structural properties of recombinant nonrepetitive and repetitive parts of major ampullate spidroin 1 from *Euprosthenops australis*: Implications for fiber formation. *Biochemistry-Us* **2008**, *47* (11), 3407-3417.
59. Stark, M.; Grip, S.; Rising, A.; Hedhammar, M.; Engstrom, W.; Hjalms, G.; Johansson, J., Macroscopic fibers self-assembled from recombinant miniature spider silk proteins. *Biomacromolecules* **2007**, *8* (5), 1695-1701.
60. Bini, E.; Foo, C. W. P.; Huang, J.; Karageorgiou, V.; Kitchel, B.; Kaplan, D. L., RGD-functionalized bioengineered spider dragline silk biomaterial. *Biomacromolecules* **2006**, *7* (11), 3139-3145.
61. Gomes, S. C.; Leonor, I. B.; Mano, J. F.; Reis, R. L.; Kaplan, D. L., Antimicrobial functionalized genetically engineered spider silk. *Biomaterials* **2011**, *32* (18), 4255-4266.
62. Dams-Kozłowska, H.; Majer, A.; Tomasiewicz, P.; Lozinska, J.; Kaplan, D. L.; Mackiewicz, A., Purification and cytotoxicity of tag-free bioengineered spider silk proteins. *J Biomed Mater Res A* **2013**, *101* (2), 456-464.
63. Moisenovich, M. M.; Pustovalova, O. L.; Arhipova, A. Y.; Vasiljeva, T. V.; Sokolova, O. S.; Bogush, V. G.; Debabov, V. G.; Sevastianov, V. I.; Kirpichnikov, M. P.; Agapov, I. I., In vitro and in vivo biocompatibility studies of a recombinant analogue of spidroin 1 scaffolds. *J Biomed Mater Res A* **2011**, *96A* (1), 125-131.
64. Teplenin, A.; Krasheninnikova, A.; Agladze, N.; Sidoruk, K.; Agapova, O.; Agapov, I.; Bogush, V.; Agladze, K., Functional Analysis of the Engineered Cardiac Tissue Grown on Recombinant Spidroin Fiber Meshes. *Plos One* **2015**, *10* (3), e0121155.
65. Agapov, I. I.; Pustovalova, O. L.; Moisenovich, M. M.; Bogush, V. G.; Sokolova, O. S.; Sevastyanov, V. I.; Debabov, V. G.; Kirpichnikov, M. P., Three-dimensional scaffold made from recombinant spider silk protein for tissue engineering. *Dokl Biochem Biophys* **2009**, *426* (1), 127-130.
66. Moisenovich, M. M.; Pustovalova, O.; Shackelford, J.; Vasiljeva, T. V.; Druzhinina, T. V.; Kamenchuk, Y. A.; Guzeev, V. V.; Sokolova, O. S.; Bogush, V. G.; Debabov, V. G.; Kirpichnikov, M. P.; Agapov, I. I., Tissue regeneration in vivo within recombinant spidroin 1 scaffolds. *Biomaterials* **2012**, *33* (15), 3887-3898.
67. Asakura, T.; Suzuki, Y.; Nagano, A.; Knight, D.; Kamiya, M.; Demura, M., Synthesis and characterization of water-soluble silk peptides and recombinant silk protein containing polyalanine, the integrin

binding site, and two glutamic acids at each terminal site as a possible candidate for use in bone repair materials. *Biomacromolecules* **2013**, *14* (10), 3731-41.

68. Weisman, S.; Haritos, V. S.; Church, J. S.; Huson, M. G.; Mudie, S. T.; Rodgers, A. J. W.; Dumsday, G. J.; Sutherland, T. D., Honeybee silk: Recombinant protein production, assembly and fiber spinning. *Biomaterials* **2010**, *31* (9), 2695-2700.

69. Wittmer, C. R.; Hu, X.; Gauthier, P. C.; Weisman, S.; Kaplan, D. L.; Sutherland, T. D., Production, structure and in vitro degradation of electrospun honeybee silk nanofibers. *Acta Biomater* **2011**, *7* (10), 3789-95.

70. Kambe, Y.; Kameda, T., Production and Cell Adhesion Activity of Recombinant Full-length Hornet Silk Protein Fused with RGDS Peptide. *The Journal of Silk Science and Technology of Japan* **2014**, *22*, 47-49.

71. Kambe, Y.; Sutherland, T. D.; Kameda, T., Recombinant production and film properties of full-length hornet silk proteins. *Acta Biomater* **2014**, *10* (8), 3590-3598.

72. Bauer, F.; Scheibel, T., Artificial Egg Stalks Made of a Recombinantly Produced Lacewing Silk Protein. *Angew Chem Int Edit* **2012**, *51* (26), 6521-6524.

73. Bauer, F.; Wohlrab, S.; Scheibel, T., Controllable cell adhesion, growth and orientation on layered silk protein films. *Biomater Sci-Uk* **2013**, *1* (12), 1244-1249.

74. Kambe, Y.; Yamamoto, K.; Kojima, K.; Tamada, Y.; Tomita, N., Effects of RGDS sequence genetically interfused in the silk fibroin light chain protein on chondrocyte adhesion and cartilage synthesis. *Biomaterials* **2010**, *31* (29), 7503-7511.

75. Inoue, S.; Tanaka, K.; Arisaka, F.; Kimura, S.; Ohtomo, K.; Mizuno, S., Silk fibroin of *Bombyx mori* is secreted, assembling a high molecular mass elementary unit consisting of H-chain, L-chain, and P25, with a 6 : 6 : 1 molar ratio. *J Biol Chem* **2000**, *275* (51), 40517-40528.

76. Cappello, J.; Crissman, J.; Dorman, M.; Mikolajczak, M.; Textor, G.; Marquet, M.; Ferrari, F., Genetic-Engineering of Structural Protein Polymers. *Biotechnol Progr* **1990**, *6* (3), 198-202.

77. Dandu, R.; Von Cresce, A.; Briber, R.; Dowell, P.; Cappello, J.; Ghandehari, H., Silk-elastinlike protein polymer hydrogels: Influence of monomer sequence on physicochemical properties. *Polymer* **2009**, *50* (2), 366-374.

78. Poursaid, A.; Price, R.; Tiede, A.; Olson, E.; Huo, E.; McGill, L.; Ghandehari, H.; Cappello, J., In situ gelling silk-elastinlike protein polymer for transarterial chemoembolization. *Biomaterials* **2015**, *57*, 142-152.

79. Nagano, A.; Tanioka, Y.; Sakurai, N.; Sezutsu, H.; Kuboyama, N.; Kiba, H.; Tanimoto, Y.; Nishiyama, N.; Asakura, T., Regeneration of the femoral epicondyle on calcium-binding silk scaffolds developed using transgenic silk fibroin produced by transgenic silkworm. *Acta Biomater* **2011**, *7* (3), 1192-1201.

80. Nagano, A.; Sato, H.; Tanioka, Y.; Nakazawa, Y.; Knight, D.; Asakura, T., Characterization of a Ca binding-amphiphathic silk-like protein and peptide with the sequence (Glu)(8)(Ala-Gly-Ser-Gly-Ala-Gly)(4) with potential for bone repair. *Soft Matter* **2012**, *8* (3), 741-748.

81. Huebnerich, D.; Helsen, C. W.; Quedzuweit, S.; Oschmann, J.; Rudolph, R.; Scheibel, T., Primary structure elements of spider dragline silks and their contribution to protein solubility. *Biochemistry-Uk* **2004**, *43* (42), 13604-13612.

82. Wohlrab, S.; Muller, S.; Schmidt, A.; Neubauer, S.; Kessler, H.; Leal-Egana, A.; Scheibel, T., Cell adhesion and proliferation on RGD-modified recombinant spider silk proteins. *Biomaterials* **2012**, *33* (28), 6650-6659.

83. Doblhofer, E.; Scheibel, T., Engineering of Recombinant Spider Silk Proteins Allows Defined Uptake and Release of Substances. *J Pharm Sci-Uk* **2015**, *104* (3), 988-994.

84. Aigner, T. B.; DeSimone, E.; Scheibel, T., Biomedical Applications of Recombinant Silk-Based Materials. *Adv Mater* **2018**, *30* (19), 1704636.

85. Widhe, M.; Johansson, U.; Hillerdahl, C. O.; Hedhammar, M., Recombinant spider silk with cell binding motifs for specific adherence of cells. *Biomaterials* **2013**, *34* (33), 8223-8234.

86. Saotome, T.; Hayashi, H.; Tanaka, R.; Kinugasa, A.; Uesugi, S.; Tatematsu, K.; Sezutsu, H.; Kuwabara, N.; Asakura, T., Introduction of VEGF or RGD sequences improves revascularization properties of *Bombyx mori* silk fibroin produced by transgenic silkworm. *J Mater Chem B* **2015**, *3* (35), 7109-7116.

87. Wu, S. Q.; Johansson, J.; Damdimopoulou, P.; Shahsavani, M.; Falk, A.; Hovatta, O.; Rising, A., Spider silk for xeno-free long-term self-renewal and differentiation of human pluripotent stem cells. *Biomaterials* **2014**, *35* (30), 8496-8502.
88. Johansson, U.; Ria, M.; Avall, K.; Shalaly, N. D.; Zaitsev, S. V.; Berggren, P. O.; Hedhammar, M., Pancreatic Islet Survival and Engraftment Is Promoted by Culture on Functionalized Spider Silk Matrices. *PLoS One* **2015**, *10* (6), e0130169.
89. Harvey, D.; Bardelang, P.; Goodacre, S. L.; Cockayne, A.; Thomas, N. R., Antibiotic Spider Silk: Site-Specific Functionalization of Recombinant Spider Silk Using "Click" Chemistry. *Adv Mater* **2017**, *29* (10).
90. Mieszawska, A. J.; Nadkarni, L. D.; Perry, C. C.; Kaplan, D. L., Nanoscale control of silica particle formation via silk-silica fusion proteins for bone regeneration. *Chemistry of materials : a publication of the American Chemical Society* **2010**, *22* (20), 5780-5785.
91. Gomes, S.; Gallego-Llamas, J.; Leonor, I. B.; Mano, J. F.; Reis, R. L.; Kaplan, D. L., Biological responses to spider silk-antibiotic fusion protein. *J Tissue Eng Regen M* **2012**, *6* (5), 356-368.
92. Zeplin, P. H.; Berninger, A. K.; Maksimovikj, N. C.; van Gelder, P.; Scheibel, T.; Walles, H., Improving the Biocompatibility of Silicone Implants Using Spider Silk Coatings: Immunohistochemical Analysis of Capsule Formation. *Handchir Mikrochir P* **2014**, *46* (6), 336-341.
93. Zeplin, P. H.; Maksimovikj, N. C.; Jordan, M. C.; Nickel, J.; Lang, G.; Leimer, A. H.; Roemer, L.; Scheibel, T., Spider Silk Coatings as a Bioshield to Reduce Periprosthetic Fibrous Capsule Formation. *Adv Funct Mater* **2014**, *24* (18), 2658-2666.
94. Harris, T. I.; Gaztambide, D. A.; Day, B. A.; Brock, C. L.; Ruben, A. L.; Jones, J. A.; Lewis, R. V., Sticky Situation: An Investigation of Robust Aqueous-Based Recombinant Spider Silk Protein Coatings and Adhesives. *Biomacromolecules* **2016**, *17* (11), 3761-3772.
95. Borkner, C. B.; Wohlrab, S.; Möller, E.; Lang, G.; Scheibel, T., Surface Modification of Polymeric Biomaterials Using Recombinant Spider Silk Proteins. *ACS Biomater. Sci. Eng.* **2017**, *3*, 767-775.
96. Heidebrecht, A.; Eisoldt, L.; Diehl, J.; Schmidt, A.; Geffers, M.; Lang, G.; Scheibel, T., Biomimetic Fibers Made of Recombinant Spidroins with the Same Toughness as Natural Spider Silk. *Adv Mater* **2015**, *27* (13), 2189-2194.
97. Andersson, M.; Jia, Q. P.; Abella, A.; Lee, X. Y.; Landreh, M.; Purhonen, P.; Hebert, H.; Tenje, M.; Robinson, C. V.; Meng, Q.; Plaza, G. R.; Johansson, J.; Rising, A., Biomimetic spinning of artificial spider silk from a chimeric minispidroin. *Nat Chem Biol* **2017**, *13* (3), 262-264.
98. Hedhammar, M.; Bramfeldt, H.; Baris, T.; Widhe, M.; Askarieh, G.; Nordling, K.; von Aulock, S.; Johansson, J., Sterilized Recombinant Spider Silk Fibers of Low Pyrogenicity. *Biomacromolecules* **2010**, *11* (4), 953-959.
99. Widhe, M.; Bysell, H.; Nystedt, S.; Schenning, I.; Malmsten, M.; Johansson, J.; Rising, A.; Hedhammar, M., Recombinant spider silk as matrices for cell culture. *Biomaterials* **2010**, *31* (36), 9575-9585.
100. Fredriksson, C.; Hedhammar, M.; Feinstein, R.; Nordling, K.; Kratz, G.; Johansson, J.; Huss, F.; Rising, A., Tissue Response to Subcutaneously Implanted Recombinant Spider Silk: An in Vivo Study. *Materials* **2009**, *2* (4), 1908-1922.
101. Nakazawa, Y.; Sato, M.; Takahashi, R.; Aytemiz, D.; Takabayashi, C.; Tamura, T.; Enomoto, S.; Sata, M.; Asakura, T., Development of Small-Diameter Vascular Grafts Based on Silk Fibroin Fibers from Bombyx mori for Vascular Regeneration. *J Biomat Sci-Polym E* **2011**, *22* (1-3), 195-206.
102. Asakura, T.; Isozaki, M.; Saotome, T.; Tatematsu, K. I.; Sezutsu, H.; Kuwabara, N.; Nakazawa, Y., Recombinant silk fibroin incorporated cell-adhesive sequences produced by transgenic silkworm as a possible candidate for use in vascular graft. *J Mater Chem B* **2014**, *2* (42), 7375-7383.
103. Leal-Egana, A.; Lang, G.; Mauerer, C.; Wickinghoff, J.; Weber, M.; Geimer, S.; Scheibel, T., Interactions of Fibroblasts with Different Morphologies Made of an Engineered Spider Silk Protein. *Adv Eng Mater* **2012**, *14* (3), B67-B75.
104. Zhu, B.; Li, W.; Lewis, R. V.; Segre, C. U.; Wang, R., E-spun composite fibers of collagen and dragline silk protein: fiber mechanics, biocompatibility, and application in stem cell differentiation. *Biomacromolecules* **2015**, *16* (1), 202-13.

105. Botchwey, E. A.; Dupree, M. A.; Pollack, S. R.; Levine, E. M.; Laurencin, C. T., Tissue engineered bone: Measurement of nutrient transport in three-dimensional matrices. *J Biomed Mater Res A* **2003**, *67A* (1), 357-367.
106. Schacht, K.; Vogt, J.; Scheibel, T., Foams Made of Engineered Recombinant Spider Silk Proteins as 3D Scaffolds for Cell Growth. *ACS Biomaterials Science & Engineering* **2016**, *2* (4), 517-525.
107. Wu, S.; Johansson, J.; Hovatta, O.; Rising, A., Efficient passage of human pluripotent stem cells on spider silk matrices under xeno-free conditions. *Cellular and molecular life sciences : CMLS* **2016**, *73* (7), 1479-88.
108. Shalaly, N. D.; Ria, M.; Johansson, U.; Avall, K.; Berggren, P. O.; Hedhammar, M., Silk matrices promote formation of insulin-secreting islet-like clusters. *Biomaterials* **2016**, *90*, 50-61.
109. Schacht, K.; Jüngst, T.; Schweinlin, M.; Ewald, A.; Groll, J.; Scheibel, T., Biofabrication of Cell-loaded, 3D Recombinant Spider Silk Constructs. *Angewandte Chemie* **2015**, *54* (9), 5, 2816-20.
110. DeSimone, E.; Schacht, K.; Pellert, A.; Scheibel, T., Recombinant spider silk-based bioinks. *Biofabrication* **2017**, *9* (4), 044104.
111. Blum, C.; Nichtl, A.; Scheibel, T., Spider Silk Capsules as Protective Reaction Containers for Enzymes. *Adv Funct Mater* **2014**, *24* (6), 763-768.
112. Lammel, A.; Schwab, M.; Slotta, U.; Winter, G.; Scheibel, T., Processing conditions for the formation of spider silk microspheres. *Chemsuschem* **2008**, *1* (5), 413-416.
113. Elsner, M. B.; Herold, H. M.; Muller-Herrmann, S.; Bargel, H.; Scheibel, T., Enhanced cellular uptake of engineered spider silk particles. *Biomater Sci-Uk* **2015**, *3* (3), 543-551.
114. Florczak, A.; Mackiewicz, A.; Dams-Kozłowska, H., Functionalized Spider Silk Spheres As Drug Carriers for Targeted Cancer Therapy. *Biomacromolecules* **2014**, *15* (8), 2971-2981.
115. Florczak, A.; Jastrzebska, K.; Mackiewicz, A.; Dams-Kozłowska, H., Blending two bioengineered spider silks to develop cancer targeting spheres. *J Mater Chem B* **2017**, *5* (16), 3000-3011.
116. Numata, K.; Reagan, M. R.; Goldstein, R. H.; Rosenblatt, M.; Kaplan, D. L., Spider Silk-Based Gene Carriers for Tumor Cell-Specific Delivery. *Bioconjugate Chem* **2011**, *22* (8), 1605-1610.
117. Gonzalez-Fernandez, T.; Sikorski, P.; Leach, J. K., Bio-instructive materials for musculoskeletal regeneration. *Acta Biomater* **2019**, *96*, 20-34.
118. Mironov, V.; Visconti, R. P.; Kasyanov, V.; Forgacs, G.; Drake, C. J.; Markwald, R. R., Organ printing: Tissue spheroids as building blocks. *Biomaterials* **2009**, *30* (12), 2164-2174.
119. Wang, L.; Hu, C.; Shao, L., The antimicrobial activity of nanoparticles: present situation and prospects for the future. *Int J Nanomed* **2017**, *12*, 1227-1249.
120. Lind, M., Growth factors: Possible new clinical tools: A review. *Acta Orthopaedica Scandinavica* **1996**, *67* (4), 407-417.
121. Caballero Aguilar, L. M.; Silva, S. M.; Moulton, S. E., Growth factor delivery: Defining the next generation platforms for tissue engineering. *J Control Release* **2019**, *306*, 40-58.
122. Hassanzadeh, P., Tissue engineering and growth factors: Updated evidence. *Biomedical Reviews* **2012**, *23*, 19.
123. Li, W. J.; Jiang, Y. J.; Tuan, R. S., Cell-nanofiber-based cartilage tissue engineering using improved cell seeding, growth factor, and bioreactor technologies. *Tissue Eng Part A* **2008**, *14* (5), 639-48.
124. Mitchell, A. C.; Briquez, P. S.; Hubbell, J. A.; Cochran, J. R., Engineering growth factors for regenerative medicine applications. *Acta Biomater* **2016**, *30*, 1-12.
125. Yan, C.; Pattani, V.; Tunnell, J. W.; Ren, P., Temperature-induced unfolding of epidermal growth factor (EGF): Insight from molecular dynamics simulation. *Journal of Molecular Graphics and Modelling* **2010**, *29* (1), 2-12.
126. Santana, H.; González, Y.; Campana, P. T.; Noda, J.; Amarantes, O.; Itri, R.; Beldarraín, A.; Páez, R., Screening for stability and compatibility conditions of recombinant human epidermal growth factor for parenteral formulation: Effect of pH, buffers, and excipients. *Int J Pharm* **2013**, *452* (1), 52-62.
127. Yancopoulos, G. D.; Davis, S.; Gale, N. W.; Rudge, J. S.; Wiegand, S. J.; Holash, J., Vascular-specific growth factors and blood vessel formation. *Nature* **2000**, *407* (6801), 242-8.

128. Zara, J. N.; Siu, R. K.; Zhang, X.; Shen, J.; Ngo, R.; Lee, M.; Li, W.; Chiang, M.; Chung, J.; Kwak, J.; Wu, B. M.; Ting, K.; Soo, C., High Doses of Bone Morphogenetic Protein 2 Induce Structurally Abnormal Bone and Inflammation In Vivo. *Tissue Eng Pt A* **2011**, *17* (9-10), 1389-1399.
129. Marchioli, G.; Luca, A. D.; de Koning, E.; Engelse, M.; Van Blitterswijk, C. A.; Karperien, M.; Van Apeldoorn, A. A.; Moroni, L., Hybrid Polycaprolactone/Alginate Scaffolds Functionalized with VEGF to Promote de Novo Vessel Formation for the Transplantation of Islets of Langerhans. **2016**, *5* (13), 1606-1616.
130. Azagarsamy, M. A.; Anseth, K. S., Wavelength-Controlled Photocleavage for the Orthogonal and Sequential Release of Multiple Proteins. *Angewandte Chemie International Edition* **2013**, *52* (51), 13803-13807.
131. Herran, E.; Requejo, C.; Ruiz-Ortega, J. A.; Aristieta, A.; Igartua, M.; Bengoetxea, H.; Ugedo, L.; Pedraz, J. L.; Lafuente, J. V.; Hernandez, R. M., Increased antiparkinson efficacy of the combined administration of VEGF- and GDNF-loaded nanospheres in a partial lesion model of Parkinson's disease. *Int J Nanomedicine* **2014**, *9*, 2677-87.
132. Delanois, R. E.; Mistry, J. B.; Gwam, C. U.; Mohamed, N. S.; Choksi, U. S.; Mont, M. A., Current Epidemiology of Revision Total Knee Arthroplasty in the United States. *J Arthroplasty* **2017**, *32* (9), 2663-2668.
133. Costerton, J. W.; Stewart, P. S.; Greenberg, E. P., Bacterial Biofilms: A Common Cause of Persistent Infections. *Science* **1999**, *284* (5418), 1318-22.
134. Xiong, M. H.; Bao, Y.; Yang, X. Z.; Zhu, Y. H.; Wang, J., Delivery of antibiotics with polymeric particles. *Adv Drug Deliv Rev* **2014**, *78*, 63-76.
135. Neoh, K. G.; Kang, E. T., Combating Bacterial Colonization on Metals via Polymer Coatings: Relevance to Marine and Medical Applications. *Acs Appl Mater Inter* **2011**, *3* (8), 2808-2819.
136. Mas-Moruno, C.; Su, B.; Dalby, M. J., Multifunctional Coatings and Nanotopographies: Toward Cell Instructive and Antibacterial Implants. *Adv Healthc Mater* **2019**, *8* (1), e1801103.
137. Kourai, H.; Yabuhara, T.; Shirai, A.; Maeda, T.; Nagamune, H., Syntheses and antimicrobial activity of a series of new bis-quaternary ammonium compounds. *Eur J Med Chem* **2006**, *41*, 437-44.
138. Tenover, F. C., Mechanisms of antimicrobial resistance in bacteria. *Am J Infect Control* **2006**, *34* (5, Supplement), S3-S10.
139. Kumar, M.; Curtis, A.; Hoskins, C., Application of Nanoparticle Technologies in the Combat against Anti-Microbial Resistance. *Pharmaceutics* **2018**, *10* (1), 11.
140. Annabi, N.; Rana, D.; Shirzaei Sani, E.; Portillo-Lara, R.; Gifford, J. L.; Fares, M. M.; Mithieux, S. M.; Weiss, A. S., Engineering a sprayable and elastic hydrogel adhesive with antimicrobial properties for wound healing. *Biomaterials* **2017**, *139*, 229-243.
141. Griffiths, G.; Nyström, B.; Sable, S. B.; Khuller, G. K., Nanobead-based interventions for the treatment and prevention of tuberculosis. *Nature Reviews Microbiology* **2010**, *8* (11), 827-834.
142. Mugabe, C.; Halwani, M.; Azghani, A. O.; Lafrenie, R. M.; Omri, A., Mechanism of Enhanced Activity of Liposome-Entrapped Aminoglycosides against Resistant Strains of *Pseudomonas aeruginosa*. *Antimicrob Agents Ch* **2006**, *50* (6), 2016.
143. Chakraborty, S. P.; Sahu, S. K.; Pramanik, P.; Roy, S., In vitro antimicrobial activity of nanoconjugated vancomycin against drug resistant *Staphylococcus aureus*. *Int J Pharm* **2012**, *436* (1), 659-676.
144. Saha, S.; Kundu, B.; Kirkham, J.; Wood, D.; Kundu, S. C.; Yang, X. B., Osteochondral tissue engineering in vivo: a comparative study using layered silk fibroin scaffolds from mulberry and nonmulberry silkworms. *Plos One* **2013**, *8* (11), e80004.
145. Uebersax, L.; Mattotti, M.; Papaloizos, M.; Merkle, H. P.; Gander, B.; Meinel, L., Silk fibroin matrices for the controlled release of nerve growth factor (NGF). *Biomaterials* **2007**, *28* (30), 4449-60.
146. Liu, Q.; Huang, J.; Shao, H.; Song, L.; Zhang, Y., Dual-factor loaded functional silk fibroin scaffolds for peripheral nerve regeneration with the aid of neovascularization. *Rsc Adv* **2016**, *6* (9), 7683-7691.
147. Zhang, W.; Wang, X.; Wang, S.; Zhao, J.; Xu, L.; Zhu, C.; Zeng, D.; Chen, J.; Zhang, Z.; Kaplan, D. L.; Jiang, X., The use of injectable sonication-induced silk hydrogel for VEGF(165) and BMP-2 delivery for elevation of the maxillary sinus floor. *Biomaterials* **2011**, *32* (35), 9415-24.

148. Lan, Y.; Li, W.; Jiao, Y.; Guo, R.; Zhang, Y.; Xue, W.; Zhang, Y., Therapeutic efficacy of antibiotic-loaded gelatin microsphere/silk fibroin scaffolds in infected full-thickness burns. *Acta Biomater* **2014**, *10* (7), 3167-76.
149. Lu, Z.; Meng, M.; Jiang, Y.; Xie, J., UV-assisted in situ synthesis of silver nanoparticles on silk fibers for antibacterial applications. *Colloids and Surfaces A: Physicochemical and Engineering Aspects* **2014**, *447*, 1-7.
150. Tomsic, B.; Ilec, E.; Zerjav, M.; Hladnik, A.; Simoncic, A.; Simoncic, B., Characterisation and functional properties of antimicrobial bio-barriers formed by natural fibres. *Colloids Surf B Biointerfaces* **2014**, *122*, 72-78.
151. Song, D. W.; Kim, S. H.; Kim, H. H.; Lee, K. H.; Ki, C. S.; Park, Y. H., Multi-biofunction of antimicrobial peptide-immobilized silk fibroin nanofiber membrane: Implications for wound healing. *Acta Biomater* **2016**, *39*, 146-155.
152. Weinhaus, A. J., *Anatomy of the Human Heart*. 3. ed.; Springer International Publishing: Switzerland, **2015**.
153. Laflamme, M. A.; Murry, C. E., Heart regeneration. *Nature* **2011**, *473* (7347), 326-335.
154. American Heart Association, Types of Heart Failure. <https://www.heart.org/en/health-topics/heart-failure/what-is-heart-failure/types-of-heart-failure> (accessed 03, 2019).
155. R. Baliga, R.; Dec, G.; Narula, J., *Practice Guidelines for the Diagnosis and Management of Systolic Heart Failure in Low- and Middle-Income Countries*. **2013**; Vol. 8, p 141-170.
156. R Baliga, R.; K Bahl, V.; Alexander, T.; Sankardas, M. A.; Manga, P.; Dec, G.; Narula, J., *Management of STEMI in Low- and Middle-Income Countries*. **2014**; Vol. 9, p 469-510.
157. Murry, C. E.; Reinecke, H.; Pabon, L. M., Regeneration gaps: observations on stem cells and cardiac repair. *J Am Coll Cardiol* **2006**, *47* (9), 1777-85.
158. Whelan, R. S.; Kaplinskiy, V.; Kitsis, R. N., Cell death in the pathogenesis of heart disease: mechanisms and significance. *Annu Rev Physiol* **2010**, *72*, 19-44.
159. Olivetti, G.; Melissari, M.; Capasso, J. M.; Anversa, P., Cardiomyopathy of the aging human heart. Myocyte loss and reactive cellular hypertrophy. *Circ Res* **1991**, *68* (6), 1560-8.
160. Bergmann, O.; Bhardwaj, R. D.; Bernard, S.; Zdunek, S.; Barnabe-Heider, F.; Walsh, S.; Zupicich, J.; Alkass, K.; Buchholz, B. A.; Druid, H.; Jovinge, S.; Frisen, J., Evidence for Cardiomyocyte Renewal in Humans. *Science* **2009**, *324* (5923), 98-102.
161. Adler, C. P., Relationship between deoxyribonucleic acid content and nucleoli in human heart muscle cells and estimation of cell number during cardiac growth and hyperfunction. *Recent Adv Stud Cardiac Struct Metab* **1975**, *8*, 373-86.
162. Adler, C. P.; Friedburg, H., Myocardial DNA content, ploidy level and cell number in geriatric hearts: post-mortem examinations of human myocardium in old age. *J Mol Cell Cardiol* **1986**, *18* (1), 39-53.
163. Zebrowski, D. C.; Vergarajauregui, S.; Wu, C.-C.; Piatkowski, T.; Becker, R.; Leone, M.; Hirth, S.; Ricciardi, F.; Falk, N.; Giessl, A.; Just, S.; Braun, T.; Weidinger, G.; Engel, F. B., Developmental alterations in centrosome integrity contribute to the post-mitotic state of mammalian cardiomyocytes. *Elife* **2015**, *4*, e05563.
164. Leri, A.; Rota, M.; Pasqualini, F. S.; Goichberg, P.; Anversa, P., Origin of cardiomyocytes in the adult heart. *Circ Res* **2015**, *116* (1), 150-166.
165. Broughton, K. M.; Wang, B. Y. J.; Firouzi, F.; Khalafalla, F.; Dimmeler, S.; Fernandez-Aviles, F.; Sussman, M. A., Mechanisms of Cardiac Repair and Regeneration. *Circ Res* **2018**, *122* (8), 1151-1163.
166. Hirt, M. N.; Hansen, A.; Eschenhagen, T., Cardiac Tissue Engineering State of the Art. *Circ Res* **2014**, *114* (2), 354-367.
167. Dow, J.; Simkhovich, B. Z.; Kedes, L.; Kloner, R. A., Washout of transplanted cells from the heart: a potential new hurdle for cell transplantation therapy. *Cardiovasc Res* **2005**, *67* (2), 301-7.
168. Naito, H.; Melnychenko, I.; Didie, M.; Schneiderbanger, K.; Schubert, P.; Rosenkranz, S.; Eschenhagen, T.; Zimmermann, W. H., Optimizing engineered heart tissue for therapeutic applications as surrogate heart muscle. *Circulation* **2006**, *114* (1 Suppl), I72-8.
169. Zeng, Q. C.; Guo, Y.; Liu, L.; Zhang, X. Z.; Li, R. X.; Zhang, C. Q.; Hao, Q. X.; Shi, C. H.; Wu, J. M.; Guan, J., Cardiac fibroblast-derived extracellular matrix produced in vitro stimulates growth and metabolism of cultured ventricular cells. *Int Heart J* **2013**, *54* (1), 40-4.

170. Ott, H. C.; Matthiesen, T. S.; Goh, S. K.; Black, L. D.; Kren, S. M.; Netoff, T. I.; Taylor, D. A., Perfusion-decellularized matrix: using nature's platform to engineer a bioartificial heart. *Nat Med* **2008**, *14* (2), 213-21.
171. Zimmermann, W. H.; Didie, M.; Wasmeier, G. H.; Nixdorff, U.; Hess, A.; Melnychenko, I.; Boy, O.; Neuhuber, W. L.; Weyand, M.; Eschenhagen, T., Cardiac grafting of engineered heart tissue in syngenic rats. *Circulation* **2002**, *106* (12 Suppl 1), I151-7.
172. Sekine, H.; Shimizu, T.; Hobo, K.; Sekiya, S.; Yang, J.; Yamato, M.; Kurosawa, H.; Kobayashi, E.; Okano, T., Endothelial Cell Coculture Within Tissue-Engineered Cardiomyocyte Sheets Enhances Neovascularization and Improves Cardiac Function of Ischemic Hearts. *Circulation* **2008**, *118* (14_suppl_1), S145-S152.
173. Stevens, K. R.; Kreutziger, K. L.; Dupras, S. K.; Korte, F. S.; Regnier, M.; Muskheli, V.; Nourse, M. B.; Bendixen, K.; Reinecke, H.; Murry, C. E., Physiological function and transplantation of scaffold-free and vascularized human cardiac muscle tissue. *Proc Natl Acad Sci U S A* **2009**, *106* (39), 16568-73.
174. Shimizu, T.; Sekine, H.; Yang, J.; Isoi, Y.; Yamato, M.; Kikuchi, A.; Kobayashi, E.; Okano, T., Polysurgery of cell sheet grafts overcomes diffusion limits to produce thick, vascularized myocardial tissues. *Faseb J* **2006**, *20* (6), 708-10.
175. Zimmermann, W. H.; Schneiderbanger, K.; Schubert, P.; Didie, M.; Munzel, F.; Heubach, J. F.; Kostin, S.; Neuhuber, W. L.; Eschenhagen, T., Tissue engineering of a differentiated cardiac muscle construct. *Circ Res* **2002**, *90* (2), 223-30.
176. Furuta, A.; Miyoshi, S.; Itabashi, Y.; Shimizu, T.; Kira, S.; Hayakawa, K.; Nishiyama, N.; Tanimoto, K.; Hagiwara, Y.; Satoh, T.; Fukuda, K.; Okano, T.; Ogawa, S., Pulsatile Cardiac Tissue Grafts Using a Novel Three-Dimensional Cell Sheet Manipulation Technique Functionally Integrates With the Host Heart, In Vivo. *Circ Res* **2006**, *98* (5), 705-712.
177. Radisic, M.; Park, H.; Shing, H.; Consi, T.; Schoen, F. J.; Langer, R.; Freed, L. E.; Vunjak-Novakovic, G., Functional assembly of engineered myocardium by electrical stimulation of cardiac myocytes cultured on scaffolds. *Proc Natl Acad Sci U S A* **2004**, *101* (52), 18129-34.
178. Zimmermann, W. H.; Melnychenko, I.; Wasmeier, G.; Didie, M.; Naito, H.; Nixdorff, U.; Hess, A.; Budinsky, L.; Brune, K.; Michaelis, B.; Dhein, S.; Schwoerer, A.; Ehmke, H.; Eschenhagen, T., Engineered heart tissue grafts improve systolic and diastolic function in infarcted rat hearts. *Nat Med* **2006**, *12* (4), 452-8.
179. Tiburcy, M.; Didie, M.; Boy, O.; Christalla, P.; Doker, S.; Naito, H.; Karikkineth, B. C.; El-Armouche, A.; Grimm, M.; Nose, M.; Eschenhagen, T.; Zieseniss, A.; Katschinski, D. M.; Hamdani, N.; Linke, W. A.; Yin, X.; Mayr, M.; Zimmermann, W. H., Terminal differentiation, advanced organotypic maturation, and modeling of hypertrophic growth in engineered heart tissue. *Circ Res* **2011**, *109* (10), 1105-14.
180. Reinecke, H.; Zhang, M.; Bartosek, T.; Murry, C. E., Survival, integration, and differentiation of cardiomyocyte grafts: a study in normal and injured rat hearts. *Circulation* **1999**, *100* (2), 193-202.
181. Yang, M. C.; Wang, S. S.; Chou, N. K.; Chi, N. H.; Huang, Y. Y.; Chang, Y. L.; Shieh, M. J.; Chung, T. W., The cardiomyogenic differentiation of rat mesenchymal stem cells on silk fibroin-polysaccharide cardiac patches in vitro. *Biomaterials* **2009**, *30* (22), 3757-3765.
182. Chi, N. H.; Yang, M. C.; Chung, T. W.; Chen, J. Y.; Chou, N. K.; Wang, S. S., Cardiac repair achieved by bone marrow mesenchymal stem cells/silk fibroin/hyaluronic acid patches in a rat of myocardial infarction model. *Biomaterials* **2012**, *33* (22), 5541-5551.
183. Chi, N. H.; Yang, M. C.; Chung, T. W.; Chou, N. K.; Wang, S. S., Cardiac repair using chitosan-hyaluronan/silk fibroin patches in a rat heart model with myocardial infarction. *Carbohydr Polym* **2013**, *92* (1), 591-597.
184. Stoppel, W. L.; Hu, D. J.; Domian, I. J.; Kaplan, D. L.; Black, L. D., Anisotropic silk biomaterials containing cardiac extracellular matrix for cardiac tissue engineering. *Biomed Mater* **2015**, *10* (3), 034105.
185. Castellano, D.; Blanes, M.; Marco, B.; Cerrada, I.; Ruiz-Sauri, A.; Pelacho, B.; Arana, M.; Montero, J. A.; Cambra, V.; Prosper, F.; Sepulveda, P., A Comparison of Electrospun Polymers Reveals Poly(3-Hydroxybutyrate) Fiber as a Superior Scaffold for Cardiac Repair. *Stem Cells Dev* **2014**, *23* (13), 1479-1490.
186. Rahimi, M.; Mohseni-Kouchesfehani, H.; Zarnani, A. H.; Mobini, S.; Nikoo, S.; Kazemnejad, S., Evaluation of menstrual blood stem cells seeded in biocompatible Bombyx mori silk fibroin scaffold for cardiac tissue engineering. *J Biomater Appl* **2014**, *29* (2), 199-208.

187. Di Felice, V.; Serradifalco, C.; Rizzuto, L.; De Luca, A.; Rappa, F.; Barone, R.; Di Marco, P.; Cassata, G.; Puleio, R.; Verin, L.; Motta, A.; Migliaresi, C.; Guercio, A.; Zummo, G., Silk fibroin scaffolds enhance cell commitment of adult rat cardiac progenitor cells. *J Tissue Eng Regen M* **2015**, *9* (11), E51-E64.
188. Patra, C.; Talukdar, S.; Novoyatleva, T.; Velagala, S. R.; Muhlfeld, C.; Kundu, B.; Kundu, S. C.; Engel, F. B., Silk protein fibroin from *Antheraea mylitta* for cardiac tissue engineering. *Biomaterials* **2012**, *33* (9), 2673-2680.
189. Mehrotra, S.; Nandi, S. K.; Mandal, B. B., Stacked silk-cell monolayers as a biomimetic three dimensional construct for cardiac tissue reconstruction. *J Mater Chem B* **2017**, *5* (31), 6325-6338.
190. Institute For Quality And Efficiency In Health Care, How does the nervous system work?, <https://www.ncbi.nlm.nih.gov/books/NBK279390/>, (accessed 3, 2019)
191. Squire, L. R. *Encyclopedia of Neuroscience*. Springer: **2009**.
192. Lackington, W. A.; Ryan, A. J.; O'Brien, F. J., Advances in Nerve Guidance Conduit-Based Therapeutics for Peripheral Nerve Repair. *ACS Biomaterials Science & Engineering* **2017**, *3* (7), 1221-1235.
193. Robinson, L. R., Traumatic injury to peripheral nerves. *Muscle Nerve* **2000**, *23* (6), 863-873.
194. Seddon, H. J., A Classification of Nerve Injuries. *Br Med J* **1942**, *2* (4260), 237-9.
195. Sunderland, S., A classification of peripheral nerve injuries producing loss of function. *Brain* **1951**, *74* (4), 491-516.
196. Waller, A., Experiments on the Section of the Glossopharyngeal and Hypoglossal Nerves of the Frog, and observations of the alterations produced thereby in the Structure of their Primitive Fibres. *Royal Society* **1850**, *140*, 7.
197. Barrette, B.; Hebert, M. A.; Filali, M.; Lafortune, K.; Vallieres, N.; Gowing, G.; Julien, J. P.; Lacroix, S., Requirement of myeloid cells for axon regeneration. *J Neurosci* **2008**, *28* (38), 9363-9376.
198. Martini, R.; Fischer, S.; Lopez-Vales, R.; David, S., Interactions Between Schwann Cells and Macrophages in Injury and Inherited Demyelinating Disease. *Glia* **2008**, *56* (14), 1566-1577.
199. Burnett, M. G.; Zager, E. L., Pathophysiology of peripheral nerve injury: a brief review. *Neurosurg Focus* **2004**, *16* (5), E1.
200. Magaz, A.; Faroni, A.; Gough, J. E.; Reid, A. J.; Li, X.; Blaker, J. J., Bioactive Silk-Based Nerve Guidance Conduits for Augmenting Peripheral Nerve Repair. *Adv Healthc Mater* **2018**, *7* (23), 1800308.
201. Ghaznavi, A. M.; Kokai, L. E.; Lovett, M. L.; Kaplan, D. L.; Marra, K. G., Silk Fibroin Conduits A Cellular and Functional Assessment of Peripheral Nerve Repair. *Ann Plas Surg* **2011**, *66* (3), 273-279.
202. Grinsell, D.; Keating, C. P., Peripheral Nerve Reconstruction after Injury: A Review of Clinical and Experimental Therapies. *Biomed Res Int* **2014**, *2014*, 698256.
203. Alberti, K. A.; Hopkins, A. M.; Tang-Schomer, M. D.; Kaplan, D. L.; Xu, Q. B., The behavior of neuronal cells on tendon-derived collagen sheets as potential substrates for nerve regeneration. *Biomaterials* **2014**, *35* (11), 3551-3557.
204. Oh, S. H.; Kim, J. H.; Song, K. S.; Jeon, B. H.; Yoon, J. H.; Seo, T. B.; Namgung, U.; Lee, I. W.; Lee, J. H., Peripheral nerve regeneration within an asymmetrically porous PLGA/Pluronic F127 nerve guide conduit. *Biomaterials* **2008**, *29* (11), 1601-9.
205. Madduri, S.; Feldman, K.; Tervoort, T.; Papaloizos, M.; Gander, B., Collagen nerve conduits releasing the neurotrophic factors GDNF and NGF. *J Control Release* **2010**, *143* (2), 168-74.
206. Rosen, J. M.; Padilla, J. A.; Nguyen, K. D.; Padilla, M. A.; Sabelman, E. E.; Pham, H. N., Artificial nerve graft using collagen as an extracellular matrix for nerve repair compared with sutured autograft in a rat model. *Ann Plast Surg* **1990**, *25* (5), 375-87.
207. Chen, Y. S.; Hsieh, C. L.; Tsai, C. C.; Chen, T. H.; Cheng, W. C.; Hu, C. L.; Yao, C. H., Peripheral nerve regeneration using silicone rubber chambers filled with collagen, laminin and fibronectin. *Biomaterials* **2000**, *21* (15), 1541-7.
208. Daly, W.; Yao, L.; Zeugolis, D.; Windebank, A.; Pandit, A., A biomaterials approach to peripheral nerve regeneration: bridging the peripheral nerve gap and enhancing functional recovery. *Journal of the Royal Society, Interface* **2012**, *9* (67), 202-21.

209. Lee, J. Y.; Giusti, G.; Friedrich, P. F.; Archibald, S. J.; Kemnitzer, J. E.; Patel, J.; Desai, N.; Bishop, A. T.; Shin, A. Y., The effect of collagen nerve conduits filled with collagen-glycosaminoglycan matrix on peripheral motor nerve regeneration in a rat model. *J Bone Joint Surg Am* **2012**, *94* (22), 2084-91.
210. Karabekmez, F. E.; Duymaz, A.; Moran, S. L., Early clinical outcomes with the use of decellularized nerve allograft for repair of sensory defects within the hand. *Hand (N Y)* **2009**, *4* (3), 245-9.
211. Terfort, A.; Bowden, N.; Whitesides, G. M., Three-dimensional self-assembly of millimetre-scale components. *Nature* **1997**, *386* (6621), 162-164.
212. Whitesides, G. M.; Grzybowski, B., Self-assembly at all scales. *Science* **2002**, *295* (5564), 2418-2421.
213. Ionov, L., Biomimetic 3D self-assembling biomicroconstructs by spontaneous deformation of thin polymer films. *J Mater Chem* **2012**, *22* (37), 19366-19375.
214. Forterre, Y.; Skotheim, J. M.; Dumais, J.; Mahadevan, L., How the Venus flytrap snaps. *Nature* **2005**, *433* (7024), 421-425.
215. Ionov, L., Soft microorigami: self-folding polymer films. *Soft Matter* **2011**, *7* (15), 6786-6791.
216. Luchnikov, V.; Ionov, L.; Stamm, M., Self-Rolled Polymer Tubes: Novel Tools for Microfluidics, Microbiology, and Drug-Delivery Systems. *Macromol Rapid Comm* **2011**, *32* (24), 1943-1952.
217. Stoychev, G.; Zakharchenko, S.; Turcaud, S.; Dunlop, J. W. C.; Ionov, L., Shape-Programmed Folding of Stimuli-Responsive Polymer Bilayers. *Acs Nano* **2012**, *6* (5), 3925-3934.
218. Zakharchenko, S.; Sperling, E.; Ionov, L., Fully Biodegradable Self-Rolled Polymer Tubes: A Candidate for Tissue Engineering Scaffolds. *Biomacromolecules* **2011**, *12* (6), 2211-2215.
219. Jager, E. W. H.; Ingnas, O.; Lundstrom, I., Microrobots for micrometer-size objects in aqueous media: Potential tools for single-cell manipulation. *Science* **2000**, *288* (5475), 2335-2338.
220. Smela, E.; Ingnas, O.; Lundstrom, I., Controlled Folding of Micrometer-Size Structures. *Science* **1995**, *268* (5218), 1735-1738.
221. Gracias, D. H.; Tien, J.; Breen, T. L.; Hsu, C.; Whitesides, G. M., Forming electrical networks in three dimensions by self-assembly. *Science* **2000**, *289* (5482), 1170-1172.
222. Leong, T.; Gu, Z. Y.; Koh, T.; Gracias, D. H., Spatially controlled chemistry using remotely guided nanoliter scale containers. *J Am Chem Soc* **2006**, *128* (35), 11336-11337.
223. Ju, X. J.; Xie, R.; Yang, L.; Chu, L. Y., Biodegradable 'intelligent' materials in response to physical stimuli for biomedical applications. *Expert Opin Ther Pat* **2009**, *19* (4), 493-507.
224. Bassik, N.; Abebe, B. T.; Laflin, K. E.; Gracias, D. H., Photolithographically patterned smart hydrogel based bilayer actuators. *Polymer* **2010**, *51* (26), 6093-6098.
225. Apsite, I.; Stoychev, G.; Zhang, W. Z.; Jehnichen, D.; Xie, J.; Ionov, L., Porous Stimuli-Responsive Self-Folding Electrospun Mats for 4D Biofabrication. *Biomacromolecules* **2017**, *18* (10), 3178-3184.
226. Liu, L.; Jiang, S. H.; Sun, Y.; Agarwal, S., Giving Direction to Motion and Surface with Ultra-Fast Speed Using Oriented Hydrogel Fibers. *Adv Funct Mater* **2016**, *26* (7), 1021-1027.
227. Chen, T. T.; Bakhshi, H.; Liu, L.; Ji, J.; Agarwal, S., Combining 3D Printing with Electrospinning for Rapid Response and Enhanced Designability of Hydrogel Actuators. *Adv Funct Mater* **2018**, *28* (19), 1800514.
228. Stroganov, V.; Zakharchenko, S.; Sperling, E.; Meyer, A. K.; Schmidt, O. G.; Ionov, L., Biodegradable Self-Folding Polymer Films with Controlled Thermo-Trigged Folding *Adv Funct Mater* **2014**, *24*, 4357-4363.
229. Ye, C. H.; Nikolov, S. V.; Calabrese, R.; Dindar, A.; Alexeev, A.; Kippelen, B.; Kaplan, D. L.; Tsukruk, V. V., Self-(Un)rolling Biopolymer Microstructures: Rings, Tubules, and Helical Tubules from the Same Material. *Angew Chem Int Edit* **2015**, *54* (29), 8490-8493.
230. Yang, Y. M.; Chen, X. M.; Ding, F.; Zhang, P. Y.; Liu, J.; Go, X. S., Biocompatibility evaluation of silk fibroin with peripheral nerve tissues and cells in vitro. *Biomaterials* **2007**, *28* (9), 1643-1652.
231. Hu, A.; Zuo, B.; Zhang, F.; Lan, Q.; Zhang, H., Electrospun silk fibroin nanofibers promote Schwann cell adhesion, growth and proliferation. *Neural Regen Res* **2012**, *7* (15), 1171-8.
232. Huang, W.; Begum, R.; Barber, T.; Ibba, V.; Tee, N. C. H.; Hussain, M.; Arastoo, M.; Yang, Q.; Robson, L. G.; Lesage, S.; Gheysens, T.; Skaer, N. J. V.; Knight, D. P.; Priestley, J. V., Regenerative potential of silk conduits in repair of peripheral nerve injury in adult rats. *Biomaterials* **2012**, *33* (1), 59-71.

233. Zhang, H.; Wang, K. F.; Xing, Y. M.; Yu, Q. Z., Lysine-doped polypyrrole/spider silk protein/poly(L-lactic) acid containing nerve growth factor composite fibers for neural application. *Mat Sci Eng C-Mater* **2015**, *56*, 564-573.
234. Allmeling, C.; Jokuszies, A.; Reimers, K.; Kall, S.; Vogt, P. M., Use of spider silk fibres as an innovative material in a biocompatible artificial nerve conduit. *J Cell Mol Med* **2006**, *10* (3), 770-777.
235. Allmeling, C.; Jokuszies, A.; Reimers, K.; Kall, S.; Choi, C. Y.; Brandes, G.; Kasper, C.; Scheper, T.; Guggenheim, M.; Vogt, P. M., Spider silk fibres in artificial nerve constructs promote peripheral nerve regeneration. *Cell Proliferat* **2008**, *41* (3), 408-420.
236. Kornfeld, T.; Vogt, P. M.; Bucan, V.; Peck, C. T.; Reimers, K.; Radtke, C., Characterization and Schwann Cell Seeding of up to 15.0 cm Long Spider Silk Nerve Conduits for Reconstruction of Peripheral Nerve Defects. *J Funct Biomater* **2016**, *7* (30), doi:10.3390/jfb704003.
237. Lewicka, M.; Hermanson, O.; Rising, A. U., Recombinant spider silk matrices for neural stem cell cultures. *Biomaterials* **2012**, *33* (31), 7712-7717.
238. An, B.; Tang-Schomer, M. D.; Huang, W. W.; He, J. Y.; Jones, J. A.; Lewis, R. V.; Kaplan, D. L., Physical and biological regulation of neuron regenerative growth and network formation on recombinant dragline silks. *Biomaterials* **2015**, *48*, 137-146.
239. Department Of Bioengineering – University Of California Bioinstrumentation. <http://bioeng.berkeley.edu/research/bioinstrumentation> (accessed 03, 2019).
240. Cammann, K., Bio-sensors based on ion-selective electrodes. *Fresenius Z. Anal. Chem.* **1977**, 287 (1).
241. Thevenot, D. R.; Toth, K.; Durst, R. A.; Wilson, G. S., Electrochemical biosensors: recommended definitions and classification. *Biosens Bioelectron* **2001**, *16*, 121-131.
242. Lottspeich, F.; Engels, J. W., *Bioanalytik*. 3 ed.; Springer Spektrum: 2012.
243. Kuchler, A.; Yoshimoto, M.; Luginbuhl, S.; Mavelli, F.; Walde, P., Enzymatic reactions in confined environments. *Nat Nanotechnol* **2016**, *11* (5), 409-420.
244. Vashist, S. K.; Lam, E.; Hrapovic, S.; Male, K. B.; Luong, J. H. T., Immobilization of Antibodies and Enzymes on 3-Aminopropyltriethoxysilane-Functionalized Bioanalytical Platforms for Biosensors and Diagnostics. *Chem Rev* **2014**, *114* (21), 11083-11130.
245. Linko, V.; Eerikäinen, M.; Kostianen, M. A., A modular DNA origami-based enzyme cascade nanoreactor. *Chem Commun* **2015**, *51* (25), 5351-5354.
246. Kadnikova, E. N.; Kostic, N. M., Oxidation of ABTS by hydrogen peroxide catalyzed by horseradish peroxidase encapsulated into sol-gel glass. Effects of glass matrix on reactivity. *J Mol Catal B-Enzym* **2002**, *18* (1-3), 39-48.
247. Walde, P.; Ichikawa, S., Enzymes inside lipid vesicles: Preparation, reactivity and applications. *Biomol Eng* **2001**, *18* (4), 143-177.
248. Hase, M.; Yamada, A.; Hamada, T.; Baigl, D.; Yoshikawa, K., Manipulation of cell-sized phospholipid-coated microdroplets and their use as biochemical microreactors. *Langmuir* **2007**, *23* (2), 348-352.
249. Vriezema, D. M.; Garcia, P. M. L.; Oltra, N. S.; Hatzakis, N. S.; Kuiper, S. M.; Nolte, R. J. M.; Rowan, A. E.; van Hest, J. C. M., Positional assembly of enzymes in polymersome nanoreactors for cascade reactions. *Angew Chem Int Edit* **2007**, *46* (39), 7378-7382.
250. Lee, H.; DeLoache, W. C.; Dueber, J. E., Spatial organization of enzymes for metabolic engineering. *Metab Eng* **2012**, *14* (3), 242-251.
251. Sintra, T. E.; Ventura, S. P. M.; Coutinho, J. A. P., Superactivity induced by micellar systems as the key for boosting the yield of enzymatic reactions. *J Mol Catal B-Enzym* **2014**, *107*, 140-151.
252. Theberge, A. B.; Courtois, F.; Schaerli, Y.; Fischlechner, M.; Abell, C.; Hollfelder, F.; Huck, W. T. S., Microdroplets in Microfluidics: An Evolving Platform for Discoveries in Chemistry and Biology. *Angew Chem Int Edit* **2010**, *49* (34), 5846-5868.
253. Sakr, O. S.; Borchard, G., Encapsulation of Enzymes in Layer-by-Layer (LbL) Structures: Latest Advances and Applications. *Biomacromolecules* **2013**, *14* (7), 2117-2135.
254. Liebherr, R. B.; Gorris, H. H., Enzyme Molecules in Solitary Confinement. *Molecules* **2014**, *19* (9), 14417-14445.

255. Zhang, Y. Q.; Zhu, J.; Gu, R. A., Improved biosensor for glucose based on glucose oxidase-immobilized silk fibroin membrane. *Appl Biochem Biotechnol* **1998**, *75* (2-3), 215-33.
256. Tao, H.; Marelli, B.; Yang, M. M.; An, B.; Onses, M. S.; Rogers, J. A.; Kaplan, D. L.; Omenetto, F. G., Inkjet Printing of Regenerated Silk Fibroin: From Printable Forms to Printable Functions. *Adv Mater* **2015**, *27* (29), 4273-4279.
257. Pritchard, E. M.; Dennis, P. B.; Omenetto, F.; Naik, R. R.; Kaplan, D. L., Physical and chemical aspects of stabilization of compounds in silk. *Biopolymers* **2012**, *97* (6), 479-498.
258. Li, A. B.; Kluge, J. A.; Guziewicz, N. A.; Omenetto, F. G.; Kaplan, D. L., Silk-based stabilization of biomacromolecules. *J Control Release* **2015**, *219*, 416-430.
259. Shchepelina, O.; Drachuk, I.; Gupta, M. K.; Lin, J.; Tsukruk, V. V., Silk-on-Silk Layer-by-Layer Microcapsules. *Adv Mater* **2011**, *23* (40), 4655-60.
260. Ye, C. H.; Shchepelina, O.; Calabrese, R.; Drachuk, I.; Kaplan, D. L.; Tsukruk, V. V., Robust and Responsive Silk Ionomer Microcapsules. *Biomacromolecules* **2011**, *12* (12), 4319-4325.
261. Hermanson, K. D.; Huemmerich, D.; Scheibel, T.; Bausch, A. R., Engineered microcapsules fabricated from reconstituted spider silk. *Adv Mater* **2007**, *19* (14), 1810-15.
262. Hermanson, K. D.; Harasim, M. B.; Scheibel, T.; Bausch, A. R., Permeability of silk microcapsules made by the interfacial adsorption of protein. *Phys Chem Chem Phys* **2007**, *9* (48), 6442-6446.
263. Humenik, M.; Mohrand, M.; Scheibel, T., Self-Assembly of Spider Silk-Fusion Proteins Comprising Enzymatic and Fluorescence Activity. *Bioconjugate Chem* **2018**, *29* (4), 898-904.
264. Lang, G. Herstellung und Charakterisierung von Fasern aus rekombinanten Spinnenseidenproteinen und deren potentielle Applikationen, PhD thesis, Uni Bayreuth, Bayreuth, 2015.
265. DeSimone, E.; Aigner, T. B.; Humenik, M.; Lang, G.; Scheibel, T., Aqueous electrospinning of recombinant spider silk proteins. *Materials Science and Engineering: C* **2020**, *106*, 110145.
266. Sievert, D. M.; Ricks, P.; Edwards, J. R.; Schneider, A.; Patel, J.; Srinivasan, A.; Kallen, A.; Limbago, B.; Fridkin, S.; Network, N. H. S.; Facilities, P. N., Antimicrobial-Resistant Pathogens Associated with Healthcare-Associated Infections: Summary of Data Reported to the National Healthcare Safety Network at the Centers for Disease Control and Prevention, 2009-2010. *Infect Cont Hosp Ep* **2013**, *34* (1), 1-14.
267. Shimizu, I.; Minamino, T., Physiological and pathological cardiac hypertrophy. *J Mol Cell Cardiol* **2016**, *97*, 245-62.
268. Petzold, J.; Aigner, T. B.; Touska, F.; Zimmermann, K.; Scheibel, T.; Engel, F. B., Surface Features of Recombinant Spider Silk Protein eADF4(κ 16)-Made Materials are Well-Suited for Cardiac Tissue Engineering. *Adv Funct Mater* **2017**, *27*, 1701427.
269. Aigner, T. B.; Haynl, C.; Salehi, S.; O'Connor, A.; Scheibel, T., Nerve guidance conduit design based on self-rolling tubes. *Materials Today Bio* **2020**, *5*, 100042.
270. Aigner, T.; Scheibel, T., Self-Rolling Refillable Tubular Enzyme Containers Made of Recombinant Spider Silk and Chitosan. *Acs Appl Mater Inter* **2019**, *11* (17), 15290-15297.

5 Publications and Manuscripts

1. **Aigner, T. B.***; DeSimone, E.*; Scheibel, T. (2018) Biomedical Applications of Recombinant Silk-Based Materials. *Advanced Materials* 30 (19): 1704636
2. DeSimone, E.; **Aigner, T. B.**, Humenik, M.; Lang, G.; Scheibel, T. (2020) Aqueous electrospinning of recombinant spider silk proteins, *Materials Science and Engineering: C* 106, 110145.
3. Huang, T.; Kumari, S.; Herold, H.; Bargel, H.; **Aigner, T. B.**; Heath, D. E.; O'Brien-Simpson, N. M., O'Connor, A. J.; Scheibel, T. (2019) Enhanced antibacterial activity of Se nanoparticles upon coating with recombinant spider silk protein eADF4 (κ 16), *manuscript submitted*
4. Petzold, J.; **Aigner, T. B.**; Touska, F.; Zimmermann, K.; Scheibel, T.; Engel, F. B. (2017) Surface Features of Recombinant Spider Silk Protein eADF4(κ 16)-Made Materials are Well-Suited for Cardiac Tissue Engineering. *Advanced Functional Materials* 27: 1701427
5. **Aigner, T. B.***; Haynl, C.*; Salehi, S.; O'Connor, A. Scheibel, T. (2020) Nerve Guidance Conduit Design based on Self-rolling Tubes, *Materials Today Bio*, 5, 100042.
6. **Aigner, T. B.**; Scheibel, T. (2019) Self-rolling Tubular Structures made of Spider Silk and Chitosan as Enzyme Containers, *ACS Appl. Mater. Interfaces* 11 (17), 15290-15297
7. Herold, H. M.; **Aigner, T. B.**; Grill C. E.; Krüger S.; Taubert A.; Scheibel T. (2019) SpiderMAEn: Recombinant Spider Silk-based Hybrid Materials for Advanced Energy Technology. *Bioinspired, Biomimetic and Nanobiomaterials* 8 (1), 99-108 (not part of this dissertation)
8. Kramer J., **Aigner T. B.**, Petzold J., Roshanbinfar K., Scheibel T., Engel F. B. (2019) Recombinant Spider Silk Protein eADF4(C16)-RGD for Cardiac Tissue Engineering, *manuscript submitted* (not part of this dissertation)

* shared authorship

6 Individual contributions to joint publications and manuscripts

The current dissertation is composed of four publications and two manuscripts written in collaboration with cooperation partners. Hereinafter, the contributions of the authors to the single papers are given.

Publication I

Aigner, T. B.*; DeSimone, E.*; Scheibel, T. (2018) Biomedical Applications of Recombinant Silk-Based Materials. *Advanced Materials* 30 (19): 1704636

The paper was conceptualized by all authors. The manuscript was written, and the figures were prepared by Elise DeSimone and me. Thomas Scheibel was involved in critical discussions as well as in finalizing the manuscript.

Publication II

DeSimone, E.; **Aigner, T. B.**, Humenik, M.; Lang, G.; Scheibel, T. (2019) Aqueous electrospinning of recombinant spider silk proteins, *Materials Science and Engineering: C* 106, 110145.

The study was conceptualized by Elise DeSimone, Thomas Scheibel and me. Elise DeSimone and Gregor Lang developed the preparation and spinning from aqueous solution. Elise DeSimone prepared all nonwoven samples. SEM images were taken by Claudia Stemmann. DSC and FTIR characterization were performed by me. CD and fluorescence spectroscopy were done by Martin Humenik. GFP activity and release studies were performed by Elise DeSimone and me. Martin Humenik provided GFP and helped design all studies related to GFP. Elise DeSimone prepared the manuscript. All authors contributed to discussing contents as well as correcting the manuscript.

Publication III

Petzold, J.; **Aigner, T. B.**; Touska, F.; Zimmermann, K.; Scheibel, T.; Engel, F. B. (2017) Surface Features of Recombinant Spider Silk Protein eADF4(κ 16)-Made Materials are Well-Suited for Cardiac Tissue Engineering. *Advanced Functional Materials* 27: 1701427

The paper was planned by Jana Petzold, Felix B. Engel, Thomas Scheibel and me. The spider silk film preparation as well as characterization and analysis via FTIR and contact angle measurements were performed by me. Jana Petzold performed all cell cultures studies, and Filip Touska performed the analysis of calcium change. The manuscript was written by Felix B. Engel, Jana Petzold and me. All other authors contributed with valuable scientific discussions and helped finalizing the publication.

Publication IV

Aigner, T. B.; Scheibel, T. (2019) Self-rolling Tubular Structures made of Spider Silk and Chitosan as Enzyme Containers, *ACS Appl. Mater. Interfaces* 11 (17), 15290-15297

The paper was conceptualized by both authors. Experimental work, manuscript writing, and figure preparation were performed by me. Thomas Scheibel gave critical input and helped finalizing the manuscript.

Publication V

Aigner, T. B.*; Haynl, C.*; Salehi, S.; O'Connor, A. Scheibel, T. (2020) Nerve Guidance Conduit Design based on Self-rolling Tubes, *Materials Today Bio*, 5, 100042.

The paper was planned by all authors. Christian Haynl prepared and analyzed the cryogels and performed the mechanical testing. The tubular structures were prepared and analyzed by me and I performed the cell culture experiments. Sahar Salehi assisted in cell culture experiments. The manuscript was written and the figures were prepared by Christian Haynl, Sahar Salehi and me. Thomas Scheibel and Andrea O'Connor helped with critical discussions to finalize the manuscript.

Manuscript I

Huang, T.; Kumari, S.; Herold, H.; Bargel, H.; **Aigner, T. B.**; Heath, D. E.; O'Brien-Simpson, N. M., O'Connor, A. J.; Scheibel, T. (2019) Enhanced antibacterial activity of Se nanoparticles upon coating with recombinant spider silk protein eADF4 ($\kappa 16$), *manuscript submitted*

The project was planned by Tao Huang, Heike Herold and Sushma Kumari. Tao Huang prepared the materials and performed the experiments with the helping hand of the co-authors. Heike Herold helped with particle coating, performed zeta potential and ICP-OES measurements. Sushma Kumari eukaryotic and prokaryotic cell experiments. Hendrik Bargel performed SEM and EDS measurement. I advised the silk film preparation and performed TEM imaging. Daniel Heath, Neil O'Brien-Simpson, Thomas Scheibel and Andrea O'Connor helped with critical discussions and finalized the manuscript.

Publications and Manuscripts

Part 1. Biomedical applications of recombinant silk

Aigner T. B.*, DeSimone E.*, Scheibel T.

Published in *Advanced Materials*, 30, 1704636

(2018)

Reprinted with kind permission from WILEY-VHC Verlag GmbH & Co

REVIEW

Biomaterials

**ADVANCED
MATERIALS**
www.advmat.de

Biomedical Applications of Recombinant Silk-Based Materials

Tamara Bernadette Aigner, Elise DeSimone, and Thomas Scheibel*

Silk is mostly known as a luxurious textile, which originates from silkworms first cultivated in China. A deeper look into the variety of silk reveals that it can be used for much more, in nature and by humanity. For medical purposes, natural silks were recognized early as a potential biomaterial for surgical threads or wound dressings; however, as biomedical engineering advances, the demand for high-performance, naturally derived biomaterials becomes more pressing and stringent. A common problem of natural materials is their large batch-to-batch variation, the quantity available, their potentially high immunogenicity, and their fast biodegradation. Some of these common problems also apply to silk; therefore, recombinant approaches for producing silk proteins have been developed. There are several research groups which study and utilize various recombinantly produced silk proteins, and many of these have also investigated their products for biomedical applications. This review gives a critical overview over of the results for applications of recombinant silk proteins in biomedical engineering.

1. Prologue

The purpose of this review is to summarize the use of recombinant silk proteins in biomedical engineering and the most beneficial characteristics of recombinant silks for these types of applications. Readers will also be given substantial amounts of background information on silks as well as important sub-fields in biomedical engineering, in hopes of making this review accommodating to specialists from different fields. The motivation is to provide a broad picture of a class of interesting biopolymers which are not as well-known as, for example, collagen, for biomedical engineering.

T. B. Aigner, E. DeSimone
University Bayreuth, Lehrstuhl Biomaterialien
Universitätsstr. 30, 95447 Bayreuth, Germany
Prof. T. Scheibel
Bayreuther Zentrum für Kolloide und Grenzflächen (BZKG)
Bayreuther Zentrum für Bio-Makromoleküle (bio-mac)
Bayreuther Zentrum für Molekulare Biowissenschaften (BZMB)
Bayreuther Materialzentrum (BayMAT)
Bayerisches Polymerinstitut (BPI)
University Bayreuth
Universitätsstr. 30, 95447 Bayreuth, Germany
E-mail: thomas.scheibel@brn.uni-bayreuth.de

 The ORCID identification number(s) for the author(s) of this article can be found under <https://doi.org/10.1002/adma.201704636>.

DOI: 10.1002/adma.201704636

2. Biomedical Engineering

Biomedical engineering (BME) is the practice of applying engineering principles to medical problems in order to improve the quality of health care. It encompasses everything from patient data collection, to medical machine design (e.g., magnetic resonance imaging), to pregnancy tests, to contributing to basic science, to tissue engineering.^[1] It seeks not only to increase lifespan but also to improve the quality of life for people afflicted with injury or disease. Generally speaking, there are four major patient populations which are in need: the elderly, the diseased or injured, those infected with “super bugs,” and those in third world countries.

The population world-wide is growing larger due to an increase in successful birth rate and life expectancy.^[2] The aging population is particularly problematic in terms of medical costs, as they are at increased risk for disease, injury, and tissue dysfunction.^[3] Common ailments of the elderly include dilapidation of joints through arthritis^[4] and failure of the heart and blood vessels through various heart diseases.^[5] Although there are many existing treatments, these are only able to alleviate the ailment, and not treat it. For example, hip implants for joint replacement are made from hard, inorganic materials. This results in improper integration with the host tissue, and there is no restoration of the original tissue. The most successful existing therapy is organs replacement.^[6] However, in this case, there is still no proper tissue integration because the organ is considered foreign by the immune system, requiring use of immune-repressive drugs and thereby increasing the patient's risk of infection. Further, the demand of organs is much greater than the supply, and the associated costs are quite high.^[7] There are also diseases which effect this population and are currently untreatable such as Alzheimer's.^[8]

A larger, broader patient demographic is those who have had nonfatal, accidental injuries (according to statistics reported by Center for Disease Control and Prevention (CDC)^[9]), for example bone fracture, anterior crucial ligament tear, peripheral nerve damage, skeletal muscle damage, and burns. Although treatments are relatively advanced for these types of injuries, there is still scarring and incomplete restoration of tissue function.^[10] More complicated injuries are those caused by disease or tissue pathology, for example osteoarthritis in the knee joint. This is particularly complicated because it requires both treatment of the disease and replacement of the damaged tissue.

Current solutions usually involve disease management through collagen injections, surgery, physical therapy, and in extreme cases joint replacement.^[11]

Another significant problem in modern medicine is that hospitals are notorious for high occurrence of transmitted diseases. In a survey from 183 hospitals in 2011 in the United States, it was found that 4% of patients contracted a healthcare-associated infection (HAIs).^[12] Of these incidents, the most predominant types were pneumonia (21.8%), surgical-site infections (21.8%), and gastrointestinal infections (17.1%). Infections in hospitals also tend to be more serious than those contracted elsewhere, as there is greater risk of antibiotic-resistant strains of bacteria. In a separate study in 2010, it was shown that nearly 20% of pathogens reported from all HAIs had multidrug-resistant phenotypes (e.g., methicillin-resistant *Staphylococcus aureus* (8.5%), vancomycin-resistant *Enterococcus* (3%)).^[13] The most common way to deal with this is through preventative medicine by sanitary protocols. However, no matter how good the sanitary protocols, infections will happen. Infections are usually handled through antibiotics, and in extreme cases the patient(s) will also be quarantined. Additionally, the overuse of antibiotics and antibiotic soaps in sanitary protocols has resulted in antibiotic resistant strains which cannot be treated by available drugs.^[14]

A last short-coming of modern medicine worth mentioning is the lack of remedies available to those in third world countries or with lower incomes. Although there are movements to improve this situation occurring in several sectors, for example, by improving water quality, providing household energy and education, and developing vaccines for vector-borne diseases (e.g., malaria), there is still much work left to do (according to Health and Environment Linkages Initiative (HELI) division of the World Health Organization (WHO)^[15]).

There are several new trends to meet these current medical problems in the BME field. Interesting examples include smart wear technology, primarily to be used for at-home patient monitoring,^[16] technology for mapping and stimulating the brain achieved through recent pushes by the BRAIN initiative as well as its internationalization,^[17] soft robotics for interaction with soft tissues,^[18] in vitro modeling for research to clinic translation for basic research and drug toxicology screening (e.g., liver on a chip),^[19] biomaterial coatings (active or passive) which physically disrupt bacteria with or without use of antibiotics to prevent disease transmission,^[20] or biofabrication for regenerative medicine.^[21] Although all of these products are novel and exciting, there are still drawbacks to even the most cutting edge designs such as poor translation from research to use in the clinic^[22] and the manufacturing readiness of the technology is low.^[23] Although there are many complicated reasons for this, one major step toward producing clinically viable products is to develop novel, suitable biomaterials. Among the suitable candidates, a particularly interesting biomaterial is the one derived from silks, due to its highly unique, inherent properties. For example, it has slow biodegradation^[24] and it is hypoallergenic.^[25] Originally, among a multiplicity of silks, only silkworm silk could be used for biomedical engineering, due to the difficulty of collecting silk from other animals and the challenges in biotechnological production. However,



Tamara Bernadette Aigner graduated from the double degree Bachelor's and joint Master's program for biological chemistry at the Johannes Kepler University (Austria, Linz) and the University of South Bohemia (Czech Republic, České Budějovice). She is currently a

Ph.D. candidate at University of Bayreuth (Germany) under the supervision of Thomas Scheibel and her research focuses on using recombinant spider silk proteins as a biomaterial for heart muscle and nerve regeneration.



Elise DeSimone received her Bachelor's degree in biomedical engineering from Rensselaer Polytechnic Institute (Troy, New York) and Master's degree in biomedical engineering from Tufts University (Medford, Massachusetts). She is currently a Ph.D. candidate at University of Bayreuth (Germany) under the

supervision of Thomas Scheibel and her current research focuses on the use of recombinant spider silk proteins as a biomaterial for biofabrication.



Thomas Scheibel has been full professor at the department of biomaterials at the Universität Bayreuth in Germany since 2007. He received both his Diploma of Biochemistry (1994) and a Dr. rer. nat. (1998) from the Universität Regensburg in Germany. After his postdoc at the University of Chicago

(1998–2001), he received his habilitation (2007) from the Technische Universität München in Germany. His research focuses on biotechnological production and processing of structural proteins, as well as their biomedical and technical application.

over the past 15 years, the recombinant production of silk proteins has been optimized to the extent that it can even be manufactured.^[26] Therefore, considering its favorable properties for biomedical applications and its recently realized availability, we believe and will try to present the case in this review that recombinant silk proteins could be one of these new biomaterials.

3. Silk

3.1. Natural Silk—What Is Silk?

Silks have a long history as a natural resource; silk from the silkworm *Bombyx mori* (*B. mori*) was used for weaving precious textiles in China, and was a greatly sought after product by the Europeans, with attempts to smuggle worms on the silk road.^[27] Natural silk even played a role in the early developments of the modern medicine, being identified as biocompatible and hypoallergenic, as well as suitable for direct use as wound dressing or surgical thread.^[28]

Craig defined silk as follows: “Silks are fibrous proteins containing highly repetitive sequences of amino acids and are stored in the animal as a liquid and configure into fibers when sheared or “spun” at secretion.”^[29] The most notable part of this definition is that silks are fibrous proteins, unlike glues, which are processed directly out of a highly concentrated solution, which is a process unlike that for other fibrous proteins such as collagen.^[29] Silks have evolved in many organisms independently, and some of their general characteristics are presented in Figure 1.

Silks are mainly composed of structural proteins, and their functionality can be traced back to their primary amino acid

sequences, which is rich in alanine, serine, and/or glycine. Although several different silk structures are possible, from β -sheets over α -helices to coiled-coil to collagen/polyglycine families, usually silk materials, depending on their equilibrium state, have either a high content of β -sheets or α -helices. When a solid silk morphology has high β -sheet content, usually these β -sheet structures resemble crystallites. Normally this would result in a material which is strong and brittle, however, silk is not brittle; silk is tough. This is because the β -sheets are surrounded by α -helices and coils, which act as a matrix phase. In other words, silks processed into water-insoluble fibers are semi-crystalline biopolymers and it follows that silk fibers with higher crystalline content are usually stronger or tougher.^[30]

Due to the significance of secondary structures to material properties, and as will be later shown to the response of cells, they are usually characterized every time a new silk protein is produced, or a different processing technique is used. To determine secondary structure content, commonly circular dichroism (CD) spectroscopy or Fourier-transform infrared (FTIR) spectroscopy in solid or liquid phase are performed. In interpreting CD measurements, core domains of silk proteins in solution at room temperature typically show random coil, polyproline II-like conformations or α -helical structures. The

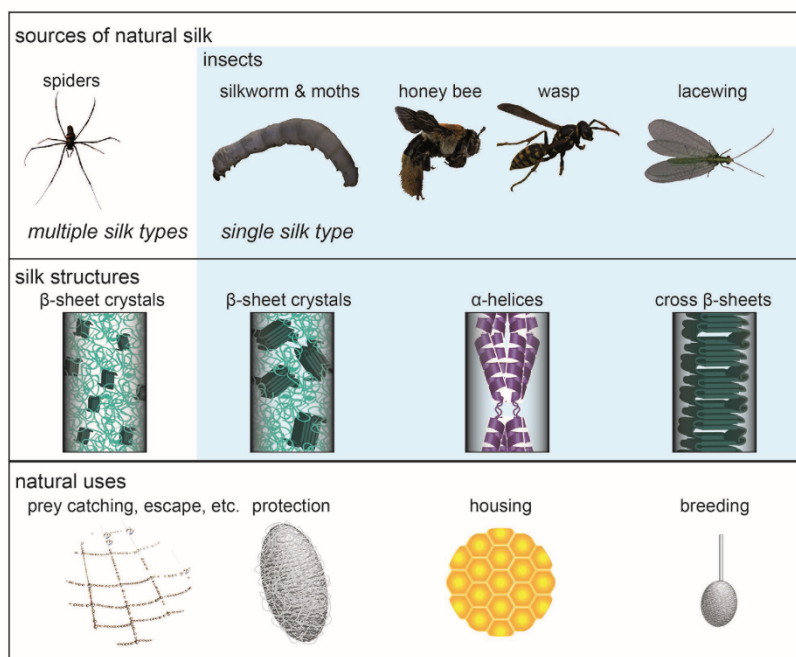


Figure 1. Natural silks. Natural silks of spiders, silkworms, moths, bees, wasps, and lacewings were used as an inspiration for the recombinant production of silk proteins to be used for biomedical applications. Spider and silkworm silk consist of β -sheet crystals embedded in an amorphous matrix. The huge difference in these two silk types is that these crystals in spider silks are much smaller and perfectly aligned along the fiber axis. Honey bee and wasp silk mainly consist of coiled-coil structures. Lacewing silk is composed of cross- β -sheet structures allowing a high bending stiffness. These secondary structural features evolved due to the desired function, e.g., a spider silk web has to withstand the force of a flying prey being caught without breaking, and the egg stalk should be able to carry an egg and protect it from predators. Silk worm, honey bee and wasp photos were taken and modified from open source images found on Pexels or Pixabay.

terminal domains in spider silk proteins, in contrast, often show α -helical structures, revealing α -helix bundles. When the protein solution is heated, conformational changes occur in the core domain forming β -sheet and/or β -turn structures.^[31] In FTIR spectroscopy the sum of these C=O stretching vibrations is found in the broad amide I band located between 1705 and 1595 cm^{-1} . Several methods were developed to retrieve information about the secondary structure content from the amide I band. To estimate the single bands which form the broad and undefined amide I band, Fourier self-deconvolution (FSD) is applied as described in Hu et al.^[32] Each of the single bands can then be assigned to a secondary structure motif, and thereby the percentage of each structural element can be calculated. The secondary structure content of solid silk samples differs remarkably between the species and the treatment of the material, for example, recombinant honey-bee silk mainly consists of coiled-coil structure (60%), whereas recombinant spider silk can reach a β -sheet content of about 40%.^[31,33]

Silks are produced in many arthropods and are important for survival and reproduction. Interestingly, different silks and their glands have evolved independently, which is the basis of some key differences in the silks between different animals. In insects, silk is produced in Malpighian tubules, labial, or dermal glands. Silks produced in the labial glands of different animals show all five known silk protein structures (coiled-coil, extended β -sheet, cross- β -sheet, collagen triple helix, polyglycine II) as they are used for various functions. In dermal glands silks only adopt β -sheet structure, and Malpighian tubule silks form either cross- β or α -helical structures.^[30]

In contrast to most insects, which can produce one silk type only,^[30] orb weaving spiders are able to produce up to seven different silks, each in a separate gland.^[34] However, dragline silk, the silk which spiders use for escaping danger and creating the strong frame of their webs, usually receives the most attention. These dragline fibers comprise primarily two protein classes, major ampullate spidroin 1 and 2 (MaSp1 and MaSp2).^[35] The main difference between MaSp1 and MaSp2 is that MaSp1 is almost proline-free, while MaSp2 contains about 15% proline residues.^[36]

3.2. Recombinant Silk—Why Go Recombinant?

There are many drawbacks to harvesting from natural biomaterial sources, these include batch-to-batch variation, impurities, risk for disease transmission, risk for rejection by immune response, and gathering in substantial (useable) quantities.^[37] In the case of silks, the main drawback of harvesting the material, with the exception of *B. mori* silk, is that large scale farming of most of the animals is not possible or harvesting the material is complicated (e.g., lacewing silk). Spiders are particularly difficult to domesticate, as most species are territorial and cannibalistic.^[38] Nevertheless, efforts have been made to harvest native silk from *Nephila* spiders and combine it with decellularized, porcine veins to prepare nerve guidance conduits.^[39] Insects such as lacewing flies or bees are easier to farm, however they produce minuscule amounts of silk, and harvesting these silks would not only be tedious, but would severely limit their applications due to the limited amount of material.^[40] Consequently,

in terms of sourcing, silk is less accessible unlike other natural materials such as collagens, which are abundant, however are at higher risk for an undesirable response upon implantation. Collagen has been associated with product impurities, disease transmission, and increased likelihood of bacterial infection.^[41]

To create an alternative source of biomaterials, biotechnological solutions have been developed to produce larger amounts of protein with more consistent quality and greater biological safety. Although this was a challenging endeavor, over the course of 15 years recombinant silk protein production has become well-established, and some variants are even available commercially.^[26] To continue with the previous comparison, collagen is also favorable for protein engineering in that it has a repetitive amino acid sequence. In the case of collagen, this repetitive sequence is characterized by motif Gly-X-Y where Y is most commonly hydroxylated proline.^[42] Hydroxylation of the proline is a highly complex process requiring special enzymes. Therefore, in spite of its repetitive amino acid sequence, collagen cannot be produced by most expression systems due to its need for extensive post-translational modification.^[41] In this respect, recombinant silk proteins could be considered more ready than recombinant collagen proteins.

For a more in depth discussion on the challenges of recombinant silk production, the authors refer readers to in-depth reviews on this subject.^[43]

Several steps are required to design and produce a recombinant protein. They can be roughly divided by natural DNA sequence determination, recombinant DNA design based on natural sequence, vector cloning, host organism transformation, induction, and purification of the protein.^[44] When engineering recombinant protein, it is often advantageous to engineer the sequence to be produced more efficiently, while maintaining its key functions. Although a demanding task, this offers huge advantage in terms of studying these proteins, and further allows for hybridizing or functionalizing recombinant silk protein (Figure 2). The most often used host organism for recombinant silk protein production is *Escherichia coli* (*E. coli*), and therefore, the process will be explained from this perspective, although other hosts are also available and have been recently reviewed.^[43c,d]

Recombinantly produced silk proteins have been in general shown to be versatile in terms of being able to form several, tailorable morphologies. They can be formed into films, capsules, particles, foams, hydrogels, micrometer-fibers and nanofibers (Figure 3). This allows a wide range of applications in different fields.

3.3. Nomenclature

The authors would also like to make a few direct comments regarding nomenclature, as this is sometimes challenging in the field of recombinant silk proteins, especially with spider silks. This is because spider silk can be characterized by species, silk type (e.g., dragline or flagelliform silk) and/or protein type (e.g., MaSp1 vs MaSp2). Further, there is sometimes confusion between silk proteins produced by insects (fibroins) versus silks produced by spiders (spidroins), and spider silk proteins are often referred to as both (fibroin

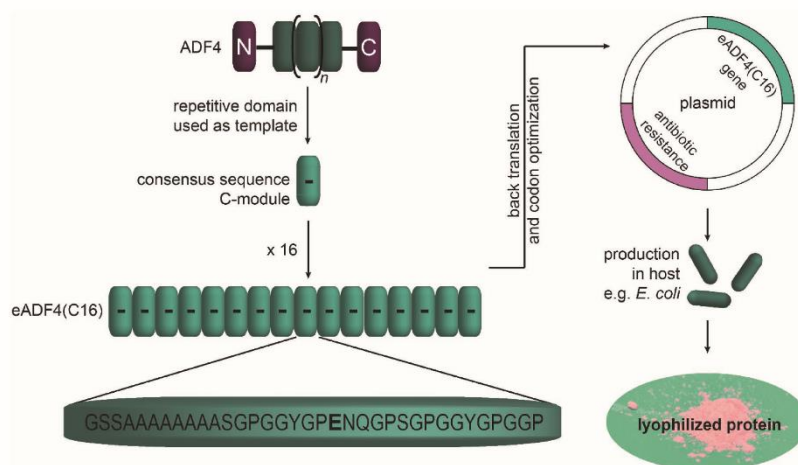


Figure 2. Development of recombinant silk protein using eADF4(C16) as an example. The repetitive core of *Araneus diadematus* fibroin 4 (ADF4) was identified and used as a template for the C-module. This C-module was then repeated 16 times to create the engineered ADF4 (eADF4(C16)). The amino acid sequence was back translated and codon optimized for the host organism (here *E. coli*). A plasmid containing the silk gene and a gene for antibiotic resistance to allow selection was created. The host was then transfected and protein production triggered. After several purification steps protein powder was obtained, which can be further processed into different morphologies.

or spidroin), whereas silkworm and insect silk proteins are referred to exclusively as silk fibroin.

Most recombinant spider silk proteins are based on *Nephila clavipes* sequences and refer to their spidroins as MaSp1 and MaSp2, depending on their proline content (MaSp1 low, MaSp2 high). Other recombinant spider silk proteins are based

on *Araneus diadematus*, which has two identified proteins in dragline silk named as fibroins 3 and 4 (ADF3–ADF4), however both are MaSp2 proteins.^[45] In most other cases, even though the recombinant spider silk protein is based on a different spider than *Nephila clavipes*, the protein will be referred to as MaSp1 or MaSp2. Another way researchers name their recombinant

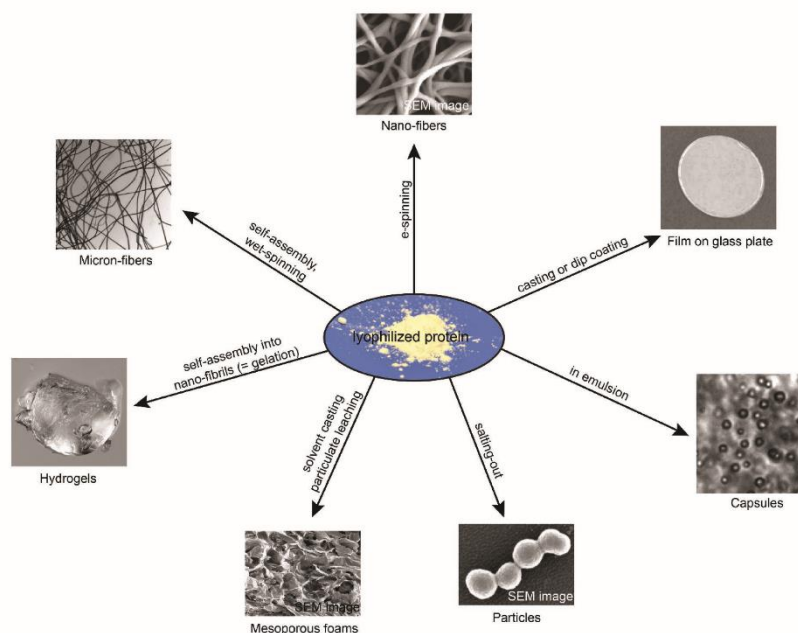


Figure 3. Processing routes for recombinant silk proteins to prepare different morphologies.

proteins is based on their molecular arrangement, or based on the number of consensus modules in the sequence.

As a further complication, throughout the course of their research, some groups will change their naming system of their proteins, making it difficult to differentiate between a newly designed recombinant protein or a variation or optimization of an earlier recombinant protein. Although the decision to rename an existing protein is often justified, it can be difficult to follow throughout the literature. A few examples in which researchers change the name of their recombinant protein is for “15mer”^[31a] also called MS1,^[46] eADF4(C16) which was originally ADF4(C16)^[47] or C₁₆,^[48] and rS1/9^[49] which is also called 1F9.^[50]

To provide a guide for the reader for this review, recombinant silk proteins used in BME are summarized in Table 1.

4. Regenerative Medicine

Damaged human tissues or organs are rarely able to completely regenerate, the regenerative capability depending directly on the tissue type and the severity of the damage. Regenerative medicine is the field dedicated to creating tissue or organ-like implants in order to heal or replace damaged tissues or organs.^[64] The important concepts and definitions will be presented here; however, the authors encourage interested readers to explore other reviews and opinion pieces, which delve into the topic of regenerative medicine and importantly touch on critical points as well as scientific debate in the field.^[65]

The largest subfield of regenerative medicine is tissue engineering, which is the selection and spatial arrangement of cells and biomaterials for artificial tissue design. The approach used is typically characterized as bottom-up or top-down, where bottom-up refers to modular assembly of building units into tissue-like constructs, and top-down refers to simply combining the components and allowing them to self-form structures.^[66] Which type of method is used, bottom up or top down, usually depends on the problem which must be solved. For example, there are some cases where a fully matured tissue must be implanted because the implant must function immediately, such as in heart or heart tissue replacement. On the other hand, there are tissues which can benefit from a slow healing process, for example in neurological tissues where there is a nerve gap. Regardless of the technique, the “building blocks” for implants made based on regenerative medicine principles are biomaterials, cells, soluble bioactive factors, and specialized, in vitro culturing conditions (e.g., mechanical stimulation through liquid flow) (reported by nibib online^[64b]). It is important to note that not all these “building blocks” must be used in one construct, and it is widely debated which of these components are truly necessary for regenerative medicine.

In this review, the tissue engineering design element focused on is biomaterials based on silk proteins. As defined by the National Institutes of Health in the 1980s a biomaterial is “any substance (other than a drug) or combination of substances, synthetic or natural in origin, which can be used for any period of time, as a whole or as a part of a system which treats, augments, or replaces any tissue, organ, or function of the body.”^[67] Biomaterials are not to be confused with

biogenic materials, which are defined as materials produced in nature.

Due to its principle role in tissue function, researchers often try to recapitulate properties of the extracellular matrix (ECM) by altering the morphology of the biomaterial, introducing gradients of biomaterials, and so on. One of the most significant design elements of a biomaterials scaffold is dimension that the cells are cultured in (1D, 2D, or 3D); in 1D cells form elongated shapes, which polarizes the cells (e.g., cortical neurons), in 2D cells tend to form monolayers as in the case of membrane tissues (e.g., endothelial cells), and in 3D cells tend to form irregular shapes with many filopodia, and this is the environment which most cells are exposed to.^[68]

4.1. Micrometer-Fibers Made of Recombinant Silk Proteins

“Micrometer-fiber” is a term which will be used by the authors to describe fibers which have diameters in the micrometer-range. In terms of silk proteins, the most classic example of producing these fibers is by biomimetic or wet spinning, the latter being the extrusion of a spinning dope into a coagulation bath.^[69] However, to the best of the authors’ knowledge, there are only limited number of papers using wet-spinning to investigate for the potential for use of silk-based micrometer-fibers for tissue engineering applications (e.g., suture materials).^[70] This is unexpected in that wet-spun fibers usually provide the best mechanical properties out of all fiber production methods (raw extracted, electrospinning, microfluidics), as well as the excellent control of fiber diameter.^[70] That this technique is used less often than other techniques is likely due to the fact that the fibers cannot be produced as quickly or in the same quantity as in the other production methods. Therefore, wet-spinning will not be extensively discussed in this review.

Micrometer-fibers have also been further processed by braiding, weaving, chopping, and combining into nonwoven meshes.^[31b,59,71]

4.1.1. Micrometer-Sized, Recombinant Silk Fibers, Fiber Meshes, or Fiber Knits in Tissue Engineering

Self-assembled 4RepCT fibers were evaluated concerning toxicity and immunogenicity by subcutaneous implantation in rats.^[72] No toxicity was detected, and the immunogenicity was low as determined by the presence of infiltrated immune cells, and the formation of fibrous capsule or granulation tissue. A particularly important point of this study was the removal of endotoxins, a common problematic by-product of recombinant proteins produced in *E. coli*. Next, it was shown that the self-assembled micrometer-fibers could be sterilized without negative effects on the fiber properties, Figure 4.^[73] This is a clear benefit of this particular protein variant toward tissue engineering, as endotoxin-free, sterile materials are necessary to qualify for Food and Drug Administration (FDA)-approval.

After pilot studies were complete, fiber meshes were produced from 4RepCT self-assembled fibers, and compared to films and foams for promoting growth of primary fibroblasts as well as maintenance of differentiation state (as measured by

Table 1. Recombinant silk proteins used in biomedical engineering applications, not including information on modified versions (e.g., with RGD sequence).

Origin species	Natural protein	Recombinant protein	Host	Molecular weight (recombinant protein)	Unique features of the recombinant protein primary sequence	Reference
<i>Antheraea pernyi</i> (moth)	Fibroin	EAEFN _{5/16}	<i>E. coli</i> strain BL21	≈11.4 kDa, ≈22.9 kDa	G-rich, poly-A repeat, repetitive unit repeated 5 or 10 times	[31d]
<i>Apis mellifera</i> (honey bee)	AmelF1-4	Recombinant AmelF1, AmelF2, AmelF3, AmelF4	<i>E. coli</i> strain Rosetta 2 (DE3) competent cells	32 kDa	29–33% alanine, amino acid sequence of recombinant protein exactly the same as natural protein	[51]
<i>Bombyx mori</i> (silkworm)	Heavy chain (H-chain)	Transgenic silk fibroin	Transgenic silkworm, <i>B. mori</i>	N/A—Variable; Natural silk fibroin = 100–400 kDa, usually ≈300	Natural silk fibroin characterized by silk fibroin block (GAGAGS)	[52]
<i>Bombyx mori</i> (silkworm)	Light chain (L-chain)	L-RGDSx2 fibroin (LRF)	Transgenic silkworm, <i>B. mori</i>	N/A—Variable; Natural silk usually ≈26 kDa	Natural silk fibroin light chain modified with RGD binding sequence	[53]
<i>Bombyx mori</i> (silkworm)	Crystalline	[(AGSGAG) ₄ E ₈ AS] ₄	Transgenic silkworm, <i>B. mori</i> and <i>E. coli</i>	19.9 kDa (theoretical 19.7 kDa)	Polyglutamic acid for calcium binding	[54]
<i>Bombyx mori</i> (silkworm) and "mammalian"	Silk fibroin and elastin	SELP-47K and SELP-815K	<i>E. coli</i> strain HB101	SELP-815K ≈65 kDa SELP-47K ≈70 kDa	Silk fibroin block (GAGAGS) and mammalian elastin-like block (GVGVP) either with silk 4 times and elastin 7 times (SELP-47K) or with silk 8 times and elastin 15 times (SELP-815K)	[55]
<i>Chrysopa carnea</i> (lacewing)	MalXB2	N[AS] ₈ C	<i>E. coli</i> strain BL21 (DE3)	53 kDa	AS module repeated 8 times	[33b,56]
<i>Vespa similima</i> (hornet)	Vsilk1-4	Recombinant Vsilk1-4	<i>E. coli</i> strain BL21	30–70 kDa	Relatively low number of repetitive sequences, amino acid sequence of recombinant protein exactly the same as natural protein	[57]
<i>Araneus diadematus</i> (spider)	ADF-4 (MaSp2)	eADF4(C16), eADF4(K16)	<i>E. coli</i> strain BL21	48 kDa	GPGXX-rich with poly-A sequence, module is repeated 16 times	[58]
<i>Euprosthenops australis</i> (spider)	MaSp1	4RepCT	<i>E. coli</i> strain BL21	23.4 kDa	G-rich, poly-A repetitive unit repeated 4 times	[31b,59]
<i>Nephila clavipes</i> (spider)	MaSp1	6mer, 15mer	<i>E. coli</i> strain or RY-3041, a mutant BLR (DE3) defective in the expression of SlyD protein	16–22 kDa, 40–50 kDa	G-rich, poly-A monomer	[31a,60]
<i>Nephila clavipes</i> (spider)	MaSp1	1F9 and rS1/9	<i>Pichia pastoris</i> (yeast) or <i>Saccharomyces cerevisiae</i> (yeast)	94 kDa	9 monomer repeats, monomer contains consensus primary repeats	[49,50,61]
<i>Nephila clavipes</i> (spider)	MaSp1, MaSp2	rMaSp1, rMaSp2	Transgenic goats	65–120 kDa	not defined	[62]
<i>Nephila clavipes</i> (spider)	MaSp1	MS1 (15mer)	<i>E. coli</i> BLR (DE3)	MS1: 39 kDa	MS1: G-rich, poly-A, repetitive unit repeated 15 times	[46,63]
	MaSp2	MS2 (9mer)		MS2: 28.15 kDa	MS2: G-rich, poly-A, 4x Q, repetitive unit repeated 9 times	

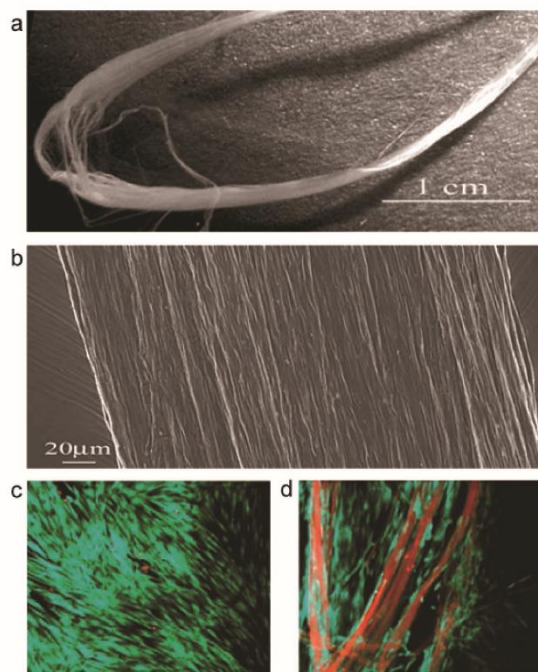


Figure 4. Sterilized, self-assembled 4RepCT micrometer-fibers as visualized by a) photography and b) SEM. Fibroblast attachment and proliferation for 7 d on c) tissue culture plastic (TCP) as a control and d) sterilized 4RepCT micrometer-fibers as evaluated by LIVE (green)/DEAD (red) staining. Micrometer-fibers were also nonspecifically stained red by the staining solution. The micrometer-fibers showed cell attachment comparable to the TCP control, and the lack of dead cells indicated there was no cytotoxicity. Reproduced with permission.^[73] Copyright 2010, American Chemical Society.

collagen I production).^[71] As in the case for most silks, it was clear that inclusion of a cell-binding peptide would be necessary for proper cell attachment, and variants modified with either the tri-peptide RGD (Arg-Gly-Asp), RGE (Arg-Gly-Glu, negative control for RGD), the penta-peptides IKVAV (Ile-Lys-Val-Ala-Val), or YIGSR (Tyr-Ile-Gly-Ser-Arg) were also tested.^[74] There was no challenge or observed changes in the self-assembly of fibers made of 4RepCT modified with cell binding peptides, however cell attachment was significantly enhanced on films made thereof. 4RepCT has also been modified with several other binding sequences, as well as antibiotics to repress bacterial growth.^[75]

The potential of self-assembling fibers 4RepCT for specific applications was introduced in Johansson et al., where the performance of 4RepCT as a biomaterial for pancreatic islet formation was evaluated. The authors compared the performance of films, foams, and meshes made of self-assembled fibers. Pancreatic donors were collected either from C57Bl/6J mice or from human islets of diseased patients. The islets were evaluated for cell viability and attachment, as well as insulin production and the amount of intracellular calcium. The best performance was on RGD functionalized 4RepCT

assembled into foams, and the details of these results are therefore described in the foams section of this review.^[76]

When silkworms build their cocoons, these consist of one long, winding thread with a protein core surrounded by sericin gum. To remove the sericin, or to “degum” the fibers, cocoons or cocoon pieces are boiled, and the remaining product is intact silk fibroin threads, usually referred to as regenerated silk fibroin (RSF). These fibers can then be used as single strands, bundled into yarns, or woven into a knit structure.^[77] In a preliminary study, wild-type and transgenic worm RSFs modified with adhesive collagen sequence were used to prepare small-diameter vascular grafts.^[77a] The grafts were created by winding onto a tube template (1.5 mm diameter, 10 mm long) using a 16-bobbins braiding machine. The grafts were further coated with aqueous RSF solution, post-treated with 50% ethanol, and then removed from the template. Male Sprague–Dawley rats were used as an animal model for implantation in the abdominal aorta. After 12 months there was significantly high patency in wild-type silk fibroin compared to poly(tetrafluoroethylene) grafts, and there was infiltration of cell types as well as structured vessel formation after 4–12 weeks. At this stage, the recombinant silk fibroin production is still needed to be optimized, and therefore only an *in vitro* examination was conducted, and showed enhanced attachment of endothelial cells.

In further work, the transgenic worms were modified to produce silk fibroin, which includes vascular endothelial growth factor (VEGF) or RGD sequences in the heavy chain.^[77c] The successful production was confirmed using western blotting and antibody staining, however there was no quantification of the ratio of modified and unmodified heavy chains. Human umbilical vein endothelial cells showed enhanced cell attachment proliferation on the modified variants. Further, the grafts were tested for attachment of serum proteins, as attachment of serum proteins results in a closing of the graft to blood flow. In this study, the attachment of platelets was evaluated *in vitro* as well as patency *in vivo*. *In vitro*, it was found that both VEGF and RGD modified silk fibroin showed enhanced attachment of platelets compared to materials made of the unmodified silk fibroin. However, materials of the RGD variant showed far less patency *in vivo* compared to that of both unmodified silk and VEGF modified variants, and the authors hypothesized this was due to thrombosis.

In conclusion, VEGF modified silk fibroin-based materials not only showed the best patency, but showed the best tissue infiltration and new vessel formation, making this variant particularly promising for future application.^[77c] Furthermore, there seemed to be a clear benefit of fibers which were fixed into some kind of morphology (braided, mesh) over free-floating fibers, implying that, although it was important to test the fibers independently, practically micrometer-fibers need to be reformed to be useful in application.

4.2. Sub-Micrometer and Nanofibers

Sub-micrometer and nanofibers are used in regenerative medicine due to the size relevance of such fibers to many natural structures found in tissues.^[78] When used alone and not in composite scaffolds, the most common tissue engineering

applications of such fibers are in the context of membrane tissues and/or hollow tubes such as vascular grafts,^[79] nerve guides,^[80] skin grafts, or wound dressings.^[81] One common technique to produce sub-micrometer and nanofibers is electrospinning.

Electrospinning is the formation of fibers in the micrometer to nanometer range by electrically charging a slowly extruded solution.^[82] First, a droplet forms at the tip of the needle, and, if the parameters are set correctly, the force of the electrical charge overcomes the tension of the droplet, and a jet is formed. Eventually, the jet undergoes whipping instabilities, thereby stretching the jet, in the ideal case, into an ultrathin fiber which forms the mat.^[82,83] The main advantages of electrospinning are that it requires low working volumes to produce large amounts of scaffold, and there is relatively fine control over what is produced. However, the disadvantage is that mats produced from electrospinning are generally 2D, although it is technically possible to produce 3D scaffolds.^[84] Further, low molecular weight (i.e., most recombinant proteins) polymers or proteins are often difficult to use in electrospinning, although this can usually be overcome by increasing the concentration.^[85] Another disadvantage to electrospinning solutions is that they are commonly produced by dissolving the solute in toxic, fast evaporating solvents. This, combined with the extreme electrical voltage, makes the process less friendly to biological agents exposed to the process, and can also be considered dangerous from a regulatory point of view.

4.2.1. Recombinant Silks Processed into Nonwoven Fiber Mats for Tissue Engineering

In an evaluation of Balb/3T3 mouse fibroblast adhesion of films, hydrogels, and nonwoven mats produced from recombinant spider silk eADF4(C16), one of the most interesting results was that, without introduction of an RGD sequence, cells were able to attach to nonwoven meshes. This was surprising, since the flat films prepared by the same recombinant protein resulted in low cell adhesion. Interestingly, there was a strong dependence of the cell attachment on the fiber diameter.^[33a] Through these studies it was shown that the bioactivity of cells on recombinant spider silk materials can also be enhanced by changing the morphology, and in this study it was assumed that the fiber diameter primarily determines the success of cell attachment. However, it is difficult to say if the negative space or the fibers themselves contributed to the cell attachment, as both the architecture of the fibers as well as the porosity play a significant role in this process.^[86]

In a similar study, attachment of primary green fluorescent protein (GFP)-expressing fibroblasts from rabbits to AmelF3 (recombinant honey bee silk, Table 1) nonwoven meshes was evaluated.^[31b] In this case, an aqueous solvent was used for electrospinning, but poly(ethylene oxide) was added as a fiber forming agent. It was shown that there was fibroblast monolayer formation in 7 d, without any modification to the protein, as in the case of eADF4(C16). However, in this case, there were no films cast as a further control, and no citations or previous work are available showing cell culture on films made of the recombinant honey bee silk protein. Therefore, it is not

possible to definitively conclude if the attachment of cells on this recombinant silk is due to its biochemical or physical character, or if it was due to the use of this morphology.

A more complex example of using nonwoven mats produced from recombinant spider silk proteins was exhibited in Zhu et al., using MaSp1/MaSp2 blended with collagen. The spinning dopes were at concentrations of 100 mg mL⁻¹ and comprised of either collagen type I, 4:1 MaSp1/MaSp2, or a blend of the two. Here, human decidual peritendal placental stem cells were cultured on the nonwoven mats and tested for proliferation and neural differentiation.^[87] MaSp-based nonwoven meshes had the advantage that they resisted degradation in Dulbecco's Modified Eagle Medium and were mechanically stronger (Young's modulus <1 GPa for collagen-based and ≈4.5 GPa for MaSp-based fibers). On the other hand, the collagen-based nonwoven mats were more biologically active with increased attachment as well as increased expression of β -tubulin III, a structural protein found in the axons of neurons. To try to achieve both of these properties, they experimented with the ratios of collagen and recombinant spider silk protein in the spinning dope, and it was found that the fibers produced from 30% MaSp content seemed to be the best balance between the two properties, mechanical stability, and bioactivity, showing resistance to degradation as well as significant differentiation of the stem cells. However, these nonwoven meshes were only cultured for 7 d, and neural cell differentiation and maturation is a much longer process, and perhaps it would have been more advantageous to use less collagen and allow for longer growth periods.^[19b] Another possible route for this would be instead to use mixtures of recombinant protein variants, which have collagen-associated cell-binding peptides, or other neuronal growth factors. Thereby, the mechanical stability of silk would not be compromised by blending.

In summary, fiber mats are an interesting morphology bridging the gap between flat films and complex 3D networks like hydrogels. It was shown that sub-micrometer fiber morphologies can enhance the cell attachment. However, there seems to be further benefits of including cell-recognition sites, which should be considered in terms of producing functional tissue, but have not been thoroughly analyzed so far.

4.3. Films

Films are the morphology of choice for screening the response of cells to the biochemical features (e.g., cell-binding sites), cytocompatibility, and physical (e.g., charge) character of the biomaterial. The small amount of material required, the ability to control the effects of topology and mechanical stiffness, as well as the ease and simplicity for high-throughput experiments, makes films a particularly powerful tool for initial characterization of the material. Especially in terms of recombinant proteins, this can be a crucial point due to the low amount of available material before the production is optimized. Films have been produced by recombinant silk proteins 4RepCT, eADF4(C16), N[AS]₆C, 6/15mer, MaSp1/MaSp2 (transgenic goats), Vssilks, EAEFN_n, transgenic fibroins and variants thereof.

4.3.1. Recombinant Silks Processed into Films

Silk films are usually produced by casting a silk solution within various solvents like 1,1,1,3,3,3-hexafluoro-2-propanol (HFIP), formic acid, aqueous buffers, or mixtures thereof. Due to the rapid evaporation of HFIP after casting, the proteins remain in the same equilibrium state of secondary structures as if they were in solution, and films must be post-treated to be rendered water insoluble. The post-treatment step usually is incubation in primary alcohols like methanol or ethanol at various percentages ranging from 70% to anhydrous.^[31a,33a,d,57b,88] One exception is that, if cast out of formic acid, the proteins tend to immediately convert into β -sheet rich structures, and therefore post-treatment is not necessarily required.^[33b,e] Films out of aqueous solutions were sometimes post-treated with alcohol,^[31a,57a,60b,89] and sometimes used as obtained.^[71,74–76,90]

The surface characteristics of silk films such as surface topography, roughness, and composition are commonly investigated by various microscopy techniques such as atomic force microscopy (AFM),^[89a,91] light microscopy, and scanning electron microscopy (SEM).^[89c,92] These types of assays have shown that generally silk films are smooth. Surface hydrophobicity is typically studied on films using contact angle measurements, which have revealed that recombinant silk films tend to be slightly hydrophilic (contact angle between 55° and 90°).^[53a,57b,88a,89a] Given how similar recombinant silk films seem in materials characterization tests, the results in cell culture were surprisingly different.

One of the most common ways to evaluate recombinant silk proteins films is by determining cell attachment and proliferation. 4RepCT films were incubated with human fibroblasts, and although no cell recognition sites were present, cells adhered, proliferated, and produced collagen I.^[71] Several cell binding motifs—RGD, IKVAV, YIGSR, and RGE as negative control—were generated. Primary human fibroblasts, keratinocytes, endothelial, and Schwann cells were seeded on silk films with the different binding motifs. Focal adhesions of fibroblasts, keratinocytes, and endothelial cells were best on films of the RGD variant, whereby Schwann cells seemed to prefer films made of the IKVAV variant.^[74] Films of different silk variants bearing a fibronectin motif, with RGD being presented in a loop similar to native ECM, were incubated with human primary cells, which showed an increased attachment, spreading stress fiber formation and focal adhesion points compared to RGD-4RepCT. Moreover, human dermal microvascular endothelial cells (HDMVEC), human mesenchymal stem cells (hMSC), and human epidermal keratinocytes (NHEK) were able to attach and proliferate, and NHEK could be directed to migrate into a wound area.^[93] By contrast, eADF4(C16) films resulted in low cell adhesion and proliferation of Balb/3T3 mouse fibroblasts, likely due to the fact that this protein lacks specific domains for cell adhesion, has a net negative charge, and the films have a smooth surface.^[33a] An RGD tag was covalently bound to the C-terminus by introducing the encoding sequence directly into the recombinant DNA sequence, or via chemical coupling of a cyclic RGD-peptide to the N-terminus; both variants tremendously improved Balb/3T3 adhesion compared to that on the RGE-modified control.^[89a]

In Kambe et al., the attachment of chondrocytes isolated from white rabbits was tested on films produced from fibroins with different numbers of RGD motifs per recombinant protein. Indeed, it was shown that primary chondrocytes exhibited a spread morphology on films of the L-RGDSx2 after 12 h, which was not found on films of native fibroin. A modified cantilever was used to determine the adhesive force and demonstrated an increase in adhesive strength on the RGD modified fibroin surface. Further, real-time polymerase chain reaction (qPCR) measurements revealed that this increased cell adhesive strength did not occur at the expense of down-regulating the chondrocyte-specific phenotype. Thus, films of the L-RGDSx2 fibroin containing two RGD motifs in the fibroin light chain were determined to be a promising substrate for primary chondrocytes.^[53a] Films made of four recombinant silk proteins of *Vespa similima* horns were also investigated. It was shown that Vssilk1 and Vssilk2 film surfaces are positively charged at physiological pH and were rather hydrophobic with water contact angles between 85° and 90°. It was therefore not surprising that there was a significant higher cell adhesion on films made of Vssilk1 and 2 than of Vssilk3 and 4. It was proposed that this effect comes from a cell–substrate interaction mediated by adsorbed negatively charged ECM proteins, for instance collagen I or fibronectin.^[57b] In a further study, an RGD motif was added to Vssilk1, which improved NIH3T3 fibroblast adhesion.^[57a]

Independent of cell-binding motifs, it was also shown that by structuring films of different eADF4(C16) variants and the lacewing egg stalk mimic N[AS]₆C, the attachment of Balb/3T3 fibroblasts and C2C12 myoblasts can be improved. Moreover, the cells aligned in the grooves of the structured films, independent of the silk proteins and variants used, and myoblasts even formed myotubes.^[33b] Films of transgenic silkworm silk have also been analyzed by several groups. In Yanagisawa et al., a collagen or an RGD motif was added to the light chain of fibroin in an attempt to improve cell adhesion. Tests using Balb/3T3 fibroblasts showed that on films of both constructs adhesion could be improved compared to that on films of native fibroin, whereby RGD modified silks resulted in the best performance.^[52c]

Recombinant silk films have also been used as screening tools for more specific applications. On 4RepCT films, mouse and human pancreatic islets were studied. The cells were investigated in terms of viability and function by their Ca²⁺ and insulin release as well as the islet morphology and immunohistochemistry were assessed.^[76] Lewicka et al. investigated neural stem cells (NSCs) on 4RepCT films and showed that before differentiation cells could proliferate and after differentiation with ciliary neurotrophic factor matured into astrocytes and after differentiation with bone morphogenetic protein matured into neurons. However, differentiation with the thyroid hormone T3 into oligodendrocytes resulted in a lower success rate compared to the positive control (poly-L-ornithine and fibronectin coated plates). These results suggest the applicability of 4RepCT films in combination with NSCs for drug screening and in the future for cell therapy-based treatments of neurological disorders like Parkinson's disease or traumatic spinal cord injuries.^[90a] In the study by An et al. MaSp1 and MaSp2 films were compared to *B. mori* silk films, and it

was shown that cortical neurons grow on MaSp1 films only. The hypothesized reason for this behavior is that MaSp1 films are not only stiffer, but also inherently positively charged at neutral pH. Thus, the neural cell adhesion molecule (NCAM), which is negatively charged, preferably attaches to this silk film. A significant increase in NCAM protein level was determined by qRT-PCR. Additionally, they found a GRGGL (Gly-Arg-Gly-Gly-Leu) motif in MaSp1, also found in brain aggrecan core protein, which seems to support neural growth.^[88b]

MaSp1 derivatives 15mer and 15mer conjugated with the RGD cell binding motif films were evaluated for the attachment of hMSCs, as well as the tendency of the MSCs to biomineralize the scaffold. Interestingly, a higher amount of calcium as well as a higher proliferation was obtained on films of the 15mer without the RGD tag. Although experimentally unconfirmed, it was speculated that the RGD motif was not accessible on the surface.^[31a] To remedy the problem, the silaffin derived R5 tag, which is responsible for silica mineralization in *Cylindrotheca fusiformis*, was tagged onto 15mer. hMSCs were grown on films with and without silica nanoparticles (SNPs) and on both a comparable cell growth and morphology was shown in comparison to growth on plain tissue culture plates. However, an up-regulation of osteogenic genes (alkaline phosphatase and bone sialoprotein (BSP)) was found mainly in SNP containing samples.^[92] In a later study, the 6mer was genetically coupled with BSP to induce bone mineralization in vitro. Calcium phosphate deposition was confirmed after 6 h incubation in accelerated calcification solution, and after 7 d in osteogenic culture media. Such films also showed a higher hMSC attachment and proliferation rate as in native 6mer, likely due to the fact that BSP contains triple RGD (Figure 5).^[89c] In the presence of calcium a higher stiffness of films of the 6mer with BSP than without BSP was found. Additionally, 6mer films treated with BSP had a much higher Young's modulus than of those which were not treated, as determined by AFM measurements. This might be due to the fact that, when calcium is present, supramolecular networks can be formed, and these

have the ability to dissipate energy in response to applied force. This is a highly promising property for bone plasticity, and therefore it was suggested to use this protein as organic glue for synthetic nanoscale composites.^[89b] Another interesting recombinant silk is the silk moth derivative EAEFN_n ($n = 5$ or 10) from *Antheraea pernyi*. On EAEFN₁₀ films, an osteoblast cell line showed an increased adhesion compared to that on *B. mori* fibroin films. Further, differentiated cells after 14 and 21 d deposited more calcium phosphate onto EAEFN₁₀ films than *B. mori* fibroin films, however, the positive control resulted in the greatest degree of biomineralization by the osteoblasts.^[31d]

In a separate study, 6mer was coupled to the antibacterial peptides, namely human neutrophil defensin 2 and 4 and hepcidin. Paper discs were immersed in these different protein solutions and placed on LB plates with gram-negative or gram-positive bacteria which resulted in clear inhibition zones for antibiotic-loaded films.^[60b] Further, films of the 6mer, 6mer with hepcidin, poly(lactic-co-glycolic acid) film, or no film were implanted into the subcutaneous pocket in mice. Flow cytometry and histology showed that there was a mild inflammatory response in all implants after two weeks. Fewer and more localized responses to scaffolds were noted after six weeks.^[89d] In their last study a tag-free purification approach of plain 6mer and 15mer was developed and shown to be noncytotoxic.^[60a]

In Petzold et al., the response of primary cardiac cells from 3-day-old Sprague–Dawley rats was evaluated on films prepared from eADF4(κ 16), a positively charged variant of eADF4(C16). Cardiomyocytes cultured on eADF4(κ 16) formed a healthy monolayer with clear cell–cell communication, and furthermore the monolayer was shown to contract (Figure 6). Cardiomyocytes on eADF4(κ 16) films showed no hypertrophic effect, reacted to pro-proliferative stimuli, and the contractions were synchronized between cells. Therefore, eADF4(κ 16) not only performs with comparable success to fibronectin, but also offers other advantages, such as no induction of hypertrophy, the possibility to be transferred into different morphologies, and it can be produced in much larger quantities.^[33c]

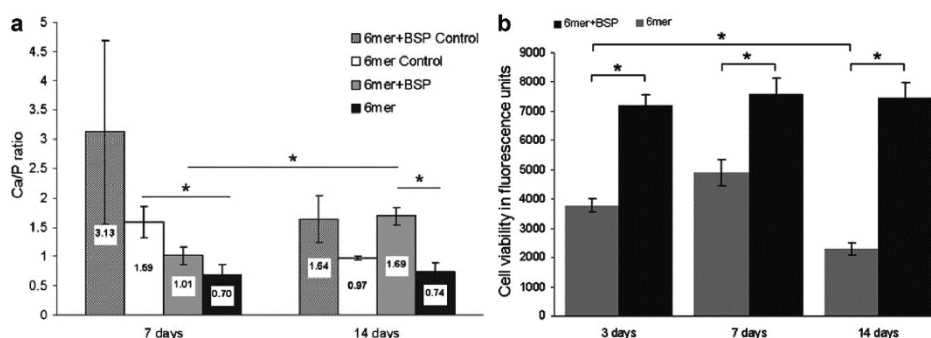


Figure 5. a) Ca/P ratios found on 6mer and 6mer+BSP films with and without (control) cells were determined using energy dispersive spectroscopy. hMSC were seeded onto silk films, and after reaching 80–90 % confluence osteogenic differentiation was induced. Controls were incubated in osteogenic medium only. The higher ratios found on 6mer+BSP samples can be explained by the affinity of the BPS domain for calcium ions. Remarkably, the ratios found after 14 d closely resemble ratios found in tricalcium phosphate (1.50) and hydroxyapatite (1.67). b) hMSC viability was investigated on 6mer and 6mer+BSP films and determined using an alamarBlue assay. Here, a higher cell viability/proliferation was found for cells on 6mer-BSP films than on plain 6mer films, probably due to the BPS binding domain, which contains three RGD sequences ($*p < 0.05$). Reproduced with permission.^[89c] Copyright 2011, Royal Society of Chemistry.

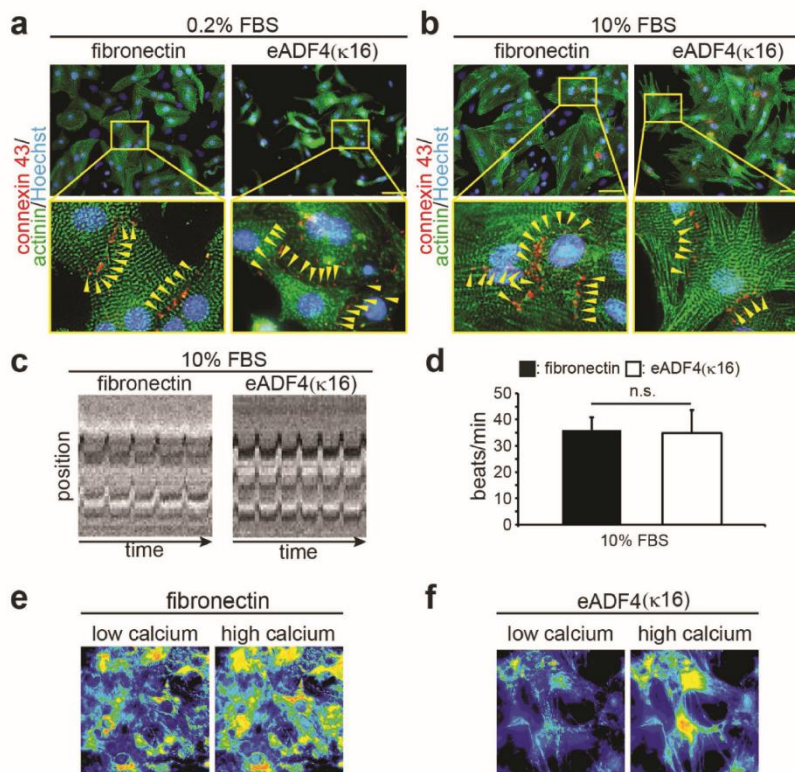


Figure 6. Cardiomyocytes cultured on fibronectin and eADF4(κ 16) films. a,b) Heart muscle cells on fibronectin and eADF4(κ 16) stimulated with 0.2% or 10% fetal bovine serum (FBS), stained for sarcomeric- α -actinin (green), connexin 43 (red), and DNA (blue). In order to allow contractility, cardiomyocytes must exhibit well-differentiated sarcomers, which can be seen in cells seeded on both materials (green stacked lines). Further, electrical coupling between the cells plays a significant role in efficient contraction. The efficient coupling in cardiomyocytes on both film types was shown by staining for the gap junction protein connexin 43 (marked with yellow arrows), where an enhancement could be achieved by stimulation with FBS. Additionally, FBS stimulation lead to an induction of hypertrophy in heart muscle cells cultivated on silk films. Scale bar: 50 μ m. c) Kymograph analysis showing contractions and d) its quantitative analysis. Neonatal cardiomyocytes spontaneously show contractile activity, which was recorded and analyzed via Kymograph analysis software, confirming that cells beat with the same frequency on both film types. e,f) Calcium imaging representing intracellular change in calcium concentration during contraction. Therefore, the matrices were loaded with a calcium sensitive dye to investigate the effects on the calcium homeostasis. It was found that neither the number of contractions nor the contraction frequency showed a significant difference between the two film materials.^[33e]

In conclusion it can be said that many different recombinant silks from different origin were investigated as materials of film scaffolds giving an insight into the basic response of various cell types. Unfortunately, some studies did not characterize the surface before seeding cells on it,^[52c] are missing important details in material and methods^[92] or did not show any microscopy images to confirm their cell culture data.^[52c,60b] Further should be mentioned that many groups use immortalized cell lines to test the performance of their silk films, which is helpful for understanding how cells might react on a basic level, but are also insensitive to more specific culture conditions.^[94] As more and more special cell binding motifs are added to the silk variants, it would be desirable that in future studies a focus is laid on primary or stem cells specific for these motifs. Nevertheless, there were some preliminary tests for use in neural, bone, and cardiac tissue engineering. Unfortunately,

bone tissue engineering showed less promising results compared to established control materials, but results were particularly interesting for cardiac tissue engineering.

4.4. Mesoporous Foams

Mesoporous foams are 3D structures comprised of 3D arranged, thin-walled pores. One of the most critical parameters is pore size, where large pores (>100 μ m) might prevent vascularization of the artificial tissue, as endothelial cells are not able to bridge pores which are larger than a cell diameter,^[95] but small pores (<100 nm) will limit the diffusion of nutrients, metabolic waste products, and gases.^[96]

There are several approaches for creating foams which are used, the most common being salt-leaching, freeze-drying,

and gas foaming. In the case of gas foaming, the polymer is saturated with a gas, such as CO₂, at high pressure. Then, the pressure is slowly released to atmospheric pressure, which reduces the solubility of the gas in the polymer and thereby gas bubbles are formed.^[97] In solvent-casting particulate leaching, salt particles are homogeneously dispersed in a polymer solution and the solvent is evaporated. The salt is leached out of the scaffold in a water bath, which leaves behind a porous foam structure.^[98] Salt leaching is the most common technique for producing foams from recombinant silk proteins.

To create a scaffold by freeze-drying, the most simple method is to freeze an aqueous polymer solution, which results in crystal formation by the solvent, and then to remove the solvent by sublimation, leading to a porous foam.^[99] Here, the pore size can be controlled by changing the pH or freezing rate.^[100] Alternatively, the pore size can also be controlled by use of emulsion freeze-drying, where an aqueous phase is mixed with a water-miscible organic solvent and subsequently frozen.^[101] To avoid the necessity of post-treatment, an alternative is to use cryogelation. In this case, a polymerizing agent is added to the polymer solution, and due to the formation of ice crystals, and hence indirect removal of solvent, the polymer solution and crosslinking agent concentration become so high that it results in matrix formation, leading to a stable foam which requires no further processing.^[102] Pore direction can also be controlled by cyrostructuring. Cryostructuring, or the directional growth of solvent crystals, occurs when a temperature gradient is applied, and it follows that the pores are also aligned into a specific structure.^[103]

4.4.1. Recombinant Silks Processed into Mesoporous Foams

eADF4(C16) foams were prepared by salt-leaching and had a β -sheet content similar to samples of post-treated eADF4(C16) films (~42%).^[33c] Scaffolds made of eADF4(C16) were found to be in the range of soft tissue (elastic compressive moduli = 0.94–3.24 kPa) which is compared to rS1/9 foams which had about 100 \times the tensile strength at $18 \pm 5 \text{ N cm}^{-2}$ (180 kPa).^[49] This, combined with gravimetric analysis of eADF4(C16) foams determining a porosity of 92%, indicated these foams could be promising for tissue engineering applications. Therefore, foams made of eADF4(C16) with and without RGD domain were further evaluated for the adhesion and proliferation of Balb/3T3 mouse fibroblasts.

Cells cultured for 10 d on eADF4(C16)-RGD foams were homogeneously distributed and exhibited a spread morphology.^[33c] In spite of its high stiffness, a similar result was obtained testing 3T3 fibroblasts on 1F9 foams after 14 d in culture, as determined by confocal laser scanning microscopy (CLSM).^[61a] Moisenovich et al. showed 3T3 fibroblasts attached and proliferated in rS1/9 scaffolds, whereby a homogeneous cell distribution throughout the material was obtained after 14 d as found by CLSM.^[49,61b] Further, rS1/9 foams were compared to *B. mori* silk fibroin ones, which showed a similar result in terms of 3T3 fibroblast attachment and proliferation,^[61b,104] but allowed a 5 \times faster migration through the network, leading to the conclusion that rS1/9 foams yielded a reduced motility of 3T3 cells.^[61b] Freeze-dried L-RGDSx2 fibroin (LRF) scaffolds with a mean pore diameter of 80 μm showed promising results

for bone and cartilage tissue engineering, where primary chondrocytes from white rabbits produced more cartilage-like tissue on the surface of LRF than on native fibroin.^[53a]

The *Euprosthenoops australis* derivative 4RepCT and variants thereof were formed into foams with pore sizes between 30 and 200 μm .^[71,74,75b,76,90a] Unfortunately, the exact mechanism of foam preparation is not explained in any of these studies. Human primary fibroblasts seeded onto 4RepCT foams exhibited attachment, spreading, proliferation, and collagen I production over 11 d.^[71] In a follow up study, NSCs were shown to successfully differentiate to astrocytes using ciliary neurotrophic factor.^[90a] Further, for culture of human induced pluripotent stem cells (hiPSCs) and human embryonic stem cells (hESC) a xeno-free system was developed where 4RepCT modified with vitronectin (VN-4RepCT) was used. hiPSCs as well as hESCs maintained their pluripotency even after 30 passages on 4RepCT films, and successfully differentiated into cardiomyocytes and neuroectoderm on foams. They were then injected in severe combined immunodeficiency mice, where they formed teratoma generating cells from all three germ layers. Further, hiPSCs seeded on silk films were successfully differentiated into endoderm, cardiomyocytes, or neuroectoderm.^[75a] In a follow up study hPSCs were cultivated over 10 passages and they were confirmed to be karyotypically normal and pluripotent.^[90b]

Two studies address pancreatic island engineering using either 4RepCT variants with N-terminal RGD, RGE, IKVAV, and YIGSR^[76] or N-terminal VN or fibronectin (FN) as well as RGD incorporated after the second or third Rep motif (2R- or 3R-4RepCT).^[75b] In Johansson et al., mouse and human pancreatic islets were seeded directly onto the scaffolds, and it was shown that the most effective adhesion took place on foams prepared from RGD-4RepCT. Even after a month in culture, the clusters maintained key functions such as insulin release upon glucose stimulation, and increase in [Ca²⁺]_i upon potassium or glucose stimulation. The cells on silk foams showed less necrosis compared to free floating clusters, and human islets were found to form sprouts and new islet like structures from donors less than 35 years old. Therefore, it was suggested to use this in vitro model for screening of potential therapeutic treatments and development of novel transplantation strategies. Islets from RGD-4RepCT and “free-floating” control samples were also transplanted into the anterior chamber of mice eyes. Islets from RGD-4RepCT were more stable in size, showed a better vascularization, lower cell death, and less insulin loss than observed in the control group.^[76] In a follow-up study, mouse and human pancreatic islets, as well as MIN6m9 mouse beta cell line, were investigated. Single cell suspensions were seeded onto the foams, and cluster formation was determined. RGD-4RepCT as well as 2R-4RepCT resulted in the best cluster formation, and these clusters also showed functionality in terms of insulin production and a change in [Ca²⁺]_i after depolarization (Figure 7). Further, the clusters from 4-RepCT and 2R-RepCT were transplanted into the anterior chamber of mice eye, and both groups facilitated insulin production and the formation of microvasculature, whereby larger vessels were found in 2R-4RepCT.^[75b]

In further studies, rS1/9 scaffolds were formed into bar shaped scaffolds and implanted into the midline dorsal subcutaneous area of BALB/c mice, where no toxicity or other tissue

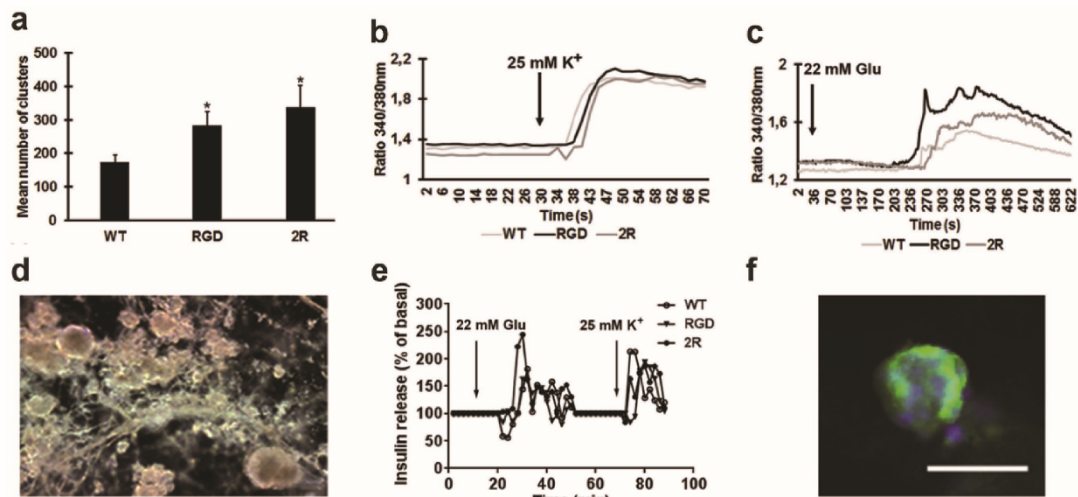


Figure 7. Human β -cells were cultured on silk protein foams and shown to form viable and functional islet-like clusters. a) Number of clusters obtained within foams after 7 d in culture on WT (4RepCT), RGD (RGD-4RepCT), and 2R (2R-4RepCT) ($n = 3$, triplicates, $*p < 0.05$) and determination of change in internal calcium concentration upon b) depolarization with potassium or c) with glucose. These tests confirm the stimulatory effect and hence the viability and functionality of the islet-like clusters. The glucose stimulation (c) performed after 7 days in culture showed a slightly more pronounced increase in internal calcium concentration on RGD compared to WT foams. d) Representative micrographs of islet-like clusters on 2R foams. e) Dynamics in insulin release after depolarization with glucose or potassium of clusters on WT, RGD, and 2R foams. Therefore, cells were stimulated with glucose first, which showed expected level of insulin production. Afterwards, the release was brought back to a basal level by lowering the glucose concentration again. Subsequent potassium stimulation showed a successful depolarization. f) Micrograph of cluster stained for insulin (green) and nucleus (blue). It shows that most cells stain positive for insulin confirming the presence of β -cells; further some glucagon producing cells were found. Scale bar: 50 μm . Reproduced with permission.^[75b] Copyright 2016, Elsevier.

pathology was observed. Histology performed after eight weeks showed clear ingrowth of adipose and fibrous tissue as well as vascularization and nerve fibers.^[49] In a separate study, *B. mori* fibroin and rS1/9 foams were implanted into midline dorsal subcutaneous area or into femoral defects. The implants were well-tolerated, and histology after eight weeks of the subcutaneous implants showed the shape of the scaffold was conserved in both, in rS1/9 and in *B. mori* fibroin scaffolds; however, in-growth of connective and fat tissue, cell mediated erosion, and vessel and nerve fiber formation was more pronounced in rS1/9 than in *B. mori* fibroin scaffolds. For the bone implants, Roentgen and CT studies revealed that after four weeks a higher recovery took place in case of rS1/9 in terms of bone formation and maturation.^[61b] Further, scanning probe nanotomography confirmed a better regeneration of bone tissue in rats using rS1/9 compared to *B. mori* fibroin, probably due to higher nanoporosity thereof.^[104]

The performance of transgenic silkworm silk foams [(AGSGAG)₄(E₈AS)₄] was also evaluated for its ability to promote bone regeneration. This silk contains additional glutamic acid residues, which should enhance calcium binding, and this was confirmed by X-ray photoelectron spectroscopy and Von Kossa staining. The sponges were analyzed in femoral defects in Japanese white rabbits and their performance was compared to that made of native silk fibroin. After four weeks, micro-CT revealed an enhanced bone formation in the transgenic silk fibroin, and further improvement was seen after eight weeks.^[54a]

In summary, salt leaching, phase-separation freeze drying, and an unknown foaming mechanism were used for foam preparation. The foams were in general very well characterized in terms of structure (SEM, CLSM), mechanical stability (compressive test), (secondary) structure content (FTIR + FSD, ¹³C crosspolarization magic angle spinning nuclear magnetic resonance), porosity (gravimetric analysis), cell attachment, and degradation (enzymatic, chemical). The only exceptions were foams prepared from 4RepCT and LRF scaffolds, which were unfortunately not as well-characterized, and therefore it is difficult to draw complete conclusions from these works. Further, foams were applied in attempts to form functional tissues including bone, peripheral nerve, and pancreas. Of these, particularly promising results were seen in terms of insulin production and calcification of foams, however many more studies must be conducted to enhance and fully characterize these tissue-like structures.

4.5. Hydrogels

Hydrogels can be most simply defined as polymer or proteins networks, induced by physical or chemical crosslinking in solution, which are primarily composed of water (>90%) but still retain their structure.^[105] Examples of physical crosslinking are chain entanglements, hydrophobic interactions, and hydrogen bonds.^[106] Physical crosslinking is normally a process which occurs spontaneously under certain

conditions, such as specific concentrations and temperatures.^[107] Chemical crosslinking is the use of a chemical agent to induce covalent bonds between polymer or protein chains, or salts for ionic bonding.^[106a,108]

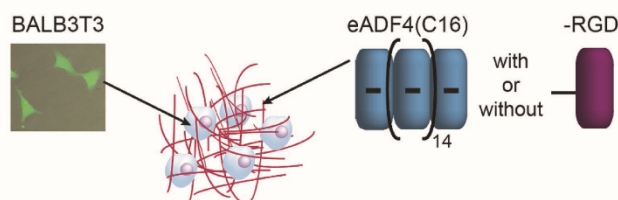
Compared to other morphologies, hydrogels are highly interesting in terms of 3D cell culture, as the cells are introduced to a truly 3D environment, as opposed to 2D or complex 2D surfaces.^[109] However, as implied from adding the 3rd dimension, significantly more protein or polymer is required to form hydrogels, as well as consumables used for evaluating the scaffolds, such as staining reagents. The diffusion of molecules (waste-nutrient exchange) is also significantly impeded. However, these disadvantages are usually out-weighed by the fact that hydrogels are the most physiologically accurate morphology. Further, they can be used as biomaterial component for 3D bioprinting, when they are able to flow under shear stress, and recover mechanical properties after the process is complete.^[110]

One of the reasons why spider silks are favorable materials for forming hydrogels for tissue engineering applications is that they can be formed without crosslinkers.^[107a,111] The formation of hydrogels through self-assembly is a thermodynamically driven process where the principle variables determining the rate of gelation are the concentration and the temperature. In the case of the investigated spider silk proteins, the nucleation phase is characterized by a structural change in the amino acid chain to more β -sheet rich structures, followed by the fibril elongation phase, followed by network formation.^[107a] To the best of the authors knowledge, there is only one case of recombinant spider silk hydrogels for tissue engineering, which is eADF4(C16), Table 1.

4.5.1. Recombinant Silk Hydrogels for Biofabrication

eADF4(C16) was shown to be effective for 3D bioprinting, Figure 8.^[112] In this study it was shown that the hydrogel was nontoxic to cells when encapsulated, and although there was a reduction in cell viability due to the encapsulation process, there was nearly 100% cell viability comparing before printing to after printing. Although there is room for improvement, this pilot study in general showed the promise for the use of eADF4(C16) for 3D bioprinting. In the future, these disadvantages should be improved, and again more specific cell types or growth factors should be used in an attempt to achieve a specific tissue function.

bioink preparation by encapsulation of cells in recombinant silk solution



bioink gelation

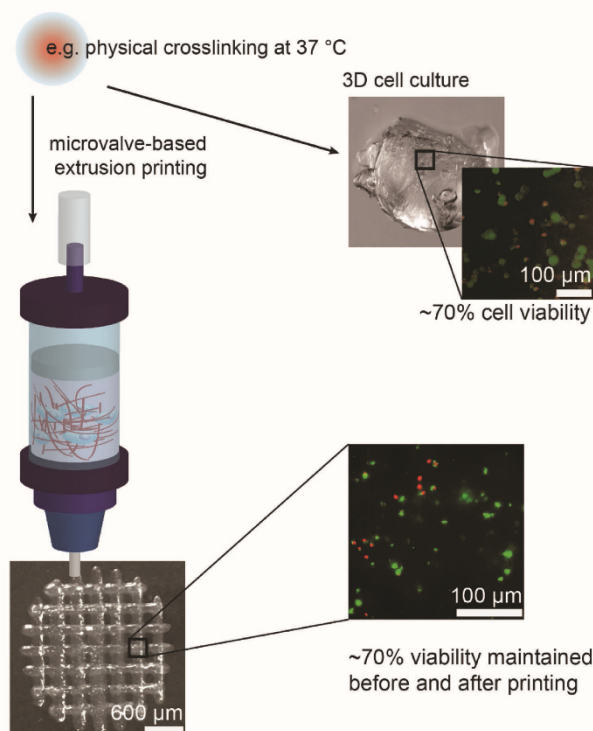


Figure 8. Biofabrication using eADF4(C16) as the biomaterial component of a bioink. Cells were encapsulated in highly concentrated eADF4(C16) solution and gelled by incubation at 37 °C. The bioink can either be used for 3D cell culture or for 3D bioprinting with reasonable cell viability.

5. Implant Coatings

When an implant is introduced into the human body there are several consequences, including high risk of infections at insertion site^[113] as well as several reactions of the body to the chemical, physical, and morphological characteristics of the implant surface. The foreign body response begins with protein adsorption followed by monocyte/macrophage adhesion, which will eventually fuse to form foreign body giant cells as they cannot digest the implant.^[114] These foreign body giant cells

then further initiate more complex inflammatory and wound healing responses, for example, scar tissue formation. Thereby, fibroblasts are attracted by the giant cells and begin synthesizing collagen, forming a complete avascular capsule around the implant.^[115] Thus, it is of great importance to understand the environment of and host response to certain biomaterials in order to use them in meaningful applications, referring to a review by Anderson et al. for more details.^[116]

5.1. Recombinant Silks Used as Implant Coatings

The number of methods used for coating hard and soft medical devices with recombinant silk proteins is limited to dip-coating or spray-coating or a combination of both. Aqueous solutions were used to avoid damaging the implant material as well as introducing residues of toxic solvents or salts in the body. In a pilot study by Zeplin et al., silicone implants were coated with a layer of eADF4(C16) $\approx 1 \mu\text{m}$ thick by dip-coating the implant into aqueous silk solution three times with the aim of reducing capsular fibrosis (Figure 9).^[25,117] In vivo studies in Sprague–Daley rats showed a decrease in fibroblast and histiocyte coverage as well as less collagen deposition on coated than on uncoated silicone samples. The reduction in capsule thickness and fibrosis factors was also confirmed by qPCR.^[25] Further, this implant coating was much more successful than others in current research. In a follow up study, eADF4(C16) was exploited to coat silicone catheters. Here, the material was prepared by oxygen plasma treatment followed by application of poly(ethyleneimine) (PEI: positive charged polymer) or eADF4(κ 16) (positively charged silk protein), to counterbalance the negative charge from plasma treatment, and finished by an eADF4(C16) (negatively charged silk protein) coating. The interaction with several cell lines (Balb/3T3 fibroblasts, B50 nerve cells, C2C12 myoblasts, and HaCaT keratinocytes) was investigated, and neither adhesion nor proliferation was observed. The coating was confirmed to be stable against delamination, even after bending.^[91] Harris et al.

also used dip-coating, spray-coating, and a combination of both to apply a 0.5–50 μm thick layer of rMaSp1/rMaSp2 onto silicon wafers, stainless steel, titanium chips, and PU or silicone catheters. A general smoothening effect of the surface was observed upon coating of catheters, which was confirmed by determining the friction coefficient. The best results for coating homogeneity were observed by using a combination of spray-coating and dip-coating. To see if this could also be used to reduce the formation of biofilms, thrombotic fouling, and protein accumulation, functional compounds or additives were added. In order to reduce the likelihood of an infection, antibiotics (kanamycin, gentamycin, tetracycline, ampicillin, or chloramphenicol), azole, and/or aminoglycosides were added. Furthermore, heparin was supplemented as a functional compound to prevent thrombosis. These silk/heparin coated silicone implants, which were incubated in blood that was induced to clot, showed a severe decrease in thrombotic fouling.^[62]

In order to functionalize implants with biologically active peptides, 4RepCT was modified with either cell-recognition peptide (FN-4RepCT) or an antimicrobial motif (Mag-4RepCT). The coating process was analyzed using quartz crystal microbalance and surface plasmon resonance, and it was shown that silk was adsorbed continuously and that the resulting layer was stable toward sodium hydroxide, hydrochloric acid (0.1/0.5 M), and ethanol treatment. The silk coating assembled into fibrils on the surface, and these nanofibrous coatings, especially FN-4RepCT, improved viability, spreading, and proliferation of HDMEC and human dermal fibroblasts. A decrease in *S. aureus* density was also observed on both 4RepCT and Mag-4RepCT.^[118]

In summary, it can be stated that recombinant silk coatings were successfully applied onto various surfaces and fulfilled the desired task in terms of tissue and cell response. For example, surfaces could be adjusted so that either cell attachment was decreased or increased. Almost all studies reported that silk coatings increased smoothness and rendered the surfaces more hydrophilic.^[25,62,91] Although

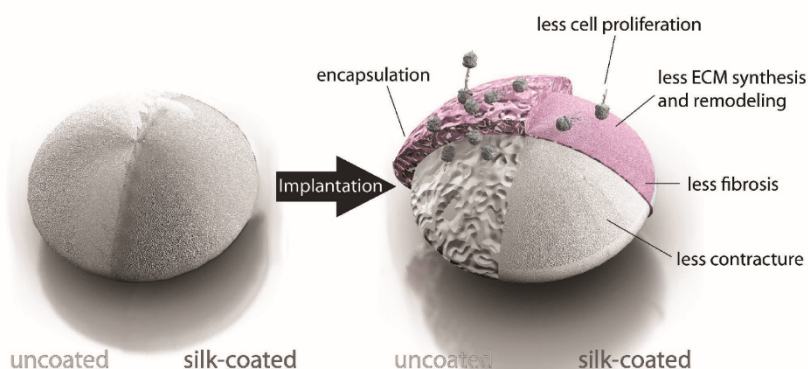


Figure 9. Scheme of bioshield function of silk coating on a silicone implant. Silicone, despite being resistant against enzymatic and hydrolytic degradation, displays a hydrophobic surface triggering adhesion of unspecific proteins and cells. This leads to a foreign body response, which might end in the formation of a fibrotic capsule, causing a deformation of the implant and pain and discomfort in patients. By applying a thin spider silk coating, which causes no immune reaction, the implant can be shielded and thereby capsule formation can be significantly reduced.^[25]

hydrophilic, it was found that 4RepCT coating formed a nanofibrillar structure.^[118] However, perhaps the most exciting result of this study was the nearly undetectable immune response as well as the slow biodegradation in vivo.

6. Drug Delivery

Drug delivery systems are designed for increasing the uptake efficiency and specificity of a drug for a target tissue.^[119] Usually the strategy is to target specific cells or characteristics of a diseased tissue, and to design the drug delivery vehicle such that it does not release its drug unless in that particular environment (Figure 10a). Other advantages of using drug delivery systems are to increase the loading efficiency of drugs which have low water solubility, and increase control over the release profile of the pharmaceutical agent.^[120] Simply stated, drug delivery systems allow for a reduction in the amount of drug administered, frequency of drug administration, as well as the potential side effects of a drug.^[121]

Drug delivery systems are often characterized as either stationary or mobile. Stationary systems act as a drug depot which are implanted in one location and slowly release drugs over a long period of time. Examples include implant coatings (films) or wound dressings (hydrogels).^[122] Biomaterial-based products are currently available in the market and are composed of polyanhydrides (Gliadel Wafer) and poly(lactic-co-glycolic acid) (Zoladex). Mobile systems on the other hand act as transporters carrying their drug load to the final destination, where it is released. Therefore, these systems are further characterized by how they target the site of interest, either actively or passively. Active target systems will attach recognition sequences for molecules such as nucleic acids, peptides, proteins, small molecules, or monoclonal antibodies which are unique to the target site. For example, ligands attached to the drug delivery system can bind to cell-specific membrane molecules on the target cell (Figure 10b).^[123]

There are many studies where *B. mori* silk fibroin was processed via different routes into microspheres and nanoparticles, and both were successfully loaded with different (model) drugs. However, *B. mori* fibroin suffers, like all naturally derived polymers, from batch-to-batch variations making quality control, necessary in biomedical applications, difficult.^[124] highlighting the use of recombinantly produced silk proteins.

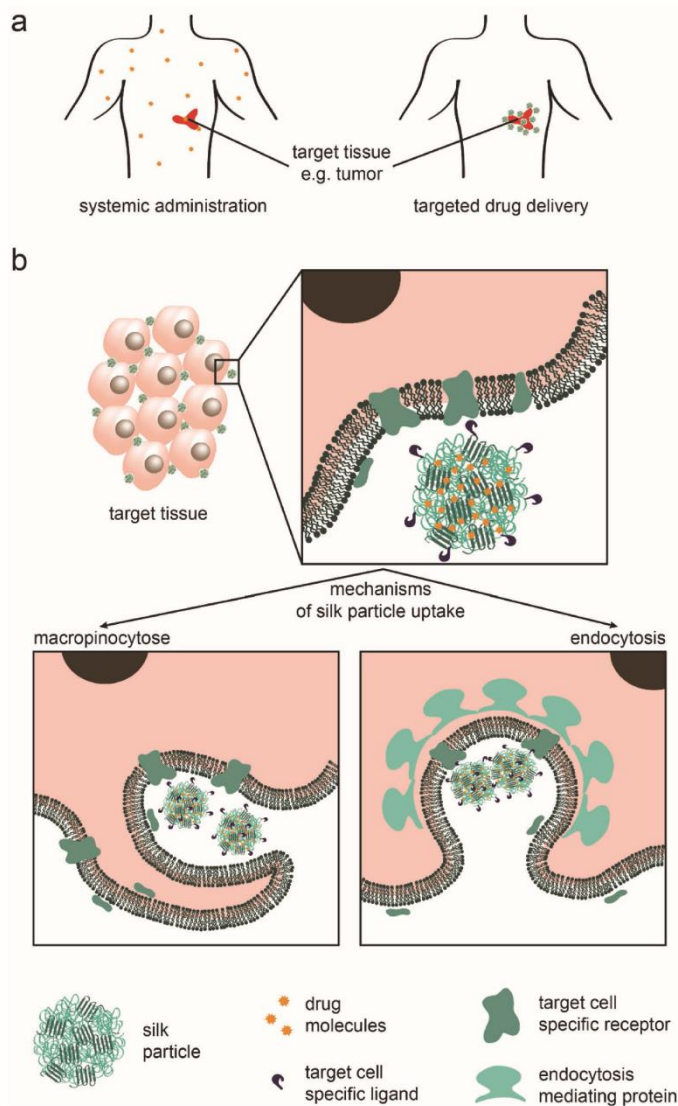


Figure 10. Drug delivery via silk particles. a) Comparison of systemic drug administration and targeted drug delivery. In systemic drug administration the whole body faces the medication, whereas in targeted drug delivery only desired cells are attacked. b) Cellular up-take of silk particles either via macropinocytosis or endocytosis. Silk particles were found to be mainly up-taken by different mechanisms, namely micropinocytosis and endocytosis, depending on the properties of the silk proteins used.

6.1. Hydrogels

Hydrogels are a particularly attractive choice for drug delivery because they can be easily loaded with relatively high amounts of water-soluble drugs by diffusion or by encapsulation.^[105,125] The drug release profile can be easily controlled

by hydrogel-specific characteristics, such as crosslinking density, environment-responsive swelling, or shrinkage. A further advantage is that preformed hydrogels are often injectable, or the hydrogel precursor solution can be injected as a liquid and gel on site. Therefore, hydrogels stay at the site of interest much more successfully than for example particles, which have a short residence time in the blood, especially at smaller size.^[126]

Challenges associated with using hydrogels as drug delivery carriers are that they often have an uncontrollable burst release, either immediately due to rapid diffusion time of small molecules, or later from a sudden, rapid degradation of the hydrogel.^[125b] However, most of these challenges are simple to overcome, for example by creating environmentally sensitive hydrogels,^[125a] or by making multimembrane hydrogels.^[127] Recombinant silk hydrogels are particularly interesting due to their slow biodegradation, however the only type examined so far is silk-elastinlike proteins (SELPs) (Table 1).

6.1.1. Recombinant Silk Hydrogels for Drug Delivery

One group focuses on the production of SELP hydrogels, in particular for cancer therapy. In the foundational publications, they investigated different variants of SELP, and showed that SELP-815K hydrogels (Table 1) had the best release of adenovirus.^[128]

In a paper by Poursaid et al. two variants of SELPs were tested as chemoembolization agents: SELP-47K and SELP-815K.^[55d] Chemoembolization is a cancer-treatment where the blood vessels to the tumor are blocked, resulting in tumor shrinkage, combined with chemotherapy drugs, to actually kill the tumor cells.^[129] First they conducted *in vitro* tests in microfluidic channels designed to imitate the hepatic vascular system, where they observed that the sol–gel transition occurred at an appropriate time point, which further resulted in clogging of the targeted channels only. It performed with similar success in rabbits, where it gelled in the site of interest and resulted in significant tumor shrinkage.^[55c]

Although these studies show these hydrogels to be promising for chemoembolization, there were a few points which were lacking conclusive comments from the researchers. For example, they reported reduction in tumor growth rate, however, they did not mention if there was complete regression of the tumor, or if this would be effective against metastatic forms of cancer. Overall, the hydrogels show highly interesting properties, and should be further investigated with more complex models and methods.

6.2. Films

Film-based and membrane-based scaffolds in drug delivery are often studied due to their simplicity and the possibility to obtain zeroth-order release kinetics allowing a constant drug administration.^[130] Hofmann et al. investigated silk fibroin films as drug delivery matrices by casting films from a protein–drug mixture. Indeed it was found that films with higher crystallinity showed no initial burst release. Further, the activity of protein drugs was evaluated and it was shown that horse radish peroxidase was still active after release from methanol treated films.^[131]

Long-term studies of enzymes entrapped in silk fibroin films showed a 40–100% activity of glucose oxidase, lipase, and horse radish peroxidase after 10 months of storage.^[132] It was further resolved that the entrapped enzyme was only released after proteolytic silk degradation, which was in turn dependent on the secondary structure of the silk matrix. Hence, controllable release kinetics of the films could be realized by adjusting the silk structure with different post-treatment techniques and/or the addition of a plasticizer like glycerol.^[133]

6.2.1. Recombinant Silk Films for Drug Delivery

The authors are only aware of two publications utilizing recombinant silk films for drug delivery. In both cases, films were formed from eADF4(C16) by film casting. In order to allow an easy removal, films were cast onto a polytetrafluorethylene surface either from organic HFIP^[134] or aqueous solution.^[121] In the study conducted by Hardy et al., eADF4(C16) was additionally blended with polycaprolactone and thermoplastic polyurethane at various ratios, and resulting films were about 100 μm thick.^[134] The films were well-characterized using differential scanning calorimetry and tensile testing (Young's moduli with 5500^[121] or 3300 MPa^[134]), as well as thermogravimetric analysis,^[124] isoelectric point,^[121] water absorption,^[121] and water contact angle^[134] measurements.

Low molecular weight drug models (methyl violet or ethacridine lactate) were loaded by incubation, and diffusion was determined in phosphate-buffered saline (PBS) via UV–vis spectrometry. The highest loading and the fastest release were observed in pure silk constructs, presumably due to the negative charge of eADF4(C16). The time of release could be further shortened by the addition of enzymes.^[134] In Agostini et al., pure and multilayered films as well as the impact of additives glycerol and 2-pyrrolidone on the release of loaded low molecular weight (etracaine HCl and paracetamol) and high molecular weight (fluorescein isothiocyanate (FITC)–bovine serum albumin (BSA) and FITC–dextran) model drugs were investigated. Paracetamol and FITC–dextran were released within one day only, and also FITC–BSA showed an initial burst followed by a steady release from the $\approx 30 \mu\text{m}$ thick monolayers. Multilayer films prepared by pressing a FITC–BSA and glycerol (glue) film between two pure silk films did not show any improvement in terms of release. Coating of FITC–BSA and 2-pyrrolidone (plasticizer) loaded films lead to a decrease in burst release to 20% followed by a steady release over 90 d.^[121]

In conclusion, films could be loaded with drugs, but not as effectively as particle systems. This could potentially be improved by using a system which allows for greater drug loading (e.g., hydrogels).

6.3. Capsules

Capsules allow the encapsulation and protection of larger molecules, small particles, or even small microorganisms.^[135] A capsule can be formed around a solid core, which is then removed afterwards. This technique was for example used to obtain 1b1-capsules from modified *B. mori* fibroin by applying the silk onto

silica particles, which are subsequently dissolved.^[136] In the field of recombinant silks capsules were formed in an emulsion process, whereby an amphiphilic molecule lines the interface between water and oil thereby forming a capsule wall.^[48,137]

6.3.1. Recombinant Silk Processed into Drug Delivery Capsules

eADF4(C16) spider silk capsules were prepared in a water-in-oil emulsion using either toluene^[48,137a] or silicon oil.^[137b] Toluene has the advantage that it induces β -sheet formation and thus, no further post-treatment is necessary (Figure 11a); however, it also has the disadvantage that it is cytotoxic.^[48] Silicon oil on the other hand is FDA-approved, but an additional post-treatment step must be included after capsule formation. The capsule diameter as determined by light microscopy was 1–30 μm . Mass balance measurements showed that the membrane thickness was 50–70 nm. Compression tests performed with AFM gave a Young's modulus of 0.7–3.6 GPa. The capsules prepared in silicon had a molecular weight cut-off (MWCO) >40 kDa,^[137b] whereby the capsules prepared in toluene had a MWCO of about 27 kDa.^[48,137a] No rupture was observed under osmotic stress up to 10⁷ Pa, and the capsules were chemically stable in 2% sodium dodecyl sulfate and 8 M urea.

In further studies by Blüm et al., β -galactosidase was loaded into capsules.^[137b] It was shown that the enzyme could be entrapped in the capsule protecting it from proteolysis. Using such a closed reaction chamber with a semi-permeable membrane, inactive enzymes or their precursors could be encapsulated and then activated from outside by α -complementation of β -galactosidase.^[137b]

All three studies show that it is possible to prepare capsules from recombinant silk proteins with reasonable stability. This drug delivery system is still in the early stages of development, and further studies are required to determine its potential. The big advantage of this approach is the possibility to encapsulate not only large molecules, but even entire microorganisms, which makes it attractive for further research.

5.4. Particles

Previously it was shown that regenerated silk fibroin particles can be used as mobile drug delivery systems.^[138] Several different methods have been developed for preparation of silk fibroin particles as for example salting out, microfluidics, phase separation with polyvinyl alcohol, desolvation in an organic solution and liquid templating. The most commonly used approach for recombinant silk proteins is salting-out in phosphate buffer (Figure 11b), taking advantage of the fact that silk proteins are less soluble at high salt concentrations due to electrolyte–nonelectrolyte interactions.^[138a]

6.4.1. Recombinant Silks Processed into Drug Delivery Particles

In Lammel et al., particles were prepared by mixing an eADF4(C16) solution and phosphate buffer with a pipette, a micromixing device with laminar or turbulent flow, and by

dialysis of protein solution against phosphate buffer. Due to the importance of particle size, it was desired to establish the relationship between the concentration of the protein solution, the concentration of phosphate buffer, as well as the mixing time for determining particle size. Particle sizes were found to be between 250 nm (micromixing with turbulent flow) and 2.1 μm (dialysis) as determined by SEM and laser diffraction spectrometry (LDS).^[139] In general it was found that the lower the protein concentration, the higher the phosphate buffer concentration and the faster the mixing time the smaller the final particles will be.

Particles were also characterized in terms of heat, mechanical, colloidal, and chemical stability. Lucke et al. showed that eADF4(C16) particles prepared by micromixing (332 nm) or in an ultrasonic atomizer (6.7 μm) could be steam sterilized without any effect on size or secondary structure.^[140] A closer look on the interfacial properties of the particle was obtained by direct force measurements with a colloidal probe. Thereby it was found that eADF4(C16) particles are surrounded by a fuzzy protein layer protruding into the solution. This diffuse layer allows long-range interactions, which are based on electrostatic and steric forces (Figure 11c).^[141] Interestingly, an increase in physical crosslinking, for example, by increasing the molecular weight, had a severe impact on elastic modulus, whereby chemical crosslinking with ammonium persulfate (APS) and tris(2,2'-bipyridyl)dichlororuthenium(II) (Rubpy) had only minor stiffening effects, as the initial β -sheet content in non-crosslinked particles was already high. Additionally, a continuous deformation behavior without buckling indicates a high homogeneity of silk particles.^[142] Interestingly crosslinking did have an effect on chemical stability: when incubated in 6 M guanidinium thiocyanate, formic acid, HFIP, 8 M guanidinium hydrochloride, and 10×10^{-3} M Tris(hydroxymethyl)aminomethane (Tris) buffer crosslinked particles were stable for 25 h, whereby non-crosslinked particles were only stable in guanidinium hydrochloride and Tris buffer.^[143]

Colloidal stability of eADF4(C16) particles and its variants was determined in several studies. It was found that eADF4(C16) particles are stable for six months in water, but a decrease in pH^[144] or the addition of kosmotropic salts^[145] leads to particle agglomeration. It is known that particles with a zeta potential below -20 mV show only little agglomeration.^[146] In a study by Elsner et al., particles made of eADF4(C16) hybridized with different motives (RGD, R₆G, Tat) and of eADF4(κ 16) were tested and the results remained consistent: particles of eADF4(C16) and the RGD variant had ≈ -25 mV (the lowest zeta potential) and showed low agglomeration, whereby Tat-eADF4(C16)Tat with -8 mV agglomerated.^[120b] Also Jastrzebska et al. found that MS2 particles showed a negative zeta potential ranging between -10 and -35 mV depending on the silk purification method, phosphate, and silk concentration, and on the pH.^[63] A later study detected that MS1 particles had a positive zeta potential of ≈ 9 mV, and interestingly a 8:2 mixture of MS1:MS2 gave an even higher value of ≈ 15 mV. Her2 binding peptides were genetically added to both variants (H2.1/2MS1/2), which had no influence on the zeta potential. The stability was tested by turbidity measurements and revealed that MS2 particles are more stable than MS1 particles, and the mixtures are found in between. Importantly, the Her2

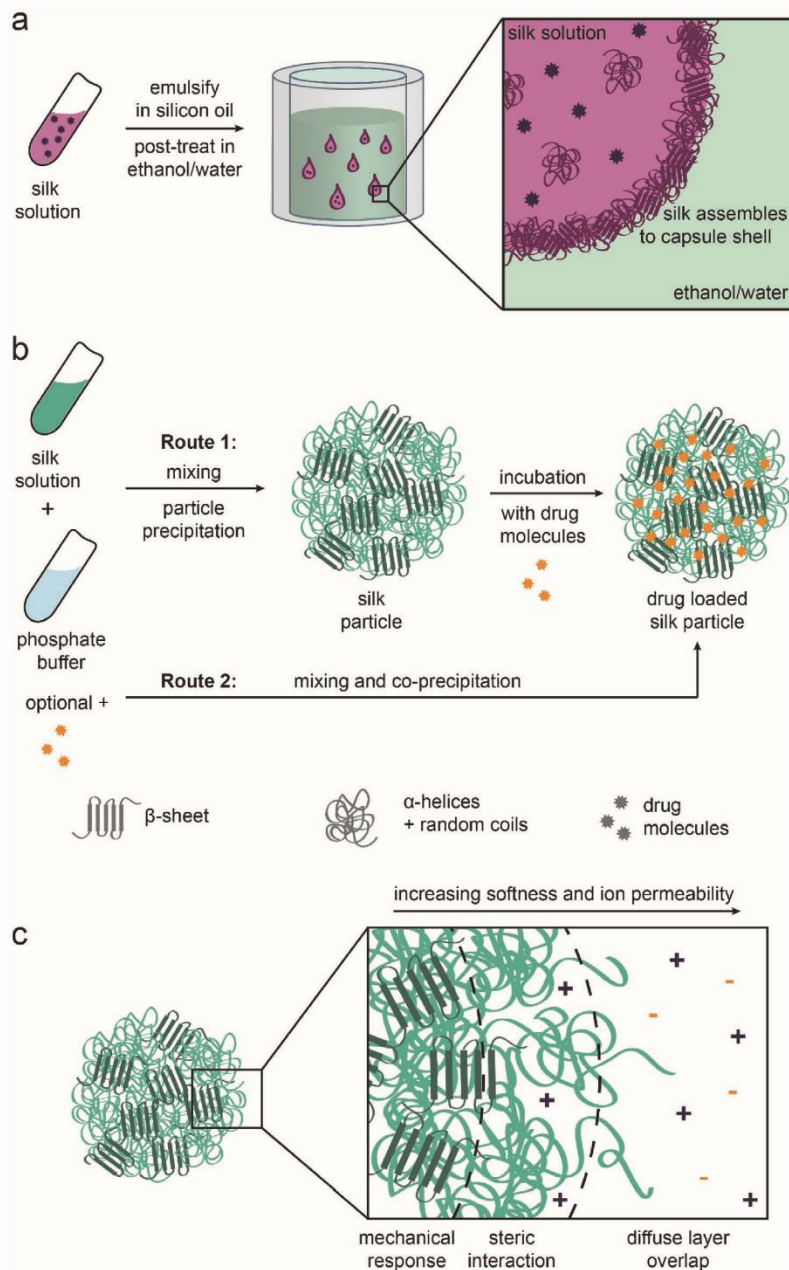


Figure 11. Preparation of mobile drug delivery systems made of silk proteins. a) Capsule formation: Silk solution is emulsified in silicon oil. The silk molecules adsorb at the water/silicon oil interface and form a film. This film is stabilized via a post-treatment step—here β -sheets are induced in an ethanol/water mixture. b) Particle formation by salting out: Route 1: the recombinant silk solution is mixed with phosphate buffer and then loaded with drug molecules by diffusion. Route 2: the recombinant silk solution is mixed with drug molecules before coprecipitation in phosphate buffer. c) Different layers in particles contributing to their properties: In the core elastic deformation takes place, which mainly determines the mechanical properties of the particles. On the particle surface brush-like structures (approximated by an Alexander–deGennes type of interaction) can be found, which determine the interaction with, e.g., drug molecules. A diffuse charged layer is located outside.

binding peptides did not influence the stability.^[147] With stable particles in solution, it is possible to consider particle loading.

In a study by Hofer et al., they could show using FITC-labeled proteins that neither uptake of uncharged FITC–dextran nor negatively charged FITC–bovine serum albumin into eADF4(C16) particles. The positively charged FITC–lysozyme could successfully be loaded, whereby again pH and ionic strength played a crucial role. Interestingly, the zeta-potential of the particles was the same before and after loading.^[144] A similar observation was also made by Schierling et al. where particles of several eADF4(C16) derivatives (negatively charged) were loaded with fluorescently labeled PEI (positively charged) or eADF4(κ 16) particles (positively charged) with labeled ssDNA (negatively charged or with a plasmid DNA doxorubicin (Dox) mixture) and this loading had no effect on the colloidal stability.^[148] Also negatively charged MS2 particles could be loaded with rhodamine B or Dox.^[63] In a later study it was shown that MS1 particles can be loaded with almost double the amount of Dox than MS2 particles (645 vs 372 ng per μ g silk), although MS1 and Dox are both positively charged. The reason might be a higher hydrophobicity as well as the looser packing of MS1 particles facilitating diffusion. Further, it was shown that Dox loading efficiency of a 8:2 mixture with or without Her2 binding peptide was between that of the pure silk particle variants.^[147] In the case of loading eADF4(C16), Lammel et al. proposed that loading is mainly driven by three parameters: (1) charge of the drug (determined by K_D), i.e., if the particle possesses a negative charge, only positively charged drugs can be loaded; (2) octanol water partition coefficient ($\log P_{o/w}$), hence the solubility of the molecule; (3) molecular weight of the drug, whereby (1) and (2) are the dominating factors.^[145]

Particle loading can also be accomplished by coprecipitation (Figure 11b). Coprecipitation was shown to efficiently load eADF4(C16) particles with the model drug rhodamine B or β -carotene.^[47,143] Similar results were observed for H2.1/2MS1, which could be successfully coprecipitated with Dox. Thereby \approx 355 ng of Dox were loaded per μ g of silk.^[46] Interestingly, this resembles only half the amount loaded via diffusion.

Release of drugs from particles was investigated in different buffer systems usually by UV–Vis spectroscopy.^[47,58b,145,147,148] Superhydrophobic β -carotene could only be released upon digestion of the silk particle. Here it was shown that the eADF4(C16) particles remained intact in artificial gastric fluid, whereby they were digested in artificial intestinal fluid.^[47] A decrease in pH caused a burst-release of lysozyme, methyl violet, or ethacridine lactate loaded eADF4(C16) particles, as well as of Dox-loaded H2.1MS1 and H2.2MS1 (H2.1/2MS1) particles. This could be explained by a change in charge due to the pH change, diminishing the electrostatic interactions between silk and drug and thereby promoting drug release.^[46,144,145] Only a small burst release of about 20% was reported by Florczak et al. in MS1, MS2, and their mixtures with or without binding peptide, and decreasing pH had less influence than in studies described before.^[147] Also an increase in ionic strength or character (i.e., kosmotropic or not) effected the kinetics.^[58b,144] Furthermore, it was found that in comparison to eADF4(C16) the lysine bearing eADF4(κ 16) revealed a burst release of small molecules like 6-carboxy-fluorescein under all tested conditions. This could be explained by the fact that lysine residues

found in eADF4(κ 16) are more hydrophilic and, hence, can be easier assessed by salts and solvents. A coating of eADF4(κ 16) particles with eADF4(C16) using a layer-by-layer technology was thought to slow down the release, but the opposite was true. Thus, the electrostatic repulsion of eADF4(C16) and the cargo overruled the desired closing effect of eADF4(C16).^[58b] In another approach crosslinking with APS and Rubpy was successfully used to slow down the release of the model drug rhodamine B. Further, it was shown that the mechanism of drug incorporation has a major influence on the release profile.^[143] The reason for this effect might be that drug release from silk particles can be described by second order kinetics. The drug molecules in the core of the particles bound via electrostatic and hydrophobic interactions first need to be transported to the surface due to a concentration gradient driven process. Then they can be slowly released from the surface, where they are bound via electrostatic interactions.^[143,145]

The last major step in evaluating drug delivery systems is the cellular uptake. Therefore, Elsner et al. investigated eADF4(C16) variants possessing different motifs, namely eADF4(C16)-RGD, eADF4(C16)-R₈G, eADF4(C16)-Tat, Tat- eADF4(C16), Tat-eADF4(C16)-Tat, and the positively charged eADF4(κ 16). First, it was confirmed that unloaded particles have no cytotoxic effect on HeLa^[120b] and Kelly neuroblastoma cell proliferation.^[148] Further uptake studies were performed using fluorescence activated cell sorting in which only 19% of HeLa cells took up eADF4(C16) particles after 72 h, but 97% internalized eADF4(κ 16) particles. The other variants were up-taken by 30–40% of HeLa cells.^[120b]

In a follow up study it was shown that even particles loaded with model drugs did not influence cell growth behavior. DNA/Dox loaded eADF4(κ 16) particles were also investigated in terms of cytotoxicity. Balb/3T3 fibroblasts, HeLa, and Kelly neuroblastoma cells were incubated with DNA/Dox loaded eADF4(κ 16) particles. All three cultures were terminated within 48 h when cultured with particle concentrations greater than 48 ng μ L⁻¹.^[148]

The up-take mechanism was found to be clathrin-mediated endocytosis in case of eADF4(C16)-RGD and eADF4(κ 16) particles, and macropinocytosis in case of eADF4(C16) and eADF4(C16)-R₈G particles (Figure 11b).^[148] CLSM confirmed that H2.1MS1 spheres not only targeted but also successfully entered Her2-overexpressing cancer cells exclusively, whereby the nucleus was not penetrated (Figure 12).^[46] A significant decrease in viability of Her2-overexpressing cancer cells was observed when H2.1/2MS1 particles loaded with Dox were added compared to MS1 control particles loaded with Dox. CLSM revealed that Dox effectively entered the nucleus. The Her2-negative control cell line on the other hand showed a general decrease in cell viability similar to the Her2-positive cells with MS1-Dox particles, but no difference between the different particles was observed.^[46] By combining MS1 with MS2 in a ratio of 8:2 the physical–chemical properties could be improved without losing these favorable drug delivering properties of MS1 particles. It was shown that the mixture containing the Her2 binding peptide successfully targeted Her2-positive cells and caused \approx 60% toxicity in these cells, whereby nonfunctionalized spheres reduced the viability by 10% only. Also Her2-negative control cells showed a rather high viability of 90%.^[147]

Besides loading of particles with drug molecules, recombinant silk can be complexed with plasmid DNA (pDNA) to

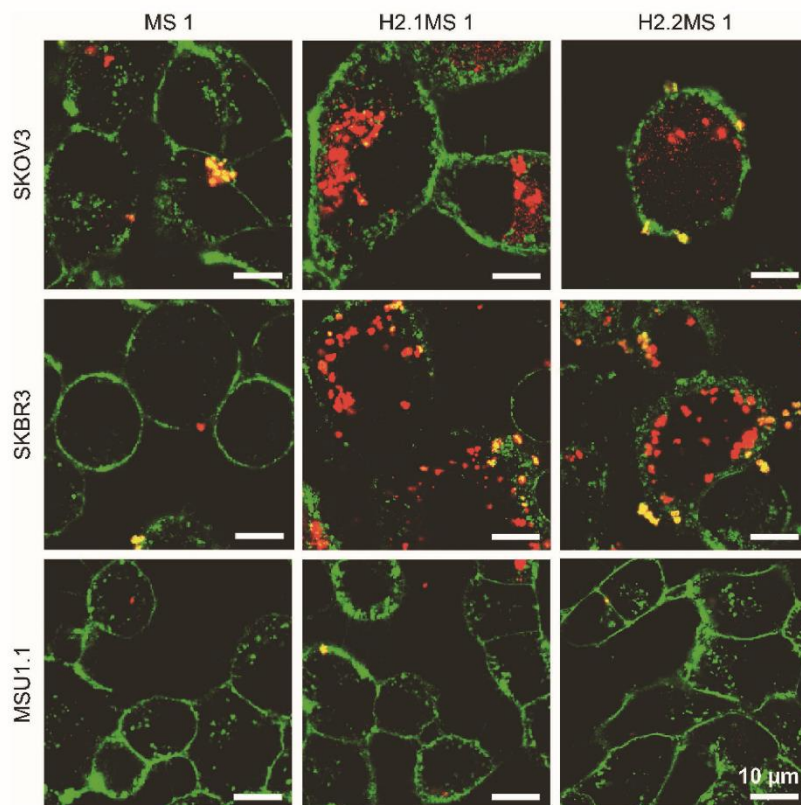


Figure 12. Interaction of Her2 positive (SKOV3 and SKBR3) and control (MSU1.1) cells with fluorescently labeled spider silk particles made of MS 1 (recombinant silk protein particles without the Her2 binding peptide) or H2.1/2MS 1 (recombinant silk protein particles with Her2 binding peptide). Cell membrane stained with ConA-FITC (green) and particles conjugated with ATTO 647N (red). The Her2/neu gene is overexpressed and/or amplified in 20–30% of invasive breast carcinomas and is thus an interesting target. Functionalized spheres (H2.1/2MS1) were effectively internalized into the cytoplasm of Her2 positive cells. Scale bar: 10 μm . Reproduced with permission.^[46] Copyright 2014, American Chemical Society.

obtain a gene delivery system. Therefore, a silk-based block copolymer comprising 6mer and a poly(L-lysine) domain was developed. This protein formed ionic complexes with pDNA encoding GFP. The complex formation was analyzed with agarose gel electrophoresis, dynamic light scattering (DLS), and AFM, showing that the protein self-assembled into globules with pDNA possessing a solution diameter of about 380 nm. Human embryonic kidney (HEK) cells were transfected with an efficiency of 14% and no cytotoxicity was observed.^[149] Several follow-up studies were performed, all including different tags to increase transfection efficiency. A ppTG1 peptide was added, which is known to destabilize and penetrate cell membranes. Here, the protein was complexed with pDNA coding for GFP or Firefly Luciferase. Transfection efficiency of the complex to HEK cells and a melanoma cell line were comparable to Lipofectamine 2000, a golden standard gene vector. The cell viability was with 75% and 69% lower than in previous studies, but similar to that in presence of Lipofectamine 2000.^[150] Further, the cell binding motif RGD was added up to eleven times to the block

copolymer, which was then complexed with pDNA coding for Firefly Luciferase. Transfection was investigated with HeLa and HEK cells, whereby the transfection efficiency was clearly the highest with the protein complex with eleven RGD motifs, but approximately an order of magnitude lower than with Lipofectamine 2000. No significant effect on cell viability was observed.^[151] In a follow-up study, the tumor-homing peptides F3 and CGKRK were genetically added to the spider silk-poly(L-Lysine) construct. Transfection experiments were performed with melanoma cells as well as highly metastatic human breast tumor cells, and nontumorigenic cells were used as control. Again, a Luciferase assay was used to determine successful transfection. All complexes preferably transfected the tumorigenic cell lines and showed almost no transfection of the nontumorigenic cells. Further, the constructs were shown to be noncytotoxic by an MTS cell proliferation assay. Additionally, an *in vivo* study in tumor-bearing mice was performed and showed that from day seven on Luciferase was significantly produced in the tumor.^[152] In the latest study by Numata et al. again tumor-homing peptides, namely

F3 and Lyp1, were investigated in combination with a shortened spider silk-poly(L-lysine) construct (1mer + 15 Lysines). The goal here was to increase the molar percentage of the tumor-homing peptides. The same cells as in the previous study were tested and it could be shown that again a selective transfection of tumorigenic cells occurred. The F3 bearing complex with a size of about 100 nm was less cytotoxic and showed an overall better transfection efficiency and is therefore the more promising candidate.^[153]

In summary, it can be said that particulate drug delivery systems made of recombinant silk proteins have been thoroughly investigated using SEM,^[46,47,58b,63,129b,139,142–145,147,148] LDS,^[139,144,145] or DLS^[25,58b,129b,144] to determine particle size. Minor changes in the recombinant silk protein, the intrinsic properties of the (model) drug, the method of preparation and loading, as well as the release conditions have a major influence on loading efficiency and release kinetics. Further it was found that positively charged particles made of eADF4(κ16) are up-taken more efficiently, showing the usefulness of recombinant silks for mechanistic cellular-uptake studies.^[120b] Additionally, systems can be cell-targeted by the introduction of binding peptides as shown for H2.1/2MS1 particles.^[46] However, all recombinant silk particles systems have to be tested in vivo to see if these drug delivery systems are effective in a clinical setting.

7. Summary of Recombinant Silk in BME

In this review, the potential of recombinant silk proteins as a biomaterial was illustrated, **Figure 13**. They have been applied with particular success in tissue engineering and medical implant coatings, where it was found that cell behavior can be controlled by altering the charge,^[33e] by introducing cell-binding peptides^[74] and by changing the morphology of the scaffold.^[33a,71] Although there is no obvious, direct correlation between secondary structure content and cell behavior, it can have indirect effects due to changes in mechanical properties or hydrophobicity. However, the secondary structure content has a direct effect on properties such as chemical stability and drug loading. Although drug delivery systems have been shown to be functional in vitro, none of the systems developed so far have been tested in animal models. Although there are many advantages of using recombinant spider silk proteins for medical applications compared to other proteins, there are three in particular which the authors believe make this class of proteins exceptional.

The de novo production of recombinant proteins guarantees reproducible quality in the necessary quantities. This thereby also enables tailoring materials to have a special functionality,^[31c,154] for example by the introduction of different binding peptides.^[77c] The latter is particularly interesting, as most materials made of unmodified recombinant silk proteins are inert to cells, not allowing for attachment or differentiation, but also not causing any cytotoxicity. This is significant in that it makes it possible to culture cells on recombinant silk, and also provides a particularly powerful tool for mechanistically studying the effects of these binding peptides, or any other property such as topography.^[87,155] A step remaining for approving this material for cell culture is the regular removal of endotoxins, a

common byproduct from gram negative bacteria (e.g., *E. coli*).^[156] However, it is clear from the studies from one group, that it is possible to achieve a complete removal of these byproducts by using purification columns, as well as sterilize silk proteins.^[73a]

The second property of recombinant silk materials which makes them particularly outstanding as a biomaterial is the way the body responds to them. First demonstrated in 1710 as a wound dressing, spider silk could prevent bleeding and promote wound healing.^[28c] It has been recently shown in animal models that there is no significant fibrous capsule formation around recombinant silk-coated implants,^[25] as well as a significant reduction in the infiltration of inflammatory cells compared to controls.^[72] Further, spider silk implanted into pigs subcutaneously was locally tolerated.^[157] Problems with biocompatibility of silkworm silk only occurred due to sericins, which are glue-like proteins that encapsulate the raw fiber (also found in transgenic silkworm silk).^[28a] Hence, no immune response was observed with silk proteins, providing the perfect base for biomedical applications.

The third exceptional property of recombinant silks is that the biodegradability is slow, and it remains mechanically stable under physiological conditions for a significant amount of time. This is true even for fragile structures such as films or foams, which is unique compared to other naturally derived biomaterials; this is likely due to the low number of available sites for hydrolysis or active biodegradation of silk materials.^[24] On the other hand, degradation is still possible given the availability of matrix metalloproteinase (MMP) degradation sites in the primary structure, making it also more advantageous compared to stable, synthetic polymers which have no biodegradation sites.^[33d] However, it is important to note that the silk materials must be tested case-by-case because protein folding alters the availability of cleavage sites,^[51b] and sometimes it is necessary to introduce additional degradation sites into the recombinant silk protein.^[135]

The performance and success of a biomaterial is greatly determined by its stability in vivo, the rate of degradation, and the degradation products. Important hereby is that the biomaterial's degradation rate is similar compared to the rate that the cells are producing their own ECM. During the degradation, the biomaterial ideally keeps its mechanical stability to avoid collapsing of the newly formed tissue. Furthermore, the degradation products should not only be nontoxic, but in addition should not negatively influence the surrounding tissue as for example by lowering the pH, which is a common problem of polyesters. This is one of the reasons why naturally occurring or derived materials such as polysaccharides and proteins are gaining interest in the biomedical field; the body recognizes the degradation products and can clear them.^[96a]

In a foundational study on recombinant silk biodegradation, Lammel et al. investigated spider silk particle degradation using elastase and trypsin. It was found that elastase and trypsin first degrade the hydrophilic parts of the eADF4(C16) particle shell, and the hydrophobic particles then agglomerate. A rearrangement in the agglomerated particles leads to exposure of hydrophilic parts, which can then again be degraded.^[145] Further it was shown that eADF4(C16) particles can be completely digested using proteinase K or artificial intestinal fluid, but not in artificial gastric fluid.^[47] In a

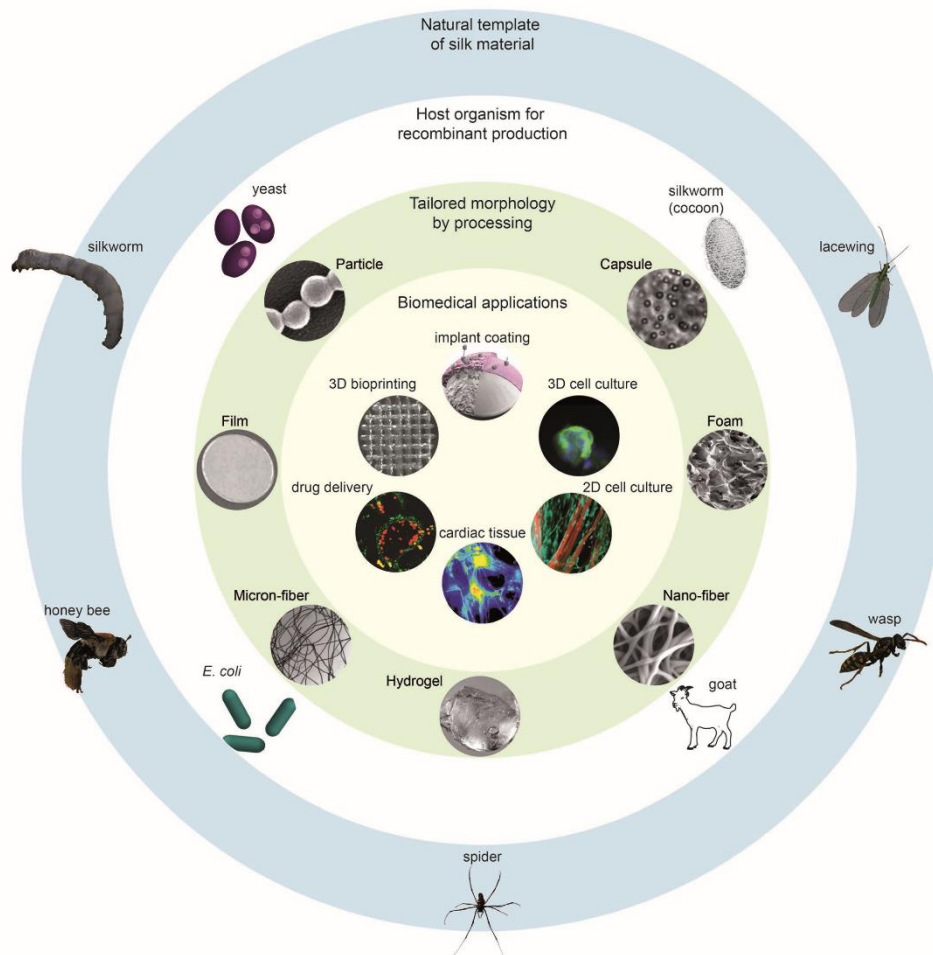


Figure 13. Recombinant silk proteins used as a biomaterial for biomedical engineering applications. Recombinant silk proteins were engineered and produced in host organisms, enabling the development of different morphologies and screening for putative applications. Silk worm, honey bee and wasp photos were taken and modified from open source images found on Pexels or Pixabay. 2D cell culture; Reproduced with permission.^[73] Copyright 2010, American Chemical Society. 3D cell culture; Reproduced with permission.^[75b] Copyright 2016, Elsevier. Cardiac tissue.^[33a] Implant coating.^[25] Drug delivery; Reproduced with permission.^[46] Copyright 2014, American Chemical Society.

follow up study *in vitro*, the degradation of several different eADF4(C16) scaffolds was investigated. It was found that the soluble protein could be immediately degraded by the recombinant human proteases MMP-2 and polymorphonuclear (PMN) elastase within less than a minute. Further, the degradation of particles, films, and nonwoven meshes with and without crosslinking was investigated over 15 d in the presence of two bacterial model proteases, namely protease type XIV (PXIV) resembling a digestive model and collagenase type IA (CHC) resembling a wound environment, and was shown to be significantly slower than for soluble silk proteins.^[33d]

In general, all scaffolds were degraded faster by PXIV than by CHC, whereby crosslinking the scaffolds with APS and Rubpy

decreased the degradation rate. In absence of proteases almost no degradation was observed during the whole experiment. Also the morphology of the silk scaffold played a major role on the proteolytic stability, here particles degraded the fastest, followed by films and nonwoven meshes. No correlation was found between initial secondary structure contents of the scaffolds and its degradation rate. A 500× higher protease concentration than occurring in natural environment had to be used in order to measure degradation in a reasonable time frame. Therefore, degradation *in vivo* is supposed to be much slower.^[33d] This slow degradation *in vivo*, indirectly determined for eADF4(C16), was still found on coated silicone implants twelve months after implantation.^[25]

Spider silk implant coatings of polydimethylsiloxane (PDMS) resulted in a similar behavior, whereby the coating was rather stable against degradation by CHC, but was fully degraded in the presence of PXIV within 6 d.^[91] Furthermore, enzymatic degradation of eADF4(C16) foams was investigated using the same enzymes. A 1300× higher protease concentration than found in natural environment was used and led to a full degradation in the presence of PXIV within 4 d, whereby 75% of the scaffolds were still left after treatment with CHC for 15 d.^[33c] Moisenovich et al. performed two studies with rS1/9 silk foams, whereby the same degradation experiment was performed. Foams were incubated in PBS and Fenton's reagent (0.1×10^{-3} M FeSO_4 , 1×10^{-3} M H_2O_2). It was shown that the foams are quite stable in PBS (20% loss), but degrade very fast in Fenton's reagent (>90% loss) over 11 weeks.^[49] Interestingly, a similar result was obtained in the follow up study already after 7 weeks.^[61b]

The degradation of recombinant honey bee silk AmelF3 was investigated using trypsin and α -chymotrypsin, both commonly found in the digestive system in the small intestine.^[159] As in the case of eADF4(C16), the protein was completely stable in buffer, and experienced rapid degradation only in presence of a protease. In a similar study, attachment of primary GFP-expressing fibroblasts from rabbits to AmelF3 nonwoven mats, and further degradation of the nonwoven meshes, was evaluated.^[51b]

Price et al. even introduced a sequence recognized by MMPs to SELP-815K in order to improve the degradability. In the presence of 40×10^{-9} M MMP-2, there was complete degradation of the protein in solution within 120 min, and hydrogels in vitro were significantly degraded after 14 d; and there was a corresponding increase in soluble protein found in solution. For in vivo testing, mice were infected with JHU-022 human head, and neck squamous cell carcinoma and the SELP-815K modified with the degradation sequence were assembled into hydrogels containing either saline or virus and were directly injected into the tumor. In vitro, hydrogels containing the degradation sequence could be degraded by MMP-2 completely after 60 min, whereas there was no degradation detected for those not containing the degradation sequence. By tailoring the hydrogel formulation, prolonged expression of the adenovirus could be achieved, and thereby there was a decreased growth rate of the tumor and an increase in the survival rate over a 50-day period, compared to the animals where adenovirus was injected alone.^[158]

8. Conclusion

In this review the use of recombinant silk proteins as a bio-material assembled into different morphologies is summarized, and particularly promising results are highlighted. It can be stated that materials prepared from recombinant silk proteins show some clear advantages for BME compared to other biomaterials, such as their high-quality de novo production, low immunogenicity, and slow biodegradation. The next important step is to obtain FDA-approval for recombinant silk materials and then it is likely that these biomaterials will be used more frequently, and with great anticipation and hope for future success.

Acknowledgements

T.B.A. and E.D. contributed equally to this work. This work was financially supported by DFG grant SFB 840 TP A8 (to T.S.), European Union grand ETZ-EFRE 2014-2020, Freistaat Bayern-Tschechien, Project ID 123 (to T.S.), and the Bavarian Research Foundation (DOK 175-15, to T.B.A.). The authors would also like to thank Heike Herold and Adrian Golser for contributing advice and knowledge, which improved the content of this review.

Conflict of Interest

The authors declare no conflict of interest.

Keywords

biomaterials, biomedical engineering, drug delivery, recombinant silk, silk processing

Received: August 15, 2017

Revised: October 26, 2017

Published online:

- [1] BMES, BMES—FAQs about BME, <http://www.bmes.org/content.asp?contentid=140> (accessed: August 2017).
- [2] a) WHO, *World Health Statistics 2016: Monitoring Health for the SDGs*, WHO Press, Geneva, Switzerland 2016; b) V. Kontis, J. E. Bennett, C. D. Mathers, G. Li, K. Foreman, M. Ezzati, *Lancet* 2017, 389, 1323.
- [3] a) T. Niccoli, L. Partridge, *Curr. Biol.* 2012, 22, R741; b) M. C. Nevitt, S. R. Cummings, E. S. Hudes, *J. Gerontol.* 1991, 46, M164.
- [4] J. M. Quintana, I. Arostegui, A. Escobar, J. Azkarate, J. I. Goenaga, I. Lafuente, *Arch. Intern. Med.* 2008, 168, 1576.
- [5] NIH, Who Needs a Pacemaker?, <https://www.nihbi.nih.gov/health/health-topics/topics/pace/whoneeds> (accessed: August 2017).
- [6] J. S. Miller, *PLoS Biol.* 2014, 12, e1001882.
- [7] M. J. Lysaght, J. A. O'Loughlin, *ASAIO J.* 2000, 46, 515.
- [8] Alzheimer's Association, *2016 Alzheimer's Disease Facts and Figures*, Chicago, Washington 2016.
- [9] CDC, Statistics Reported by Center for Disease Control and Prevention, <https://www.cdc.gov/> (accessed: August 2017).
- [10] *Stem Cells, Tissue Engineering and Regenerative Medicine* (Eds: D. Warburton), World Scientific Publishing Co. Pte. Ltd., Singapore 2015.
- [11] a) J. W. Michael, K. U. Schluter-Brust, P. Eysel, *Dtsch. Arztebl. Int.* 2010, 107, 152; b) E. A. Makris, A. H. Gomoll, K. N. Malizos, J. C. Hu, K. A. Athanasiou, *Nat. Rev. Rheumatol.* 2015, 11, 21.
- [12] S. S. Magill, J. R. Edwards, W. Bamberg, Z. G. Beldavs, G. Dumyati, M. A. Kainer, R. Lynfield, M. Maloney, L. McAllister-Hollod, J. Nadle, S. M. Ray, D. L. Thompson, L. E. Wilson, S. K. Fridkin, E. I. P. Healthcare, *N. Engl. J. Med.* 2014, 370, 1198.
- [13] D. M. Sievert, P. Ricks, J. R. Edwards, A. Schneider, J. Patel, A. Srinivasan, A. Kallen, B. Limbago, S. Fridkin, N. H. S. Network, P. N. Facilities, *Infect. Control Hosp. Epidemiol.* 2013, 34, 1.
- [14] S. B. Levy, B. Marshall, *Nat. Med.* 2004, 10, S122.
- [15] HELI, Health and Environment Linkages Initiative, <http://www.who.int/heli/en/> (accessed: August 2017).
- [16] M. M. Rodgers, V. M. Pai, R. S. Conroy, *IEEE Sens. J.* 2015, 15, 3119.

- [17] BRAIN-Initiative, Brain stimulation, <http://www.braininitiative.org/> (accessed: August 2017).
- [18] E. Strickland, 3 Squishy Medical Robots That Are as Soft as You Are, <http://spectrum.ieee.org/biomedical/devices/3-squishy-medical-robots-that-are-as-soft-as-you-are> (accessed: August 2017).
- [19] a) D. Huh, B. D. Matthews, A. Marmiroto, M. Montoya-Zavala, H. Y. Hsin, D. E. Ingber, *Science* 2010, 328, 1662; b) A. M. Hopkins, E. DeSimone, K. Chwalek, D. L. Kaplan, *Prog. Neurobiol.* 2015, 125, 1.
- [20] D. Campoccia, L. Montanaro, C. R. Arciola, *Biomaterials* 2013, 34, 8533.
- [21] J. Groll, T. Boland, T. Blunk, J. A. Burdick, D. W. Cho, P. D. Dalton, B. Derby, G. Forgacs, Q. Li, V. A. Mironov, L. Moroni, M. Nakamura, W. Shu, S. Takeuchi, G. Vozzi, T. B. Woodfield, T. Xu, J. J. Yoo, J. Malda, *Biofabrication* 2016, 8, 013001.
- [22] J. P. Ioannidis, *PLoS Med.* 2005, 2, e124.
- [23] C. Wu, B. Wang, C. Zhang, R. A. Wysk, Y. W. Chen, *Crit. Rev. Biotechnol.* 2017, 37, 333.
- [24] L. S. Nair, C. T. Laurencin, *Prog. Polym. Sci.* 2007, 32, 762.
- [25] P. H. Zepelin, N. C. Maksimovikj, M. C. Jordan, J. Nickel, G. Lang, A. H. Leimer, L. Roemer, T. Scheibel, *Adv. Funct. Mater.* 2014, 24, 2658.
- [26] L. DeFrancesco, *Nat. Biotechnol.* 2017, 35, 496.
- [27] V. Elisseeff, in *The Silk Roads: Highways of Culture and Commerce* (Ed: V. Elisseeff), Berghahn Books, UNESCO Publishing, New York, USA 2000.
- [28] a) M. Bon, *Philos. Trans. R. Soc., B* 1710, 27, 2; b) M. Santin, A. Motta, G. Freddi, M. Cannas, *J. Biomed. Mater. Res.* 1999, 46, 382; c) G. H. Altman, F. Diaz, C. Jakuba, T. Calabro, R. L. Horan, J. S. Chen, H. Lu, J. Richmond, D. L. Kaplan, *Biomaterials* 2003, 24, 401.
- [29] C. L. Craig, *Annu. Rev. Entomol.* 1997, 42, 231.
- [30] T. D. Sutherland, J. H. Young, S. Weisman, C. Y. Hayashi, D. J. Merriitt, *Annu. Rev. Entomol.* 2010, 55, 171.
- [31] a) E. Bini, C. W. P. Foo, J. Huang, V. Karageorgiou, B. Kitchel, D. L. Kaplan, *Biomacromolecules* 2006, 7, 3139; b) M. Hedhammar, A. Rising, S. Grip, A. S. Martinez, K. Nordling, C. Casals, M. Stark, J. Johansson, *Biochemistry* 2008, 47, 3407; c) S. Wohlrab, K. Spiess, T. Scheibel, *J. Mater. Chem.* 2012, 22, 22050; d) T. Asakura, Y. Suzuki, A. Nagano, D. Knight, M. Kamiya, M. Dernura, *Biomacromolecules* 2013, 14, 3731.
- [32] X. Hu, D. Kaplan, P. Cebe, *Macromolecules* 2006, 39, 6161.
- [33] a) A. Leal-Egana, G. Lang, C. Mauerer, J. Wickinghoff, M. Weber, S. Geirner, T. Scheibel, *Adv. Eng. Mater.* 2012, 14, B67; b) F. Bauer, S. Wohlrab, T. Scheibel, *Biomater. Sci.* 2013, 1, 1244; c) K. Schacht, J. Vogt, T. Scheibel, *ACS Biomater. Sci. Eng.* 2016, 2, 517; d) S. Müller-Herrmann, T. Scheibel, *ACS Biomater. Sci. Eng.* 2015, 1, 247; e) J. Petzold, T. B. Aigner, F. Touska, K. Zimmermann, T. Scheibel, F. B. Engel, *Adv. Funct. Mater.* 2017, 27, 1701427.
- [34] R. Foelix, *Biology of Spiders*, 3rd ed., Oxford University Press, Oxford, UK 2011.
- [35] C. Thamm, T. Scheibel, *Biomacromolecules* 2017, 18, 1365.
- [36] a) O. Tokareva, V. A. Michalczyk-Lacerda, E. L. Rech, D. L. Kaplan, *Microb. Biotechnol.* 2013, 6, 651; b) X. Hu, K. Vasanthavada, K. Kohler, S. McNary, A. M. Moore, C. A. Vierra, *Cell. Mol. Life Sci.* 2006, 63, 1986; c) A. E. Brooks, H. B. Steinkraus, S. R. Nelson, R. V. Lewis, *Biomacromolecules* 2005, 6, 3095; d) C. Y. Hayashi, N. H. Shipley, R. V. Lewis, *Int. J. Biol. Macromol.* 1999, 24, 271.
- [37] J. M. Aarnodt, D. W. Grainger, *Biomaterials* 2016, 86, 68.
- [38] a) F. Vollrath, *Int. J. Biol. Macromol.* 1999, 24, 81; b) B. Madsen, Z. Z. Shao, F. Vollrath, *Int. J. Biol. Macromol.* 1999, 24, 301; c) A. Spöner, W. Vater, S. Monajernbashi, E. Unger, F. Grosse, K. Weisshart, *PLoS One* 2007, 2, e998; d) K. H. Guehrs, B. Schlott, F. Grosse, K. Weisshart, *Insect Mol. Biol.* 2008, 17, 553; e) L. Eisoldt, A. Smitth, T. Scheibel, *Mater. Today* 2011, 14, 80.
- [39] C. Radtke, C. Allmeling, K. H. Waldmann, K. Reiners, K. Thies, H. C. Schenk, A. Hillmer, M. Guggenheirn, G. Brandes, P. M. Vogt, *PLoS One* 2011, 6, e16990.
- [40] M. Neuenfeldt, T. Scheibel, *Biomolecules* 2017, 7, 43.
- [41] J. A. M. Ramshaw, J. A. Werkmeister, G. J. Dumsday, *Bioengineered* 2014, 5, 227.
- [42] S. Chattopadhyay, R. T. Raines, *Biopolymers* 2014, 101, 821.
- [43] a) H. M. Herold, T. Scheibel, *Z. Naturforsch. C: J. Biosci.* 2017, 72, 365; b) T. Asakura, T. Miller, in *The Power of Recombinant Spider Silk Proteins* (Eds: S. Wohlrab, C. Thamm, T. Scheibel), Springer Science+Business Media Dordrecht, Dordrecht 2014; c) D. L. Kaplan, T. Scheibel, in *Reference Module in Materials Science and Materials Engineering* (Ed: S. Hashmi), Elsevier Inc., Amsterdam 2017; d) A. Heidebrecht, T. Scheibel, in *Advances in Applied Microbiology*, Vol. 82, (Eds: G. Gadd, S. Sariaslani), Elsevier Inc., Amsterdam, Netherlands 2013; e) T. Kato, M. Kajikawa, K. Maenaka, E. Y. Park, *Appl. Microbiol. Biotechnol.* 2010, 85, 459.
- [44] G. L. Rosano, E. A. Ceccarelli, *Front. Microbiol.* 2014, 5, 172.
- [45] D. Huemmerich, T. Scheibel, F. Vollrath, S. Cohen, U. Gar, S. Iltah, *Curr. Biol.* 2004, 14, 2070.
- [46] A. Florczak, A. Mackiewicz, H. Dams-Kozłowska, *Biomacromolecules* 2014, 15, 2971.
- [47] B. Liebmann, D. Huemmerich, T. Scheibel, M. Fehr, *Colloids Surf., A* 2008, 337, 126.
- [48] K. D. Hermanson, D. Huemmerich, T. Scheibel, A. R. Bausch, *Adv. Mater.* 2007, 19, 1810.
- [49] M. M. Moisenovich, O. L. Pustovalova, A. Y. Arhipova, T. V. Vasiljeva, O. S. Sokolova, V. G. Bogush, V. G. Debabov, V. I. Sevastianov, M. P. Kirpichnikov, I. I. Agapov, *J. Biomed. Mater. Res., Part A* 2011, 96A, 125.
- [50] A. Teplenin, A. Krasheninnikova, N. Agladze, K. Sidoruk, O. Agapova, I. Agapov, V. Bogush, K. Agladze, *PLoS One* 2015, 10, e0121155.
- [51] a) S. Weisman, V. S. Haritos, J. S. Church, M. G. Huson, S. T. Mudie, A. J. W. Rodgers, G. J. Dumsday, T. D. Sutherland, *Biomaterials* 2010, 31, 2695; b) C. R. Wittner, X. Hu, P. C. Gauthier, S. Weisman, D. L. Kaplan, T. D. Sutherland, *Acta Biomater.* 2011, 7, 3789.
- [52] a) T. Tamura, C. Thibert, C. Royer, T. Kanda, E. Abraham, M. Kamba, N. Kornoto, J. L. Thomas, B. Mauchamp, G. Chavancy, P. Shirk, M. Fraser, J. C. Prudhomme, P. Couble, *Nat. Biotechnol.* 2000, 18, 559; b) K. Kojima, Y. Kuwana, H. Sezutsu, I. Kobayashi, K. Uchino, T. Tamura, Y. Tamada, *Biosci., Biotechnol., Biochem.* 2007, 71, 2943; c) S. Yanagisawa, Z. H. Zhu, I. Kobayashi, K. Uchino, Y. Tamada, T. Tamura, T. Asakura, *Biomacromolecules* 2007, 8, 3487.
- [53] a) Y. Kambe, K. Yamamoto, K. Kojima, Y. Tamada, N. Torrita, *Biomaterials* 2010, 31, 7503; b) S. Inoue, K. Tanaka, F. Arisaka, S. Kimura, K. Ohtomo, S. Mizuno, *J. Biol. Chem.* 2000, 275, 40517.
- [54] a) A. Nagano, Y. Tanioka, N. Sakurai, H. Sezutsu, N. Kuboyama, H. Kiba, Y. Tanimoto, N. Nishiyama, T. Asakura, *Acta Biomater.* 2011, 7, 1192; b) A. Nagano, H. Sato, Y. Tanioka, Y. Nakazawa, D. Knight, T. Asakura, *Soft Matter* 2012, 8, 741.
- [55] a) J. Cappello, J. Crissman, M. Dornan, M. Mikolajczak, G. Textor, M. Marquet, F. Ferrari, *Biotechnol. Prog.* 1990, 6, 198; b) R. Dandu, A. Von Cresce, R. Briber, P. Dowell, J. Cappello, H. Ghandehari, *Polymer* 2009, 50, 366; c) A. Poursaid, R. Price, A. Tiede, E. Olson, E. Huo, L. McGill, H. Ghandehari, J. Cappello, *Biomaterials* 2015, 57, 142.
- [56] F. Bauer, T. Scheibel, *Angew. Chem., Int. Ed.* 2012, 51, 6521.
- [57] a) Y. Kambe, T. Karneda, *J. Silk Sci. Technol. Jpn.* 2014, 22, 47; b) Y. Kambe, T. D. Sutherland, T. Karneda, *Acta Biomater.* 2014, 10, 3590.

- [58] a) D. Huemmerich, C. W. Helsen, S. Quedzuweit, J. Oschmann, R. Rudolph, T. Scheibel, *Biochemistry* 2004, 43, 13604; b) E. Doblhofer, T. Scheibel, *J. Pharm. Sci.* 2015, 104, 988.
- [59] M. Stark, S. Grip, A. Rising, M. Hedhammar, W. Engstrom, G. Hjalm, J. Johansson, *Biomacromolecules* 2007, 8, 1695.
- [60] a) H. Darns-Kozłowska, A. Majer, P. Tomaszewicz, J. Lozinska, D. L. Kaplan, A. Mackiewicz, *J. Biomed. Mater. Res., Part A* 2013, 701, 456; b) S. C. Gomes, I. B. Leonor, J. F. Mano, R. L. Reis, D. L. Kaplan, *Biomaterials* 2011, 32, 4255.
- [61] a) I. I. Agapov, O. L. Pustovalova, M. M. Moisenovich, V. G. Bogush, O. S. Sokolova, V. I. Sevastyanov, V. G. Debabov, M. P. Kirpichnikov, *Dokl. Biochem. Biophys.* 2009, 426, 127; b) M. M. Moisenovich, O. Pustovalova, J. Shackelford, T. V. Vasiljeva, T. V. Druzhinina, Y. A. Karnenchuk, V. V. Guzeev, O. S. Sokolova, V. G. Bogush, V. G. Debabov, M. P. Kirpichnikov, I. I. Agapov, *Biomaterials* 2012, 33, 3887.
- [62] T. I. Harris, D. A. Gaztambide, B. A. Day, C. L. Brock, A. L. Ruben, J. A. Jones, R. V. Lewis, *Biomacromolecules* 2016, 17, 3761.
- [63] K. Jastrzebska, E. Felcyn, M. Kozak, M. Szybowicz, T. Buchwald, Z. Pietralik, T. Jesionowski, A. Mackiewicz, H. Darns-Kozłowska, *Sci. Rep.* 2016, 6, 28106.
- [64] a) C. Mason, P. Dunnill, *Regener. Med.* 2008, 3, 1; b) NIBIB, Tissue Engineering and Regenerative Medicine, <https://www.nibib.nih.gov/science-education/science-topics/tissue-engineering-and-regenerative-medicine> (accessed: August 2017).
- [65] a) A. Khadernhosseini, R. Langer, *Nat. Protoc.* 2016, 11, 1775; b) M. J. Webber, O. F. Khan, S. A. Sydlík, B. C. Tang, R. Langer, *Ann. Biomed. Eng.* 2015, 43, 641; c) H. Sadri-Ardekani, A. Atala, *Methods* 2016, 99, 1; d) D. F. Williams, *Biomaterials* 2014, 35, 10009.
- [66] J. W. Nichol, A. Khadernhosseini, *Soft Matter* 2009, 5, 1312.
- [67] NIH, *NIH Consens Statement Online* 1982, 4, 19.
- [68] a) A. D. Doyle, F. W. Wang, K. Matsumoto, K. M. Yamada, *J. Cell Biol.* 2009, 184, 481; b) G. Charras, E. Sahai, *Nat. Rev. Mol. Cell Biol.* 2014, 15, 813.
- [69] a) A. Heidebrecht, L. Eisoldt, J. Diehl, A. Schmidt, M. Geffers, G. Lang, T. Scheibel, *Adv. Mater.* 2015, 27, 2189; b) M. Andersson, Q. P. Jia, A. Abella, X. Y. Lee, M. Landreh, P. Purhonen, H. Hebert, M. Tenje, C. V. Robinson, Q. Meng, G. R. Plaza, J. Johansson, A. Rising, *Nat. Chem. Biol.* 2017, 13, 262.
- [70] G. Li, Y. Li, G. Q. Chen, J. H. He, Y. F. Han, X. Q. Wang, D. L. Kaplan, *Adv. Healthcare Mater.* 2015, 4, 1134.
- [71] M. Widhe, H. Byssell, S. Nystedt, I. Schenning, M. Malrsten, J. Johansson, A. Rising, M. Hedhammar, *Biomaterials* 2010, 31, 9575.
- [72] C. Fredriksson, M. Hedhammar, R. Feinstein, K. Nordling, G. Kratz, J. Johansson, F. Huss, A. Rising, *Materials* 2009, 2, 1908.
- [73] M. Hedhammar, H. Brarrfeldt, T. Baris, M. Widhe, G. Askarieh, K. Nordling, S. von Aulock, J. Johansson, *Biomacromolecules* 2010, 11, 953.
- [74] M. Widhe, U. Johansson, C. O. Hillerdahl, M. Hedhammar, *Biomaterials* 2013, 34, 8223.
- [75] a) S. Q. Wu, J. Johansson, P. Dardimopoulou, M. Shahsavani, A. Falk, O. Hovatta, A. Rising, *Biomaterials* 2014, 35, 8496; b) N. D. Shalaly, M. Ria, U. Johansson, K. Avall, P. O. Berggren, M. Hedhammar, *Biomaterials* 2016, 90, 50; c) D. Harvey, P. Bardelang, S. L. Goodacre, A. Cockayne, N. R. Thomas, *Adv. Mater.* 2017, 29, 1604245.
- [76] U. Johansson, M. Ria, K. Avall, N. D. Shalaly, S. V. Zaitsev, P. O. Berggren, M. Hedhammar, *PLoS One* 2015, 10, e0130169.
- [77] a) Y. Nakazawa, M. Sato, R. Takahashi, D. Aytterniz, C. Takabayashi, T. Tamura, S. Enomoto, M. Sata, T. Asakura, *J. Biomater. Sci., Polym. Ed.* 2011, 22, 195; b) T. Asakura, M. Isozaki, T. Saotome, K. I. Tatematsu, H. Sezutsu, N. Kuwabara, Y. Nakazawa, *J. Mater. Chem. B* 2014, 2, 7375; c) T. Saotome, H. Hayashi, R. Tanaka, A. Kinugasa, S. Uesugi, K. Tatematsu, H. Sezutsu, N. Kuwabara, T. Asakura, *J. Mater. Chem. B* 2015, 3, 7109.
- [78] R. Vasita, D. S. Katti, *Int. J. Nanomed.* 2006, 1, 15.
- [79] T. Fukunishi, C. A. Best, T. Sugijura, J. Opfermann, C. S. Ong, T. Shinoka, C. K. Breuer, A. Krieger, J. Johnson, N. Hibino, *J. Thorac. Cardiovasc. Surg* 2017, 153, 924.
- [80] S. K. Seidlits, J. Y. Lee, C. E. Schmidt, *Nanomedicine (London, U. K.)* 2008, 3, 183.
- [81] a) Z. X. Cai, X. M. Mo, K. H. Zhang, L. P. Fan, A. L. Yin, C. L. He, H. S. Wang, *Int. J. Mol. Sci.* 2010, 11, 3529; b) J. P. Chen, G. Y. Chang, J. K. Chen, *Colloid Surf., A* 2008, 313, 183.
- [82] N. Bhardwaj, S. C. Kundu, *Biotechnol. Adv.* 2010, 28, 325.
- [83] G. Taylor, *Proc. R. Soc. London, Ser. A* 1964, 280, 383.
- [84] S. B. Cai, H. L. Xu, Q. R. Jiang, Y. Q. Yang, *Langmuir* 2013, 29, 2311.
- [85] A. Koski, K. Yim, S. Shivkumar, *Mater. Lett.* 2004, 58, 493.
- [86] J. L. Lowery, N. Datta, G. C. Rutledge, *Biomaterials* 2010, 31, 491.
- [87] B. Zhu, W. Li, R. V. Lewis, C. U. Segre, R. Wang, *Biomacromolecules* 2015, 16, 202.
- [88] a) J. G. Hardy, A. Pfaff, A. Leal-Egana, A. H. E. Muller, T. R. Scheibel, *Macromol. Biosci.* 2014, 14, 936; b) B. An, M. D. Tang-Schorner, W. W. Huang, J. Y. He, J. A. Jones, R. V. Lewis, D. L. Kaplan, *Biomaterials* 2015, 48, 137.
- [89] a) S. Wohlrab, S. Muller, A. Schmidt, S. Neubauer, H. Kessler, A. Leal-Egana, T. Scheibel, *Biomaterials* 2012, 33, 6650; b) S. Gomes, K. Nurnata, I. B. Leonor, J. F. Mano, R. L. Reis, D. L. Kaplan, *Biomacromolecules* 2011, 12, 1675; c) S. Gomes, I. B. Leonor, J. F. Mano, R. L. Reis, D. L. Kaplan, *Soft Matter* 2011, 7, 4964; d) S. Gomes, J. Gallego-Llomas, I. B. Leonor, J. F. Mano, R. L. Reis, D. L. Kaplan, *J. Tissue Eng. Regen. Med.* 2012, 6, 356.
- [90] a) M. Lewicka, O. Hermanson, A. U. Rising, *Biomaterials* 2012, 33, 7712; b) S. Wu, J. Johansson, O. Hovatta, A. Rising, *Cell. Mol. Life Sci.* 2016, 73, 1479.
- [91] C. B. Borkner, S. Wohlrab, E. Möller, G. Lang, T. Scheibel, *ACS Biomater. Sci. Eng.* 2017, 3, 767.
- [92] A. J. Mieszawska, L. D. Nadkarni, C. C. Perry, D. L. Kaplan, *Chem. Mater.* 2010, 22, 5780.
- [93] M. Widhe, N. D. Shalaly, M. Hedhammar, *Biomaterials* 2016, 74, 256.
- [94] J. Johansson, A. Rising, *Front. Bioeng. Biotechnol.* 2014, 2, 50.
- [95] A. K. Salern, R. Stevens, R. G. Pearson, M. C. Davies, S. J. B. Tendler, C. J. Roberts, P. M. Williams, K. M. Shakesheff, *J. Biomed. Mater. Res.* 2002, 61, 212.
- [96] a) H. Naderi, M. M. Matin, A. R. Bahrami, *J. Biomater. Appl.* 2011, 26, 383; b) E. A. Botchwey, M. A. Dupree, S. R. Pollack, E. M. Levine, C. T. Laurencin, *J. Biomed. Mater. Res., Part A* 2003, 67A, 357.
- [97] D. J. Mooney, D. F. Baldwin, N. P. Suh, L. P. Vacanti, R. Langer, *Biomaterials* 1996, 17, 1417.
- [98] A. G. Mikos, G. Sarakinos, S. M. Leite, J. P. Vacanti, R. Langer, *Biomaterials* 1993, 14, 323.
- [99] I. V. Yannas, J. F. Burke, P. L. Gordon, C. Huang, R. H. Rubenstein, *J. Biomed. Mater. Res.* 1980, 14, 107.
- [100] C. J. Doillon, C. F. Whyne, S. Brandwein, F. H. Silver, *J. Biomed. Mater. Res.* 1986, 20, 1219.
- [101] K. Whang, C. H. Thomas, K. E. Healy, G. Nuber, *Polymer* 1995, 36, 837.
- [102] N. Bolgen, F. Plieva, I. Y. Galaev, B. Mattiasson, E. Piskin, *J. Biomater. Sci., Polym. Ed.* 2007, 18, 1165.
- [103] J. Groll, U. Gbureck, K. Stuckensen, *Germany WO2013083844 A2*, 2013.
- [104] O. I. Agapova, A. E. Efimov, M. M. Moisenovich, V. G. Bogush, I. I. Agapov, *Russ. J. Transplantol. Artif. Organs* 2015, 17, 37.

- [105] Y. Qiu, K. Park, *Adv. Drug Delivery Rev.* 2001, 53, 321.
- [106] a) J. Maitra, V. K. Shukla, *Am. J. Polym. Sci.* 2014, 4, 7; b) Q. Chai, Y. Jiao, X. Yu, *Gels* 2017, 3, 15.
- [107] a) K. Schacht, T. Scheibel, *Biomacromolecules* 2011, 12, 2488; b) M. R. Matanovic, J. Kristl, P. A. Grabnar, *Int. J. Pharm.* 2014, 472, 262.
- [108] E. DeSimone, K. Schacht, T. Scheibel, *Mater. Lett.* 2016, 183, 101.
- [109] J. Thiele, Y. J. Ma, S. M. C. Bruekers, S. H. Ma, W. T. S. Huck, *Adv. Mater.* 2014, 26, 125.
- [110] K. Hölzl, S. M. Lin, L. Tytgat, S. Van Vlierberghe, L. X. Gu, A. Ovsianikov, *Biofabrication* 2016, 8, 032002.
- [111] U. J. Kim, J. Y. Park, C. M. Li, H. J. Jin, R. Valluzzi, D. L. Kaplan, *Biomacromolecules* 2004, 5, 786.
- [112] K. Schacht, T. Jüngst, M. Schweinlin, A. Ewald, J. Groll, T. Scheibel, *Angew. Chem.* 2015, 54, 5.
- [113] G. Donelli, I. Francolini, *J. Chemother.* 2001, 13, 595.
- [114] a) M. C. Shen, I. Garcia, R. V. Maier, T. A. Horbett, *J. Biomed. Mater. Res., Part A* 2004, 70A, 533; b) A. K. McNally, J. M. Anderson, *Am. J. Pathol.* 1995, 147, 1487.
- [115] D. G. Castner, B. D. Ratner, *Surf. Sci.* 2002, 500, 28.
- [116] J. M. Anderson, A. Rodriguez, D. T. Chang, *Semin. Immunol.* 2008, 20, 86.
- [117] P. H. Zepelin, A. K. Beminger, N. C. Maksimovikj, P. van Gelder, T. Scheibel, H. Walles, *Handchir. Mikrochir. Plast. Chir.* 2014, 46, 336.
- [118] L. Nileback, J. Hedin, M. Widhe, L. S. Floderus, A. Krona, H. Bysell, M. Hedhammar, *Biomacromolecules* 2017, 18, 846.
- [119] Y. Wang, D. S. Kohane, *Nat. Rev. Mater.* 2017, 2, 17020.
- [120] a) R. Langer, *Science* 1990, 249, 1527; b) M. B. Elsner, H. M. Herold, S. Müller-Herrmann, H. Barge, T. Scheibel, *Biomater. Sci.* 2015, 3, 543.
- [121] E. Agostini, G. Winter, J. Engert, *J. Controlled Release* 2015, 213, 134.
- [122] R. Langer, N. A. Peppas, *AIChE J.* 2003, 49, 2990.
- [123] V. Sanna, N. Pala, M. Sechi, *Int. J. Nanomed.* 2014, 9, 467.
- [124] a) X. Q. Wang, E. Wenk, A. Matsumoto, L. Meinel, C. M. Li, D. L. Kaplan, *J. Controlled Release* 2007, 117, 360; b) E. Wenk, A. J. Wandrey, H. P. Merkle, L. Meinel, *J. Controlled Release* 2008, 132, 26; c) E. Wenk, H. P. Merkle, L. Meinel, *J. Controlled Release* 2011, 150, 128.
- [125] a) P. Gupta, K. Vermani, S. Garg, *Drug Discovery Today* 2002, 7, 569; b) T. R. Hoare, D. S. Kohane, *Polymer* 2008, 49, 1993.
- [126] T. Banerjee, S. Mitra, A. K. Singh, R. K. Sharma, A. Maitra, *Int. J. Pharm.* 2002, 243, 93.
- [127] S. Ladet, L. David, A. Dornard, *Nature* 2008, 452, 76.
- [128] J. Gustafson, K. Greish, J. Frandsen, J. Cappello, H. Ghandehari, *J. Controlled Release* 2009, 140, 256.
- [129] a) J. M. Llovet, J. Bruix, B. C. L. C. Grp, *Hepatology* 2003, 37, 429; b) RSNA, Chemoembolization, <https://www.radiologyinfo.org/en/info.cfm?pg=chemoembol> (accessed: August 2017).
- [130] Y. F. Huang, K. Bailey, S. Wang, X. S. Feng, *React. Funct. Polym.* 2017, 116, 57.
- [131] S. Hofmann, C. T. W. P. Foo, F. Rossetti, M. Textor, G. Vunjak-Novakovic, D. L. Kaplan, H. P. Merkle, L. Meinel, *J. Controlled Release* 2006, 111, 219.
- [132] S. Z. Lu, X. Q. Wang, Q. Lu, X. Hu, N. Uppal, F. G. Omenetto, D. L. Kaplan, *Biomacromolecules* 2009, 10, 1032.
- [133] Q. Lu, X. Q. Wang, X. Hu, P. Cebe, F. Omenetto, D. L. Kaplan, *Macromol. Biosci.* 2010, 10, 359.
- [134] J. G. Hardy, A. Leal-Egana, T. R. Scheibel, *Macromol. Biosci.* 2013, 13, 1431.
- [135] T. M. S. Chang, *Nat. Rev. Drug Discovery* 2005, 4, 221.
- [136] a) O. Shchepelina, I. Drachuk, M. K. Gupta, J. Lin, V. V. Tsukruk, *Adv. Mater.* 2011, 23, 4655; b) C. H. Ye, O. Shchepelina, R. Calabrese, I. Drachuk, D. L. Kaplan, V. V. Tsukruk, *Biomacromolecules* 2011, 12, 4319; c) C. H. Ye, I. Drachuk, R. Calabrese, H. Q. Dai, D. L. Kaplan, V. V. Tsukruk, *Langmuir* 2012, 28, 12235.
- [137] a) K. D. Herrmannson, M. B. Harasim, T. Scheibel, A. R. Bausch, *Phys. Chem. Chem. Phys.* 2007, 9, 6442; b) C. Blum, A. Nichtl, T. Scheibel, *Adv. Funct. Mater.* 2014, 24, 763.
- [138] a) A. S. Lammell, X. Hu, S. H. Park, D. L. Kaplan, T. R. Scheibel, *Biomaterials* 2010, 31, 4583; b) F. P. Seib, G. T. Jones, J. Rnjak-Kovacina, Y. N. Lin, D. L. Kaplan, *Adv. Healthcare Mater.* 2013, 2, 1606.
- [139] A. Lammell, M. Schwab, U. Slotta, G. Winter, T. Scheibel, *Chemoschem* 2008, 1, 413.
- [140] M. Lucke, G. Winter, J. Engert, *Int. J. Pharm.* 2015, 487, 125.
- [141] N. Helfricht, M. Klug, A. Mark, V. Kuznetsov, C. Blum, T. Scheibel, G. Papastavrou, *Biomater. Sci.* 2013, 1, 1166.
- [142] M. P. Neubauer, C. Blum, E. Agostini, J. Engert, T. Scheibel, *A. Fery, Biomater. Sci.* 2013, 1, 1160.
- [143] C. Blüm, T. Scheibel, *BioNanoScience* 2012, 2, 67.
- [144] M. Hofer, G. Winter, J. Myschik, *Biomaterials* 2012, 33, 1554.
- [145] A. Lammell, M. Schwab, M. Hofer, G. Winter, T. Scheibel, *Biomaterials* 2011, 32, 2233.
- [146] R. H. Müller, *Zetapotential und Partikelladung in der Laborpraxis*, Wissenschaftlicher Verlagsgesellschaft mbH Stuttgart, Stuttgart, Germany 1996.
- [147] A. Florczak, K. Jastrzebska, A. Mackiewicz, H. Darns-Kozłowska, *J. Mater. Chem. B* 2017, 5, 3000.
- [148] M. B. Schierling, E. Doblhofer, T. Scheibel, *Biomater. Sci.* 2016, 4, 1515.
- [149] K. Nurnata, B. Subramanian, H. A. Currie, D. L. Kaplan, *Biomaterials* 2009, 30, 5775.
- [150] K. Nurnata, D. L. Kaplan, *Biomacromolecules* 2010, 11, 3189.
- [151] K. Numata, J. Hamasaki, B. Subramanian, D. L. Kaplan, *J. Controlled Release* 2010, 146, 136.
- [152] K. Numata, M. R. Reagan, R. H. Goldstein, M. Rosenblatt, D. L. Kaplan, *Bioconjugate Chem.* 2011, 22, 1605.
- [153] K. Nurnata, A. J. Mieszawska-Czajkowska, L. A. Kvenvold, D. L. Kaplan, *Macromol. Biosci.* 2012, 12, 75.
- [154] W. W. Huang, D. Ebrahimi, N. Dinjaski, A. Tarakanova, M. J. Buehler, J. Y. Wong, D. L. Kaplan, *Acc. Chem. Res.* 2017, 50, 866.
- [155] K. Y. Lee, D. J. Mooney, *Prog. Polym. Sci.* 2012, 37, 106.
- [156] M. B. Gorbet, M. V. Sefton, *Biomaterials* 2005, 26, 6811.
- [157] F. Vollrath, P. Barth, A. Basedow, W. Engstorn, H. List, *In Vivo* 2002, 16, 229.
- [158] R. Price, A. Poursaid, J. Cappello, H. Ghandehari, *J. Controlled Release* 2015, 213, 96.
- [159] E. Vandermarliere, M. Mueller, L. Martens, *Mass Spectrom. Rev.* 2013, 32, 453.

Part 2. Aqueous electrospinning of recombinant spider silk proteins

DeSimone, E.; **Aigner, T. B.**; Humenik, M.; Lang, G.; Scheibel, T.

Published in Materials Science & Engineering C, 106, 110145

(2020)

Reprinted with kind permission from Elsevier GmbH



Contents lists available at ScienceDirect

Materials Science & Engineering C

journal homepage: www.elsevier.com/locate/msec

Aqueous electrospinning of recombinant spider silk proteins

Elise DeSimone^a, Tamara B. Aigner^a, Martin Humenik^a, Gregor Lang^b, Thomas Scheibel^{a,c,*}^a University of Bayreuth, Dept. of Biomaterials, Prof.-Rüdiger-Bormann-Str. 1, 95447 Bayreuth, Germany^b University of Bayreuth, Biopolymer Processing Group, Ludwig-Thomas-Str. 36a, 95447 Bayreuth, Germany^c University of Bayreuth, Biomaterials, Bayreuther Zentrum für Kolloide und Grenzflächen (BZKG), Bayreuther Zentrum für Molekulare Biowissenschaften (BZMB), Bayreuther Materialzentrum (BayMAT), Bayerisches Polymerinstitut (BPI), Universitätsstr. 30, 95447 Bayreuth, Germany

ARTICLE INFO

Keywords:

Electrospinning
Aqueous dope
Recombinant spider silk
Bioactivity
Post-treatment

ABSTRACT

There has been a significant increase in the use of sensitive biological components, e.g., growth factors or enzymes, in implanted scaffolds/devices. To prevent diffusion away from the targeted area and to maximize access of the biological agent to the desired target, it is necessary to provide a supportive substrate to immobilize and protect biological agents from the environment. For this purpose, nanofiber fabrics are highly promising due to their high porosity, capacity for solution flow-through and high surface-to-volume ratio. However, electrospinning often requires harsh processing conditions, such as the use of volatile solutions, which can result in loss of activity of the incorporated biological components. In this study we developed a mild process for electrospinning of eADF4(C16), a recombinant spider silk protein. eADF4(C16) is non-cytotoxic, displays excellent stability against hydrolytic and enzymatic degradation and opens the opportunity for genetic addition of bioactive factors. Therefore, an aqueous spinning dope of eADF4(C16) was loaded with either green fluorescence protein (GFP) or the recombinant fusion protein GFP-eADF4(C16). The fluorescence activity of GFP is dependent on its proper folding, which does not occur in organic solvents, making it an attractive model protein. We were able to demonstrate the usability as well as the significance of the all-aqueous processing conditions for the activity of GFP in electrospun spider silk scaffolds.

1. Introduction

Implant devices that incorporate biological components (e.g. enzymes, DNA, antibodies, cells) are increasing in use due to the desire to create devices with more complex functions. Such carriers are required to retain and protect the biological function of the incorporated biomacromolecules under the ambient environmental conditions without reducing their accessibility. For example, a growth factor should be accessible to a target cell or an enzyme should be accessible to a substrate. Further, other “wet-environment” devices such as biosensors (used to detect a chemical or biological analyte in solution) impose similar requirements [1,2]. Consequently, efficient immobilization of accessible biologically active components onto/into substrate/matrix materials is regarded the most critical aspect to produce such devices. Simple approaches such as incorporation of biological components into/onto films are commonly used, but do not exploit the high potential, that can be achieved by advanced processing techniques. For example, to improve diffusion rates (i.e. increase in accessibility) nanofiber nonwovens or hydrogels are much more promising candidates as scaffolds. In this respect, nanofiber fabrics are of particular interest,

as they have high porosity, capacity for solution flow-through and high surface-to-volume ratio. Further, it is beneficial to prepare the nanofibers from biopolymers, so that they can degrade without producing toxic byproducts.

Many types of polymers or biopolymers can be electrospun, given that the electrospinning solutions (spinning dopes) are highly concentrated (e.g. viscous) and the solvent is sufficiently volatile. Therefore, organic solvents tend to prevail as the most common choice for a solvent due to the ease of processing (high solubility and high volatility). Frequently used solvents include 1,1,1,3,3,3-Hexafluoro-2-propanol (HFIP), chloroform, acetic acid, and dimethylformamide (DMF) [3]. An aqueous electrospinning dope is more difficult to prepare, but increases safety of production and possibility for direct incorporation of sensitive components without loss of their functionality [4–6]. Due to the low solubility of many fiber-forming biopolymers in aqueous buffers, usually an additive is required. Frequently high molecular weight poly(ethylene oxide) (PEO) is used as an additive as it is inert, cheap and comes in several different molecular weights, which allows easy to tune the viscosity. PEO has been widely used to help to produce fibers, e.g., from alginate [7] collagen [8] or silk [9–11].

* Corresponding author at: University of Bayreuth, Dept. of Biomaterials, Prof.-Rüdiger-Bormann-Str. 1, 95447 Bayreuth, Germany.
E-mail address: thomas.scheibel@bm.uni-bayreuth.de (T. Scheibel).

<https://doi.org/10.1016/j.msec.2019.110145>

Received 5 June 2019; Received in revised form 28 August 2019; Accepted 28 August 2019

Available online 29 August 2019

0928-4931/© 2019 Elsevier B.V. All rights reserved.

Silks are a class of fibrous proteins composed of highly repetitive amino acid sequences [12]. Due to their combination of strength and flexibility, silk fibers are attractive materials for various technical applications. In addition to their mechanical properties, silks are well-tolerated by cells and organisms and at the same time are resistant to hydrolytic degradation as well as degradation by most enzymes [13–17]. Therefore, silks are particularly interesting for use as a substrate being exposed to physiological fluids or implanted directly into a patient. Although silk is produced by several different species, the two most reliable sources for industrial use are silkworm silk (commonly from *Bombyx mori*) and recombinant spider silk proteins. A particularly promising example of recombinant spider silk is engineered *Araneus diadematus* fibroin-4 with a consensus sequence, the ‘C-module’, repeated 16 times (eADF4(C16)) [18,19]. Recombinant Spider silks have the advantage of excellent mechanical properties [20] and low immunogenicity [21]. Further, they are biocompatible when processed as films or electrospun nonwoven fiber mats [14,22]. Recombinant production allows for manipulation and modification of the proteins at the genetic level enabling incorporation of biological entities in hybrid proteins. *Bombyx mori* silk, on the other hand, is available in large quantities and already well established for several applications where bioactive components are incorporated into the scaffold including tissue engineering [6,23] and biosensing [24–26]. In order to prepare silk scaffolds incorporating sensitive biological components, it is necessary to prepare the desired morphology (e.g. film, hydrogel, electrospun fibers) using an aqueous process to preserve the biological activity of the bioreceptor. Further, in the case of films and fibers, a post-treatment step is required in order to induce formation of beta-sheet crystal to render the morphology insoluble in water. Consequently, it is necessary to not only prepare an aqueous electrospinning dope, but also to use an aqueous post-treatment (i.e. water annealing).

In this study, an all aqueous electrospinning process was developed using the recombinant spider silk eADF4(C16) to demonstrate the potential of spider silk-based fibers for incorporation of biologically active components. The “all aqueous process” refers to the use of an aqueous electrospinning dope and the use of water annealing as a mild post-treatment method. Electrospun fiber mats were the scaffold morphology chosen, as in the future they can be used to promote cell attachment [27] or to allow for air [28] or liquid flow-through for biosensing applications. Green fluorescent protein (GFP) was used as a model for the biologically active component of the system. The fluorescence activity can be detected at low concentrations and is highly sensitive to proper protein folding [29,30]. Moreover, the genetic fusion of GFP to recombinant spider silk (GFP-eADF4(C16)) enabled the immobilization of the GFP within the support material. Comparing conventional processing of organic solutions and post-treatment with this new approach, we demonstrated the significance of using mild conditions for each processing step (solution preparation, electrospinning, post-treatment and incubation in buffer) on the activity of GFP.

2. Materials and methods

2.1. Preparation of aqueous eADF4(C16) protein solution

The recombinant spider silk protein eADF4(C16) (MW: 47,698 Da) is an engineered protein with the amino acid sequence (module C) representing the consensus sequence core motif of the natural dragline silk *Araneus diadematus* fibroin 4 (ADF4) of the European garden spider. The module C (GSSAATAAAASGPGGYGPENQGPSGPGGYGPGGP) is repeated 16 times [18,19]. Recombinant production and purification of eADF4(C16) was completed as described previously [18]. Lyophilized protein was dissolved in 6 M guanidinium thiocyanate at a concentration of 4 mg/mL and dialyzed against 10 mM Tris/HCl, pH 7.5 overnight with 4 buffer changes. The solution was then centrifuged for 20 min at 8500 rpm, 23 °C. Separately, poly(ethylene oxide) with MW of 400,000 Da (PEO400) (Sigma Aldrich, Germany) was dissolved in

10 mM Tris/HCl, pH 7.5 at 5 w/v %. This stock solution was used for either electrospinning pure PEO400 nanofibers, or for further preparation of the aqueous eADF4(C16) electrospinning dope. eADF4(C16) and PEO400 solutions were blended at mass to mass ratio of 3:1 (eADF4(C16) to PEO400). The low concentrated mixture was subsequently dialyzed against (MWCO 8-10 kDa) 25 w/v % poly(ethylene glycol) with MW of 20,000 Da (PEG20) (Sigma Aldrich, Germany) to adjust the desired final concentration. To remove protein aggregates or undissolved PEO, the solution was centrifuged for 20 min at 8500 rpm, 23 °C before further use. The concentration of eADF4(C16) was determined by UV absorption.

2.2. Preparation of organic eADF4(C16) protein solution

For control experiments, lyophilized eADF4(C16) was directly dissolved in 1,1,1,3,3,3-Hexafluoro-2-propanol (HFIP) (Alfa Aesar, Germany) to a desired final concentration as described previously [27,28]. The solution was vortexed for 60 s and left on a tumbling reactor overnight at room temperature. This solution was prepared in concentrations of 10.0, 12.5 and 15.0 w/v % for electrospinning.

For the simplicity of this text, aqueous eADF4(C16) with ~1.7 w/v % PEO400 as an additive will be referred to as C16_{H₂O} or ‘aqueous solution’, and the organic eADF4(C16) solution in HFIP will be referred to as C16_{HFIP} or ‘organic solution’.

2.3. Electrospinning parameters

Electrospinning was conducted for 5 min per sample according to the parameters outlined in Table 1. The initial parameters were based on values reported previously [28]. Electrospinning was conducted in a closed container to better control the environmental conditions. The humidity was controlled by either using condensed air to reduce the humidity or by using a humidifier to increase the humidity.

Electrospun fibers were post-treated using vapor treatment of either p.a. anhydrous, ethanol (EtOH) (Sigma, Germany) or Millipore-purified (MilliQ) water. Undiluted, anhydrous, ethanol p.a. is referred to throughout this paper as 100% EtOH. To evaluate the various post-treatment methods, it was necessary to prepare a positive control with the maximum possible beta sheet content. To prepare the nanofiber mats with maximum beta-sheet content, nonwoven samples were post-treated using 100% EtOH vapor at 60 °C for 12 h and further washed in 70% EtOH overnight. The fibers prepared using this procedure are

Table 1
Processing parameters applied in the production of electrospun mats.

Parameters		Spider silk-based electrospinning dopes	
		Aqueous solvent	Organic solvent
Solution	Solvent	10 mM Tris/HCl, pH 7.5	HFIP
	Additives	400 kDa PEO (PEO400)	none
Set-up	eADF4(C16) concentration(s) (wt/v %)	3.0–5.0w/v%	10–15w/v%
	Needle voltage	+ 15 kV	+ 22.5 kV
	Collector voltage	– 5 kV	– 5 kV
	Flow rate	7 μL/min	
	Needle length	22 mm	
	Needle diameter	0.80 mm	
	Needle counter electrode	5 cm aluminum ring, 5 cm wide	
	Working distance	18.5 cm	
	Collector geometry	2D circle, 8 cm diameter	
	Environmental	Relative humidity	15–30%
	Temperature	Ambient	Ambient

referred to throughout this paper as 'fully processed' (FP). The washing step also removed the PEO400 from aqueous dope-derived samples. Therefore, this control served two purposes: One was to determine maximum beta-sheet content and compare to the conventional preparation approach [28], the other was to confirm that PEO400 had no effect on the folding of eADF4(C16). Experimental groups studied the effect of post-treatment type (EtOH or MilliQ H₂O) and temperature (37 °C or 60 °C) on post-treatment time.

2.4. Scanning electron microscopy (SEM)

Samples of electrospun fibers were prepared for SEM by mounting onto studs with carbon tape such that the area being viewed would not be affected by the glue. Mounted samples were sputter coated with 2.0 nm of platinum. Images were obtained using the SEM 1540EsB Cross Beam (Zeiss, Germany). SEM was operated at 3 kV with a collector bias of 400. The SE2 lens and 30 μm aperture were used, and a line averaging method was used for noise reduction. Fiber diameters were determined using the measuring tool in ImageJ software. 20,000× images were dissected into quadrants, and five random measurements were taken in each quadrant. Four regions for each sample were analyzed for three samples per experimental group ($n = 3$).

2.5. Fourier-transform infrared spectroscopy (FTIR)

Secondary structure content of the eADF4(C16) electrospun fibers at different processing steps was determined using Fourier self-deconvolution (FSD) analysis of spectra collected using a Bruker Tensor 27 spectrometer (Bruker, Germany). Samples were formed as pellets for these measurements, and the same pellets were later analyzed by differential scanning calorimetry (DSC) measurements. Spectra were detected by attenuated total reflection (ATR) with a resolution of 4 cm⁻¹, and 120 scans were averaged for a range of 4000–800 cm⁻¹. FSD was conducted for the amide I band (1595–1705 cm⁻¹) to determine individual secondary structure elements as described previously [31,32]. A sample number of 4–6 ($n = 4–6$) was used for each experimental group, each sample was scanned three times, and the FSD was conducted on the spectra with the best signal-to-noise ratio.

2.6. Differential scanning calorimetry (DSC)

DSC measurements were conducted in the DSC1, STAR^c-System (Mettler Toledo, Germany). Samples were first heated to 110 °C for 10 min to remove any water, and then returned to 25 °C to further equilibrate for 10 min. The samples were then measured from 25 °C to 400 °C for endothermic and exothermic behavior and allowed to equilibrate at the final temperature for 10 min. Heating rate was 4.98 K min⁻¹ and cooling rate was -4.98 K min⁻¹. Modification and analysis of the DSC curves were conducted with the instrument software STAR^c. Curves were modified for baseline correction, and all integrals of peaks were normalized by mass.

2.7. Recombinant green fluorescent protein (GFP) and GFP-eADF (C16) fusion

Recombinant green fluorescent protein (GFP) derived from the sequence of *Aequorea victoria* GFP as well as the fusion protein GFP-eADF4(C16) were produced as described previously [30]. The recombinant GFP had a molecular weight of 28,400 Da and an extinction coefficient of 0.7, (A₂₀ for 0.15% w/v aq. solution) and the fusion protein GFP-eADF4(C16) had a molecular weight of 74,800 Da and an extinction coefficient of 0.92. GFP was stored in a 50 v/v % 25 mM Tris/HCl, 50 mM NaCl, pH 8 and 50 v/v % glycerol mixture and GFP-eADF4(C16) as a freeze-dried powder and resolved and refolded into active state as described [30].

2.8. Loading recombinant spider silk fibers with GFP

The influence of solvent conditions used for the preparation of electrospinning dopes on the GFP emission was determined either in 10 mM Tris/HCl, pH 7.5 and HFIP in the presence or absence of PEO400 additive. Fluorescence intensity was determined using a plate reader (Berthold, Germany, ex: 485 nm/em: 535 nm) by diluting the stock GFP solution in the concentration range from 1.1 to 22.9 μM and 1.1 to 57.2 μM for aqueous and organic solutions, respectively. To prepare the electrospinning dope, GFP or GFP-eADF4(C16) were mixed directly with highly concentrated eADF4(C16) solutions (4.5–5 w/v %).

2.9. Circular dichroism (CD) and fluorescence spectroscopy

Circular dichroism (CD) spectra were recorded on a J-815 CD Spectrometer (Jasco, Germany) using a 0.1 cm quartz cuvette (Hellma GmbH & Co. KG, Germany). Fluorescence spectra were recorded at excitation wavelength of 495 nm using a FP-6500 fluorescence spectrometer (Jasco, Germany). Stock solution of GFP (6 mg/mL) was diluted in PBS at 0.2 mg/mL containing 0–50 v/v % EtOH or 5 v/v % HFIP and incubated at room temperature for 30 min before spectra recording.

2.10. GFP activity studies

4.0 w/v % C16_{H₂O} and 12.5 w/v % C16_{HF} were loaded with 0.72 mg/mL GFP in the spinning dope (a molar ratio of 3 mol% eADF4(C16) to GFP was obtained). After electrospinning and undergoing different post-treatment conditions, the samples were analyzed in wet state with an Eitan DIGE Imager (Cy2 filter: ex: 480/30 nm, em: 530/40 nm) to determine GFP activity.

2.11. GFP release studies

3.4 w/v % C16_{H₂O} was loaded with either 0.2 mg/mL GFP (a molar ratio of 1 mol% eADF4(C16) to GFP) or with GFP-eADF4(C16) fusion protein (a molar ratio of 2.77 mol%). The samples were post-treated at 37 °C with MilliQ vapor for 15 min. The cumulative release of GFP or GFP-eADF4(C16) from electrospun fibers was determined by incubating nonwoven fibers in 300 μl phosphate buffered saline (PBS) and analyzing the supernatant after certain time intervals (ex: 485 nm/em: 535 nm). The results were normalized for the amount of eADF4(C16). Therefore, the electrospun fibers were re-dissolved in 6 M guanidinium thiocyanate followed by dilution in 25 mM Tris/HCl, pH 7.5 (5:95). This silk solution was analyzed using UV-vis spectroscopy, and protein concentration was determined using absorption at 280 nm.

2.12. Fluorescent imaging

To confirm results shown for both activity and release studies, fluorescent images were acquired using a fluorescence microscope (Leica, Germany). The images, within a particular test, were taken using the same exposure time or signal enhancement.

3. Results and discussion

For the simplicity of this text, several abbreviations will be used. 400 kDa poly(ethylene oxide) will be referred to as PEO400. Engineered *Araneus diadematus* fibroin-4 with the 'C-module' repeated 16 times will be referred to as eADF4(C16) (MW: 47,698 Da). eADF4(C16) fusion to green fluorescent protein (GFP) will be referred to as GFP-eADF4(C16). 5 wt/v% eADF4(C16) dissolved in ~1.7 wt/vol% 400 kDa poly(ethylene oxide) (PEO400)/10 mM Tris (pH 7.5) will be referred to as C16_{H₂O} or 'aqueous solution'. eADF4(C16) dissolved in 1,1,1,3,3,3-Hexafluoro-2-propanol (HFIP) will be referred to as C16_{HF} or 'organic solution'.

3.1. Development of an aqueous electrospinning process for recombinant spider silk proteins

Electrospinning of recombinant spider silk eADF4(C16) from an aqueous solution was tested in the presence or absence of PEO400 at different concentrations. As reported previously, it was not possible to conduct electrospinning without an additive [9,10], and PEO400 was utilized at its minimum possible concentration (~1.7 w/v %) to develop a suitable spinning dope for eADF4(C16). It was further determined that concentrations in the range of 3.0–5.0 w/v % eADF4(C16) resulted in fiber formation, whereas concentrations below 3 w/v % resulted in electrospinning and concentrations above 5 wt/v% resulted in gelation during dope preparation time to spinning. Another important parameter was the relative humidity inside the electrospinning device; at a relative humidity $\geq 30\%$ fiber production was not possible. As shown by De Vrieze et al., humidity is often the “forgotten” parameter, which can be critical in determining if electrospinning will be successful or not [33].

Produced fibers were characterized using scanning electron microscopy (SEM), differential scanning calorimetry (DSC) and Fourier-transform infrared spectroscopy (FTIR); key results for the optimized, aqueous processing route are summarized in Fig. 1. Additional data for SEM (SI Figs. 1 & 2) and FTIR (SI Fig. 3) can be found in the supplementary information. DSC measurements indicated that after post-treatment and washing steps, PEO is successfully removed from the C16_{H₂O} fibers. After electrospinning, it is necessary to post-treat silk fibers to convert the protein structure from prevalently amorphous random coil into compact beta-sheets, which renders the electrospun fibers water insoluble [34]. Therefore, electrospun fibers were evaluated immediately after electrospinning and post-treatment for secondary structure content analyzing the amide I band. Water annealing of C16_{H₂O} fibers at 37 °C resulted in maximum conversion to beta-sheets after 10 min.

Fiber diameter, as determined from “fully processed (FP)” samples, demonstrated that there is a clear advantage of the aqueous electrospinning since the fiber diameter distribution is much narrower than that of HFIP-derived fibers (Fig. 1, SI Fig. 1, SI Fig. 2). This is likely due to the presence of PEO400, which is known for being advantageous in terms of a consistent viscosity. Further, it can be seen that there is no significant difference in the secondary structure content between the nonwoven mats derived from the two different solutions. In previous studies on silk films it was shown that, depending on the solvent used, the secondary structure content after casting and drying was different, being higher after casting in aqueous solvents and lower when cast from organic solvents [35]. However, in case of films from aqueous solution drying takes over an hour and, therefore, allows the proteins to fold into beta-sheet rich structures, whereas in electrospinning drying occurs within milliseconds. Thus, the proteins are frozen immediately in the solution-like state rich in random coil/alpha helical structures, which is likely the reason for the lack of differences in secondary structure content immediately after electrospinning.

Concerning post-treatment, water annealing and ethanol post-treatment work by opposite principles; ethanol removes water and the dehydration results in hydrogen bond formation, and the peptide chain remains less mobile. On the other hand, during water annealing water molecules incorporate into the scaffold inducing chain flexibility (plasticizer) contributing to fast peptide backbone transformation into more stable beta-sheets. Inducing flexibility as opposed to dehydrating could explain the fiber melting.

3.2. Incorporation and release of GFP within electrospun silk fibers

As a proof-of-concept for using eADF4(C16) electrospun fibers as a substrate encapsulating sensitive biologicals (e.g. growth factors, DNA, enzymes), green fluorescence protein (GFP) was incorporated into electrospun fibers. GFP was chosen as an analytical tool to assess the

compatibility of the material and the processing conditions for several reasons. GFP is a globular protein, and its fluorescence activity is directly related to its native tertiary structure [29,30]. Further, previous studies demonstrated that GFP and eADF4(C16) are compatible. The folding and self-assembly of the spider silk protein into dense beta-sheet structures did not restrict the native GFP folding, even in GFP-eADF4(C16) fusion constructs. Similarly, the folding of GFP did not affect the assembly of eADF4(C16) [30]. Herein, the activity of GFP was observed after each major processing step (dissolution in the solvent, electrospinning and post-treatment).

To observe the effects of the solution preparation step, the fluorescence activity of GFP was measured in solution using a plate reader, fluorescence spectrometer as well as by circular dichroism (CD) spectroscopy (Fig. 2A–C, SI Fig. 4). Dissolution of GFP in HFIP based silk spinning dope resulted in significantly diminished fluorescence activity, whereas GFP in the aqueous silk dope retained its activity. Addition of PEO400 had no significant impact on the fluorescence activity of GFP in organic or aqueous solutions. To observe the effect of electrospinning, fibers were observed using an Ettan DIGE Imager or fluorescence microscope. Fibers produced from C16_{H₂O} exhibited a strong fluorescence, whereas there was no recovery of GFP in C16_{HF}-derived fibers (Fig. 2D&E). To observe the effects of post-treatment, GFP was either dissolved in EtOH or GFP-containing fibers were post-treated with ethanol vapor. Dissolved GFP was measured using CD or fluorescence spectroscopy, which demonstrated that GFP activity was lost above concentrations of 30 v/v% EtOH (Fig. 2B&C, SI Fig. 4). GFP-loaded fibers were imaged using an Ettan DIGE Imager or fluorescence microscopy. Post-treatment with water vapor at 37 °C or 60 °C had no apparent effect on GFP activity, and treatment with 100% ethanol vapor strongly diminished the fluorescence of GFP, independent of the temperature (Fig. 2D&E).

As a further step, to determine the release of GFP from electrospun fibers, GFP or GFP-eADF4(C16) were added to the dope and processed using the all-aqueous procedure. The release of GFP was detected by incubating the electrospun fibers in phosphate buffered saline (PBS, pH 7.2) and measuring the fluorescence of the supernatant (Fig. 2F). There was a clear burst release of the unbound GFP from the fibers, and there was complete release within 30 min incubation in PBS. There was no observed release of GFP from fibers incorporating GFP-eADF4(C16).

In solution, only minimal changes of the protein secondary structure were observed as reflected by the CD spectra with a minimum at 218 nm indicative of a significant presence of β -sheets of the β -barrel fold [36]. When GFP was in solution, increasing EtOH concentration up to 40 v/v % enhanced the emission of the fluorophore, an effect which can be attributed to the hydrophobicity of the alkyl chain of the alcohol [37], or changing the dielectric constant. At concentrations above this or at low concentrations of HFIP (5 v/v %), there was a shift of the minimum towards 230 nm. This shift towards a higher wavelength is indicative of loss of the native conformation due to aggregation [38,39].

GFP-loaded fibers prepared from HFIP solution did not regain fluorescence activity after electrospinning or post-treatment. The likelihood that GFP could refold into its native structure within the dense spider silk fiber matrix after electrospinning is low due to steric hindrances, hydrophobic interactions and electrostatic effects. Interestingly, in the case of C16_{H₂O}, there was not a complete loss of GFP activity after fibers were post-treated with 100% EtOH vapor at 37 °C. This indicates that using a lower temperature could also be significant for retaining GFP activity. Therefore, for release studies C16_{H₂O} solutions and a post-treatment at 37 °C (water annealing) were used to prepare the fibers.

As a further step, the release of GFP from the fibers was observed in PBS. The ratio of activity of GFP from before electrospinning to after release was calculated to be 90%. Although this was an excellent result in terms of activity, as mentioned in the introduction, it was desired that GFP remains in the fibers (or is released from them in a slow, controlled manner). Although it was not surprising to observe a burst

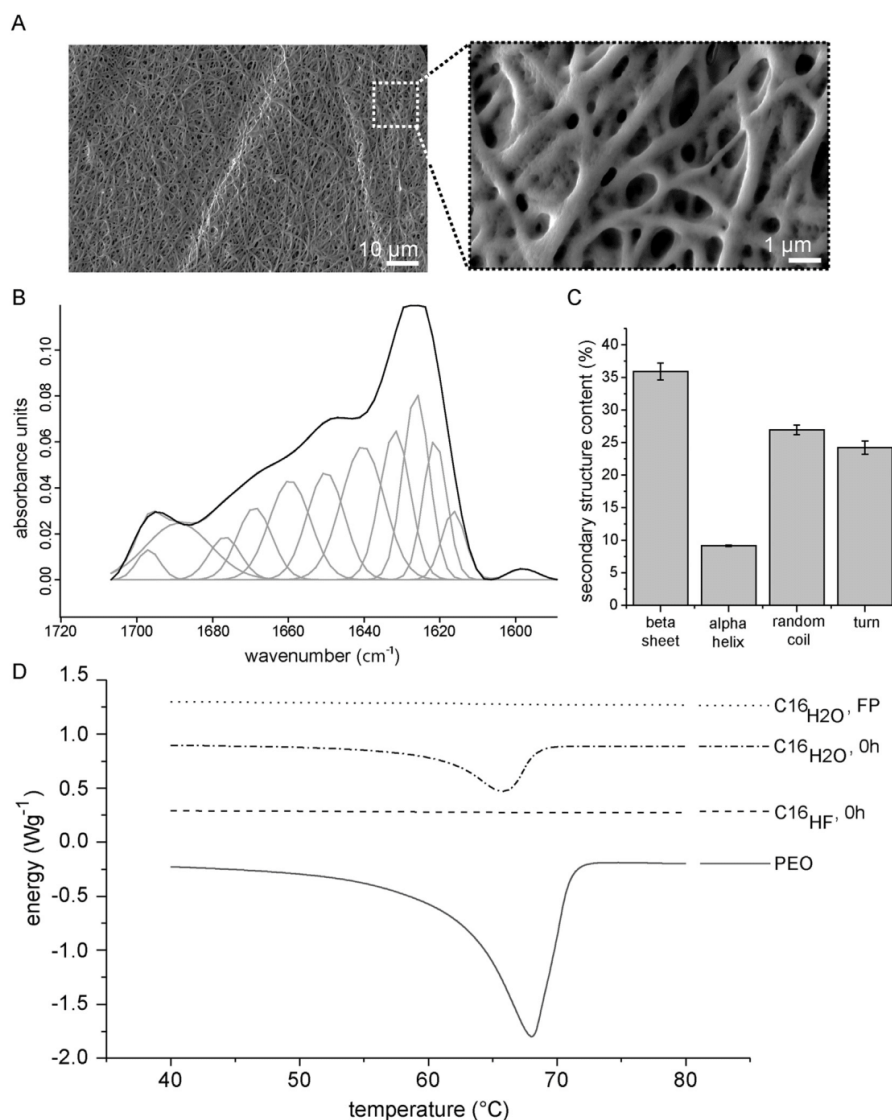


Fig. 1. Characterization of C16_{H2O} electrospun fibers post-treated at 37 °C using water vapor (A) Representative SEM images of electrospun fibers and post-treated (water-annealing). All samples were washed before imaging. Scale bar = 1 μm or = 10 μm as indicated in the images. (B) Representative FTIR spectrum as well as the Lorentz oscillators (C) The secondary structure content as determined by Fourier self-deconvolution (FSD). (D) DSC measurements of 4.5 wt/vol% C16_{H2O} or 12.5 wt/vol% C16_{HF} nonwoven mats, either measured immediately after electrospinning (no post-treatment, 0 h) or after post-treatment with 100% EtOH at 60 °C and washing steps in 70% EtOH (fully processed (FP)) as a positive control DSC curves were offset by 0.5 Wg⁻¹ for clarity. 400 kDa PEO powder (solid black line) was used as a further control; the PEO melting peak was detected between 60 and 70 °C. Characterization for all experimental and control groups can be found in the supplementary information, SI Figs. 1–3.

release, as negatively charged biologicals have shown rapid release from eADF4(C16) scaffolds [40], eADF4(C16) has a unique advantage. As it is produced using recombinant technology, it is relatively simple to engineer new sequences in order to add a functionality [30,41]. Therefore, the fusion protein GFP-eADF4(C16) was added to the aqueous spinning dope of eADF4(C16) before electrospinning, and the fibers were water annealed at 37 °C. In this case, the release of GFP was completely inhibited (Fig. 2F & SI Fig. 5), and GFP activity was maintained within the fibers for three days at room temperature in PBS (data not shown). In GFP-loaded fibers stored dry at room temperature, GFP

was stable for weeks (data not shown).

4. Conclusion and outlook

We have shown that eADF4(C16) can be used to electrospin sub-micron fibers through an all-aqueous processing route for incorporation of sensitive biological compounds. Green fluorescent protein (GFP) was used as a model to follow activity changes throughout the fabrication of the electrospun fibers. Through this work, we were able to demonstrate the significance of using an all-aqueous processing route for retaining

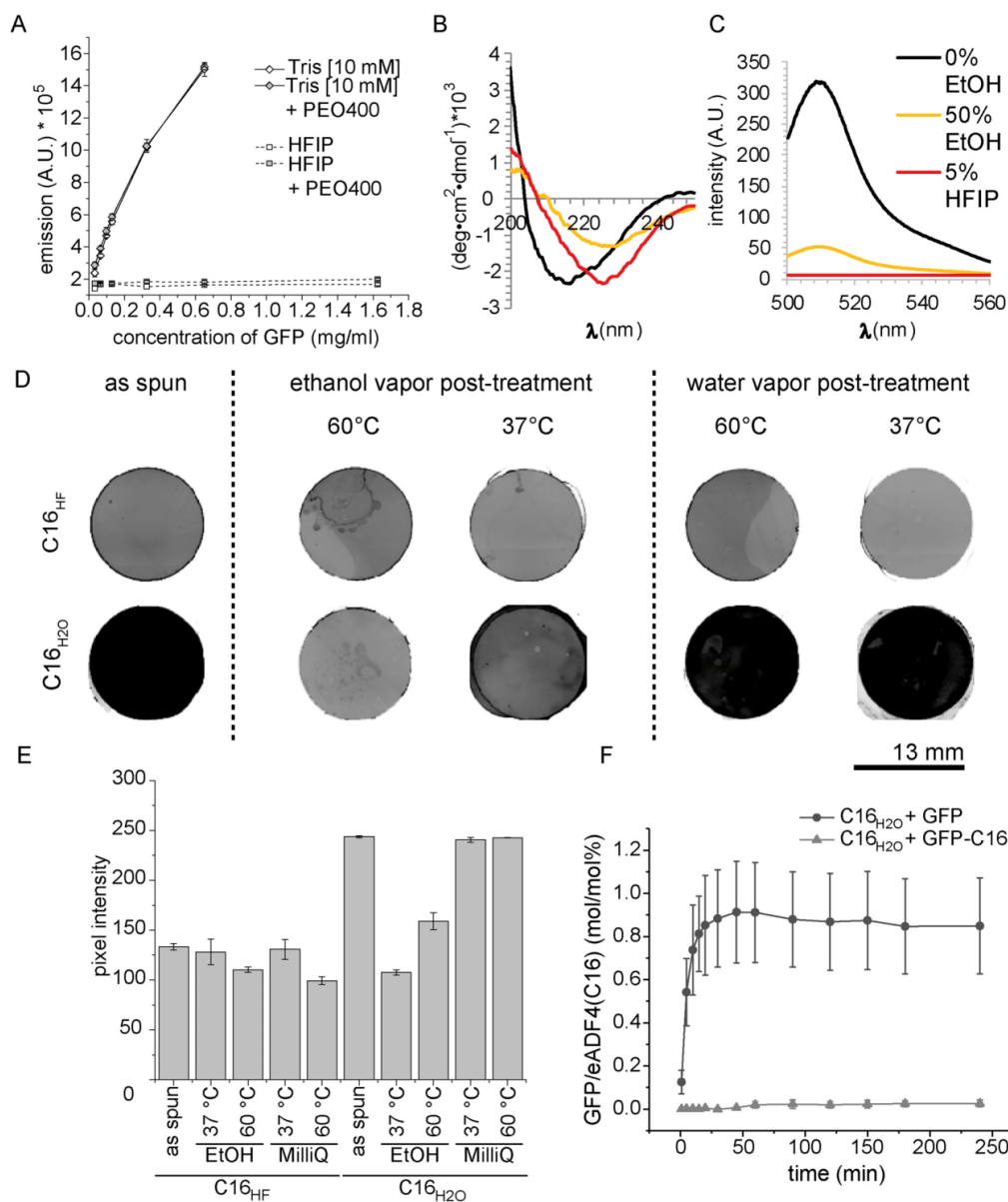


Fig. 2. Secondary structure and fluorescence activity of GFP in solution, within electrospun fibers or released from fibers into solution. (A-C) GFP was diluted in either 10 mM Tris/HCl, pH 7.5 with or without PEO400, HFIP with or without PEO400 or EtOH and measured by (A) plate reader (B) CD (0.2 mg/mL GFP) (C) and fluorescence spectroscopy (0.2 mg/mL GFP). (D) Activity of GFP as observed by inverted fluorescence scanner images immediately after electrospinning or after post-treatment. Post-treatments was either 100% EtOH vapor (60 °C or 37 °C), or 100% MilliQ vapor (60 °C or 37 °C). The intensity goes from white (no fluorescence) to black (maximum fluorescence detected). (E) quantified pixel intensity of the images shown in section D. (F) Cumulative release of GFP in PBS, implemented with or fused to eADF4(C16), from C16_{H2O} electrospun fibers post-treated with 100% MilliQ vapor at 37 °C.

high activity of sensitive biological agents through various processing steps. Further, we exploited the compatibility of globular and structural moieties in the fusion construct GFP-eADF4(C16) to prevent burst release of the biological model as observed in the case of unmodified GFP. eADF4(C16) is a bacteriostatic material [42], and nonwoven fiber meshes based thereof have exceptional mechanical properties and durability in high mechanical stress environments [43,44] and are

biocompatible [22]. Considering these and previous published results, the same platform could potentially be modified for biosensor or tissue engineering applications; e.g., a growth factor could be implemented with a linker which allows for triggered release (e.g., by enzymatic cleavage).

Acknowledgements

We would like to thank Claudia Stemmann for operating the scanning electron microscope (SEM) and Madeleine Mohrand for fermenting and purifying the fusion protein GFP-eADF4(C16). We would also like to thank Dr. Stephen Strassburg for proof-reading the manuscript.

We would like to acknowledge our funding source, Bavarian Research Foundation (DOK-175-15, T.B.A.), which made this work possible.

Appendix A. Supplementary data

Supplementary data to this article can be found online at <https://doi.org/10.1016/j.msec.2019.110145>.

References

- [1] N. Bhalla, et al., Introduction to biosensors, *Essays Biochem.* 60 (1) (2016) 1–8.
- [2] D.R. Thevenot, et al., Electrochemical biosensors: recommended definitions and classification, *Biosens. Bioelectron.* 16 (1–2) (2001) 121–131.
- [3] Z.M. Huang, et al., A review on polymer nanofibers by electrospinning and their applications in nanocomposites, *Compos. Sci. Technol.* 63 (15) (2003) 2223–2253.
- [4] P.D. Dalton, et al., Direct in vitro electrospinning with polymer melts, *Biomacromolecules* 7 (3) (2006) 686–690.
- [5] Z. Wang, et al., BMP-2 encapsulated polysaccharide nanoparticle modified biphasic calcium phosphate scaffolds for bone tissue regeneration, *J. Biomed. Mater. Res. A* 103 (4) (2015) 1520–1532.
- [6] T.M. Dinis, et al., Method to form a fiber/growth factor dual-gradient along electrospun silk for nerve regeneration, *ACS Appl. Mater. Interfaces* 6 (19) (2014) 16817–16826.
- [7] J.W. Lu, et al., Electrospinning of sodium alginate with poly(ethylene oxide), *Polymer* 47 (23) (2006) 8026–8031.
- [8] L. Buttafoco, et al., Electrospinning of collagen and elastin for tissue engineering applications, *Biomaterials* 27 (5) (2006) 724–734.
- [9] H.J. Jin, et al., Electrospinning Bombyx mori silk with poly(ethylene oxide), *Biomacromolecules* 3 (6) (2002) 1233–1239.
- [10] T. Hodgkinson, et al., Rheology and electrospinning of regenerated bombyx mori silk fibroin aqueous solutions, *Biomacromolecules* 15 (4) (2014) 1288–1298.
- [11] C.R. Wittmer, et al., Production, structure and in vitro degradation of electrospun honeybee silk nanofibers, *Acta Biomater.* 7 (10) (2011) 3789–3795.
- [12] C.L. Craig, Evolution of arthropod silks, *Annu. Rev. Entomol.* 42 (1997) 231–267.
- [13] S. Muller-Herrmann, T. Scheibel, Enzymatic degradation of films, particles, and nonwoven meshes made of a recombinant spider silk protein, *ACS Biomaterials Science & Engineering* 1 (4) (2015) 247–259.
- [14] P.H. Zepelin, et al., Improving the biocompatibility of silicone implants using spider silk coatings: immunohistochemical analysis of capsule formation, *Handchirurgie, Mikrochirurgie, plastische Chirurgie : Organ der Deutschsprachigen Arbeitsgemeinschaft für Handchirurgie : Organ der Deutschsprachigen Arbeitsgemeinschaft für Mikrochirurgie der Peripheren Nerven und Gefässe : Organ der V.* 46 (6) (2014) 336–341.
- [15] Y. Cao, B. Wang, Biodegradation of silk biomaterials, *Int. J. Mol. Sci.* 10 (4) (2009) 1514–1524.
- [16] R.L. Horan, et al., In vitro degradation of silk fibroin, *Biomaterials* 26 (17) (2005) 3385–3393.
- [17] S. Li, et al., In vivo degradation and neovascularization of silk fibroin implants monitored by multiple modes ultrasound for surgical applications, *Biomed. Eng. Online* 17 (1) (2018) 87.
- [18] C. Vendrely, T. Scheibel, Biotechnological production of spider-silk proteins enables new applications, *Macromol. Biosci.* 7 (4) (2007) 401–409.
- [19] D. Huenmerich, et al., Novel assembly properties of recombinant spider dragline silk proteins, *Curr. Biol.* 14 (22) (2004) 2070–2074.
- [20] A. Heidebrecht, et al., Biomimetic fibers made of recombinant Spidroins with the same toughness as natural spider silk, *Adv. Mater.* 27 (13) (2015) 2189.
- [21] P.H. Zepelin, et al., Spider silk coatings as a bioshield to reduce Periprosthetic fibrous capsule formation, *Adv. Funct. Mater.* 24 (18) (2014) 2658–2666.
- [22] D. Steiner, et al., Intrinsic vascularization of recombinant eADF4(C16) spider silk matrices in the arteriovenous loop model, *Tissue Eng. A* (2019), <https://doi.org/10.1089/ten.tea.2018.0360>.
- [23] C.M. Li, et al., Electrospun silk-BMP-2 scaffolds for bone tissue engineering, *Biomaterials* 27 (16) (2006) 3115–3124.
- [24] S. Chakravarty, et al., Silk fibroin as a platform for dual sensing of vitamin B-12 using photoluminescence and electrical techniques, *Biosens. Bioelectron.* 112 (2018) 18–22.
- [25] K. Min, S. Kim, C.G. Kim, Colored and fluorescent nanofibrous silk as a physically transient chemosensor and vitamin deliverer, *Sci. Rep.* 7 (1) (2017) 5448.
- [26] S.L. Burrs, et al., A comparative study of graphene-hydrogel hybrid bionanocomposites for biosensing, *Analyst* 140 (5) (2015) 1466–1476.
- [27] A. Leal-Egana, et al., Interactions of fibroblasts with different morphologies made of an engineered spider silk protein, *Adv. Eng. Mater.* 14 (3) (2012) B67–B75.
- [28] Lang, G., S. Jokisch, and T. Scheibel, Air filter devices including nonwoven meshes of electrospun recombinant spider silk proteins. *Jove-Journal of Visualized Experiments*, 2013 pp(75).
- [29] R.Y. Tsien, The green fluorescent protein, *Annu. Rev. Biochem.* 67 (1998) 509–544.
- [30] M. Humenik, M. Mohrand, T. Scheibel, Self-assembly of spider silk-fusion proteins comprising enzymatic and fluorescence activity, *Bioconjug. Chem.* 29 (4) (2018) 898–904.
- [31] X. Hu, D. Kaplan, P. Cebe, Determining beta-sheet crystallinity in fibrous proteins by thermal analysis and infrared spectroscopy, *Macromolecules* 39 (18) (2006) 6161–6170.
- [32] A.S. Lammel, et al., Controlling silk fibroin particle features for drug delivery, *Biomaterials* 31 (16) (2010) 4583–4591.
- [33] S. De Vrieze, et al., The effect of temperature and humidity on electrospinning, *J. Mater. Sci.* 44 (5) (2009) 1357–1362.
- [34] X. Hu, et al., Regulation of silk material structure by temperature-controlled water vapor annealing, *Biomacromolecules* 12 (5) (2011) 1686–1696.
- [35] K. Spiess, et al., Impact of initial solvent on thermal stability and mechanical properties of recombinant spider silk films, *J. Mater. Chem.* 21 (35) (2011) 13594–13604.
- [36] N.V. Visser, et al., Circular dichroism spectroscopy of fluorescent proteins, *FEBS Lett.* 521 (1–3) (2002) 31–35.
- [37] A.D. Kummer, et al., Viscosity-dependent fluorescence decay of the GFP chromophore in solution due to fast internal conversion, *J. Phys. Chem. B* 106 (30) (2002) 7554–7559.
- [38] D.K. Eggers, J.S. Valentine, Molecular confinement influences protein structure and enhances thermal protein stability, *Protein Sci.* 10 (2) (2001) 250–261.
- [39] V. Joshi, et al., Circular dichroism spectroscopy as a tool for monitoring aggregation in monoclonal antibody therapeutics, *Anal. Chem.* 86 (23) (2014) 11606–11613.
- [40] S. Kumari, et al., Recombinant spider silk hydrogels for sustained release of biologicals, *ACS Biomaterials Science & Engineering* 4 (5) (2018) 1750–1759.
- [41] S. Wohlrab, et al., Cell adhesion and proliferation on RGD-modified recombinant spider silk proteins, *Biomaterials* 33 (28) (2012) 6650–6659.
- [42] R.H. Zha, et al., Universal nanofiber silk coatings via controlled spidroin self-assembly, *Biomaterials Science* 7 (2) (2019) 683–695.
- [43] G. Lang, et al., Mechanical testing of engineered spider silk filaments provides insights into molecular features on a mesoscale, *ACS Appl. Mater. Interfaces* 9 (1) (2017) 892–900.
- [44] S. Jokisch, M. Neuenfeldt, T. Scheibel, Silk-based fine dust filters for air filtration, *Advanced Sustainable Systems* 1 (10) (2017).

Supplementary information

Aqueous electrospinning of recombinant spider silk proteins

Elise DeSimone¹, Tamara B. Aigner¹, Martin Humenik¹, Gregor Lang², Thomas Scheibel^{1,3,*}

¹University of Bayreuth

Dept. of Biomaterials

Prof.-Rüdiger-Bormann-Str. 1

95447 Bayreuth

Germany

²University of Bayreuth

Biopolymer Processing Group

Ludwig-Thomas-Str. 36a

95447 Bayreuth

Germany

³University of Bayreuth

Biomaterials

Bayreuther Zentrum für Kolloide und Grenzflächen (BZKG)

Bayreuther Zentrum für Molekulare Biowissenschaften (BZMB)

Bayreuther Materialzentrum (BayMAT), Bayerisches Polymerinstitut (BPI)

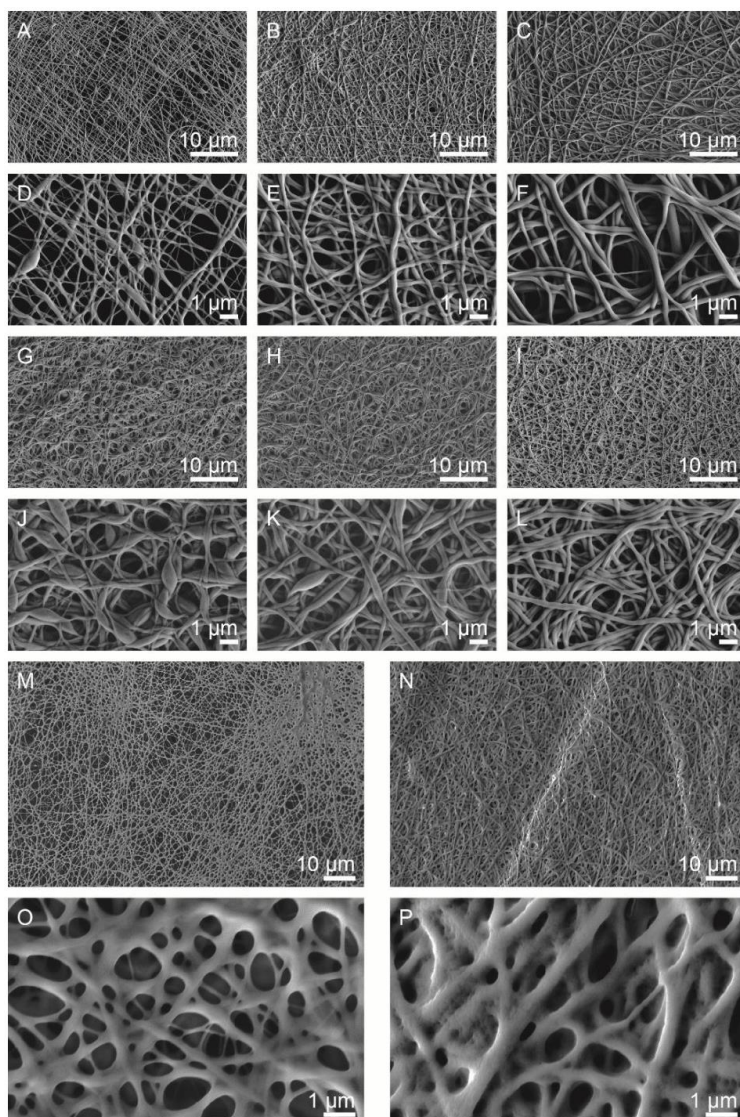
Universitätsstr. 30

95447 Bayreuth

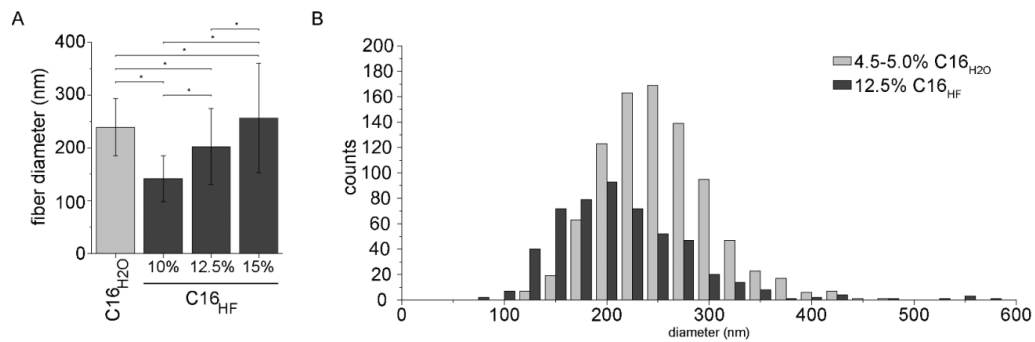
Germany

E-Mail: thomas.scheibel@bm.uni-bayreuth.de

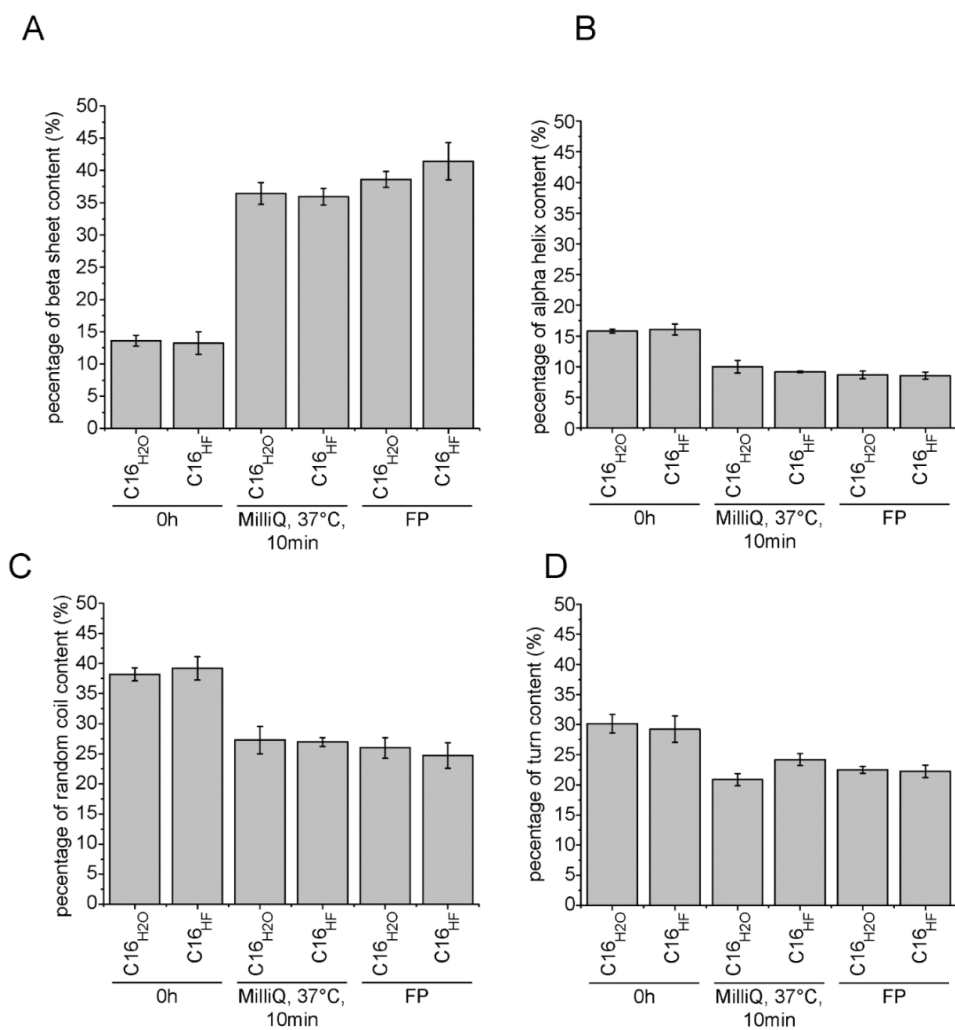
* corresponding author



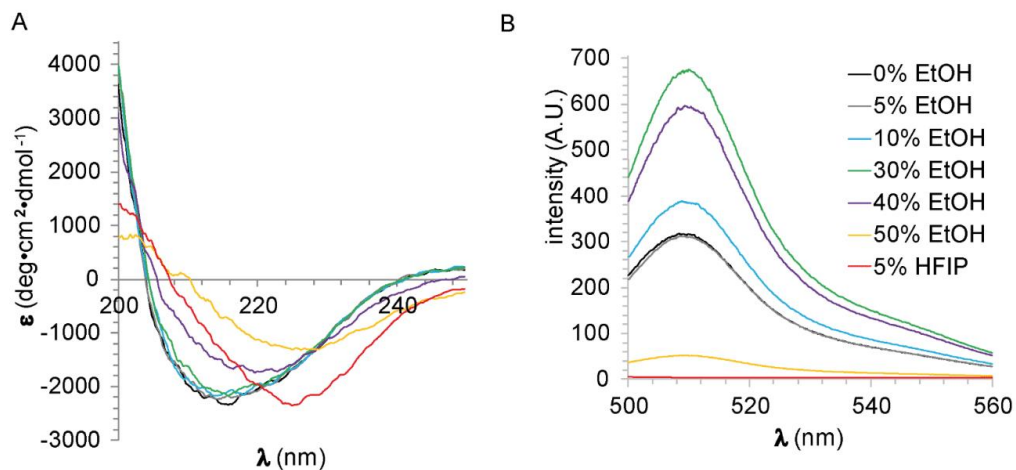
SI Figure 1: Representative SEM images of nonwoven meshes produced from C16_{HF} (A-F, M&O) and C16_{H₂O} (G-L, N&P). A&D: 10 w/v % eADF4(C16), B&E: 12.5 w/v % eADF4(C16) C&F: 15.0 w/v % eADF4(C16). G&J: 4.0 w/v % eADF4(C16), H&K: 4.5 w/v % eADF4(C16), I&L: 5.0 w/v % eADF4(C16). For images A-L, all samples were 'fully processed' (FP) as a positive control. Nonwoven meshes were also post-treated using water vapor at 37 °C (M-P). M&O: 12.5 w/v % C16_{HF} N&P: 5 w/v % C16_{H₂O}. All samples were washed before imaging. Scale bar = 10 μm or 1 μm as indicated in each image.



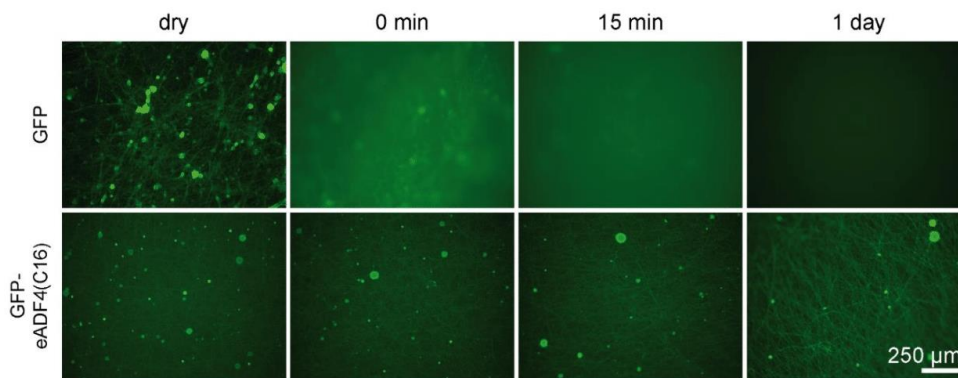
SI Figure 2: Fiber diameter as determined from SEM images of eADF4(C16) in aqueous solution (4.5 w/v %, light gray) or in HFIP solution (12.5 w/v %, dark gray); (A) the average fiber diameter and (B) the distribution of fiber diameters. All samples were post-treated for 12 hours using 100 % EtOH at 60 °C vapor, as well as washing with 70 % EtOH (fully processed (FP)).



SI Figure 3: The secondary structure content as determined using Fourier self-deconvolution (FSD) of C16_{H₂O} and C16_{HF} electrospun fibers immediately after electrospinning (no post-treatment (0h)), after post-treatment for 10 min with 100 % MilliQ vapor (MQ, 37 °C, 10min) and after post-treatment with 100 % EtOH at 60 °C and washing steps in 70 % EtOH (fully processed (FP)) as a positive control.



SI Figure 4: Secondary structure and fluorescence activity of GFP in solution (0.2 mg/ml GFP). GFP was diluted with PBS (0 % EtOH), 5 % HFIP or EtOH (5 v/v %, 10 v/v %, 30 v/v %, 40 v/v %, 50 v/v %) and measured using (A) CD and (B) fluorescence spectroscopy.



SI Figure 5: Fluorescence microscopy to visualize release of incorporated GFP or fused GFP from C16_{H20} electrospun fibers post-treated for 10 min with 100 % MillQ at 37 °C. Fluorescence images were taken directly after electrospinning or after 0 min, 15 min, and 1 d in PBS buffer.

Part 3. Enhanced antibacterial activity of Se nanoparticles upon coating with recombinant spider silk protein eADF4(κ 16)

Huang, T.; Kumari, S.; Herold, H.; Bargel, H.; **Aigner, T.B.**; Heath, D.E.; O'Brien-Simpson, N.M.; O'Connor, A.J. and Scheibel, T.

Manuscript submitted

1 ORIGINAL RESEARCH

2 **Enhanced antibacterial activity of Se nanoparticles upon**
3 **coating with recombinant spider silk protein eADF4(κ 16)**

4 Tao Huang^{1,2}

5 Sushma Kumari²

6 Heike Herold²

7 Hendrik Bargel²

8 Tamara B. Aigner²

9 Daniel E. Heath¹

10 Neil M. O'Brien-Simpson³

11 Andrea J. O'Connor¹

12 Thomas Scheibel^{2,4}

13

14 ¹Department of Biomedical Engineering, Melbourne School of Engineering, University of
15 Melbourne, Parkville, VIC 3010, Australia; ²Department for Biomaterials, Faculty of Engineering
16 Science, University of Bayreuth, Prof. Rüdiger Bormann Str. 1, 95447 Bayreuth, Germany;
17 ³Melbourne Dental School and The Bio21 Institute of Molecular Science and Biotechnology, The
18 University of Melbourne, Parkville, VIC 3010, Australia; ⁴Bavarian Polymer Institute (BPI), Bayreuth
19 Center for Material Science and Engineering (BayMAT), Bayreuth Center for Colloids and
20 Interfaces (BZKG), Bayreuth Center for Molecular Biosciences (BZMB), University of Bayreuth,
21 95447 Bayreuth, Germany

22

23 Correspondence: Andrea J. O'Connor

24 Tel +61 3 8344 8962

25 Email a.oconnor@unimelb.edu.au

26 Thomas Scheibel

27 Tel +49 (0)921 / 55-6701

28 Email thomas.scheibel@bm.uni-bayreuth.de

29

30 **Abstract:**

31 **Purpose:** Selenium nanoparticles (Se NPs) are promising antibacterial agents to tackle the
32 growing problem of antimicrobial resistance. The aim of this study was to fabricate Se NPs with a
33 net positive charge to enhance their antibacterial efficacy.

34 **Methods:** Se NPs were coated with a positively charged protein – recombinant spider silk protein
35 eADF4(κ 16) – to give them a net positive surface charge. Their cytotoxicity and antibacterial activity
36 were investigated, with negatively charged polyvinyl alcohol coated Se NPs as a control. Besides,
37 these eADF4(κ 16) coated Se NPs were immobilized on the spider silk films, and the antibacterial
38 activity of these films was investigated.

39 **Results:** Compared to the negatively charged polyvinyl alcohol coated Se NPs, the positively
40 charged eADF4(κ 16) coated Se NPs demonstrated a much higher bactericidal efficacy against the
41 Gram-negative bacteria *E. coli*, with a minimum bactericidal concentration (MBC) approximately 50
42 times lower than that of negatively charged Se NPs. Cytotoxicity testing showed that the
43 eADF4(κ 16) coated Se NPs are safe to both Balb/3T3 mouse embryo fibroblasts and HaCaT
44 human skin keratinocytes up to 31 μ g/mL, which is much higher than the MBC of these particles
45 against *E. coli* ($8 \pm 1 \mu$ g/mL). In addition, antibacterial coatings were created by immobilising the
46 eADF4(κ 16) coated Se NPs on positively charged spider silk films and these were shown to retain
47 good bactericidal efficacy and overcome the issue of low particle stability in culture broth. It was
48 found that these Se NPs needed to be released from the film surface in order to exert their
49 antibacterial effects and this release can be regulated by the surface charge of the film, such as
50 the change of the spider silk protein used.

51 **Conclusion:** Overall, eADF4(κ 16) coated Se NPs are promising new antibacterial agents against
52 life-threatening bacteria.

53 **Keywords:** Gram-positive, Gram-negative, *E. coli*, antibacterial film, cytotoxicity

54

55

56 **Introduction**

57 Bacterial infections are a major cause of chronic wounds and mortality.¹ Currently used antibiotics
58 kill bacteria mainly targeting cell wall synthesis, translational machinery, or DNA replication
59 machinery.¹ However, bacteria can develop resistance to antibiotics by producing modified
60 enzymes that decompose antibiotics,² changing cell components to inhibit antibiotic interaction,³
61 and increase the expression of efflux pumps to excrete different types of antibiotics.⁴ In recent
62 years, excessive use of antibiotics has induced the rapid development of drug-resistant bacteria.⁵
63 Bacteria resistant to all antibiotics (pandrug-resistant bacteria) have already been reported.⁶ These
64 multi drug-resistant bacteria have become a potential global public health threat. Therefore, new
65 antibacterial strategies are urgently needed to tackle the growing problem of these pandrug-
66 resistant bacteria, the so-called “superbugs”.

67 Nanoparticles (NPs) are considered to be promising antimicrobial agents to kill antibiotic-
68 resistant bacteria, as most of the antibiotic resistance mechanisms have very limited effect on NPs.¹
69 Several types of NPs have been explored for antimicrobial applications, such as Ag NPs,⁷ Au NPs,⁸
70 Se NPs,⁹ Pd NPs,¹⁰ Ti₂O NPs,¹¹ CuO NPs,¹² and so on. Among these NPs, the antibacterial Se
71 NPs have attracted increasing attention, with studies showing promising antimicrobial activities
72 against bacteria and fungi^{13,14,15,16} as well as the ability to disrupt biofilms.¹⁷ Unlike Ag, Au, Pd, Ti
73 and Cu, selenium is a trace element in the human body.¹⁸ It is an important component in at least
74 25 selenoenzymes and a cofactor for glutathione peroxidases and thioredoxin reductases.¹⁹ Ag
75 NPs, as the most widely researched nanoparticles for antibacterial applications exhibit excellent
76 antibacterial activity, but at the same time, show high toxicity to human cell lines.^{20,21} Our previous
77 work compared the cytotoxicity and antibacterial activity of chitosan/polyvinyl alcohol scaffolds
78 loaded with either Ag NPs or Se NPs. Both types of scaffolds showed antibacterial activity, but the
79 scaffolds decorated with Se NPs were more cytocompatible with fibroblasts than the Ag NPs loaded
80 scaffolds.²² Recent reports from our group^{9,23} and others^{24,25} showed that negatively charged Se
81 NPs showed strong antibacterial effects against Gram-positive bacteria but were less effective

82 against Gram-negative bacteria. The electrostatic attraction between positively charged
83 nanoparticles and the negatively charged membranes of bacterial cells plays an important role in
84 the antibacterial activity of nanoparticles.^{26,27} Since the membrane of Gram-negative bacteria is
85 generally more negatively charged than that of Gram-positive bacteria,^{28,29} they have been
86 observed to be more sensitive to positively charged nanoparticles.²⁸ Therefore, positively charged
87 nanoparticles have been explored for effective antibacterial applications.^{30,31,32} For example, Liu *et*
88 *al* reported that positively charged Ag NPs showed a much lower minimum inhibitory concentration
89 (MIC) than negatively charged Ag NPs against the Gram-positive bacteria *Bacillus subtilis*, the
90 Gram-negative bacteria *E. coli*, and the pathogenic yeast *Candida albicans*.³³ Thus, modifying the
91 surface of Se NPs with positive charge is a promising approach to improve the antibacterial activity
92 of Se NPs against Gram-negative bacteria. However, most previous studies on antibacterial Se
93 NPs have used negatively charged coatings to stabilize the particles.^{9,23,24,25,34} One study that did
94 use a positively charged chitosan coating on Se NPs did not find that it improved their antibacterial
95 efficacy over negatively charged polyvinyl alcohol (PVA) coated Se NPs. In fact, the chitosan
96 coated Se NPs were found to show much higher MIC than the PVA coated Se NPs against both *S.*
97 *aureus* (500 µg/mL vs. 125 µg/mL) and *E. coli* (500 µg/mL vs. 250 µg/mL).³⁵ This unexpected result
98 may be due to different sized NPs being used with the different coatings (195 nm for the chitosan
99 coated Se NPs vs. 136 nm for the PVA coated Se NPs). Importantly, size is one key factor
100 influencing the uptake of NPs by cells in general and the antibacterial efficacy of Se NPs in
101 particular.²³ Another factor could be surface charge, as a positively charged surface coating has
102 been shown to increase the uptake of Se NPs by cancer cells.³⁶ Thus, the influence of positive
103 charge on cytotoxicity and antibacterial activity of Se NPs still needs to be investigated.

104 Several synthetic and biopolymers with positive charge have been previously used as
105 coatings of inorganic nanoparticles to enhance the antimicrobial activity, such as branched
106 polyethyleneimine (PEI),³⁷ poly-allylamine hydrochloride (PAH),³⁸ chitosan^{39,40} and oligochitosan.⁴¹
107 The PEI has disadvantages including toxicity and nonbiodegradability.⁴² PAH has high toxicity
108 toward various mammalian cells.⁴³ Although chitosan has good biocompatibility and antibacterial
109 activity,⁴⁴ its physical properties are highly pH dependent.⁴⁵ To overcome the poor solubility, water

110 soluble oligochitosan has been made by hydrolysis of chitosan.⁴⁶ However, the yields of
111 oligochitosan were often low and lead to a mixture of products.^{46,47} Moreover, since chitin is sourced
112 from shellfish, and chitosan and oligochitosan are derivatives of chitin, their use may not be
113 appropriate for people with shellfish allergies.⁴⁸ Compared to these polymers, the positively
114 charged spider silk protein eADF4(κ 16) has several advantages, including good biocompatibility,
115 low immunogenicity, nontoxicity, and biodegradability.^{49,50,51,52,53,54} Recombinant spider silk protein
116 eADF4(κ 16) is a variant of polyanionic eADF4(C16), where the naturally occurring glutamic acid
117 residue in the sequence of the eADF4 core C-module (GSSAAA AAAAAS GPGGYG PENQGP
118 SGPGGYGPGGP) is replaced with lysine.⁴⁹ eADF4(C16) is based on the consensus core
119 sequence of the garden spider *Araneus diadematus* dragline silk fibroin 4 (ADF4) and comprises a
120 consensus (C) module repeated 16 times.⁵⁵ Importantly, both recombinant spider silk proteins have
121 similar physicochemical properties and therefore can be processed into several morphologies like
122 particles, films, coatings, and fibers.⁵⁶ These properties show that recombinant spider silk can be
123 used as a suitable biopolymer to modify the surface charge of nanoparticles to enhance their
124 antibacterial activity.

125 In this work, the positively charged spider silk protein eADF4(κ 16) was selected to stabilize
126 Se NPs and provide a net positive surface charge. Se NPs coated with the positively charged
127 eADF4(κ 16) were expected to show increased interactions with negatively charged bacterial cell
128 membranes. Their antibacterial properties against Gram-negative bacteria, such as *E. coli*, and
129 cytotoxicity for mammalian cells were assessed. In addition, PVA coated Se NPs were studied in
130 comparison to the eADF4(κ 16) coated NPs. PVA is a commonly used stabilizing agent for Se
131 NPs,^{57,58} and the antibacterial activity of PVA coated Se NPs have been investigated in many
132 studies.^{9,23,35,59} Furthermore, the eADF4(κ 16) coated NPs were immobilised on positively or
133 negatively charged spider silk protein films, and their ability to exert their antibacterial activity was
134 assessed.

135 **Material and methods**

136 ***Materials***

137 Selenium dioxide (SeO₂, 98%), PVA (MW 9000-10000, 80% hydrolysed), formic acid (≥ 98%) and
138 Mueller-Hinton broth were purchased from Sigma Aldrich (Germany). L-ascorbic acid (≥ 99%) and
139 agar were obtained from Roth Carl Roth GmbH (Germany). 1,1,1,3,3,3-Hexafluoro-2-propanol
140 (HFIP, 99+%) was purchased from Alfa Aesar (Germany). Dimethyl sulfoxide (DMSO, ≥ 99.5%)
141 was bought from Fluka (Australia). Phosphate-buffered saline (PBS) tablets were bought from
142 Gibco (UK). In all the experiments, ultrapure water from a Milli-Q-system (Billerica, MA, USA) was
143 used.

144 Proteins: eADF4(C16) was purchased from AMSilk GmbH (Planegg/München, Germany).
145 eADF4(κ16) was produced and purified as described previously.^{49,55}

146 ***Se NPs synthesis***

147 For fabrication of positively charged Se NPs, the recombinant spider silk protein eADF4(κ16) was
148 first dissolved in formic acid (≥98%) at a concentration of 4 mg/mL and further diluted with water to
149 obtain a concentration of 0.1 mg/mL. SeO₂ powder was added into this solution to a concentration
150 of 5 mM. Then, 4 mL of 0.1M L-ascorbic acid was added into 4 mL of 0.1 mg/mL eADF4(κ16) and
151 5 mM SeO₂ solution. The reaction mixture was stirred at a speed of 300 rpm using a magnetic
152 stirrer. After 10 min, the solution was transferred into 2 mL Eppendorf tubes and was centrifuged
153 at a speed of 13300 rpm (17000 g) for 3 min using a Heraeus Pico 17 centrifuge (Thermo Scientific),
154 followed by removal of supernatant and washing the particles twice with water. Particles were
155 stored in water for all experiments. Similarly, negatively charged Se NPs were fabricated using
156 PVA dissolved in water at a concentration of 2 mg/mL.

157 **Characterization of Se NPs**

158 The zeta potential of Se NPs was measured using a Zetasizer (Malvern, ATA Scientific). Zeta
159 potential was measured at 25 °C; selenium with a refractive index (RI) of 2.6 and absorption of 0.5
160 was set as the material, a dielectric constant of 78.5 for water as the dispersant.⁶⁰ The morphology
161 of the Se NPs was observed using transmission electron microscopy (TEM, JEOL, Japan) at an
162 accelerating voltage of 80 keV. The particle sizes were determined by measuring 200 nanoparticles
163 from more than 4 TEM images of each sample in different areas. Energy Dispersive Spectroscopy
164 (EDS) within an equipped-on scanning electron microscope (SEM, Zeiss Sigma 300 VP,
165 Oberkochen, Germany) was used to detect the component elements of the nanoparticles. The
166 interaction between Se NPs and eADF4(κ 16) or PVA was investigated by measuring their
167 Attenuated Total Reflection-Fourier Transform Infrared (ATR-FTIR) Spectra in the range of 4000-
168 800 cm^{-1} on a Bruker Tensor 27 spectrometer (Bruker, Germany). For each spectrum, 100 scans
169 were recorded at a resolution of 4 cm^{-1} . The individual secondary structure elements were
170 determined by analysing the amide I region (1595-1705 cm^{-1}) with Fourier self-deconvolution (FSD)
171 using Opus software (Bruker, Germany). To measure the Se concentration of the Se NPs solutions,
172 nitric acid (HNO_3) was used to dissolve the Se NPs into ions, and ICP-OES (Perkin Elmer Optima
173 7300 DV, USA) was adopted to test the Se ion concentrations.

174

175 **Cytotoxicity tests of Se NPs**

176 AlamarBlue[®] was used to test the cytotoxicity of Se NPs. Balb/3T3 mouse embryo fibroblasts and
177 HaCaT human skin keratinocytes (European Collection of Cell Cultures) were used to evaluate the
178 cytotoxicity of Se NPs. The cells were cultured in Dulbecco's modified Eagle's medium (DMEM)
179 with 10% fetal bovine serum (FBS), 100 $\text{U}\cdot\text{mL}^{-1}$ gentamycin and 100 $\mu\text{g}\cdot\text{mL}^{-1}$ glutamine, 5% CO_2 ,
180 95% relative humidity, and at 37 °C.

181 Se NPs solution at a concentration of 500 $\mu\text{g}/\text{mL}$ in water was serially diluted with DMEM
182 from concentrations of 0.97 to 31.2 $\mu\text{g}/\text{mL}$. The control groups comprised DMEM medium as the
183 negative control and DMEM with 10% (v/v) DMSO as the positive control, according to ISO 10993-

184 5 standard.⁶¹ Cells at a density of 5×10^3 per 100 μL medium per well were added into the 96-well
185 plates and incubated for 24 h at 37 °C to allow attachment. The medium was then replaced by 100
186 μL of DMEM with Se NPs or control media. After 24 h incubation, the DMEM with Se NPs was
187 removed and washed once by PBS. Then, 120 μL of DMEM with 10% alamarBlue[®] reagent was
188 added to all wells and incubated at 37 °C. After an incubation time period of 3 h, 100 μL medium
189 was transferred from each well to a black 96-well plate. The transformation of the blue fluorescent
190 dye resazurin into red fluorescent resorufin ($\lambda_{\text{ex}} = 530 \text{ nm}$; $\lambda_{\text{em}} = 590 \text{ nm}$) was measured using a
191 plate reader (Mithras LB 940, Bertold, Bad Wildbach, Germany) with 530 nm excitation and 600
192 nm emission filters and a counting time of 0.5 s. The cell viability (X) of each experimental group
193 was calculated based on three samples according the formula below according to ISO 10993-5.⁶¹

$$194 \quad X = \frac{(OD_1 - OD_b)}{(OD_2 - OD_b)} \times 100\% \quad (1)$$

195 where OD_1 represents the mean fluorescence density of the experimental groups or the
196 positive control group, OD_2 represents the mean fluorescence density of the negative control group,
197 OD_b represents the mean fluorescence density of the blank control.

198 **Antibacterial tests of Se NPs**

199 Colony forming units (CFU) assays using *Escherichia coli* (*E. coli*, strain BL21-Gold, Novagen,
200 Merck, Germany) were performed for testing the antibacterial activity of Se NPs and the particles
201 made of plain eADF4(κ 16). Firstly, a single colony of *E. coli* taken from an agar plate was inoculated
202 into 20 mL Mueller Hinton Broth (MHB) and was cultured overnight at 37 °C. Then 200 μL of the
203 overnight bacterial solution was transferred into 10 mL fresh MHB and cultured for 4h at 37 °C. 100
204 μL of water with different concentrations of Se NPs or plain eADF4(κ 16) particles was added into
205 each well of 96-well plates. The bacteria were centrifuged at 13300 rpm (17000 g) for 15 min, then
206 washed using water once and resuspend into water. 100 μL of 1×10^7 cells/mL of *E. coli* in water
207 were added into each well. After 4 h incubation at 37 °C, the bacterial suspensions were diluted to
208 10^{-1} , 10^{-2} , 10^{-3} and 10^{-4} times with water, then 10 μL of these solutions were transferred to agar
209 plates with MHB. The agar plates were incubated overnight at 37 °C, then the bacterial colony

210 forming units were observed and counted. The minimum bactericidal concentration (MBC) was
211 calculated according to the method published in Ref. 62. Concentration-killing curves were plotted
212 with CFUs/mL as a function of antibacterial agent concentration, and linear regression analysis was
213 used to determine the lowest concentration (MBC) at which the CFU/mL becomes zero.

214 ***Bacterial morphology imaging***

215 The morphology of *E. coli* cells after treatment with Se NPs was imaged using SEM (Zeiss Sigma
216 300 VP, Oberkochen, Germany). The samples were prepared as follows: 100 μ L of 150 μ g/mL Se
217 NPs in water was added into each well of 96-well plates, then 100 μ L MHB with 5×10^7 cells/mL
218 bacteria was added into each well. After 2 h incubation, 10 μ L of the bacteria with Se nanoparticles
219 solution was dropped onto a clean silicon wafer, followed by drying at 37 °C for 40 min. Afterwards,
220 2.5% v/v glutaraldehyde was used to fix the bacteria cells for 1 h, then gradient ethanol solutions
221 (30%, 50%, 60%, 70%, 80%, 90%, 95% and 100% v/v) were used for dehydration. After overnight
222 drying in the air, the samples were coated with platinum prior to imaging.

223 ***Fabrication of eADF4(κ 16) coated Se NPs immobilized on spider***

224 ***silk protein films***

225 To prepare films, recombinant spider silk proteins eADF4(κ 16) or eADF4(C16) were first dissolved
226 in HFIP to a concentration of 30 mg/mL, and 10 μ L of the solution were dropped into each well of
227 a 48-well plate. The samples were allowed to dry inside a fume hood and were post-treated with
228 70% ethanol to induce β -sheet formation.^{63,64} Then, 10 μ L of eADF4(κ 16) coated Se NPs at a
229 concentration of 3 mg/mL in HFIP were quickly dropped onto the films and allowed to dry in a fume
230 hood. All the films were sterilized by UV exposure for 1 h.

231 ***Antibacterial tests of Se NPs immobilized on spider silk protein***
232 ***films***

233 CFU assays on *E. coli* were performed for testing the antibacterial activity of Se NPs immobilized
234 on spider silk protein films. Firstly, a single colony of *E. coli* taken from an agar plate was inoculated
235 into 20 mL MHB and was cultured overnight at 37 °C. Then, 200 µL of the overnight bacterial
236 solution was transferred into 10 mL fresh MHB and cultured for 4h at 37 °C. 250 µL of 1×10⁶
237 cells/mL of *E. coli* in MHB were added into a 48-well plate with films and incubated for 4h. The later
238 steps for diluting the bacteria suspensions and culturing colonies on agar plates were the same as
239 those used for CFU assays on Se NPs.

240 ***Releasing tests of Se NPs immobilized on spider silk protein films***

241 The eADF4(κ16) coated Se NPs immobilized on eADF4(κ16) films or eADF4(C16) films were
242 fabricated into a 48-well plate, as mentioned above. For each type of films, 250 µL of MHB was
243 added into each well of six sample wells and incubated at 37 °C for 4 h. In three of these six sample
244 wells, 150 µL of MHB was directly taken from each well and transferred to a 10 mL centrifuge tube.
245 For the other three sample wells, 150 µL of MHB was taken after 5 times pipetting from the surface
246 of films using a 1 mL pipette (Eppendorf® Research® Plus) and transferred to a 10 mL centrifuge
247 tube. 350 µL HNO₃ was added into each of the centrifuge tubes and allowed to react overnight to
248 dissolve the Se NPs. Then the solution was diluted using water and analysed by inductively coupled
249 plasma-optical emission spectrometry (ICP-OES, Varian 720-ES) to determine the Se ion
250 concentrations.

251 ***Statistical analysis***

252 Data in this work are expressed as means ± standard deviation of three measurements. Statistical
253 analyses for all results were performed by one-way analysis of variance (ANOVA with Tukey's Post
254 Hoc Test using SPSS 25.0) and p-values less than 0.05 were considered statistically significant.

255 **Results and discussion**

256 ***Synthesis and characterization of selenium nanoparticles***

257 Selenium nanoparticles (Se NPs) were synthesized by chemical reduction of selenous acid,
258 obtained by adding selenium dioxide in water. eADF4(κ 16) and polyvinyl alcohol (PVA) were used
259 as stabilizing agents and L-ascorbic acid as reducing agent. TEM images of different sized Se NPs
260 are shown in [Figure 1 a-b](#). These nanoparticles were all spherical and quite monodisperse,
261 indicating that both eADF4(κ 16) and PVA are good stabilizers for Se NPs yielding a stable surface
262 coating. The size distribution of these nanoparticles evaluated from their TEM images is shown in
263 [Figure 1 c-d](#). The mean diameter of Se NPs stabilized with 0.1 mg/mL eADF4(κ 16) (46 nm)
264 matched that of 2 mg/mL PVA stabilized Se NPs (46 nm). The zeta potentials of the eADF4(κ 16)
265 coated Se NPs and PVA coated Se NPs were $+46.0 \pm 0.6$ mV and -7.3 ± 0.1 mV, respectively. The
266 zeta potential distributions are shown in [Figure S1](#).

267 Energy Dispersive Spectroscopy (EDS) analysis of eADF4(κ 16) coated Se NPs is shown
268 in [Figure S2 a](#). Peaks corresponding to O, N and Se confirm the eADF4(κ 16) coating of the Se
269 NPs. Also, EDS of control samples was measured, prepared by washing the eADF4(κ 16) coated
270 Se NPs with guanidinium thiocyanate, as shown in [Figure S2 b](#). Guanidinium thiocyanate denatures
271 the protein structure of the eADF4(κ 16) coating, which is thereby removed from the Se NP surface,
272 leading to aggregation of Se NPs and disappearance of the nitrogen peak in the EDS. The
273 eADF4(κ 16) coated Se NPs were observed visibly to be stable in water for more than 3 months,
274 indicating that the coating made of eADF4(κ 16) on the Se NPs was stable, preventing particle
275 aggregation.

276 FT-IR was used to investigate the structural features of Se NPs and eADF4(κ 16), and the
277 spectra are shown in [Figure 1 e](#). eADF4(κ 16) coated Se NPs showed very similar spectra to that
278 of plain eADF4(κ 16) particles used as controls. After washing with guanidinium thiocyanate, the
279 protein peaks of the coated Se NPs significantly decreased. Fourier self-deconvoluted absorbance
280 spectra of the amide I band of eADF4(κ 16) particles and eADF4(κ 16) coated Se NPs were
281 evaluated and are shown in [Figure S3](#). The percentages of the secondary structure elements are

282 listed in Table 1. Comparing to eADF4(κ 16) particles, eADF4(κ 16) coated Se NPs showed similar
283 features with a slightly decreased percentage of side chains and increased percentage of turns.

284 FT-IR was also used to investigate the structural features of Se NPs coated with PVA
285 (Figure 1 f). Plain PVA showed a peak at 3307 cm^{-1} corresponding to O-H stretching vibrations.
286 The peaks at 2850 cm^{-1} , 2920 cm^{-1} and 2941 cm^{-1} corresponded to C-H stretching from the alkyl
287 group. In comparison, PVA coated Se NPs showed a shift in the hydroxyl peak to 3369 cm^{-1} . This
288 blue-shift indicated that PVA was conjugated to the surface of Se NPs through the –OH group.³⁶

289 ***Cytotoxicity test of selenium nanoparticles using fibroblasts and*** 290 ***keratinocytes***

291 The cell viability of Balb/3T3 mouse embryo fibroblasts and HaCaT human skin keratinocytes
292 exposed to different concentrations of eADF4(κ 16) coated Se NPs and PVA coated Se NPs were
293 measured using the alamarBlue® assay (Figure 2). Balb/3T3 mouse embryo fibroblasts are
294 frequently used to test materials' carcinogenicity⁶⁵ and cytotoxicity,^{66,67} and HaCaT keratinocytes
295 are a preliminary in vitro model to investigate skin toxicity.⁶⁸ Both of these cell lines have been
296 widely used for cytotoxicity tests of nanoparticles.^{67,69,70,71} The PVA coated Se NPs exhibited no
297 obvious cytotoxicity at concentrations up to 31.2 $\mu\text{g/mL}$. The viability of Balb/3T3 mouse embryo
298 fibroblasts did decrease somewhat with increasing concentrations of Se NPs, but their viability was
299 not below 70% even at the highest dose of 31 $\mu\text{g/mL}$ (one-sample t-test, $p=0.41$). According to ISO
300 10993-5,⁶¹ a material reducing cell viability below 70% of the negative control is considered to be
301 potentially cytotoxic, so the effects of these Se NPs would not be classified as cytotoxic at these
302 doses. All in all, up to 31 $\mu\text{g/mL}$, eADF4(κ 16) coated Se NPs and PVA coated Se NPs were not
303 considered to be potentially cytotoxic for Balb/3T3 mouse embryo fibroblasts.

304 After 24 hours' exposure, both the eADF4(κ 16) coated Se NPs and the PVA coated Se
305 NPs showed no significant cytotoxicity to the HaCaT human skin keratinocytes at doses up to 31.2
306 $\mu\text{g/mL}$. The viability of HaCaT human skin keratinocytes exposed to PVA coated Se NPs showed
307 a trend of first increasing to $153\pm 12\%$ with 3.9 $\mu\text{g/mL}$ of PVA coated Se NPs and then decreasing
308 with increasing Se concentrations. This trend, which is consistent with our previous findings,²³ may

309 be attributed to the antioxidant activity of Se NPs.^{16,72} At low levels, Se cannot sufficiently scavenge
310 reactive oxygen species (ROS), whereas at high levels, Se can catalyse the production of ROS,
311 which can be toxic to human cells, making an intermediate dose favourable. The eADF4(κ 16)
312 coated Se NPs did not show this trend, possibly due to differences in their interactions and uptake
313 by the cells. As selenium has a very low solubility in physiological conditions, the ways the NPs
314 themselves interact with the cells is expected to govern their effects.

315 The greater decrease in the viability of the Balb/3T3 mouse embryo fibroblasts with the
316 eADF4(κ 16) coated Se NPs compared to the PVA coated Se NPs may be ascribed to the surface
317 charge of the Se NPs. High positive surface charge of NPs has been reported to be more cytotoxic
318 than negative surface charge.⁷³ The cellular uptake process can be divided into two steps: first,
319 particles attach to the cell membrane, and second, they are internalized by the cells.⁷⁴ The step of
320 attachment is mostly affected by the surface charge of the nanoparticle.^{75,76} As the cell membrane
321 is dominated by negatively charged sulphated proteoglycans,⁷⁷ nanoparticles with high positive
322 surface charge can therefore more easily approach cells and become strongly bound to the cell
323 membrane, resulting in a higher cellular uptake.⁷⁸ As the eADF4(κ 16) coated Se NPs have a high
324 positive surface charge ($+46.0 \pm 0.6$ mV), they may induce higher cellular uptake resulting in greater
325 effects on the cells. The PVA coated Se NPs have a slightly negative surface charge (-7.3 ± 0.1
326 mV), which may reduce their ability to be taken up by the cells, consistent with them being less
327 cytotoxic.

328 ***Antibacterial activity of selenium nanoparticles***

329 eADF4(κ 16) coated Se NPs and PVA coated Se NPs were tested for their antibacterial activity
330 against *E. coli* as a model organism. Both types of Se NPs showed dose-dependent antibacterial
331 effects against *E. coli* (Figure 3 a). However, the bactericidal effect of eADF4(κ 16) coated Se NPs
332 was much higher than that of its counterpart, with a minimum bactericidal concentration (MBC)
333 against *E. coli* of 8 ± 1 $\mu\text{g/mL}$, which is 50 times lower than that of the PVA coated Se NPs with a
334 MBC of 405 ± 80 $\mu\text{g/mL}$. Figure 3 b-d shows the agar plates with *E. coli* colonies after treatment
335 with Se NPs. It could be clearly shown that no colonies were detected when treated with at least

336 15.6 µg/mL of eADF4(κ16) coated Se NPs. By contrast, a large number of colonies appeared even
337 after treatment with 31.2 µg/mL of PVA coated Se NPs. As shown above, eADF4(κ16) coated Se
338 NPs are safe for both Balb/3T3 mouse embryo fibroblasts and HaCaT human skin keratinocytes
339 up to 31 µg/mL, which is much higher than the MBC (8 ± 1 µg/mL) of these NPs against *E. coli*.
340 Therefore, it should be safe and effective to use these particles at doses below 31 µg/mL for
341 antibacterial applications. However, further testing would be needed to confirm their
342 biocompatibility for specific in vivo applications.

343 The morphologies of *E. coli* before and after treatment with the Se NPs are shown in [Figure](#)
344 [3 e-g](#). The negatively charged PVA coated Se NPs were repelled by *E. coli* ([Figure 3 f](#)), whereas
345 the eADF4(κ16) coated Se NPs were able to attach to *E. coli* ([Figure 3 g](#)). The greater attachment
346 of the Se NPs with the positively charged coating to *E. coli* correlates well with the lower
347 concentration of these NPs required to show antibacterial efficacy, as demonstrated in [Figure 3 a](#).
348 These results confirmed the importance of electrostatic attraction between positively charged
349 nanoparticles and negatively charged membrane of bacterial cells for the antibacterial activity of
350 nanoparticles.^{26,79}

351 Particles made of plain eADF4(κ16) alone showed no antibacterial effects up to 250 µg/mL
352 against *E. coli* ([Figure S4](#)), so the antibacterial activity of the eADF4(κ16) coated Se NPs can be
353 primarily attributed to their selenium content. Our previous work revealed that Se NPs show multi-
354 modal mechanisms of action on Gram-positive bacteria, including depletion of internal adenosine
355 triphosphate (ATP), promotion of ROS production, and disruption of membrane potential.²³ ATP is
356 an important energy source of living organisms, the depletion of ATP can seriously affect both
357 respiration and metabolism of bacteria.^{80,81} Over production of ROS can induce the damage of
358 cellular components including lipids, DNA and proteins.^{82,83} Disruption of membrane potential can
359 cause changes of a series of cellular processes.⁸⁴ Chudobova *et al* also found that Se NPs could
360 impair the bacterial DNA structure of the *zntR* gene amplified *in vitro*⁸⁵ and Liu *et al* reported that
361 Se NPs could weaken bacterial membranes and decrease the function of adhesion-mediating
362 proteins.⁸⁶ Tran *et al* proposed that the antibacterial effect of Se NPs is also related to free
363 intracellular thiol depletion of Se NPs.⁸⁷ Besides, the positive charge could enhance the interactions

364 between NPs and cell membranes, and then induce more intense membrane damage,⁸⁸ which can
365 also be an antibacterial mechanism of eADF4(κ 16) coated Se NPs. Further studies would be
366 needed to elucidate the specific mechanisms of action of eADF4(κ 16) coated Se NPs.

367 In a previous study, PVA coated Se NPs with effective antibacterial activity against Gram-
368 positive bacteria *S. aureus* were fabricated.²³ However, these particles were found to be less
369 effective against the Gram-negative bacteria *E. coli*. In the present work, the eADF4(κ 16) coated
370 Se NPs showed a much higher antibacterial activity against *E. coli* than PVA coated ones.
371 Meanwhile, these particles also retained good antibacterial activity against *S. aureus* (Figure S5),
372 with a MBC value of 32 ± 1 $\mu\text{g/mL}$. Notably, the MBC of eADF4(κ 16) coated Se NPs against *E. coli*
373 was four times lower than that against *S. aureus*. Positively charged NPs often work better against
374 Gram-negative bacteria than Gram-positive bacteria as the Gram-negative bacteria are more
375 sensitive to positively charged materials.^{89,90} The antibacterial activity of these eADF4(κ 16) coated
376 Se NPs is very high compared to previously reported PVA coated Se NPs, which normally show a
377 minimum inhibitory concentration (MIC) higher than 60 $\mu\text{g/mL}$ ^{9,17,34,35} against *S. aureus*, and even
378 worse performance against *E. coli*, with no significant effect,^{9,24,25,35} or MIC values higher than 100
379 $\mu\text{g/mL}$ ^{17,34,91}. Although the MBC was not tested in most of these studies, the MBC is generally
380 higher than the MIC. By contrast, the eADF4(κ 16) coated Se NPs showed relatively low MBC
381 values of 32 ± 1 $\mu\text{g/mL}$ against *S. aureus*, and 8 ± 1 $\mu\text{g/mL}$ against *E. coli*. The PVA coated Se
382 NPs showed a MBC of 35 ± 16 $\mu\text{g/mL}$ against *S. aureus*,²³ but they were found to have only weak
383 antibacterial effects against *E. coli* as mentioned above. One study showed Se NPs with MIC of 4
384 $\mu\text{g/mL}$ against both *S. aureus* and *E. coli*.⁹² However, this required additional antimicrobial
385 compounds to boost the efficacy of Se NPs. Although the eADF4(κ 16) coated Se NPs showed
386 higher antibacterial activity than previously reported Se NPs, it is worth noting that the antibacterial
387 tests of these eADF4(κ 16) coated Se NPs were conducted in water rather than bacterial culture
388 medium as used for other studies due to the tendency of the eADF4(κ 16) coated Se NPs to
389 aggregate in bacterial culture medium.

390 ***Antibacterial test of spider silk coated Se NPs immobilized on***
391 ***spider silk films***

392 The eADF4(κ 16) coated Se NPs were found to quickly aggregate and deposit in Mueller-Hinton
393 broth (MHB). MHB is a nutrient-rich medium, which is representative of the physiological
394 environment⁹³ and regarded to be the gold standard culture media for antibacterial susceptibility
395 testing.^{94,95} Thus, in order to stabilize the particles against aggregation in MHB, they were
396 immobilized on the surfaces of films made of the positively charged eADF4(κ 16) and negatively
397 charged eADF4(C16). Physicochemical properties as well as secondary structure of spider silk
398 films have been thoroughly characterised in previous studies.^{64,96} Then, the antibacterial activity of
399 the immobilized Se NPs was tested. The charge of the films was expected to influence both the
400 immobilization and potential release of the eADF4(κ 16) coated Se NPs.

401 The CFU test results for *E. coli* after treatment with eADF4(κ 16) coated Se NPs
402 immobilized on the two types of spider silk protein films are shown in [Figure 4 a](#). eADF4(κ 16) coated
403 Se NPs immobilized on eADF4(κ 16) films (with the identical surface charge) showed a significant
404 antibacterial activity, whereas particles on eADF4(C16) films (with the opposite surface charge)
405 showed no significant difference in CFU counts relative to the control.

406 These results demonstrated the effect of the charge of the surface used to immobilize the
407 coated Se NPs. The positively charged eADF4(κ 16) coated Se NPs would be expected to adsorb
408 more strongly to the negatively charged eADF4(C16) films through electrostatic interactions than
409 to the positively charged eADF4(κ 16) films. This was confirmed by comparison of the amounts of
410 Se released from the two types of films with immobilized eADF4(κ 16) coated Se NPs ([Figure 4 b](#)).
411 Very little Se was released from the films after 4 h under static immersion in MHB. Upon applying
412 gentle shear forces via pipetting, the positively charged eADF4(κ 16) films released significant
413 amounts of selenium into the culture broth, however, no significant release was seen from
414 negatively charged films. Thus, the Se NPs could be more easily released from the eADF4(κ 16)
415 films, and this correlates with the lower CFU counts found for *E. coli* exposed to these films. This
416 indicates that these Se NPs need to be released from the spider silk surface in order to exert their

417 antibacterial effects on *E. coli*. Besides, unlike Ag NP coatings which could rely on the released
418 silver ions to provide the antibacterial activity,⁹⁷ the present work implied that Se NP coatings need
419 to rely on NPs themselves to combat bacteria rather than operating via the release of selenium
420 ions. This correlates well with the much lower solubility of selenium compared to that of silver.^{97,98}
421 These new insights will help enable the future design of effective antibacterial surface coatings
422 based on Se NPs.

423 **Conclusion**

424 Previous studies have reported that negatively charged Se NPs showed good antibacterial activity
425 against Gram-positive bacteria, but they are less effective against Gram-negative bacteria which
426 are more sensitive to positively charged nanoparticles. In this work, positively charged eADF4(κ 16)
427 coated Se NPs and negatively charged PVA coated Se NPs with the same mean diameter (46 nm)
428 were fabricated. Both the eADF4(κ 16) coated Se NPs and PVA coated Se NPs were safe to
429 Balb/3T3 mouse embryo fibroblasts and HaCaT human skin keratinocytes up to 31 μ g/mL.
430 Comparing to PVA coated Se NPs, eADF4(κ 16) stabilized Se NPs showed a much higher
431 bactericidal efficacy against the Gram-negative bacteria *E. coli*. Particularly, the MBC of
432 eADF4(κ 16) coated Se NPs (8 ± 1 μ g/mL) was approximately 50 times lower than that of PVA
433 coated Se NPs (405 ± 80 μ g/mL). Immobilizing the eADF4(κ 16) stabilized Se NPs on positively
434 charged eADF4(κ 16) films showed a good bactericidal effect against *E. coli* in culture broth.
435 Together, these results indicated that eADF4(κ 16) coated Se NPs can be considered as promising
436 new antibacterial agents.
437

438 **Acknowledgments**

439 The authors acknowledge financial support by the German Academic Exchange service (DAAD)
440 through its Thematic Network Melbourne-Bayreuth Polymer/Colloid Network sponsored from funds
441 of the Federal Ministry of Education and Research (BMBF), and European Union Grand ETZ-EFRE
442 2014–2020, Freistaat Bayern–Tschechien, Project Nr. 123. Bavarian Research Foundation for

443 financial support (DOK-175-15, T.B.A). TH gratefully acknowledges the support of the University of
444 Melbourne and an Australian Government Research Training Program Scholarship (Melbourne
445 International Research Scholarship).

446

447 Disclosure

448 Thomas Scheibel is founder and shareholder of AMSilk GmbH, Germany.

449

450 References

- 451 1. Wang L, Hu C, Shao L. The antimicrobial activity of nanoparticles: present situation and
452 prospects for the future. *Int. J. Nanomedicine* 2017;**12**:1227
- 453 2. Poole K. Mechanisms of bacterial biocide and antibiotic resistance. *J. Appl. Microbiol.*
454 2002;**92**:55S-64S
- 455 3. Jayaraman R. Antibiotic resistance: an overview of mechanisms and a paradigm shift. *Curr. Sci.*
456 2009:1475-84
- 457 4. Knetsch ML, Koole LH. New strategies in the development of antimicrobial coatings: the
458 example of increasing usage of silver and silver nanoparticles. *Polymers* 2011;**3**(1):340-66
- 459 5. Theuretzbacher U. Global antibacterial resistance: The never-ending story. *J. Glob. Antimicrob.*
460 *Resist.* 2013;**1**(2):63-69
- 461 6. Basak S, Singh P, Rajurkar M. Multidrug resistant and extensively drug resistant bacteria: A
462 study. *J. Pathog.* 2016;**2016**:1-5
- 463 7. Ivask A, Kurvet I, Kasemets K, et al. Size-dependent toxicity of silver nanoparticles to bacteria,
464 yeast, algae, crustaceans and mammalian cells in vitro. *PLoS One* 2014;**9**(7):e102108
- 465 8. Xie Y, Liu Y, Yang J, et al. Gold Nanoclusters for Targeting Methicillin-Resistant *Staphylococcus*
466 *aureus* In Vivo. *Angew. Chem. Int. Ed.* 2018;**57**(15):3958-62
- 467 9. Tran PA, O'Brien-Simpson N, Reynolds EC, Pantarat N, Biswas DP, O'Connor AJ. Low
468 cytotoxic trace element selenium nanoparticles and their differential antimicrobial properties
469 against *S. aureus* and *E. coli*. *Nanotechnology* 2015;**27**(4):045101
- 470 10. Adams CP, Walker KA, Obare SO, Docherty KM. Size-dependent antimicrobial effects of novel
471 palladium nanoparticles. *PLoS One* 2014;**9**(1):e85981
- 472 11. Kühn KP, Chaberny IF, Massholder K, et al. Disinfection of surfaces by photocatalytic oxidation
473 with titanium dioxide and UVA light. *Chemosphere* 2003;**53**(1):71-77
- 474 12. Bondarenko O, Juganson K, Ivask A, Kasemets K, Mortimer M, Kahru A. Toxicity of Ag, CuO
475 and ZnO nanoparticles to selected environmentally relevant test organisms and mammalian
476 cells in vitro: a critical review. *Arch. Toxicol.* 2013;**87**(7):1181-200
- 477 13. Wadhvani SA, Shedbalkar UU, Singh R, Chopade BA. Biogenic selenium nanoparticles: current
478 status and future prospects. *Appl. Microbiol. Biotechnol.* 2016;**100**(6):2555-66
- 479 14. Ionin A, Ivanova A, Khmel'nitskii R, et al. Antibacterial effect of the laser-generated Se
480 nanocoatings on *Staphylococcus aureus* and *Pseudomonas aeruginosa* biofilms. *Laser Phys.*
481 *Lett.* 2017;**15**(1):015604
- 482 15. Ismail A-WA, Sidkey NM, Arafa RA, Fathy RM, El-Batal AI. Evaluation of in vitro antifungal
483 activity of silver and selenium nanoparticles against *Alternaria solani* caused early blight disease
484 on potato. *Br. Biotechnol. J.* 2016;**12**(3):1

- 485 16. Yazhiniprabha M, Vaseeharan B. In vitro and in vivo toxicity assessment of selenium
486 nanoparticles with significant larvicidal and bacteriostatic properties. *Materials Science and*
487 *Engineering: C* 2019;**103**:109763
- 488 17. Zonaro E, Lampis S, Turner RJ, Qazi SJS, Vallini G. Biogenic selenium and tellurium
489 nanoparticles synthesized by environmental microbial isolates efficaciously inhibit bacterial
490 planktonic cultures and biofilms. *Front. Microbiol.* 2015;**6**:584
- 491 18. Underwood E. *Trace elements in human and animal nutrition*: Elsevier, 2012.
- 492 19. Tan VIC, Hinchman A, Williams R, Tran PA, Fox K. Nanostructured biomedical selenium at the
493 biological interface. *Biointerphases* 2018;**13**(6):06D301
- 494 20. AshaRani P, Low Kah Mun G, Hande MP, Valiyaveetil S. Cytotoxicity and genotoxicity of silver
495 nanoparticles in human cells. *ACS nano* 2008;**3**(2):279-90
- 496 21. Tran PA, Hocking DM, O'Connor AJ. In situ formation of antimicrobial silver nanoparticles and
497 the impregnation of hydrophobic polycaprolactone matrix for antimicrobial medical device
498 applications. *Materials Science and Engineering: C* 2015;**47**:63-69
- 499 22. Biswas DP, O'Brien-Simpson NM, Reynolds EC, O'Connor AJ, Tran PA. Comparative study of
500 novel in situ decorated porous chitosan-selenium scaffolds and porous chitosan-silver scaffolds
501 towards antimicrobial wound dressing application. *J. Colloid Interface Sci.* 2018;**515**:78-91
- 502 23. Huang T, Holden JA, Heath DE, O'Brien-Simpson NM, O'Connor AJ. Engineering highly
503 effective antimicrobial selenium nanoparticles through control of particle size. *Nanoscale*
504 2019;**11**:14937-51
- 505 24. Bartůněk V, Junková J, Šuman J, et al. Preparation of amorphous antimicrobial selenium
506 nanoparticles stabilized by odor suppressing surfactant polysorbate 20. *Mater. Lett.*
507 2015;**152**:207-09
- 508 25. Nguyen TH, Vardhanabhuti B, Lin M, Mustapha A. Antibacterial properties of selenium
509 nanoparticles and their toxicity to Caco-2 cells. *Food Control* 2017;**77**:17-24
- 510 26. Stoimenov PK, Klinger RL, Marchin GL, Klabunde KJ. Metal oxide nanoparticles as bactericidal
511 agents. *Langmuir* 2002;**18**(17):6679-86
- 512 27. Radovic-Moreno AF, Lu TK, Puscasu VA, Yoon CJ, Langer R, Farokhzad OC. Surface charge-
513 switching polymeric nanoparticles for bacterial cell wall-targeted delivery of antibiotics. *ACS*
514 *nano* 2012;**6**(5):4279-87
- 515 28. Chung Y-C, Su YP, Chen C-C, et al. Relationship between antibacterial activity of chitosan and
516 surface characteristics of cell wall. *Acta Pharmacol. Sin.* 2004;**25**(7):932-36
- 517 29. Gross M, Cramton SE, Götz F, Peschel A. Key role of teichoic acid net charge in staphylococcus
518 aureus colonization of artificial surfaces. *Infect. Immun.* 2001;**69**(5):3423-26
- 519 30. Franci G, Falanga A, Galdiero S, et al. Silver nanoparticles as potential antibacterial agents.
520 *Molecules* 2015;**20**(5):8856-74
- 521 31. El Badawy AM, Silva RG, Morris B, Scheckel KG, Suidan MT, Tolaymat TM. Surface charge-
522 dependent toxicity of silver nanoparticles. *Environ. Sci. Technol.* 2010;**45**(1):283-87
- 523 32. Abbaszadegan A, Ghahramani Y, Gholami A, et al. The effect of charge at the surface of silver
524 nanoparticles on antimicrobial activity against Gram-positive and Gram-negative bacteria: a
525 preliminary study. *J. Nanomater.* 2015;**16**(1):53
- 526 33. Liu L, Yang J, Xie J, et al. The potent antimicrobial properties of cell penetrating peptide-
527 conjugated silver nanoparticles with excellent selectivity for Gram-positive bacteria over
528 erythrocytes. *Nanoscale* 2013;**5**(9):3834-40
- 529 34. Guisbiers G, Wang Q, Khachatryan E, et al. Inhibition of *E. coli* and *S. aureus* with selenium
530 nanoparticles synthesized by pulsed laser ablation in deionized water. *Int. J. Nanomedicine*
531 2016;**11**:3731
- 532 35. Boroumand S, Safari M, Shaabani E, Shirzad M, Faridi-Majidi R. Selenium nanoparticles:
533 synthesis, characterization and study of their cytotoxicity, antioxidant and antibacterial activity.
534 *Mater. Res. Express* 2019;**6**(8):0850d8
- 535 36. Yu B, Zhang Y, Zheng W, Fan C, Chen T. Positive surface charge enhances selective cellular
536 uptake and anticancer efficacy of selenium nanoparticles. *Inorg. Chem.* 2012;**51**(16):8956-63
- 537 37. Silva T, Pokhrel LR, Dubey B, Tolaymat TM, Maier KJ, Liu X. Particle size, surface charge and
538 concentration dependent ecotoxicity of three organo-coated silver nanoparticles: comparison
539 between general linear model-predicted and observed toxicity. *Sci. Total Environ.*
540 2014;**468**:968-76

- 541 38. Buchman JT, Rahnamoun A, Landy KM, et al. Using an environmentally-relevant panel of Gram-
542 negative bacteria to assess the toxicity of polyallylamine hydrochloride-wrapped gold
543 nanoparticles. *Environ. Sci. Nano* 2018;**5**(2):279-88
- 544 39. Yoksan R, Chirachanchai S. Silver nanoparticle-loaded chitosan–starch based films:
545 Fabrication and evaluation of tensile, barrier and antimicrobial properties. *Mater. Sci. Eng., C*
546 2010;**30**(6):891-97
- 547 40. Cu TS, Nguyen CK, Tran NQ. Preparation of silver core-chitosan shell nanoparticles using
548 catechol-functionalized chitosan and antibacterial studies. *Macromol. Res.* 2014;**22**(4):418-23
- 549 41. Nguyen VT, Tran KVQ, Tran QN. Effect of oligochitosan-coated silver nanoparticles (OCAgNPs)
550 on the growth and reproduction of three species *Phytophthora* in vitro. *Arch. Phytopathol. Plant*
551 *Protect.* 2018;**51**(5-6):227-40
- 552 42. Clamme JP, Azoulay J, Mély Y. Monitoring of the formation and dissociation of
553 polyethylenimine/DNA complexes by two photon fluorescence correlation spectroscopy.
554 *Biophys. J.* 2003;**84**(3):1960-68
- 555 43. Wyrwal M, Koczurkiewicz P, Wojcik K, et al. Synthesis of strong polycations with improved
556 biological properties. *J. Biomed. Mater. Res. A* 2014;**102**(3):721-31
- 557 44. Dai T, Tanaka M, Huang Y-Y, Hamblin MR. Chitosan preparations for wounds and burns:
558 antimicrobial and wound-healing effects. *Expert Rev. Anti-Infect. Ther.* 2011;**9**(7):857-79
- 559 45. El-Sherbiny I, Abdel-Bary E, Harding D. Swelling characteristics and in vitro drug release study
560 with pH- and thermally sensitive hydrogels based on modified chitosan. *J. Appl. Polym. Sci.*
561 2006;**102**(2):977-85
- 562 46. Kim S-K, Rajapakse N. Enzymatic production and biological activities of chitosan
563 oligosaccharides (COS): A review. *Carbohydr. Polym.* 2005;**62**(4):357-68
- 564 47. Einbu A, Grasdalen H, Vårum KM. Kinetics of hydrolysis of chitin/chitosan oligomers in
565 concentrated hydrochloric acid. *Carbohydr. Res.* 2007;**342**(8):1055-62
- 566 48. Fai AEC, Stamford T, Stamford-Arnaud TM, et al. Physico-chemical characteristics and
567 functional properties of chitin and chitosan produced by *Mucor circinelloides* using yam bean as
568 substrate. *Molecules* 2011;**16**(8):7143-54
- 569 49. Dobilhofer E, Scheibel T. Engineering of recombinant spider silk proteins allows defined uptake
570 and release of substances. *J. Pharm. Sci.* 2015;**104**(3):988-94
- 571 50. Petzold J, Aigner TB, Touska F, Zimmermann K, Scheibel T, Engel FB. Surface Features of
572 Recombinant Spider Silk Protein eADF4 (κ 16)-Made Materials are Well-Suited for Cardiac
573 Tissue Engineering. *Adv. Funct. Mater.* 2017;**27**(36):1701427
- 574 51. Humenik M, Smith AM, Scheibel T. Recombinant spider silks—biopolymers with potential for
575 future applications. *Polymers* 2011;**3**(1):640-61
- 576 52. Müller-Herrmann S, Scheibel T. Enzymatic degradation of films, particles, and nonwoven
577 meshes made of a recombinant spider silk protein. *ACS Biomater. Sci. Eng.* 2015;**1**(4):247-59
- 578 53. Leal-Egaña A, Scheibel T. Silk-based materials for biomedical applications. *Biotechnol. Appl.*
579 *Biochem.* 2010;**55**(3):155-67
- 580 54. Zeplin PH, Maksimovikj NC, Jordan MC, et al. Spider silk coatings as a bioshield to reduce
581 periprosthetic fibrous capsule formation. *Adv. Funct. Mater.* 2014;**24**(18):2658-66
- 582 55. Huemmerich D, Helsen CW, Quedzuweit S, Oschmann J, Rudolph R, Scheibel T. Primary
583 structure elements of spider dragline silks and their contribution to protein solubility.
584 *Biochemistry* 2004;**43**(42):13604-12
- 585 56. Aigner TB, DeSimone E, Scheibel T. Biomedical applications of recombinant silk-based
586 materials. *Adv. Mater.* 2018;**30**(19):1704636
- 587 57. Shah C, Kumar M, Bajaj P. Acid-induced synthesis of polyvinyl alcohol-stabilized selenium
588 nanoparticles. *Nanotechnology* 2007;**18**(38):385607
- 589 58. Shah CP, Singh KK, Kumar M, Bajaj PN. Vinyl monomers-induced synthesis of polyvinyl
590 alcohol-stabilized selenium nanoparticles. *Mater. Res. Bull.* 2010;**45**(1):56-62
- 591 59. Tran PA, O'Brien-Simpson N, Palmer JA, et al. Selenium nanoparticles as anti-infective implant
592 coatings for trauma orthopedics against methicillin-resistant *Staphylococcus aureus* and
593 epidermidis: in vitro and in vivo assessment. *Int. J. Nanomedicine* 2019;**14**:4613
- 594 60. Hinterwirth H, Wiedmer SK, Moilanen M, et al. Comparative method evaluation for size and size-
595 distribution analysis of gold nanoparticles. *J. Sep. Sci.* 2013;**36**(17):2952-61
- 596 61. Iso E. 10993-5: Biological evaluation of medical devices. Tests for in vitro cytotoxicity 2009

- 597 62.Lam SJ, O'Brien-Simpson NM, Pantarat N, et al. Combating multidrug-resistant Gram-negative
598 bacteria with structurally nanoengineered antimicrobial peptide polymers. *Nat. Microbiol.*
599 2016;**1**:16162
- 600 63.Agostini E, Winter G, Engert J. Scale-up of water-based spider silk film casting using a film
601 applicator. *Int. J. Pharm.* 2017;**532**(1):13-20
- 602 64.Huemmerich D, Slotta U, Scheibel T. Processing and modification of films made from
603 recombinant spider silk proteins. *Appl. Phys. A* 2006;**82**(2):219-22
- 604 65.DiPaolo J, Takano K, Popescu N. Quantitation of chemically induced neoplastic transformation
605 of BALB/3T3 cloned cell lines. *Cancer Res.* 1972;**32**(12):2686-95
- 606 66.Terpiłowska S, Siwicka-Gieroba D, Siwicki AK. Cytotoxicity of iron (III), molybdenum (III), and
607 their mixtures in BALB/3T3 and HepG2 cells. *Journal of veterinary research* 2018;**62**(4):527-33
- 608 67.Uboldi C, Urbán P, Gilliland D, et al. Role of the crystalline form of titanium dioxide nanoparticles:
609 Rutile, and not anatase, induces toxic effects in Balb/3T3 mouse fibroblasts. *Toxicol. In Vitro*
610 2016;**31**:137-45
- 611 68.Pelin M, Fusco L, Martín C, et al. Graphene and graphene oxide induce ROS production in
612 human HaCaT skin keratinocytes: the role of xanthine oxidase and NADH dehydrogenase.
613 *Nanoscale* 2018;**10**(25):11820-30
- 614 69.Sighinolfi G, Artoni E, Gatti A, Corsi L. Carcinogenic potential of metal nanoparticles in BALB/3
615 T 3 cell transformation assay. *Environ. Toxicol.* 2016;**31**(5):509-19
- 616 70.Paolini A, Guarch CP, Ramos-López D, et al. Rhamnose-coated superparamagnetic iron-oxide
617 nanoparticles: an evaluation of their in vitro cytotoxicity, genotoxicity and carcinogenicity. *J.*
618 *Appl. Toxicol.* 2016;**36**(4):510-20
- 619 71.Senthil B, Devasena T, Prakash B, Rajasekar A. Non-cytotoxic effect of green synthesized silver
620 nanoparticles and its antibacterial activity. *J. Photochem. Photobiol. B: Biol.* 2017;**177**:1-7
- 621 72.Zeng H, Combs GF. Selenium as an anticancer nutrient: roles in cell proliferation and tumor cell
622 invasion. *J. Nutr. Biochem.* 2008;**19**(1):1-7
- 623 73.Fröhlich E. The role of surface charge in cellular uptake and cytotoxicity of medical
624 nanoparticles. *Int. J. Nanomedicine* 2012;**7**:5577
- 625 74.Ciani L, Ristori S, Bonechi C, Rossi C, Martini G. Effect of the preparation procedure on the
626 structural properties of oligonucleotide/cationic liposome complexes (lipoplexes) studied by
627 electron spin resonance and Zeta potential. *Biophys. Chem.* 2007;**131**(1-3):80-87
- 628 75.Patil S, Sandberg A, Heckert E, Self W, Seal S. Protein adsorption and cellular uptake of cerium
629 oxide nanoparticles as a function of zeta potential. *Biomaterials* 2007;**28**(31):4600-07
- 630 76.Chen C-C, Tsai T-H, Huang Z-R, Fang J-Y. Effects of lipophilic emulsifiers on the oral
631 administration of lovastatin from nanostructured lipid carriers: physicochemical characterization
632 and pharmacokinetics. *Eur. J. Pharm. Biopharm.* 2010;**74**(3):474-82
- 633 77.Bernfield M, Götte M, Park PW, et al. Functions of cell surface heparan sulfate proteoglycans.
634 *Annu. Rev. Biochem.* 1999;**68**(1):729-77
- 635 78.Honary S, Zahir F. Effect of zeta potential on the properties of nano-drug delivery systems-a
636 review (Part 1). *Trop. J. Pharm. Res.* 2013;**12**(2):255-64
- 637 79.Hamouda T, Baker Jr J. Antimicrobial mechanism of action of surfactant lipid preparations in
638 enteric Gram-negative bacilli. *J. Appl. Microbiol.* 2000;**89**(3):397-403
- 639 80.Mempin R, Tran H, Chen C, Gong H, Ho KK, Lu S. Release of extracellular ATP by bacteria
640 during growth. *BMC Microbiol.* 2013;**13**(1):301
- 641 81.Lok C-N, Ho C-M, Chen R, et al. Silver nanoparticles: partial oxidation and antibacterial
642 activities. *JBIC Journal of Biological Inorganic Chemistry* 2007;**12**(4):527-34
- 643 82.Applerot G, Lipovsky A, Dror R, et al. Enhanced antibacterial activity of nanocrystalline ZnO due
644 to increased ROS-mediated cell injury. *Adv. Funct. Mater.* 2009;**19**(6):842-52
- 645 83.Tong G, Du F, Wu W, Wu R, Liu F, Liang Y. Enhanced reactive oxygen species (ROS) yields
646 and antibacterial activity of spongy ZnO/ZnFe₂O₄ hybrid micro-hexahedra selectively
647 synthesized through a versatile glucose-engineered co-precipitation/annealing process. *J.*
648 *Mater. Chem. B* 2013;**1**(20):2647-57
- 649 84.Páez PL, Becerra MC, Albasa I. Impact of ciprofloxacin and chloramphenicol on the lipid bilayer
650 of *Staphylococcus aureus*: changes in membrane potential. *BioMed research international*
651 2013;**2013**:276524

- 652 85.Chudobova D, Cihalova K, Dostalova S, et al. Comparison of the effects of silver phosphate and
653 selenium nanoparticles on *Staphylococcus aureus* growth reveals potential for selenium
654 particles to prevent infection. *FEMS Microbiol. Lett.* 2014;**351**(2):195-201
- 655 86.Liu W, Golshan NH, Deng X, et al. Selenium nanoparticles incorporated into titania nanotubes
656 inhibit bacterial growth and macrophage proliferation. *Nanoscale* 2016;**8**(34):15783-94
- 657 87.Webster TJ, Tran PA. Antipathogenic surfaces having selenium nanoclusters: Google Patents,
658 2016.
- 659 88.Xing X, Ma W, Zhao X, et al. Interaction between Surface Charge-Modified Gold Nanoparticles
660 and Phospholipid Membranes. *Langmuir* 2018;**34**(42):12583-89
- 661 89.Banerjee M, Sharma S, Chattopadhyay A, Ghosh SS. Enhanced antibacterial activity of
662 bimetallic gold-silver core-shell nanoparticles at low silver concentration. *Nanoscale*
663 2011;**3**(12):5120-25
- 664 90.Fayaz AM, Balaji K, Girilal M, Yadav R, Kalaichelvan PT, Venketesan R. Biogenic synthesis of
665 silver nanoparticles and their synergistic effect with antibiotics: a study against gram-positive
666 and gram-negative bacteria. *Nanomed. Nanotechnol. Biol. Med.* 2010;**6**(1):103-09
- 667 91.Beladi M, Sepahi AA, Mehrabian S, Esmaili A, Sharifnia F. Antibacterial activities of selenium
668 and selenium nano-particles (products from *Lactobacillus acidophilus*) on nosocomial strains
669 resistant to antibiotics. *J. Pure Appl. Microbiol.* 2015;**9**(4):2843-52
- 670 92.Huang X, Chen X, Chen Q, Yu Q, Sun D, Liu J. Investigation of functional selenium
671 nanoparticles as potent antimicrobial agents against superbugs. *Acta Biomater.* 2016;**30**:397-
672 407
- 673 93.Wiegand I, Hilpert K, Hancock RE. Agar and broth dilution methods to determine the minimal
674 inhibitory concentration (MIC) of antimicrobial substances. *Nat. Protoc.* 2008;**3**(2):163
- 675 94.EUCAST. Determination of minimum inhibitory concentrations (MICs) of antibacterial agents by
676 broth dilution. *Clin. Microbiol. Infect.* 2003;**9**(8):ix-xv
- 677 95.CLSI. Methods for dilution antimicrobial susceptibility tests for
678 bacteria that grow aerobically; Approved standard: M07-A10. Wayne, PA: Clinical and Laboratory
679 Standards Institute 2015
- 680 96.Borkner CB, Wohlrab S, Möller E, Lang G, Scheibel T. Surface modification of polymeric
681 biomaterials using recombinant spider silk proteins. *ACS Biomater. Sci. Eng.* 2016;**3**(5):767-75
- 682 97.Eby DM, Luckarift HR, Johnson GR. Hybrid antimicrobial enzyme and silver nanoparticle
683 coatings for medical instruments. *ACS Appl. Mater. Interfaces* 2009;**1**(7):1553-60
- 684 98.Skalickova S, Milosavljevic V, Cihalova K, Horiky P, Richtera L, Adam V. Selenium nanoparticles
685 as a nutritional supplement. *Nutrition* 2017;**33**:83-90
- 686

687

688

689 **Table 1** Percentages of secondary structure elements of eADF4(κ 16) and eADF4(κ 16) coated Se
690 NPs based on the Fourier self-deconvoluted absorbance spectrum of the amide I band

Samples	Percentage of secondary structure elements (%)				
	Side chains	β -sheets	Random coils	α -helices	Turns
eADF4(κ 16) particles	5 \pm 1	41 \pm 1	24 \pm 1	7 \pm 1	22 \pm 1
eADF4(κ 16) coated Se NPs	2 \pm 1	39 \pm 2	25 \pm 1	9 \pm 1	26 \pm 1

691

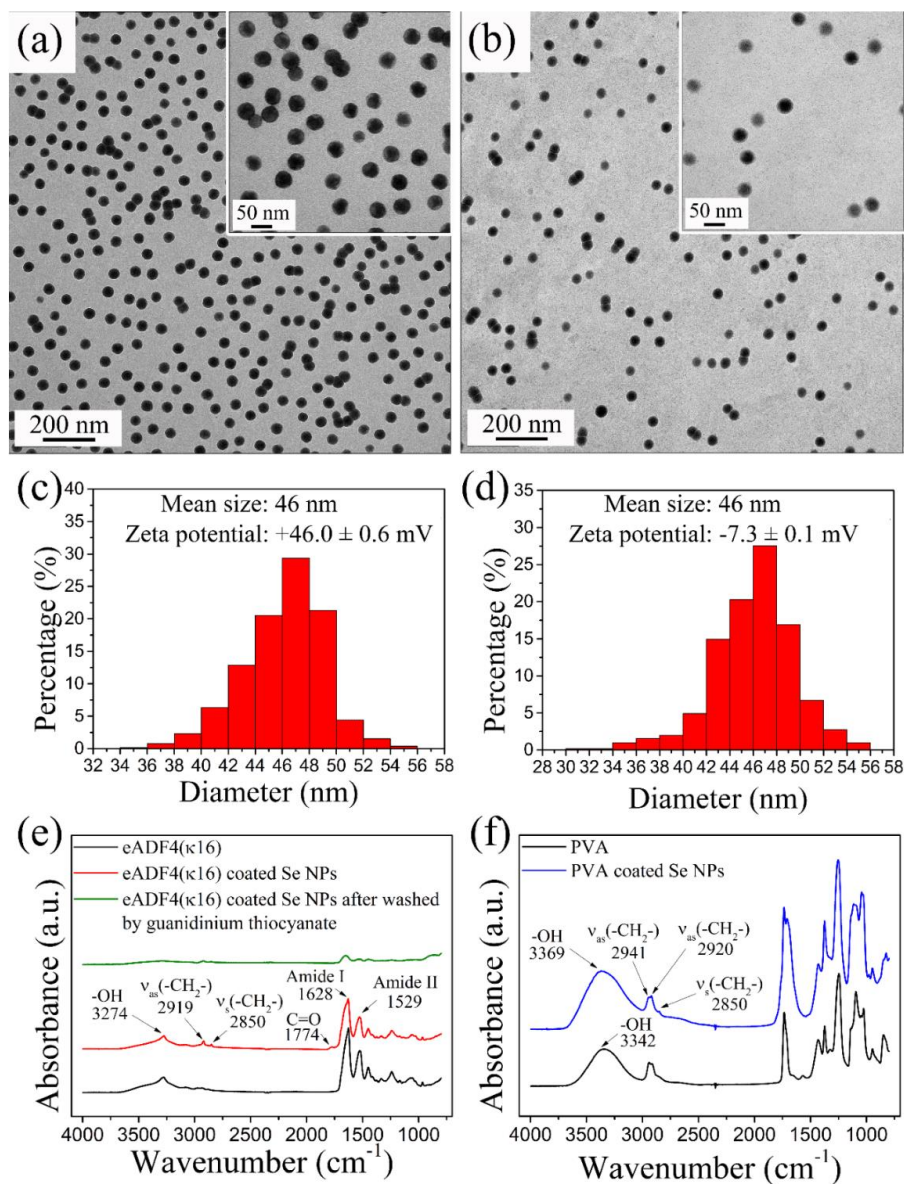
692

693

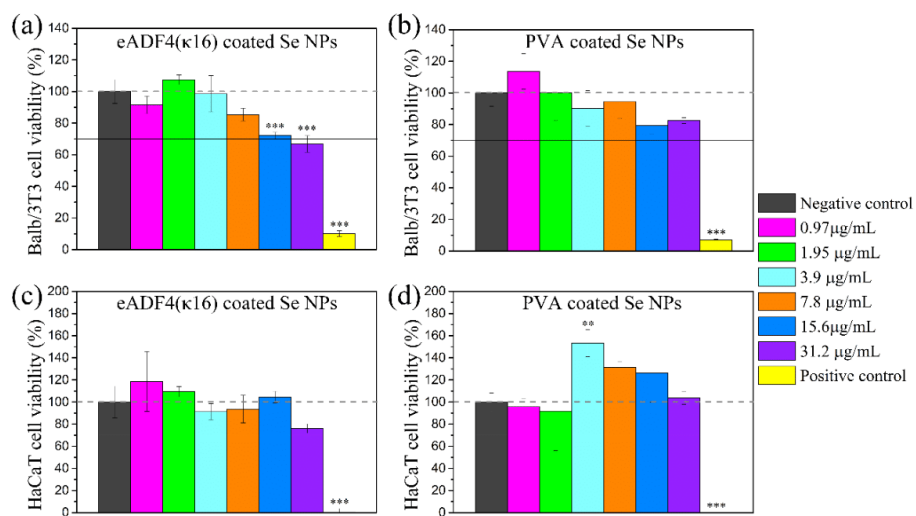
694

695

696



697
 698 **Figure 1** TEM images and the corresponding size distributions of Se NPs coated with (a, c)
 699 0.1mg/mL eADF4(κ 16), and (b, d) 2mg/mL PVA. Inset images inside (a, b) are high resolution
 700 images. FT-IR spectra of Se NPs coated with (e) 0.1mg/mL eADF4(κ 16), and (f) 2mg/mL PVA and
 701 comparison with control spectra of eADF4(κ 16) and PVA.



702

703

Figure 2 Effects of Se NPs on the viability of mammalian cells in culture. Balb/3T3 mouse

704

embryo fibroblasts incubated with (a) eADF4(κ16) coated Se NPs, and (b) PVA coated Se NPs;

705

HaCaT human skin keratinocytes incubated with (c) eADF4(κ16) coated Se NPs, and (d) PVA

706

coated Se NPs for 24 h, at 37 °C. One-Way ANOVA with Tukey's Post Hoc Test was used to

707

compare means of experimental groups to that of the negative control group, * p-value < 0.05, **

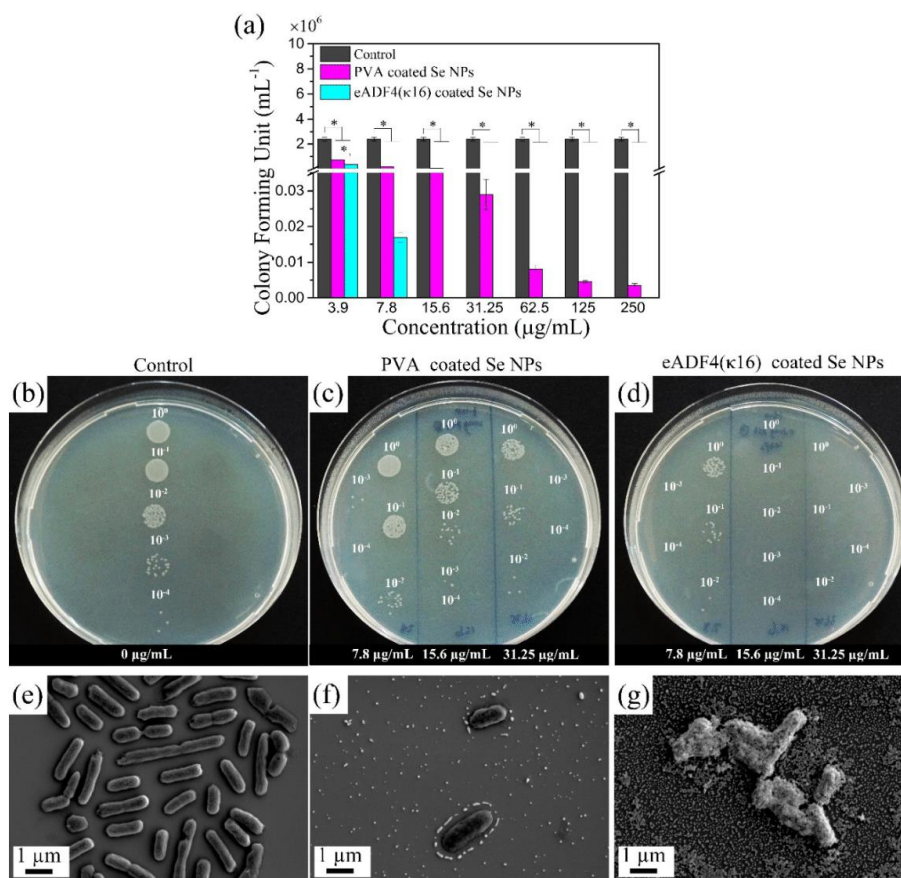
708

p-value < 0.01, *** p-value < 0.001. The dashed horizontal line represents 100% viability, and the

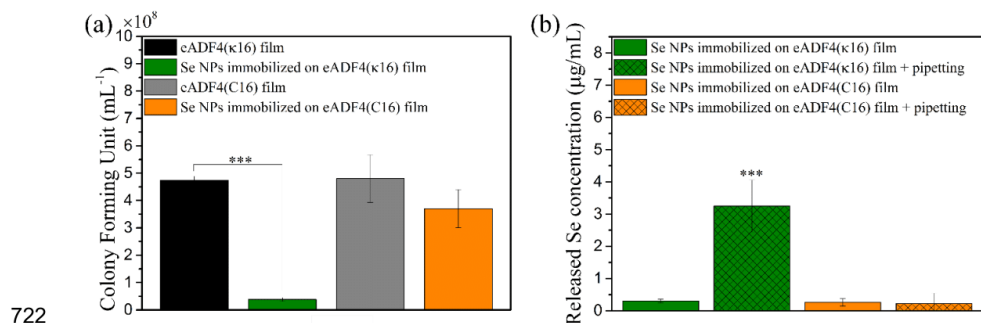
709

solid line represents 70% viability.

710



711
 712 **Figure 3** Colony forming units (CFU) assay using *E. coli* after treatment with eADF4(κ 16) and
 713 PVA coated Se NPs with varying concentrations from 3.9 $\mu\text{g/mL}$ to 250 $\mu\text{g/mL}$. One-Way ANOVA
 714 with Tukey's Post Hoc Test was used to compare means of experimental groups at each
 715 concentration, * p-value < 0.05. (b-d) Agar plate images of CFU test of *E. coli*, (b) control without
 716 particles, (c) PVA coated Se NPs, (d) eADF4(κ 16) coated Se NPs. 10^0 is the original (bacteria +
 717 Se NPs) solution, 10^{-1} , 10^{-2} , 10^{-3} and 10^{-4} mean diluting the original solution 10, 100, 1000 and
 718 10000 times, respectively, to make the colonies more countable. SEM images of 2.5×10^7
 719 cells/mL *E. coli* before and after treatment with 75 $\mu\text{g/mL}$ Se NPs: (e) plain *E. coli*, (f) *E. coli*
 720 incubated with PVA coated Se NPs, and (g) *E. coli* incubated with eADF4(κ 16) coated Se NPs.
 721



722

723 **Figure 4** (a) CFU test results of *E. coli* after treatment with 46 nm eADF4(κ 16) coated Se NPs
724 immobilized on eADF4(κ 16) or eADF4(C16) films; (b) The Se concentrations released from films
725 after 4 h static immersion in MHB or 4 h static immersion in MHB with 5 times pipetting on the
726 surface of the films. One-Way ANOVA with Tukey's Post Hoc Test was used to compare means
727 of experimental groups, *** p-value < 0.001.

728

729

Supporting Information

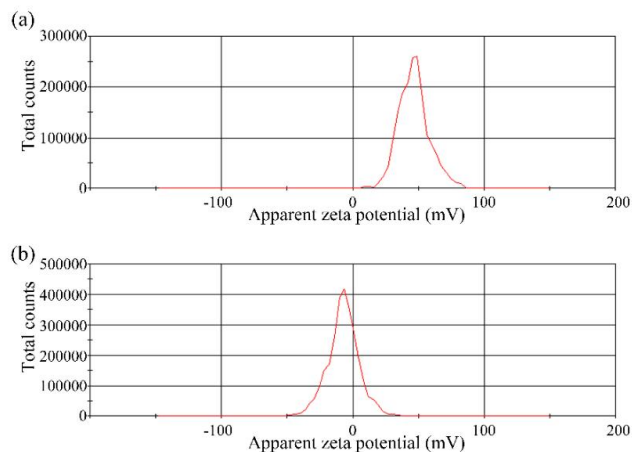
1
2
3
4
5
6
7
8
9
10
11
12
13
14
15
16
17
18
19
20
21
22
23
24
25
26
27
28
29

Enhanced antibacterial activity of Se nanoparticles upon coating with recombinant spider silk protein eADF4(κ16)

Tao Huang^{1,2}
Sushma Kumari²
Heike Herold²
Hendrik Bargel²
Tamara B. Aigner²
Daniel E. Heath¹
Neil M. O'Brien-Simpson³
Andrea J. O'Connor¹
Thomas Scheibel^{2,4}

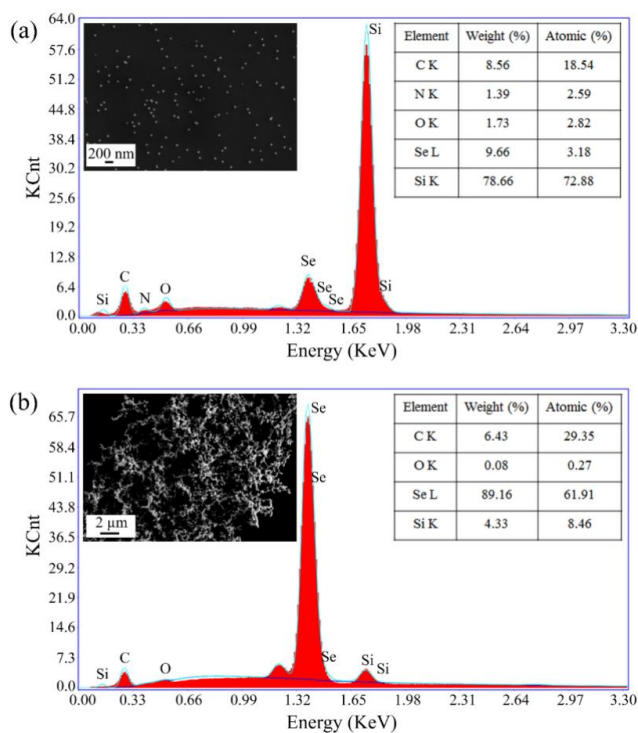
¹Department of Biomedical Engineering, Melbourne School of Engineering, University of Melbourne, Parkville, VIC 3010, Australia; ²Department for Biomaterials, Faculty of Engineering Science, University of Bayreuth, Prof. Rüdiger Bormann Str. 1, 95447 Bayreuth, Germany; ³Melbourne Dental School and The Bio21 Institute of Molecular Science and Biotechnology, The University of Melbourne, Parkville, VIC 3010, Australia; ⁴Bavarian Polymer Institute (BPI), Bayreuth Center for Material Science and Engineering (BayMAT), Bayreuth Center for Colloids and Interfaces (BZKG), Bayreuth Center for Molecular Biosciences (BZMB), University of Bayreuth, 95447 Bayreuth, Germany

Correspondence: Andrea J. O'Connor
Tel +61 3 8344 8962
Email a.oconnor@unimelb.edu.au
Thomas Scheibel
Tel +49 (0)921 / 55-6701
Email thomas.scheibel@bm.uni-bayreuth.de



30

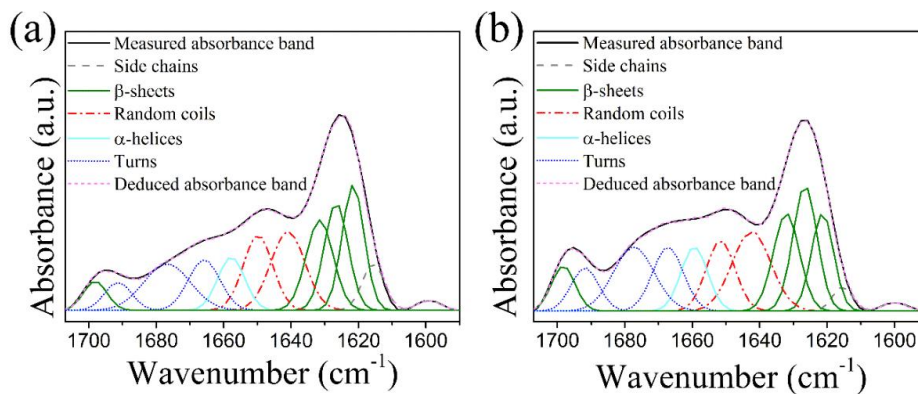
31 **Figure S1.** Zeta potential distribution of (a) 46 nm eADF4(κ 16) stabilized Se NPs and (b) 46 nm PVA
 32 stabilized Se NPs.



33

34 **Figure S2.** EDS of Se NPs: (a) eADF4(κ 16) stabilized Se NPs, (b) eADF4(κ 16) stabilized Se NPs after
 35 washing with guanidinium thiocyanate. High intensity for Se NPs in (b) shows aggregation of particles
 36 because of protein removal.

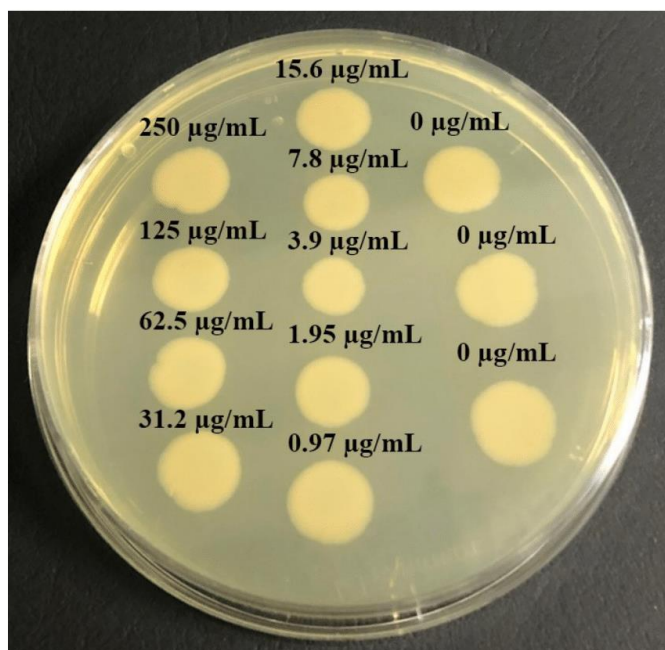
37



38

39 **Figure S3.** Fourier self-deconvoluted absorbance spectra of the amide I band of (a) eADF4(κ 16) particles
 40 and (b) 46 nm eADF4(κ 16) coated Se NPs.

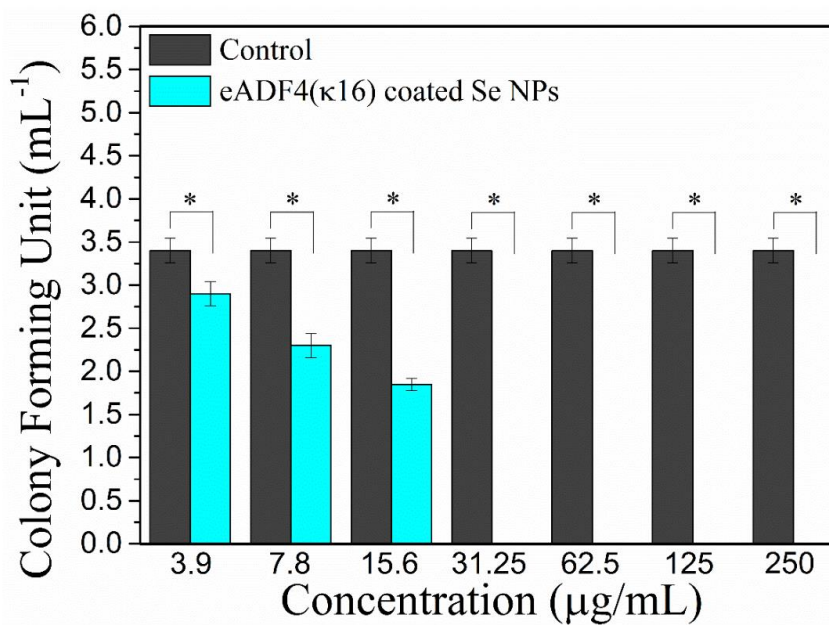
41



42

43 **Figure S4.** Colony forming units (CFU) assay using *E. coli* after treatment with eADF4(κ 16) particles. No
 44 antibacterial activity was observed at concentrations from 0.97 μ g/mL to 250 μ g/mL.

45



46

47 **Figure S5.** Colony forming units (CFU) assay using *S. aureus* (ATCC 29213) after treatment with
48 eADF4(κ16) with varying concentrations from 3.9 μg/mL to 250 μg/mL. Student's t-test was used to
49 compare means of experimental groups at each concentration, * p-value < 0.05.

50

51

**Part 4. Surface Features of Recombinant Spider Silk Protein
eADF4(κ 16)-Made Materials are Well-Suited for Cardiac Tissue
Engineering**

Petzold, J.; **Aigner, T. B.**; Touska, F.; Zimmermann, K.; Scheibel, T.; Engel, F. B.

Published in *Advanced Functional Materials*, 27, 1701427

(2017)

Reprinted with kind permission from WILEY-VHC Verlag GmbH & Co

FULL PAPER

Tissue Engineering

ADVANCED
FUNCTIONAL
MATERIALS
www.afm-journal.de

Surface Features of Recombinant Spider Silk Protein eADF4(κ 16)-Made Materials are Well-Suited for Cardiac Tissue Engineering

Jana Petzold, Tamara B. Aigner, Filip Touska, Katharina Zimmermann, Thomas Scheibel, and Felix B. Engel*

Cardiovascular diseases causing high morbidity and mortality represent a major socioeconomic burden. The primary cause of impaired heart function is often the loss of cardiomyocytes. Thus, novel therapies aim at restoring the lost myocardial tissue. One promising approach is cardiac tissue engineering. Previously, it is shown that *Antheraea mylitta* silk protein fibroin is a suitable material for cardiac tissue engineering, however, its quality is difficult to control. To overcome this limitation, the interaction of primary rat heart cells with engineered *Araneus diadematus* fibroin 4 (κ 16) (eADF4(κ 16)) is investigated here, which is engineered based on the sequence of ADF4 by replacing the glutamic acid residue in the repetitive unit of its core domain with lysine. The data demonstrate that cardiomyocytes, fibroblasts, endothelial cells, and smooth muscle cells attach well to eADF4(κ 16) films on glass coverslips which provide an engineered surface with a polycationic character. Moreover, eADF4(κ 16) films have, in contrast to fibronectin films, no hypertrophic effect but allow the induction of cardiomyocyte hypertrophy. Finally, cardiomyocytes grown on eADF4(κ 16) films respond to pro-proliferative factors and exhibit proper cell-to-cell communication and electric coupling. Collectively, these data demonstrate that designed recombinant eADF4(κ 16)-based materials are promising materials for cardiac tissue engineering.

1. Introduction

The adult mammal is unable to regenerate heart tissue after an injury, resulting in the loss of cardiomyocytes, the contractile muscle cells of the heart.^[1] Due to the major socioeconomic burden of cardiovascular disease, which has been predicted to further increase,^[2] there is a great interest in the development of approaches to reverse the loss of cardiomyocytes. Promising approaches are the activation of endogenous stem cells, induction of cardiomyocyte proliferation, stem cell therapy, and cardiac tissue engineering.^[3]

In recent years, cardiac tissue engineering has been established as a prospective option for the treatment of cardiac disease. In a landmark study, Zimmermann et al. showed that cardiomyocytes embedded in a nonstructured composite hydrogel made of type I collagen and Matrigel significantly improved heart function after implantation on myocardial infarcts in immune-suppressed rats.^[4] Subsequently,

J. Petzold
Department of Nephropathology
Institute of Pathology
Friedrich-Alexander-Universität Erlangen–Nürnberg (FAU)
Schwabachanlage 12, 91054 Erlangen, Germany

T. B. Aigner
Lehrstuhl Biomaterialien
Universität Bayreuth
Universitätsstraße 30, Bayreuth D-95447, Germany

F. Touska, Prof. K. Zimmermann
Klinik für Anästhesiologie am Universitätsklinikum Erlangen
Friedrich-Alexander-Universität Erlangen-Nürnberg (FAU)
Krankenhausstrasse 12, 91054 Erlangen, Germany

Prof. T. Scheibel
Lehrstuhl Biomaterialien
Bayreuther Zentrum für Kolloide und Grenzflächen (BZKG)
Bayreuther Zentrum für Bio-Makromoleküle (bio-mac)
Bayreuther Zentrum für Molekulare Biowissenschaften (BZMB)
Bayreuther Materialzentrum (BayMAT)
Bayerisches Polymerinstitut (BPI)
Universität Bayreuth
Universitätsstraße 30, Bayreuth D-95447, Germany

DOI: 10.1002/adfm.201701427

Prof. F. B. Engel
Department of Nephropathology
Institute of Pathology
Muscle Research Center Erlangen (MURCE)
Friedrich-Alexander-Universität Erlangen–Nürnberg (FAU)
Schwabachanlage 12, 91054 Erlangen, Germany
E-mail: felix.engel@uk-erlangen.de

 The ORCID identification number(s) for the author(s) of this article can be found under <https://doi.org/10.1002/adfm.201701427>.

it has been confirmed that tissue-engineered cardiac patches can improve recovery from myocardial injury in small and large animal models.^[5] Moreover, first clinical trials applying tissue engineering to heart disease patients have been performed. In the most recent trial, Menasché et al. delivered human embryonic stem cell-derived cardiac progenitor cells in a fibrin patch into heart failure patients, demonstrating the overall feasibility and safety of cardiac tissue engineering to treat heart failure.^[6] Nevertheless, the field is still in its infancy and it remains to be shown that the application of tissue engineering can indeed improve heart function in heart failure patients.

Currently, cardiac tissue engineering faces many problems, such as: (i) the choice of cell type or combination of cell types to generate a cardiac patch; (ii) providing hierarchically structured scaffolds to enable vascularization of cardiac patches to enlarge graft sizes; (iii) connecting the graft to the host vascularization; (iv) ensuring electrical coupling within the graft; (v) electromechanically integrating the graft to avoid arrhythmia; and (vi) the correct choice of biocompatible scaffold material with proper hierarchical structures and mechanical characteristics.^[3b,7]

Previously, it has been demonstrated that silk materials are excellently suited for tissue engineering applications.^[8] Silk proteins are natural products which have several advantages compared to other materials that are currently used in cardiac tissue engineering. They can be fabricated into diverse morphologies. Moreover, silk materials have unique mechanical strength, biocompatibility, and silks exhibit noncytotoxic properties as well as low level of inflammatory response.^[8,9] In addition, we have demonstrated that the natural *Antheraea mylitta* silk fibroin is a suitable material for cardiac tissue engineering.^[10] It enables efficient attachment of cardiomyocytes without affecting their response to extracellular stimuli, promotes sarcomere alignment, synchronous contraction, and electrical coupling.^[10] However, naturally obtained silk fibroins have also significant limitations. For example, *Antheraea mylitta* cannot efficiently be bred in captivity, and thus its silk fibroin cannot be mass-produced and the latter's quality depends on a variety of variables that cannot be controlled (e.g., feedstock quality and uptake). The resulting batch-to-batch variation of this natural polymer and the lack of suitable quantitative and qualitative in vivo analyses are some of the issues currently restricting its medical application.^[8b]

In order to overcome these limitations, we utilized here genetically engineered spider silk proteins, which make it possible to provide new biopolymers with a complexity and functionality not found in nature. The cell membranes of animal cells contain negatively charged proteoglycans, glycolipids, and glycoproteins. Therefore, mammalian cells attach preferentially to polycationic surfaces.^[11] Consequently, the aim of this study was to determine if engineered recombinant spider silk protein engineered *Araneus diadematus* fibroin 4 (κ 16) (eADF4(κ 16)) processed into films with a polycationic surface is a suitable adhesive for cardiac cells.

2. Results and Discussion

2.1. Surface Properties of Recombinant Spider Silk Protein eADF4(κ 16) Films

eADF4(C16) is engineered based on the sequence of ADF4, a component of the major ampullate silk of the European garden

spider, also called the dragline or "lifeline." Previously, we have shown that polyanionic eADF4(C16) films are not suitable substrates for cell adhesion.^[12] As the extracellular side of most mammalian cells is negatively charged and thus cells preferentially attach to polycationic surfaces,^[11] we engineered a so-called κ -module by replacing the naturally occurring glutamic acid residue in the repetitive units of the ADF4 core domain with lysine: GSSAAAAAASGPGGYGPKNQGPSGPGGYG-PGGP (Figure 1a).^[13] The κ -module was adjusted to *Escherichia coli* (*E. coli*) codon-usage and then repeated 16 times to mimic the repetitive core of ADF4. The product is the engineered positively charged spider silk protein eADF4(κ 16) (Figure 1a).

In order to determine the interaction of cardiac cells with eADF4(κ 16), glass coverslips were dip coated with eADF4(κ 16) out of formic acid (Figure 1b). Successful coating of glass coverslips was confirmed by Hoechst 33342 staining, resulting in apparent background illumination (Figure S1a, Supporting Information). Previously, eADF4(C16) film coatings showed already the formation of thermodynamically stable β -sheet rich structure during solvent evaporation.^[14] To assess the secondary structure content of eADF4(κ 16) coated glass coverslips, ATR-FTIR measurements were performed (Figure 1c). Fourier self-deconvolution (FSD) was performed analyzing the amide I band according to Hu et al.^[15] As expected, the here investigated eADF4(κ 16) films showed a high β -sheet content ($34 \pm 1\%$; α -helix: $9 \pm 0.4\%$; turns: $26 \pm 2\%$; random coils: $15 \pm 1\%$; side chains: $16 \pm 2\%$), explaining its insolubility in water even without methanol post-treatment (Figure 1c).

To determine if the high β -sheet content results in a hydrophobic film-air surface as previously described for cast eADF4(C16) films on glass,^[14b] we characterized the surface hydrophilicity of all tested protein surfaces by using water contact angle measurements (Figure 1d). As control, in addition to eADF4(C16)-coated glass coverslips, we utilized noncoated as well as glass coverslips coated with fibronectin (dissolved in water or phosphate-buffered saline (PBS)) and gelatin that are often used as adhesive for cardiomyocytes.^[10,16] Coating with eADF4(κ 16) as well as gelatin reduced the contact angle of glass ($38^\circ \pm 9^\circ$ and $29^\circ \pm 7^\circ$, respectively, vs $56^\circ \pm 5^\circ$, Figure 1d). The contact angle on fibronectin-coated surfaces was in comparison quite hydrophobic (H_2O : $111^\circ \pm 2^\circ$, PBS: $80^\circ \pm 7^\circ$, Figure 1d). These data demonstrate that eADF4(κ 16) films are hydrophilic. Thus, in contrast to cast eADF4(C16) films on glass,^[14b] eADF4(κ 16) films are not covered by a layer of β -sheets (Figure 1b).

While we have previously shown that cast eADF4(C16) films on glass are hydrophobic,^[14b] our data revealed that the eADF4(C16) film-air surface on silanized glass was more hydrophilic ($54^\circ \pm 14^\circ$, Figure 1d). Note that dip coating required the silanization of the glass coverslips, making them hydrophobic, in order to immobilize eADF4(C16) films. In contrast, eADF4(κ 16) films directly adhered to glass surfaces upon dip coating.

Importantly, it is unknown at what water contact angles cardiomyocytes attach well. For fibroblasts, maximal cell adherence occurs at water contact angles between 55° and 85° .^[17] However, it is known that the attachment of cells to surfaces is also strongly dependent on the presence of surface charges and functional groups.^[11,18] Arginine-Glycine-Aspartic acid (Arg-Gly-Asp or RGD) domains, which are present in fibronectin, improve, for example, cardiomyocyte attachment.^[10]

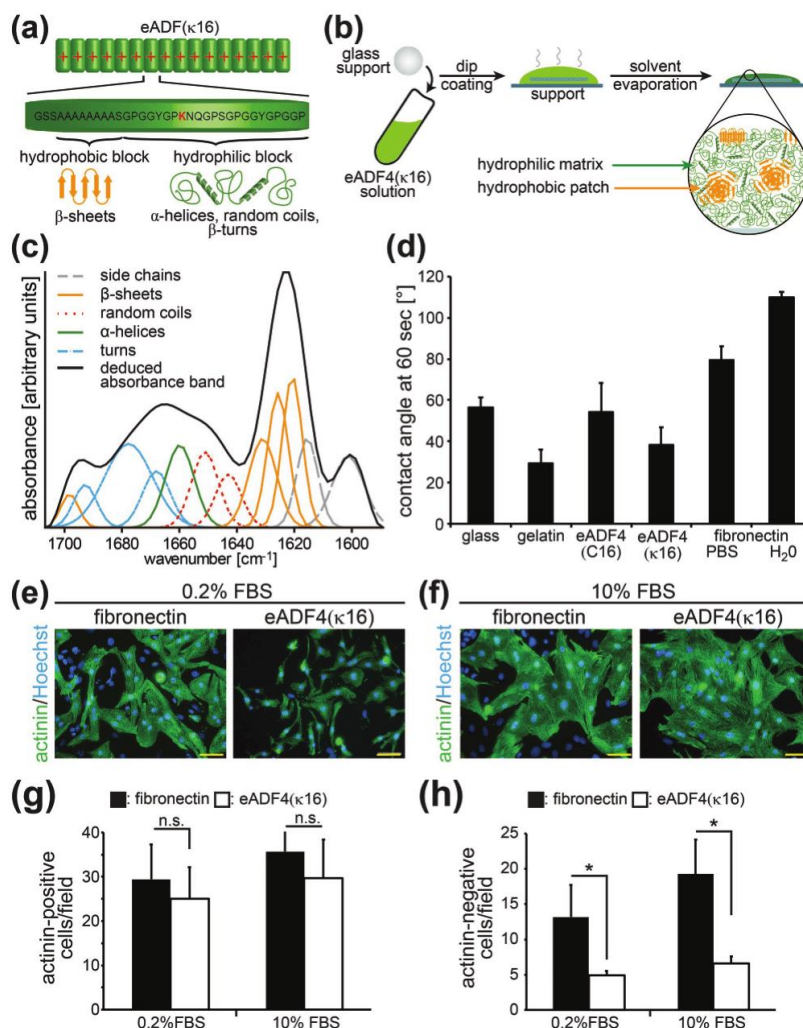


Figure 1. Cardiomyocytes efficiently attach to eADF4(κ16) films. a) Design of eADF4(κ16). b) Processing of eADF4(κ16) into films. c) Fourier self-deconvoluted absorbance spectrum of the amide I band of an eADF4(κ16) film on glass. Black line: deduced absorbance band, others: individual contributions to the amide I band assigned according to values published in literature ($n = 5$). d) Water contact angle measurements ($n = 8-10$). e, f) Cardiac cells isolated from ventricles of 3 d old rats were cultured after attachment overnight for 48 h on the indicated matrices in the presence of 0.2% (e) or 10% FBS (f). Subsequently, cardiomyocytes were stained with sarcomeric- α -actinin (actinin, green) and Hoechst 33342 (nuclei, blue). g) Quantitative analysis of sarcomeric- α -actinin-positive cardiomyocytes. h) Quantitative analysis of sarcomeric- α -actinin-negative nonmyocytes. Data are mean \pm SD. $n = 4$ independent experiments. *: $p < 0.05$. n.s.: statistically not significant. Scale bars: 50 μ m.

2.2. Cardiomyocytes, Nonmyocytes, and Human Umbilical Vein Endothelial Cells (HUVECs) Attach to eADF4(κ16) Films

To determine if polycationic eADF4(κ16) films are a suitable adhesive for cardiac cells, cells from postnatal day 3 (P3) rat hearts were isolated and cultured on eADF4(κ16) films after attachment overnight for 48 h. In parallel to attachment assays, we performed live/dead assays to verify that the recombinant spider silk protein eADF4(κ16) exhibits no cytotoxic effect on

cardiac cells. Previously, it had already been demonstrated that engineered recombinant spider silk proteins based on ADF4 are nontoxic.^[19] As control, adhesive fibronectin was chosen since it is a component of the cardiac extracellular matrix and a well-established material for neonatal cardiomyocyte attachment.^[10,20] Moreover, we have previously demonstrated that it exhibits similar properties as *Antheraea mylitta* silk fibroin.^[10] The cells were cultured in presence of 0.2% as well as 10% (v/v) fetal bovine serum (FBS) as 10% FBS is commonly used to seed

cardiomyocytes for improved attachment.^[21] However, 10% FBS is known to induce hypertrophy and/or cell cycle activity in neonatal cardiomyocytes as well as cardiomyocytes derived from human induced pluripotent stem cells.^[22] Moreover, this hypertrophy might result in pathological hypertrophy.^[23] Thus, it is pertinent to examine the effect of materials on cardiomyocytes also in culture media without or in low concentrations of serum.

Cells were stained with calcein-acetoxymethyl ester (calcein-AM) (0.25 $\mu\text{L mL}^{-1}$)/ethidium homodimer-1 (EthD-1, 1 $\mu\text{L mL}^{-1}$)/PBS (live/dead assay) (Figure S2, Supporting Information). Our data demonstrate that cardiac cells attach to eADF4(κ 16) films (Figure S2a,b, Supporting Information). Moreover, there was no statistically significant difference in the number of attached calcein-AM-positive (live) or EthD-positive (dead) cells per field between eADF4(κ 16) and fibronectin films ($n = 3$ independent experiments, $p > 0.2$; Figure S2c,d, Supporting Information). These data suggest that eADF4(κ 16)-based materials are suitable for cardiac tissue engineering. In contrast, cardiomyocytes attached as expected poorly to polyanionic eADF4(C16) as previously shown for fibroblasts (Figure S2e,f, Supporting Information).^[12]

It is important to note that the heart contains a large variety of cell types including fibroblasts, endothelial cells, smooth muscle cells, and cardiomyocytes.^[24] Thus, we assessed next whether cardiomyocytes, the primary functional cell type of the heart, attach to eADF4(κ 16) films. After cell isolation and cardiomyocyte enrichment, cells were allowed to attach overnight. After 48 h of culture in the presence of 0.2% or 10% FBS, cell cultures were stained for the cardiomyocyte-specific protein sarcomeric- α -actinin (Figure 1e,f). Quantitative analyses revealed that cardiomyocytes equally efficiently attached to eADF4(κ 16) films as to fibronectin films (Figure 1g).

Previously, it has been shown that cardiac patches that contain both cardiomyocytes and nonmyocytes exhibit improved tissue structure and function.^[25] In addition, vascularization of cardiac patches is required to ensure cardiomyocyte survival.^[7a] Consequently, it is important to assess if also nonmyocytes can attach to eADF4(κ 16)-based materials. A closer analysis of the cardiomyocyte attachment data revealed that the number of nonmyocytes (sarcomeric- α -actinin-negative) on eADF4(κ 16) films was significantly lower than on fibronectin films (0.2% FBS: 4 ± 1 vs 10 ± 5 nonmyocytes; 10% FBS: 7 ± 1 vs 18 ± 5 nonmyocytes; data are mean \pm standard deviation (SD), $n = 4$ independent experiments, $p < 0.05$; Figure 1h). To determine if the most important cell types for cardiac tissue engineering (cardiomyocytes, endothelial cells, fibroblasts, and smooth muscle cells) can attach to eADF4(κ 16) films, cardiac cells were isolated without cardiomyocyte enrichment. Cells were allowed to attach for 3 h as well as 48 h. Subsequently, cells were stained with cell type-specific markers to identify cardiomyocytes (sarcomeric- α -actinin or troponin I), fibroblasts (collagen 1), smooth muscle cells (smooth muscle actin), and endothelial cells (vascular endothelial- (VE)-cadherin). Our data demonstrate that fibroblasts (yellow arrowheads, Figure 2a), smooth muscle cells (blue arrowheads, Figure 2b), as well as endothelial cells (orange arrowheads, Figure 2c) can attach to eADF4(κ 16) films. However, the data suggest that nonmyocytes attached less efficiently to eADF4(κ 16) than to fibronectin films.

As the number of endothelial cells in the cultures was low, we tested whether eADF4(κ 16) films are suitable for the attachment of HUVECs, which are often used to investigate the proangiogenic effect of materials or to engineer vessels.^[26] HUVECs were cultured on eADF4(κ 16) as well as fibronectin films and stained for VE-cadherin. HUVECs attached to and grew on both matrices to 100% confluency (Figure 2d). VE-cadherin staining on both matrices indicated a narrow adherens junction architecture. Collectively, our data demonstrate that eADF4(κ 16) films allow not only the attachment of cardiomyocytes but also of other cell types present in the heart. The fact that nonmyocytes attach less to eADF4(κ 16) films might be of advantage considering that they proliferate in contrast to cardiomyocytes. Thus, the use of eADF4(κ 16) might be beneficial in generating cardiac tissue patches with a higher concentration of cardiomyocytes.

2.3. eADF4(κ 16) Films Have No Hypertrophic Effect but Allow Cardiomyocytes to Respond to Hypertrophic Stimuli

Hearts, and especially cardiomyocytes, respond to a variety of extracellular stimuli that modulate heart function. For example, cardiomyocytes undergo physiological hypertrophy (increase in cell size) induced by hormones and growth factors that are released upon increased workload in athletes or during pregnancy.^[23] To determine if eADF4(κ 16) affects cardiomyocyte hypertrophy, we assessed cell size by determining the area of individual cardiomyocytes. While fibronectin is an obvious control for cardiomyocyte attachment, it is not the right negative control to determine whether a material exhibits a prohypertrophic effect as it has been demonstrated that fibronectin induces hypertrophy on neonatal cardiomyocytes and contributes to pathophysiological hypertrophy in vivo.^[27] Therefore, we utilized gelatin, a commonly used and cheap moderate adhesive for cardiomyocytes,^[10,16] as it has so far not been described to exhibit a prohypertrophic effect. In agreement with these data, we observed that the size of neonatal cardiomyocytes on fibronectin films was increased 1.34-fold compared to that of cardiomyocytes on gelatin films at low serum conditions (0.2% FBS, $n = 3$ independent experiments, $p < 0.05$, Figure 3a,d). Cardiomyocytes cultured on eADF4(κ 16) films were similar in size to cardiomyocytes cultured on films made of inert gelatin (1.05-fold, $n = 3$ independent experiments, $p > 0.05$, Figure 3a,d). These data suggest that eADF4(κ 16) films exhibit no pharmacological effect.

In order to assess whether neonatal cardiomyocytes on eADF4(κ 16) films respond properly to hypertrophic stimuli, we subjected cardiomyocytes to a weak (50×10^{-6} M phenylephrine, PE) as well as a strong hypertrophic stimulus (10% FBS) (Figure 3b,c). Quantitative analyses of cell size showed that neonatal cardiomyocytes on all matrices stimulated with 10% FBS increased significantly in cell size by around twofold ($n = 3$ independent experiments, $p < 0.05$, Figure 3d). While stimulation with PE also showed a trend toward increased cell size, the change was not statistically significant. It should be noted that cell size was measured based on cross-sectional area which neglects that cells can also grow in size by increasing their thickness. Moreover, cross-sectional area is greatly affected

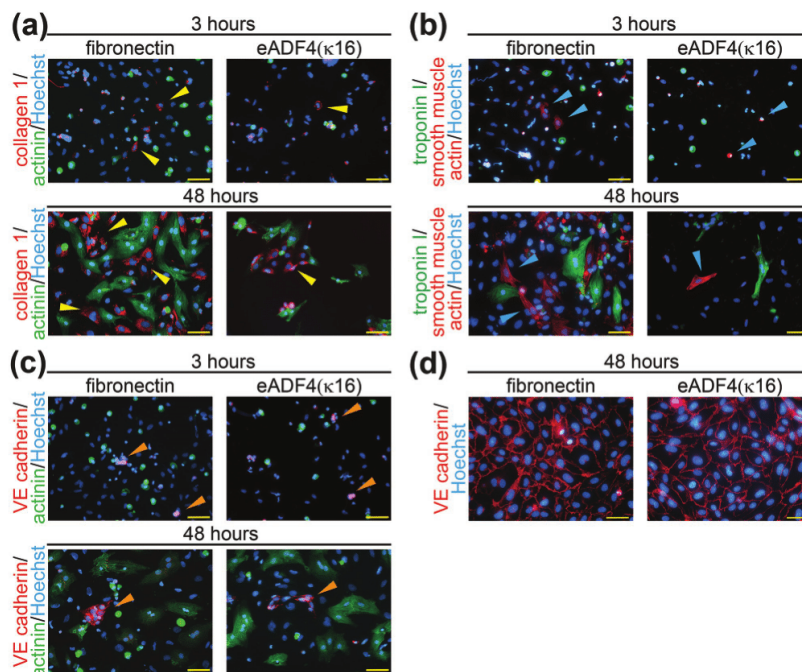


Figure 2. Nonmyocyte attachment on eADF4(κ 16) films. Isolated neonatal rat cardiac cells (no enrichment) were seeded for 3 or 48 h on different matrices as indicated. a–c) Cells were stained with (a) anti-collagen 1 antibodies (fibroblasts, red) and anti-sarcomeric- α -actinin (cardiomyocytes, green), (b) anti-smooth muscle actin (marks smooth muscle cells and a subpopulation of cardiomyocytes, red) and anti-troponin I (cardiomyocytes, green), and (c) anti-VE-cadherin antibodies (endothelial cells, red) and anti-sarcomeric- α -actinin (cardiomyocytes, green). Nuclei were visualized with Hoechst 33342 (blue). Yellow arrowheads: examples of fibroblasts. Blue arrowheads: examples of smooth muscle cells. Orange arrowheads: examples of endothelial cells. d) HUVEC cell culture on matrices as indicated stained for VE-cadherin (red) and nuclei (Hoechst 33342, blue). Scale bars: 50 μ m.

by cell density. Therefore, we stained cardiomyocytes in parallel for atrial natriuretic factor (ANF, also atrial natriuretic peptide, ANP), which is expressed around the nucleus in hypertrophic cardiomyocytes.^[28]

Quantitative analysis of ANF-positive cardiomyocytes indicates also that only fibronectin films exert a prohypertrophic effect ($n = 3$ independent experiments, $p < 0.05$, Figure 3e). Moreover, ANF expression analyses revealed that cardiomyocytes on all matrices responded to 10% FBS as well as PE. Note that cardiomyocytes on gelatin and on eADF4(κ 16) films responded in a similar manner to both stimulations in regards to cell size and ANF expression ($n = 3$ independent experiments, $p > 0.05$, Figure 3d,e). Collectively, these data indicate that eADF4(κ 16) is an inert material exhibiting no pharmacological effect but allows cardiomyocytes to respond properly to hypertrophic stimuli.

2.4. Cardiomyocytes on eADF4(κ 16) Films Respond Properly to Pro-Proliferative Stimuli

A current problem in cardiac tissue engineering is to generate cardiac tissues containing high densities of cardiomyocytes.^[10,29] This is due to the problem of seeding 3D

scaffolds with cardiomyocytes or printing bioinks with high cell densities. Thus, it might be of advantage to utilize proliferative factors to promote cardiomyocyte proliferation in the generated constructs to increase cardiomyocyte density and thus contractility. Previously, it has been shown that stimulation of cardiomyocytes with FBS or fibroblast growth factor 1 (FGF1) plus an inhibitor of the mitogen-activated protein kinase p38 (p38i) induces cell cycle re-entry in neonatal as well as adult cardiomyocytes resulting in the synthesis of deoxyribonucleic acid (DNA).^[30] Our data demonstrate that FBS, in a concentration-dependent manner, as well as FGF1/p38i, induce DNA synthesis in cardiomyocytes attached to eADF4(κ 16) or fibronectin films (white asterisks, incorporation of the nucleoside analog of thymidine 5-ethynyl-2'-deoxyuridine (EdU), Figure 4), with no statistically significant difference between the two matrices (Figure 4d). These data indicate that eADF4(κ 16) is a neutral substrate that does not influence cardiomyocyte behavior but permits the proper response of cardiomyocytes to extracellular stimuli. In addition, we observed that cardiomyocytes stimulated with FGF1/p38i exhibited on eADF4(κ 16) an elongated morphology, a similar phenotype as previously observed for neonatal and adult cardiomyocytes cultured on the inert substrate gelatin (see also Figure S3a in the Supporting Information).^[30a]

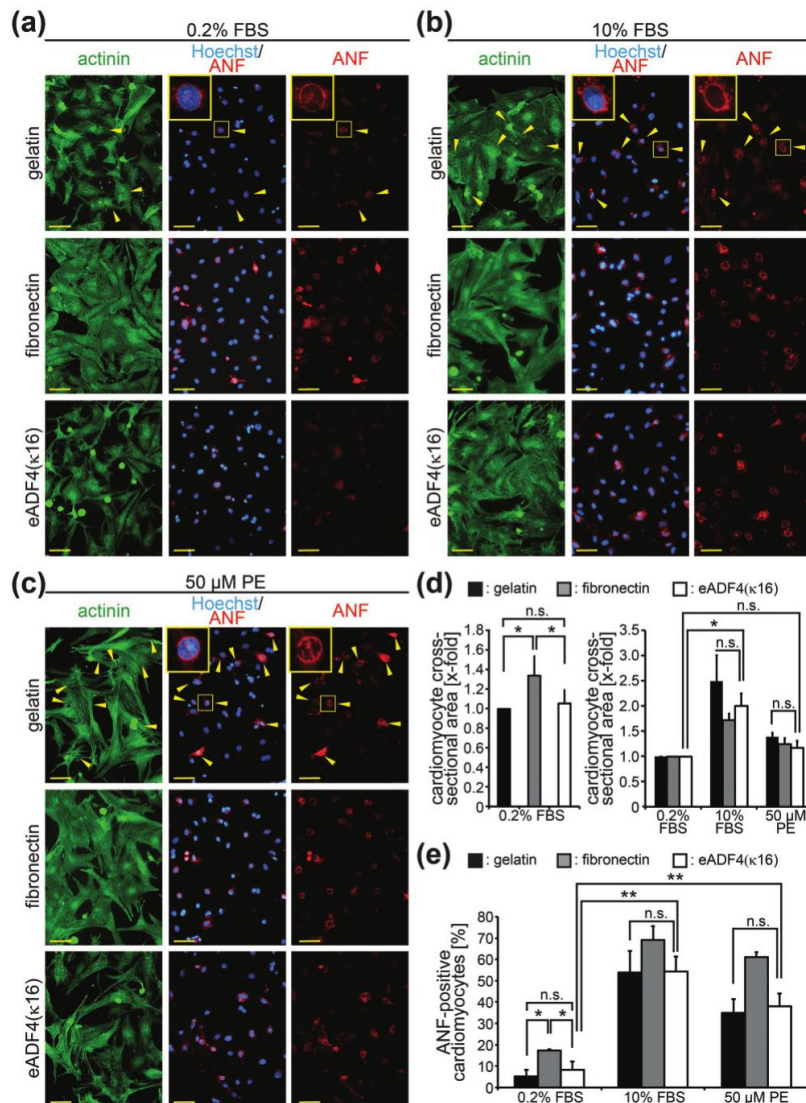


Figure 3. Cardiomyocytes respond properly to prohypertrophic stimuli on eADF4(κ16) films. Cardiomyocytes were stimulated with 0.2% or 10% FBS or 50×10^{-6} M phenylephrine (PE) and analyzed for a hypertrophic response (perinuclear ANF expression, cross-sectional area). a–c) Cardiomyocytes stained for sarcomeric- α -actinin (green), ANF (red), and DNA (Hoechst 33342, nuclei, blue). Yellow arrowheads: examples of ANF-positive cardiomyocytes exhibiting a clear perinuclear ANF signal (see inserts). d) Quantitative analysis of the cross-sectional area of sarcomeric- α -actinin-positive cardiomyocytes. Left panel: fold-change in relation to the mean cardiomyocyte size on gelatin films. Right panel: fold-change in relation to the mean cardiomyocyte size upon 0.2% stimulation on the respective matrix. e) Quantitative analysis of the number of ANF-/sarcomeric- α -actinin-positive cardiomyocytes ($n = 3$ independent experiments, mean \pm SD, *: $p < 0.05$, **: $p < 0.01$. n.s.: statistically not significant). Scale bars: 50 μ m.

2.5. Cardiomyocytes on eADF4(κ16) Films Exhibit Proper Cell-to-cell Communication and Contractility

Since the major function of the heart is to contract, it is important to assess if cardiomyocytes contract well on eADF4(κ16) films. To allow high contractility, it is crucial that

cardiomyocytes exhibit well-differentiated sarcomeres. This was observed in all our experiments based on the staining of sarcomeric proteins (Figure S3b,c, Supporting Information). In addition, we utilized the fact that neonatal cardiomyocytes exhibit spontaneous contractile activity and recorded movies of cultures grown on eADF4(κ16) and fibronectin films and analyzed

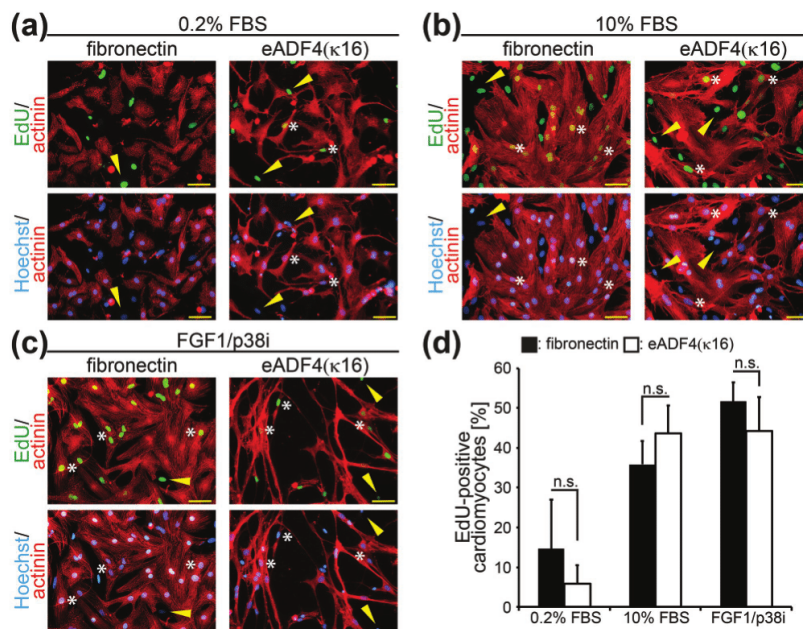


Figure 4. Cardiomyocytes respond properly to pro-proliferative stimuli on eADF4(κ 16) films. Cardiomyocytes were stimulated with 0.2% or 10% FBS or FGF1 and a p38 inhibitor (p38i) and analyzed for DNA synthesis (EdU incorporation). a–c) Cardiomyocytes stained for sarcomeric- α -actinin (red), EdU (green), and DNA (Hoechst 33342, nuclei, blue). White asterisks: examples of EdU-positive cardiomyocytes. Yellow arrowheads: examples of EdU-positive nonmyocytes. d) Quantitative analysis of the number of EdU-/sarcomeric- α -actinin-positive cardiomyocytes ($n = 3$ independent experiments, mean \pm SD, n.s.: statistically not significant). Scale bars: 50 μ m.

them via Kymograph analysis software (Image J). This analysis showed that cardiomyocytes contract with the same frequency on eADF4(κ 16) films as on fibronectin films and exhibit no arrhythmia (Figure 5a,b and Movies S1 and S2 (Supporting Information)).

In addition to proper contractility, it is important to determine if cardiomyocytes can communicate and electrically couple with each other, as efficient contraction of the heart is coordinated by propagating excitation waves. To assess if cardiomyocytes grown on eADF4(κ 16) films are able to couple electrically, cardiomyocyte cultures were stained for the gap junctional protein connexin 43, which takes part in regulating electrical signal propagation between cardiomyocytes.^[31] Immunofluorescence analyses revealed that cardiomyocytes grown on eADF4(κ 16) and fibronectin films expressed connexin 43 along cellular junctions. This was enhanced upon stimulation with 10% FBS (Figure 5c,d).

Finally, to test effects on the calcium homeostasis, cultures on either matrix were loaded with the Ca^{2+} -sensitive indicator Fura-2 AM. This allowed the visualization of Ca^{2+} carried excitation waves (Figure 5e–j). The number of contractions on either fibronectin or eADF4(κ 16) films was not significantly different. The contraction frequency for cardiomyocytes cultured on fibronectin films was on average $12 \pm 4 \text{ min}^{-1}$ ($n = 15$) and for eADF4(κ 16) films 12 ± 4 ($n = 16$) (data are mean \pm SD, Figure 5e). Peak amplitude of intracellular calcium was 0.54 ± 0.10 (arbitrary units) on fibronectin films

($n = 15$) and 0.53 ± 0.06 on eADF4(κ 16) films ($n = 16$) (data are mean \pm SD, Figure 5f).

To visualize the changes of intracellular calcium, sample recordings were extracted from cardiomyocytes plated on fibronectin (Figure 5g and Movie S3 (Supporting Information)) or eADF4(κ 16) films (Figure 5h and Movie S4 (Supporting Information)). Examples of local calcium minima (left panel) and peak calcium concentration (right panel) for cardiomyocytes grown on fibronectin or eADF4(κ 16) films are shown in Figure 5i,j, respectively. In conclusion, these data demonstrate that cardiomyocytes grown on eADF4(κ 16) films exhibit proper cell-to-cell communication and electric coupling.

3. Conclusion

We have demonstrated that eADF4(κ 16) films exhibit adhesion properties for the most important cell types in cardiac tissue engineering (cardiomyocytes, endothelial cells, fibroblasts, and smooth muscle cells) comparable to that of films made of fibronectin, a component of the native extracellular matrix of the heart and well-established coating material for neonatal cardiomyocytes. In addition, our data show that eADF4(κ 16) films are noncytotoxic and have no pharmacological effect. Moreover, cardiomyocytes grown on eADF4(κ 16) films respond properly to extracellular stimuli and exhibit proper

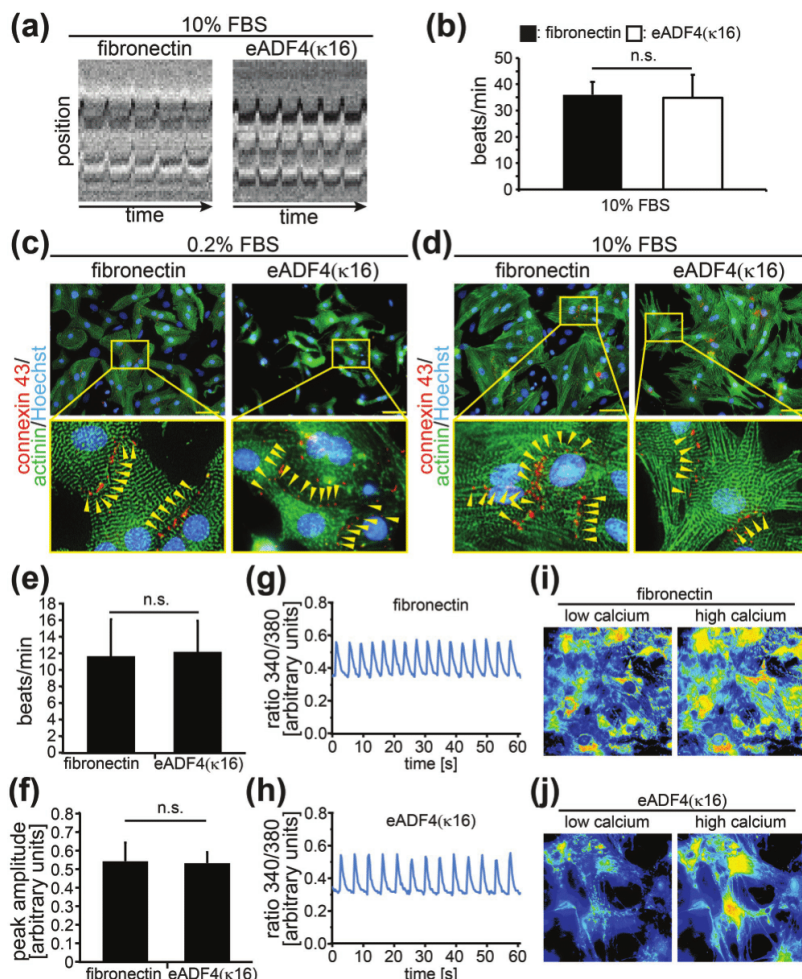


Figure 5. Cardiomyocytes on eADF4(κ 16) films exhibit proper cell-to-cell communication and contractility. a) Example of Kymograph analysis visualizing contractions (peaks). b) Quantitative analysis of (a). c, d) Examples of cardiomyocytes seeded on different matrices stimulated with 0.2% (c) or 10% FBS (d) and subsequently stained for connexin 43 (red), sarcomeric- α -actinin (green) and DNA (Hoechst 33342, nuclei, blue). Note that cardiomyocytes on eADF4(κ 16) films express connexin 43 (yellow arrowheads) suggesting well-established cell-to-cell communication. Ratiometric intracellular calcium imaging of cultured cardiomyocytes. e, f) Quantification of cardiomyocyte contraction frequency (e) and peak amplitude of intracellular calcium concentration (f) on fibronectin or eADF4(κ 16) films. Note that the contraction frequency is lower than in (b) as data collection was performed at room temperature and in a different medium. g, h) Representative examples of intracellular calcium changes of cardiomyocytes cultured on either fibronectin (g) or eADF4(κ 16) films (h). i, j) Representative images of local calcium minima (left panel) and peak calcium concentration (right panel) for cardiomyocytes cultured on either fibronectin (i) or eADF4(κ 16) films (j). Left image depicts cardiomyocytes between contractions. Right image depicts cardiomyocytes during contraction. Scale bars: 50 μ m.

excitation propagation. Our data demonstrate that eADF4(κ 16) exhibits similar properties as fibronectin and thus also as *Antheraea mylitta* silk fibroin. In conclusion, we introduce the designed recombinant eADF4(κ 16), previously developed for drug delivery applications,^[13] as a new promising material for cardiac tissue engineering that also provides the known advantages of silk proteins^[8,10] such as biodegradability^[32] and low immunogenicity.^[19c] As shown previously, eADF4 variants can be produced at large scale with high yields and high purity.^[13]

Interestingly, eADF4(κ 16) could in the future even be further genetically modified in order to optimize its performance as a substrate for cardiac tissue regeneration, for instance, by integrating additional functional domains.^[12,33] Recombinant spider silk proteins can be processed into a diverse set of morphologies including fibers, foams, hydrogels, particles, nonwoven meshes, capsules, and films.^[34] Moreover, we have recently demonstrated that cell-loaded recombinant spider silk bioinks can be printed by robotic dispensing without the

need for crosslinking additives or thickeners for mechanical stabilization,^[35] it could be assessed whether it is possible to print stem-cell derived cardiomyocytes in eADF4(κ 16)-based bioinks in order to biofabricate cardiac tissues for therapeutic applications.

4. Experimental Section

Rat Neonatal Cardiomyocyte Isolation and Cell Culture: The investigation conforms with the Guide for the Care and Use of Laboratory Animals published by the Directive 2010/63/EU of the European Parliament. Extraction of organs and preparation of primary cell cultures were approved by the local Animal Ethics Committee in accordance with governmental and international guidelines on animal experimentation (protocol TS—5/13 Nephropatho). Ventricular cardiac cells were isolated from 3 d old (P3) Sprague Dawley rats using the gentleMACS Dissociation kit (Milteny Biotec) according to the manufacturer's instructions. In order to isolate nonmyocytes, hearts were processed as previously reported.^[36] For cardiomyocyte enrichment, cells were preplated for 90 min in Dulbecco's Modified Eagle Medium (DMEM)/F12 + GLUTAMAX (GIBCO) containing penicillin/streptomycin (100 U mg⁻¹ mL⁻¹) and FBS (10%). Nonattached cells, enriched in cardiomyocytes, were then collected, centrifuged for 5 min at 330 × g, resuspended in DMEM/F12 + GLUTAMAX containing penicillin/streptomycin (100 U mg⁻¹ mL⁻¹), and counted. Before seeding, serum was added as indicated in the figures or as described below. Cells were seeded in 24-well plates at a density of 150 000 cells after cardiomyocyte enrichment, 200 000 nonmyocytes, or 50 000 HUVECs per 500 μ L per well and were cultured at 37 °C in a CO₂/air humidified atmosphere (5%/95%).

Preparation of Silk: The recombinant spider silk protein eADF4(κ 16) consists of 16 repeats of a κ -module (sequence: GSSAAAAAASGPGGYGPKNQGPSGGYGGYGGP).^[13] The spider silk protein was produced and purified as described before.^[37] Briefly, eADF4(κ 16) was produced in *E. coli* (BL21 gold), which was grown in a fed batch fermenter. The protein was purified using a heating step and ammonium sulfate precipitation.

Coating Procedure: Glass coverslips (\varnothing 12 mm, Thermo Fisher Scientific) were placed in 24-well tissue culture plates, washed twice for 5 min with 70% ethanol, once with 100% ethanol for 5 min, and air dried under UV light for 30 min. For fibronectin-coating, coverslips were incubated with 100 μ L of fibronectin (Sigma-Aldrich, F1141)/PBS (25 μ g mL⁻¹) for 1 h at 37 °C. Cells were seeded immediately after removing the remaining solution on the coverslips. For gelatin-coating, coverslips were incubated for 2 h at 37 °C with 500 μ L gelatin (Sigma-Aldrich, G1890)/water (1%, w/v). Subsequently, the gelatin solution was replaced with fresh 500 μ L gelatin solution. After 2 h incubation at 37 °C, the remaining solution on the coverslips was removed and coverslips were dried for another 1 h at 37 °C. For spider silk-processing, purified and lyophilized eADF4(κ 16) or eADF4(C16) was dissolved in formic acid and subsequently diluted with water (5:1, formic acid:water) to obtain a silk solution (0.34%, w/v). Coverslips were dip coated in this silk solution and dried on Parafilm M. Spider silk coatings from formic acid are water insoluble, therefore, further post-treatment was not necessary.^[38] Before coating with eADF4(C16) (and only in that case), the coverslips were silanized with (3-aminopropyl) trimethoxysilane to prevent detachment of eADF4(C16) films due to electrostatic repulsion of the silk and plain glass. A homogeneous spreading of silk films was confirmed by subsequent Hoechst 33342-staining. For recording movies, cells were grown on eADF4(κ 16)- or fibronectin-coated 8-well IBIDI slides. Note, eADF4(κ 16)-coating was not performed as described above but according to another previously described method.^[39] Briefly, purified and lyophilized eADF4(κ 16) was dissolved in 1,1,1,3,3,3-hexafluoro-2-propanol (HFIP) and films were cast from a solution (2%, w/v) directly into the wells (0.15 mg cm⁻²). After evaporation of HFIP, the water-soluble and α -helix-rich films

were post-treated with ethanol in order to induce β -sheet formation, rendering them water-insoluble.^[38]

Water Contact Angle Measurements: Coating was performed as described above with the following changes. All films were dried overnight on Parafilm. Fibronectin was diluted either in water (for better comparison to the other films) or PBS (as in the other experiments). Note that glass coverslips coated with fibronectin diluted in PBS were washed once with water before their transfer to Parafilm. Contact angles of coated glass coverslips were measured by sessile drop method at room temperature (RT) using a contact angle goniometer OCA-20 (DataPhysics Instruments, Filderstadt, Germany) and evaluated with the software SCA20-F. Uniform drops with a volume of 7 μ L were deposited using an automated dispensing system. The contact angles were determined 60 s after drop deposition using Young–Laplace algorithm. For each material, eight to ten measurements were performed ($n = 8–10$).

Attenuated Total Reflection-Fourier Transform Infrared (ATR-FTIR) Spectroscopy: ATR-FTIR spectra of eADF4(κ 16) films on glass and glass as control were measured in the range of 4000–800 cm⁻¹ on a Ge-crystal with a Bruker Tensor 27 spectrometer (Bruker, Germany). For each spectrum, 100 scans were recorded at a resolution of 4 cm⁻¹. The secondary structure content was determined by analyzing the amide I region (1595–1705 cm⁻¹) with FSD using Opus software (Bruker, Germany) according to Hu et al.^[15] Five samples were analyzed ($n = 5$).

Live/Dead Assay (Calcein-AM/Ethidium Homodimer-1): Cells were seeded on coated coverslips, allowed to attach for 24 h, and after washing once with PBS, incubated in medium for another 48 h. Cells were then washed three times with PBS for 5 min and incubated with calcein-AM (0.25 μ L mL⁻¹)/EthD-1 (1 μ L mL⁻¹)/PBS (Life Technologies, L2334) for 10 min at 37 °C in a CO₂/air humidified atmosphere (5%/95%). Subsequently, live images from ten randomly chosen microscopic fields (0.1 mm²) per experiment were taken to quantify living and dead cells.

Immunofluorescence Staining: Cultured cells were fixed in formaldehyde (3.7%, Sigma-Aldrich; F1635) for 20 min. All antibodies were diluted in blocking buffer (5% Bovine Serum Albumin (BSA)/0.2% Tween 20/PBS) and all manipulations were carried out at RT. Samples were permeabilized for 10 min with Triton X-100/PBS (0.5%), blocked for 20 min in blocking buffer, and incubated for 1 h with primary antibodies. Primary antibodies used in this study were: mouse monoclonal anti-sarcomeric- α -actinin (Abcam, ab9465, 1:500), rabbit polyclonal anti-connexin 43 (Santa Cruz Biotechnology, sc-9059, 1:500), rabbit polyclonal anti-ANP/ANF (Phoenix Pharmaceuticals, H-005-24, 1:500), rabbit polyclonal anti-collagen 1 (Rockland, 600-401-103-0, 1:250), rabbit polyclonal anti-VE-cadherin (Abcam, ab33168, 1:200), rabbit polyclonal anti-Troponin I (Santa Cruz Biotechnology, sc-15368, 1:50), and mouse anti-smooth muscle actin (Sigma-Aldrich, A2547, 1:250). For EdU (a thymidine analog which will be incorporated into the DNA during DNA synthesis) incorporation assays, cells were seeded in 1% FBS and allowed to attach for 48 h. Cells were then washed with PBS and stimulated as indicated for 72 h. Note that the p38 inhibitor (p38i, 10 × 10⁻⁶ M, SB203580-HCl, Tocris) was added every 24 h and that FGF1 (50 ng mL⁻¹, R&D Systems)/p38i stimulation was in the presence of 0.2% FBS. EdU (30 × 10⁻⁶ M, Life Technologies, C10337) was added after 24 and 48 h. Cells were fixed after 72 h and stained for EdU according to manufacturer's instructions. Immune complexes were detected with ALEXA 488- or ALEXA 594-conjugated donkey anti-mouse or anti-rabbit antibodies (1:500, Life Technologies). DNA was visualized by incubation with Hoechst 33342 (1:5000/PBS) for 10 min.

Cell Adhesion: Cell adhesion was quantified by determining the average number of attached cells from ten randomly chosen microscopic fields (0.1 mm²) per experiment.

Hypertrophy Assay: Cells were seeded in 0.2% FBS and allowed to attach for 24–48 h. Then, cells were washed and cultured in DMEM/F12 + GLUTAMAX containing 100 U mg⁻¹ mL⁻¹ penicillin/streptomycin and 0.2% FBS, 10% FBS, or phenylephrine (50 × 10⁻⁶ M, Sigma-Aldrich, P6126). After 48 h, cells were fixed and ten randomly chosen microscopic fields (0.1 mm²) per experiment were analyzed to determine the number of ANF-positive cardiomyocytes. In addition, the cross-sectional area of

at least 50 cardiomyocytes from five randomly chosen microscopic fields per experiment was determined via Photoshop.

Movie Capture and Kymograph Analysis: Movies of beating cardiomyocytes were recorded on a Keyence BZ9000 Fluorescence Microscope (Keyence, Osaka, Japan) and analyzed using the Image J Kymograph, which allows velocity measurements of moving structures in image time series. The x-axis of the kymograph is a time axis. A line in the kymograph in parallel to the x-axis indicates that there is no movement. A peak represents one contraction.

Intracellular Calcium Imaging: Cells were seeded in 10% FBS and allowed to attach for 48 h. Then, cells were washed once with PBS and cultured with DMEM/F12 + GLUTAMAX containing 100 U mg⁻¹ mL⁻¹ penicillin/streptomycin and 10% FBS for 5 d. Subsequently, cardiomyocyte medium was replaced with bathing solution (145 × 10⁻³ M NaCl, 5 × 10⁻³ M KCl, 1.25 × 10⁻³ M CaCl₂, 1 × 10⁻³ M MgCl₂, 10 × 10⁻³ M 2-(4-(2-hydroxyethyl)-1-piperazinyl)-ethansulfonic acid (HEPES), 10 × 10⁻³ M glucose, adjusted to pH 7.4 with NaOH) and loaded with Fura-2 AM (3 × 10⁻⁶ M) (Invitrogen, USA) supplemented with 0.02% pluronic acid (Molecular Probes, USA). The cells were incubated for 30 min, followed by a 15 min washout period at 37 °C in a CO₂/air humidified atmosphere (5%/95%). Afterward, cells were imaged within 5–15 min at RT. Several samples of three independent cultures were analyzed. Fura-2 AM was excited at 340 and 380 nm with 30 ms exposure time at 7 Hz sampling frequency using Lambda DG-4 Plus (Sutter Instrument, USA). Note that due to the measurement at RT and the different ionic composition of the incubation medium, the contraction frequency of cardiomyocytes was reduced. Ratiometric calcium imaging was performed using an Olympus IX83 microscope and acquired with a complementary metal-oxide-semiconductor (CMOS) camera (Orca-Flash4.0 LT, Hamamatsu, Japan) using SlideBook 6 software (3i, USA).

Statistical Analysis: Data are expressed as the mean ± SD of at least three independent experiments. Statistical significance of differences was evaluated by a two-tailed Student's *t*-test (Excel) or where appropriate by one way analysis of variance (ANOVA) followed by Bonferroni's post hoc test (GraphPad Prism). *p* < 0.05 was considered statistically significant.

Supporting Information

Supporting Information is available from the Wiley Online Library or from the author.

Acknowledgements

The authors would like to thank Robert Becker, Silvia Vergarajaregui, Kaveh Roshanbinfar, Johannes Kramer, David Zebrowski, and Johannes Diehl for technical support and the lab of Michael Stürzl for providing HUVECs. This work was supported by the Deutsche Forschungsgemeinschaft (DFG, EN 453/11-1 and FOR2149 to F.B.E.), the Bavarian Research Foundation (DOK-175-15, to T.B.A.), and by the Bavarian Polymerinstitute Keylab Adaptive Biomanufacturing (to T.S.).

Conflict of Interest

The authors declare no conflict of interest.

Keywords

adhesion, cardiac tissue engineering, cell–material interactions, eADF4(κ16), engineered spider silk proteins

Received: March 17, 2017

Revised: June 2, 2017

Published online:

- [1] M. A. Laflamme, C. E. Murry, *Nature* **2011**, 473, 326.
- [2] D. Mozaffarian, E. J. Benjamin, A. S. Go, D. K. Arnett, M. J. Blaha, M. Cushman, S. R. Das, S. de Ferranti, J. P. Despres, H. J. Fullerton, V. J. Howard, M. D. Huffman, C. R. Isasi, M. C. Jimenez, S. E. Judd, B. M. Kissela, J. H. Lichtman, L. D. Lisabeth, S. Liu, R. H. Mackey, D. J. Magid, D. K. McGuire, E. R. Mohler 3rd, C. S. Moy, P. Muntner, M. E. Mussolino, K. Nasir, R. W. Neumar, G. S. Nichol, L. Palaniappan, D. K. Pandey, M. J. Reeves, C. J. Rodriguez, W. Rosamond, P. D. Sorlie, J. Stein, A. Towfighi, T. N. Turan, S. S. Virani, D. Woo, R. W. Yeh, M. B. Turner, *Circulation* **2016**, 133, e38.
- [3] a) R. Madonna, L. W. Van Laake, S. M. Davidson, F. B. Engel, D. J. Hausenloy, S. Lecour, J. Leor, C. Perrino, R. Schulz, K. Ytrehus, U. Landmesser, C. L. Mumery, S. Janssens, J. Willerson, T. Eschenhagen, P. Ferdinandy, J. P. Sluijter, *Eur. Heart J.* **2016**, 37, 1789; b) B. M. Ogle, N. Bursac, I. Domian, N. F. Huang, P. Menasche, C. E. Murry, B. Pruitt, M. Radisic, J. C. Wu, S. M. Wu, J. Zhang, W. H. Zimmermann, G. Vunjak-Novakovic, *Sci. Transl. Med.* **2016**, 8, 342ps13; c) D. C. Zebrowski, R. Becker, F. B. Engel, *Am. J. Physiol.: Heart Circ. Physiol.* **2016**, 310, H1045; d) P. P. Zwetsloot, A. M. Vegh, S. J. Jansen of Lorkeers, G. P. van Hout, G. L. Currie, E. S. Sena, H. Gremmels, J. W. Buikema, M. J. Goumans, M. R. Macleod, P. A. Doevendans, S. A. Chamuleau, J. P. Sluijter, *Circ. Res.* **2016**, 118, 1223.
- [4] W. H. Zimmermann, I. Melnychenko, G. Wasmeier, M. Didie, H. Naito, U. Nixdorff, A. Hess, L. Budinsky, K. Brune, B. Michaelis, S. Dhein, A. Schwoerer, H. Ehmke, T. Eschenhagen, *Nat. Med.* **2006**, 12, 452.
- [5] a) M. Kawamura, S. Miyagawa, K. Miki, A. Saito, S. Fukushima, T. Higuchi, T. Kawamura, T. Kuratani, T. Daimon, T. Shimizu, T. Okano, Y. Sawa, *Circulation* **2012**, 126, S29; b) Y. Shiba, S. Fernandes, W. Z. Zhu, D. Filice, V. Muskheji, J. Kim, N. J. Palpant, J. Gantz, K. W. Moyes, H. Reinecke, B. Van Biber, T. Dardas, J. L. Mignone, A. Izawa, R. Hanna, M. Viswanathan, J. D. Gold, M. I. Kotlikoff, N. Sarvazyan, M. W. Kay, C. E. Murry, M. A. Laflamme, *Nature* **2012**, 489, 322; c) F. Weinberger, K. Breckwoldt, S. Pecha, A. Kelly, B. Geertz, J. Starbatty, T. Yorgan, K. H. Cheng, K. Lessmann, T. Stolen, M. Scherrer-Crosbie, G. Smith, H. Reichenspurner, A. Hansen, T. Eschenhagen, *Sci. Transl. Med.* **2016**, 8, 363ra148.
- [6] P. Menasché, V. Vanneaux, A. Hagege, A. Bel, B. Cholley, I. Cacciapuoti, A. Parouchev, N. Benhamouda, G. Tachdjian, L. Tosca, J. H. Trouvin, J. R. Fabreguettes, V. Bellamy, R. Guillemain, C. Suberbielle Boissel, E. Tartour, M. Desnos, J. Larghero, *Eur. Heart J.* **2015**, 36, 2011.
- [7] a) C. Patra, A. R. Boccaccini, F. B. Engel, *Thromb. Haemostasis* **2015**, 113, 532; b) M. N. Hirt, A. Hansen, T. Eschenhagen, *Circ. Res.* **2014**, 114, 354.
- [8] a) D. Jao, X. Mou, X. Hu, *J. Funct. Biomater.* **2016**, 7, 22; b) B. Kundu, N. E. Kurland, S. Bano, C. Patra, F. B. Engel, V. K. Yadavalli, S. C. Kundu, *Prog. Polym. Sci.* **2014**, 39, 251.
- [9] A. E. Thurber, F. G. Omenetto, D. L. Kaplan, *Biomaterials* **2015**, 71, 145.
- [10] C. Patra, S. Talukdar, T. Novoyatleva, S. R. Velagala, C. Muhlfield, B. Kundu, S. C. Kundu, F. B. Engel, *Biomaterials* **2012**, 33, 2673.
- [11] a) A. Blau, *Curr. Opin. Colloid Interface Sci.* **2013**, 18, 481; b) M. De Rosa, M. Carteni, O. Petillo, A. Calarco, S. Margarucci, F. Rosso, A. De Rosa, E. Farina, P. Grippo, G. Peluso, *J. Cell. Physiol.* **2004**, 198, 133.
- [12] S. Wohlrab, S. Muller, A. Schmidt, S. Neubauer, H. Kessler, A. Leal-Egana, T. Scheibel, *Biomaterials* **2012**, 33, 6650.
- [13] E. Doblhofer, T. Scheibel, *J. Pharm. Sci.* **2015**, 104, 988.

- [14] a) I. C. Um, H. Y. Kweon, K. G. Lee, Y. H. Park, *Int. J. Biol. Macromol.* **2003**, *33*, 203; b) S. Wohlrab, K. Spiess, T. Scheibel, *J. Mater. Chem.* **2012**, *22*, 22050.
- [15] X. Hu, D. Kaplan, P. Cebe, *Macromolecules* **2006**, *39*, 6161.
- [16] C. Patra, F. Ricciardi, F. B. Engel, *Biomaterials* **2012**, *33*, 4327.
- [17] Y. Tamada, Y. Ikada, *J. Biomed. Mater. Res.* **1994**, *28*, 783.
- [18] M. J. Lydon, T. W. Minett, B. J. Tighe, *Biomaterials* **1985**, *6*, 396.
- [19] a) C. B. Borkner, M. B. Elsner, T. Scheibel, *ACS Appl. Mater. Interfaces* **2014**, *6*, 15611; b) A. Leal-Egana, T. Scheibel, *Biotechnol. Appl. Biochem.* **2010**, *55*, 155; c) P. H. Zeplin, N. C. Maksimovikj, M. C. Jordan, J. Nickel, G. Lang, A. H. Leimer, L. Römer, T. Scheibel, *Adv. Funct. Mater.* **2014**, *24*, 2658.
- [20] T. K. Borg, K. Rubin, E. Lundgren, K. Borg, B. Obrink, *Dev. Biol.* **1984**, *104*, 86.
- [21] a) Y. Li, X. Shi, L. Tian, H. Sun, Y. Wu, X. Li, J. Li, Y. Wei, X. Han, J. Zhang, X. Jia, R. Bai, L. Jing, P. Ding, H. Liu, D. Han, *Adv. Mater.* **2016**, *28*, 10230; b) S. R. Shin, B. Aghaei-Ghareh-Bolagh, X. Gao, M. Nikkiah, S. M. Jung, A. Dolatshahi-Pirouz, S. B. Kim, S. M. Kim, M. R. Dokmeci, X. S. Tang, A. Khademhosseini, *Adv. Funct. Mater.* **2014**, *24*, 6136; c) S. R. Shin, R. Farzad, A. Tamayol, V. Manoharan, P. Mostafalu, Y. S. Zhang, M. Akbari, S. M. Jung, D. Kim, M. Comotto, N. Annabi, F. E. Al-Hazmi, M. R. Dokmeci, A. Khademhosseini, *Adv. Mater.* **2016**, *28*, 3280; d) S. R. Shin, C. Shin, A. Memic, S. Shadmehr, M. Miscuglio, H. Y. Jung, S. M. Jung, H. Bae, A. Khademhosseini, X. S. Tang, M. R. Dokmeci, *Adv. Funct. Mater.* **2015**, *25*, 4486.
- [22] a) C. Dambrot, S. R. Braam, L. G. Tertoolen, M. Birket, D. E. Atsma, C. L. Mummery, *J. Cell. Mol. Med.* **2014**, *18*, 1509; b) M. Qi, K. Ojamaa, E. G. Eleftheriades, I. Klein, A. M. Samarel, *Am. J. Physiol.* **1994**, *267*, C520; c) J. Sadoshima, H. Aoki, S. Izumo, *Circ. Res.* **1997**, *80*, 228.
- [23] I. Shimizu, T. Minamino, *J. Mol. Cell. Cardiol.* **2016**, *97*, 245.
- [24] a) I. Banerjee, J. W. Fuseler, R. L. Price, T. K. Borg, T. A. Baudino, *Am. J. Physiol.: Heart Circ. Physiol.* **2007**, *293*, H1883; b) H. W. Vliegen, A. van der Laarse, C. J. Cornelisse, F. Eulerink, *Eur. Heart J.* **1991**, *12*, 488.
- [25] H. Naito, I. Melnychenko, M. Didie, K. Schneiderbanger, P. Schubert, S. Rosenkranz, T. Eschenhagen, W. H. Zimmermann, *Circulation* **2006**, *114*, 172.
- [26] a) S. Zhao, L. Li, H. Wang, Y. Zhang, X. Cheng, N. Zhou, M. N. Rahaman, Z. Liu, W. Huang, C. Zhang, *Biomaterials* **2015**, *53*, 379; b) Z. Zhao, J. Wang, J. Lu, Y. Yu, F. Fu, H. Wang, Y. Liu, Y. Zhao, Z. Gu, *Nanoscale* **2016**, *8*, 13574.
- [27] M. H. Konstandin, M. Volkers, B. Collins, P. Quijada, M. Quintana, A. De La Torre, L. Ormachea, S. Din, N. Gude, H. Toko, M. A. Sussman, *Basic Res. Cardiol.* **2013**, *108*, 375.
- [28] C. Putinski, M. Abdul-Ghani, R. Stiles, S. Brunette, S. A. Dick, P. Fernando, L. A. Megoney, *Proc. Natl. Acad. Sci. USA* **2013**, *110*, E4079.
- [29] a) R. Gaetani, P. A. Doevendans, C. H. Metz, J. Alblas, E. Messina, A. Giacomello, J. P. Sluijter, *Biomaterials* **2012**, *33*, 1782; b) R. Gaetani, D. A. Feyen, V. Verhage, R. Slaats, E. Messina, K. L. Christman, A. Giacomello, P. A. Doevendans, J. P. Sluijter, *Biomaterials* **2015**, *61*, 339; c) J. Jang, H. J. Park, S. W. Kim, H. Kim, J. Y. Park, S. J. Na, H. J. Kim, M. N. Park, S. H. Choi, S. H. Park, S. W. Kim, S. M. Kwon, P. J. Kim, D. W. Cho, *Biomaterials* **2017**, *112*, 264.
- [30] a) F. B. Engel, M. Schebesta, M. T. Duong, G. Lu, S. Ren, J. B. Madwed, H. Jiang, Y. Wang, M. T. Keating, *Genes Dev.* **2005**, *19*, 1175; b) F. B. Engel, M. Schebesta, M. T. Keating, *J. Mol. Cell. Cardiol.* **2006**, *41*, 601.
- [31] P. A. Guerrero, R. B. Schuessler, L. M. Davis, E. C. Beyer, C. M. Johnson, K. A. Yamada, J. E. Saffitz, *J. Clin. Invest.* **1997**, *99*, 1991.
- [32] a) A. Lammel, M. Schwab, M. Hofer, G. Winter, T. Scheibel, *Biomaterials* **2011**, *32*, 2233; b) S. Müller-Herrmann, T. Scheibel, *ACS Biomater. Sci. Eng.* **2015**, *1*, 247.
- [33] K. Schacht, T. Scheibel, *Curr. Opin. Biotechnol.* **2014**, *29*, 62.
- [34] a) J. G. Hardy, T. R. Scheibel, *Biochem. Soc. Trans.* **2009**, *37*, 677; b) E. Doblhofer, A. Heidebrecht, T. Scheibel, *Appl. Microbiol. Biotechnol.* **2015**, *99*, 9361.
- [35] K. Schacht, T. Jungst, M. Schweinlin, A. Ewald, J. Groll, T. Scheibel, *Angew. Chem. Int. Ed.* **2015**, *54*, 2816.
- [36] F. B. Engel, L. Hauck, M. C. Cardoso, H. Leonhardt, R. Dietz, R. von Harsdorf, *Circ. Res.* **1999**, *85*, 294.
- [37] D. Huemmerich, C. W. Helsen, S. Quedzuweit, J. Oschmann, R. Rudolph, T. Scheibel, *Biochemistry* **2004**, *43*, 13604.
- [38] K. Spiess, R. Ene, C. D. Keenan, J. Senker, F. Kremer, T. Scheibel, *J. Mater. Chem.* **2011**, *21*, 13594.
- [39] A. Leal-Egana, G. Lang, C. Mauerer, J. Wickinghoff, M. Weber, S. Geimer, T. Scheibel, *Adv. Eng. Mater.* **2012**, *14*, B67.

Copyright WILEY-VCH Verlag GmbH & Co. KGaA, 69469 Weinheim, Germany, 2017.

**ADVANCED
FUNCTIONAL
MATERIALS**

Supporting Information

for *Adv. Funct. Mater.*, DOI: 10.1002/adfm.201701427

Surface Features of Recombinant Spider Silk Protein
eADF4(κ 16)-Made Materials are Well-Suited for Cardiac
Tissue Engineering

*Jana Petzold, Tamara B. Aigner, Filip Touska, Katharina
Zimmermann, Thomas Scheibel, and Felix B. Engel**

WILEY-VCH

Supporting Information**Surface features of recombinant spider silk protein eADF4(κ 16)-made materials are well-suited for cardiac tissue engineering**

*Jana Petzold, Tamara B. Aigner, Filip Touska, Katharina Zimmermann, Thomas Scheibel, Felix B. Engel**

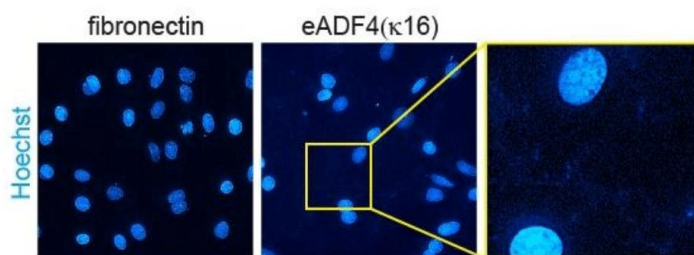


Figure S1. Hoechst 33342 to visualize eADF4(κ 16). Cell-loaded coverslips were stained with Hoechst 33342 to visualize eADF4(κ 16). Staining of nuclei (DNA) was used as internal control.

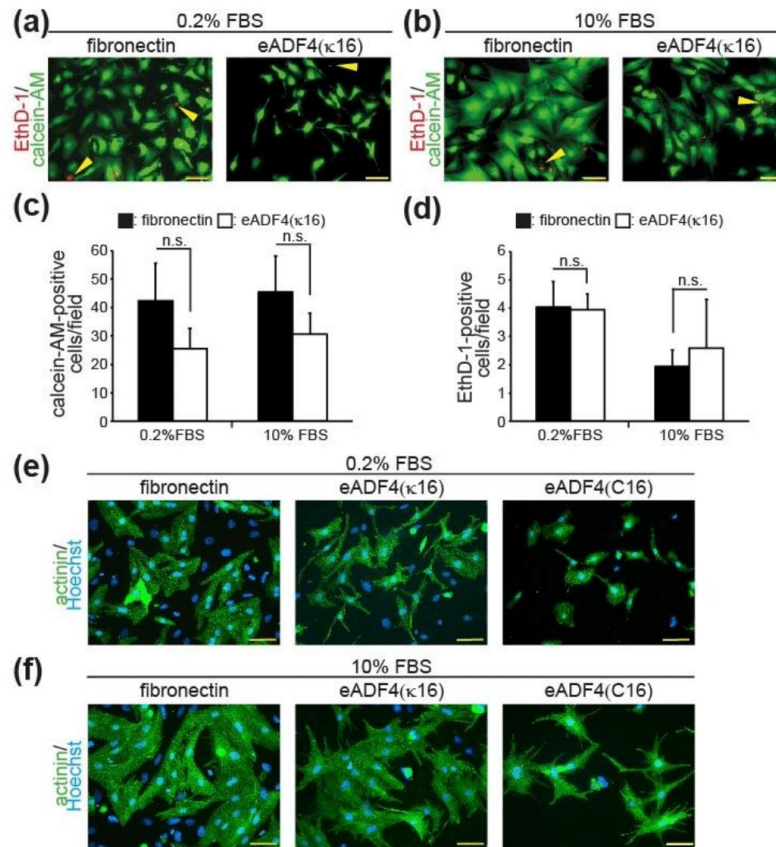


Figure S2. eADF4(κ16) is non-cytotoxic. a,b) Cardiac cells isolated from ventricles of 3-days-old rats were cultured in the presence of 0.2% (a) or 10% FBS (b). Living and dead cells were stained by calcein-AM (0.25 μl/ml, green, living) and ethidium homodimer-1 (EthD-1, 1 μl/ml, red, dead) (life/dead assay), respectively. Yellow arrowheads: examples of dead cells. c) Quantitative analysis of calcein-AM-positive living cells. d) Quantitative analysis of EthD-1-positive dead cells. e,f) Cardiac cells isolated from ventricles of 3-days-old rats were cultured after attachment overnight for 48 hours on the indicated matrices in the presence of 0.2% (e) or 10% FBS (f). Subsequently, cardiomyocytes were stained with sarcomeric- α -actinin (actinin, green) and Hoechst 33342 (nuclei, blue). Data are mean \pm SD. n = 3 independent experiments. n.s.: statistically not significant. Scale bars: 50 μm.

WILEY-VCH

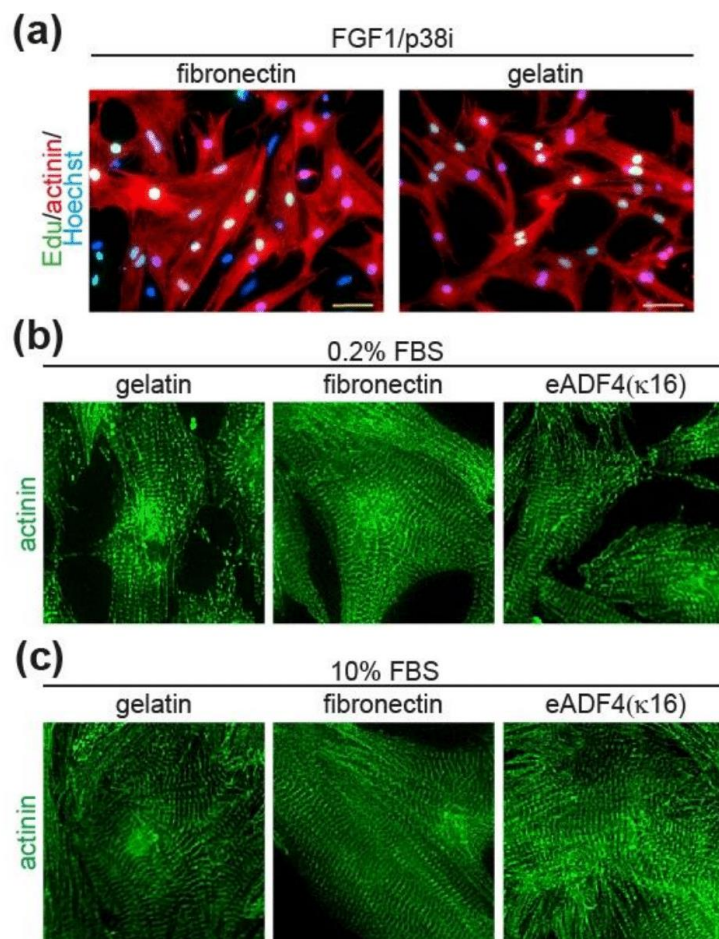


Figure S3. Cardiomyocytes respond to FGF1/p38i stimulation and exhibit well-differentiated sarcomeres on eADF4(κ 16) films. a) Cardiomyocytes were stimulated with FGF1 and a p38 inhibitor (p38i) and stained for sarcomeric- α -actinin (red), EdU (green), and DNA (Hoechst 33342, nuclei, blue). Note, cardiomyocytes on gelatin exhibit an elongated morphology. b,c) Examples of cardiomyocytes stimulated with 0.2% (b) or 10% FBS (c) stained for sarcomeric- α -actinin to visualize sarcomeres.

WILEY-VCH

Supplementary Movie Captions

Movie S1. Cardiomyocyte culture on a fibronectin film

Movie S2. Cardiomyocyte culture on an eADF4(κ 16) film

Movie S3. Calcium imaging of a cardiomyocyte culture on a fibronectin film

Movie S4. Calcium imaging of a cardiomyocyte culture on an eADF4(κ 16) film

Part 5. Nerve Guidance Conduit Design based on Self-rolling Tubes

Aigner, T. B.*; Haynl, C.*; Salehi, S.; O'Connor, A. Scheibel, T.

Published in Materials Today Bio, 5, 100042

(2020)

Reprinted with kind permission from Elsevier GmbH



Contents lists available at ScienceDirect

Materials Today Bio

journal homepage: www.journals.elsevier.com/materials-today-bio

Nerve guidance conduit design based on self-rolling tubes

T.B. Aigner^{a,g}, C. Haynl^{a,g}, S. Salehi^a, A. O'Connor^b, T. Scheibel^{a,c,d,e,f,*}



^a University of Bayreuth, Department of Biomaterials, Prof.-Rüdiger-Bormann-Str.1, 95447, Bayreuth, Germany

^b University of Melbourne, Department of Biomedical Engineering, Melbourne, Victoria, 3010, Australia

^c University of Bayreuth, Bayreuther Zentrum für Kolloide und Grenzflächen (BZKG), Universitätsstraße 30, 95447, Bayreuth, Germany

^d University of Bayreuth, Bayreuther Zentrum für Molekulare Biowissenschaften (BZMB), Universitätsstraße 30, 95447, Bayreuth, Germany

^e University of Bayreuth, Bayreuther Materialzentrum (BayMAT), Universitätsstraße 30, 95447, Bayreuth, Germany

^f University of Bayreuth, Bayerisches Polymerinstitut (BPI), Universitätsstraße 30, 95447, Bayreuth, Germany

ARTICLE INFO

Keywords:

Peripheral nerve repair
Electrospinning
Layer-by-layer film
Recombinant spider silk
Collagen
Cryogel

ABSTRACT

The current gold standard in peripheral nerve repair is nerve autografts for bridging gaps larger than a centimeter. However, autografts are associated with a low availability and the loss of function at the donor site. Nerve guidance conduits (NGCs) made of biocompatible and biodegradable materials reflect suitable alternatives. Clinically approved NGCs comprise either wraps that are rolled around the loose ends of the nerve or steady-state tubes; however, both lack internal guidance structures. Here, we established self-rolling NGCs to allow for gentle encapsulation of nerve cells together with supportive microenvironments, such as (1) an inner tube wall coating with a bioactive spider silk film, (2) an inner tube wall lining using an anisotropic spider silk non-woven mat, or (3) a luminal filler using an anisotropic collagen cryogel. Neuronal cells adhered and differentiated inside the modified tubes and formed neurites, which were oriented along the guidance structures provided by the spider silk non-woven mat or by the fibrillary structure of the collagen cryogel. Thus, our size-adaptable NGCs provide several features useful for peripheral nerve repair, and distinct combinations of the used elements might support and enhance the clinical outcome.

1. Introduction

Peripheral nerve injuries, such as crushes or sections, can be consequences of vehicle or industrial accidents, falls, or penetrating trauma [1]. The peripheral nervous system in vertebrates reacts to such injuries by active degeneration and regeneration [2,3]. Problematic are gaps, which are larger than 1 cm, thus, original nerve function cannot be restored using bioinert nerve guidance conduits (NGCs) [4,5]. In those cases, the current gold standard is nerve autografts, providing the extracellular matrix, viable Schwann cells, and growth factors needed for optimal regeneration [6–8]. Therewith, a physical guidance is given, allowing the nerve tissue cells to sprout their axons from the proximal end to the distal stump [9]. Unfortunately, the number of supplies in donor nerve tissue is limited and nerve removal causes a loss of function at the donor site. Further, a complete functional restoration cannot be guaranteed at the acceptor site [6,10]. An alternative to nerve autografts is using artificial NGCs [11–13].

Basically, there are several properties the NGC has to meet to increase the success of the clinical outcome. The NGC must be biocompatible and biodegradable to not provoke any immunological reaction or other side-effects and to avoid compression caused by non-degraded components [13]. The NGC must be flexible and soft because the gap to be bridged might cross a joint but at the same time should possess enough stability to be implanted by surgeons [13]. NGCs, which are mostly based on tubular structures, should be semipermeable allowing the diffusion of gases and nutrients but should avoid infiltration of inflammatory cells and scar tissue formation. Furthermore, the presence of bioactive molecules and adhesion of supporting cells, such as, for instance, Schwann cells, has been found to be crucial [11–14].

Filler materials within the tubular structure can create a cell friendly microenvironment promoting cell adhesion, proliferation, migration and differentiation, and directed growth of neuronal cells and their neurites. For instance, multilumen or microporous fillers, hydrogels or fiber containing conduits, and microgrooves or nanoimprints on the inner wall have been under investigation [11,12]. Another possibility is the use of

* Corresponding author.

E-mail address: thomas.scheibel@bm.uni-bayreuth.de (T. Scheibel).

^g contributed equally.

<https://doi.org/10.1016/j.mtbio.2020.100042>

Received 21 October 2019; Received in revised form 17 January 2020; Accepted 18 January 2020

Available online 27 January 2020

2590-0064/© 2020 The Authors. Published by Elsevier Ltd. This is an open access article under the CC BY-NC-ND license (<http://creativecommons.org/licenses/by-nc-nd/4.0/>).

cryogels, which provide a three-dimensional environment [15,16] favorable for this application.

Clinically approved NGCs are either wraps that are rolled around the loose ends of the nerve or steady-state tubes, in which both nerve ends are inserted [17]. Those NGC variants are not modified with internal guidance structures and they are made of either synthetic polymers, such as polyglycolic acid (Neurotube®), polylactide-caprolactone (Neurolac™) and polyvinyl alcohol (Salutunnel™), or collagen type I (NeuraGen®, NeuraWrap™, NeuroMend™, NeuroMatrix™, NeuroFlex™) [17], which is an extracellular matrix protein also found in peripheral nerves, providing myelinated axons with functional support [12,18,19] and generally exhibiting excellent biocompatibility, extremely low immunogenicity, chemotaxis, and biodegradability [20, 21].

Besides collagen, other naturally derived materials such as chitosan and spider silk are promising candidates for NGC fabrication because of their excellent compatibility with the human body. Chitosan is a derivative of naturally occurring chitin, a by-product of the seafood industry. It shows antimicrobial properties [22] and is used in food, cosmetics, and pharmaceutical and biomedical applications [23, 24], including peripheral nerve repair [25,26]. Natural spider silk fibers exhibit remarkable mechanical properties [27,28] and have performed well in *in vivo* peripheral nerve repair studies [29,30]. Owing to the difficulties (i.e., cannibalism) in spider farming, which prevent the production of large amounts and a constant material quality [31], recombinant spider silk proteins can nowadays be provided, and materials made thereof have exhibited suitable properties in neuronal *in vitro* tests [32–34]. Recombinant spider silks can be processed into several tailorable morphologies, for example, films, foams, non-woven mats, or hydrogels [35–42], and these materials were shown to not induce an immune response in the body and to degrade rather slowly [43–46]. In comparison with electro-spun collagen nanofibers, recombinant spider silk nanofibers are less prone to swelling [47], allowing a higher degree of nerve cell orientation along the fiber axes. Furthermore, different modifications are possible on the genetic level, for instance, the introduction of an arginine—glycine-aspartic acid (RGD)-bearing cell binding motif [48].

We have recently shown the application of self-rolling tubes as containers for enzymatic reactions [49]. In the present study, we designed a biocompatible and biodegradable self-rolling tubular NGC. Although the commercially available NeuroMend™ exhibits self-rolling properties, its lack of internal structures, which would be beneficial for cell vitality and differentiation, as well as directed nerve growth and neurite elongation, is regarded as one severe drawback limiting the success of the clinical outcome. Therefore, we studied the benefit of a self-rolling tube made of chitosan and different filler morphologies, which adapts to the dimensions of the injured peripheral nerve upon rolling around the loose ends and the filler material. It could be shown that the new NGCs ensured the viability of neuronal cells during encapsulation. In this study, all variants tested allowed differentiation of neuronal PC-12 cells within the NGCs, and anisotropic structures provided guidance of neurites. Our study combines the usefulness of the self-rolling property of a tube with the incorporation of suitable internal morphologies and is therefore of high importance to the development of new materials for peripheral nerve repair.

2. Materials and methods

2.1. Fabrication of self-rolling chitosan films

A filtered chitosan solution (1% w/v in 2% v/v formic acid, 190–310,000 g mol⁻¹, Sigma-Aldrich) was cast into a Petri dish (Sterilin™, diameter: 90 mm) yielding a density of 2.36 mg cm⁻², and the film was air dried overnight. This film was post-treated with 0.2 M NaOH for 5 min and subsequently washed with ultrapure water.

2.2. Fabrication of self-rolling chitosan films with an internal eADF4(C16)-RGD coating

The preparation of self-rolling chitosan tubes with an internal spider silk eADF4(C16)-RGD coating was conducted according to Aigner and Scheibel [49]. In brief, an eADF4(C16)-RGD [48] solution in 1,1,1,3,3,3-hexafluoro-2-propanol (HFIP, 8.33 mg ml⁻¹, 0.08 mg cm⁻², 48, 583 g mol⁻¹) was cast into a Petri dish (Sterilin™, diameter: 90 mm) and, after drying, post-treated with 70% (v/v) ethanol to render the silk film to be insoluble in water by inducing β -sheet formation. Then, a chitosan film was cast on top of the eADF4(C16)-RGD film according to the procedure outlined in Section 2.1.

2.3. Fabrication of self-rolling chitosan films with an internal eADF4(C16) anisotropic non-woven mat

A chitosan film was prepared as depicted in 2.1 and removed from the Petri dish and fixed on a rotating drum with double-sided tape. The rotating drum allowed production of aligned fibers yielding an anisotropic non-woven mat. Electrospinning of eADF4(C16) was performed according to the study by Lang [50]. A 150 mg ml⁻¹ solution of eADF4(C16) (47, 698 g mol⁻¹, AMSilk GmbH) in HFIP was electrospun onto the chitosan film (voltage: 30 kV; distance to collector: 15 cm; flow rate: 300 μ l min⁻¹; relative humidity: 50%). The spider silk non-woven mat was post-treated first in pure ethanol vapor for 3 h, followed by a treatment in 90% ethanol in the vapor phase (corresponds to 87% v/v ethanol) for 2 h to render the mat to be insoluble in water and to obtain a tight connection between the spider silk non-woven mat and the chitosan film.

2.4. Fabrication of anisotropic collagen cryogels

Collagen type I extracted from calf skin (Sigma-Aldrich) was dissolved in 0.5% (v/v) acetic acid at pH 3 for 20 h. After centrifugation at 17,700 g for 10 min, the supernatant was removed and showed a collagen concentration of 4.8 mg ml⁻¹. Then, an aqueous glutaraldehyde solution (25% v/v in water, Carl Roth GmbH + Co. KG) was mixed with the collagen solution yielding a final concentration of 1% glutaraldehyde (v/v). This solution was then immediately transferred into a vertically standing plastic tube, which was tightly fixed to a copper plate. After sealing the top opening of the filled plastic tube with parafilm and mounting a thermal insulation (tube filled with cotton wool) on top, the whole setup was transferred into a –20 °C temperature freezer for 48 h. Subsequently, the frozen collagen cryogel precursor was pushed out of the tube into phosphate buffered saline (PBS), pH 7.4 at room temperature to neutralize the acidic pH, thereby preventing reversible dissolution of the collagen cryogel. After 20 h gelation in PBS, the collagen cryogel was washed three times with PBS containing 0.1 M glycine. The washing was continued using two further washing steps during the next 24 h to ensure complete capture of any free glutaraldehyde groups. Finally, the collagen cryogel was washed using PBS and stored in PBS until further experiments were carried out.

2.5. Chitosan tube formation

The underlying self-rolling mechanism of the used chitosan film was based on the difference of the swelling behavior between its bottom and top layer (Section 2.1). A more detailed explanation of this process can be found in the study by Ionov [51]. Here, chitosan films were cut into rectangles with desired sizes. The self-rolling process was induced by immersing this film into an aqueous solution, that is, into phosphate buffered saline (pH 7.4). However, self-rolling was induced as well in contact with cell culture medium, which resulted in entrapping the cell suspension. To encapsulate cryogels, they were placed on the film, which self-rolled forming a tube filled with cryogel. The tube diameter could be tailored to a certain extent by varying the film thickness and the diameter of the filler, for example, the cryogel.

2.6. Morphological characterization of NGCs

NGC components were analyzed using stereo microscopy (Leica M205C) and scanning electron microscopy (SEM; Sigma VP 300, Zeiss). For SEM, the samples were mounted on aluminum studs with adhesive carbon tape and then sputter coated with platinum (2 nm). Collagen cryogels were prepared for imaging by washing and storing them for further use in 10 mM ammonium hydrogen carbonate buffer. After flash freezing in liquid nitrogen, the collagen cryogels were placed in a lyophilization device (Alpha 1–2 LDplus, Christ) for one week. The cryogel cross-section was prepared in advance to flash freezing and lyophilization by cutting the soaked cryogel using a sharp razor blade.

2.7. Determination of water content and swelling degree of collagen cryogels

Collagen cryogels were prepared having 2 cm in length (number of samples $n = 6$). The weight of the fully soaked cryogels in PBS (m_{soaked}) and of the cryogels after removing unbound PBS with a paper tissue (m_{removed}) was determined using a microbalance (Practum 224-1S, Sartorius Lab Instruments). The water content in soaked cryogels was calculated using Eq. (1).

$$\text{water content of collagen cryogels } [\%] = (m_{\text{soaked}} - m_{\text{removed}}) / m_{\text{soaked}} \times 100 \quad (1)$$

The swelling ratio of the collagen cryogels was calculated using Eq. (2). Therefore, the diameter of the fully soaked cryogels was measured in PBS (V_{soaked}) and that of the cryogels after removing unbound water with a paper tissue (V_{removed}) using a stereo microscope (Leica M205C) (number of samples $n = 4$). The cryogels were assumed to be tubular, and their volumes were calculated using their diameter values.

$$\text{swelling ratio } [\%] = (V_{\text{soaked}} - V_{\text{removed}}) / V_{\text{removed}} \times 100 \quad (2)$$

2.8. Mechanical characterization of chitosan films and collagen cryogels

The chitosan films used for conduit fabrication and the collagen cryogels were analyzed using a tensile testing device (Bose Electroforce 3220) equipped with a 2.45 N load cell. Dry chitosan films were glued onto plastic frames using a high viscosity glue (UHU® Supergel), and they were immediately transferred into a fume hood for drying. The films on the frames were incubated in PBS before analysis using a strain rate of 0.05 mm s^{-1} (number of samples $n = 5$). Engineering stress of the films was calculated as the force divided by their cross-sectional areas assumed to be rectangular (film width \times film thickness).

The mechanical properties of the collagen cryogel were analyzed referring to its longitudinal axis. Free PBS in collagen cryogels was removed using a paper tissue, and the diameters after this procedure were measured at three different positions. The moist cryogel was clamped between two plastic frames, applied to the tensile testing device, and measured at a strain rate of 0.05 mm s^{-1} (number of samples $n = 4$). Engineering stress of the cryogels was calculated as the force divided by the respective cross-sectional area, which was assumed to be circular. In terms of the films and the cryogels, the gauge length was adjusted to 2 mm. Strain was defined as the change in sample length divided by its original length. The Young's modulus was determined as the slope of the stress-strain plot in the linear elastic deformation range.

2.9. Seeding of PC-12 cells on the individual components and in the NGC

The different NGC components were prepared in untreated cell culture plates (24 wells, Thermo Fisher). For collagen surface treatment, the collagen type I solution (diluted 1:5 with sterile PBS, Cellmatrix®, Nitta Gelatin Inc) was used to coat the wells for 30 s. Then the solution was removed and the film was air dried. The eADF4(C16)-RGD film was cast

directly into the wells using HFIP (33.3 mg ml^{-1} , 0.25 mg cm^{-2}) as a solvent. After drying, films were post-treated with 70% ethanol (v/v). The eADF4(C16) non-woven mats were prepared by electrospinning of a 150 mg ml^{-1} eADF4(C16) solution in HFIP onto plastic coverslips (12 mm diameter, Thermo Fisher). The same spinning and post-treatment conditions were used as explained in section 2.3. A fixation of the plastic coverslips onto the rotating drum for fiber alignment was not possible, thus, an isotropic non-woven mat was spun onto the coverslips. The collagen cryogel was glued into well plates using a silicon glue.

The neuronal cell line PC-12 (ATCC® CRL1721™) [52] was cultured in the growth medium (Dulbecco's Modified Eagle's Medium (DMEM) with 10% (v/v) heat inactivated horse serum (Gibco), 5% (v/v) fetal bovine serum (FBS, Merck), 1% (v/v) GlutaMAX (Gibco), 1% (v/v) penicillin/streptomycin ($10,000 \text{ U ml}^{-1}$, Thermo Fisher), 20 mM 4-(2-hydroxyethyl)-1-piperazineethanesulfonic acid buffer (HEPES, Carl Roth)). For the adhesion test, 25–30,000 cells were seeded per square centimeter on the aforementioned materials and allowed to adhere for 7 days with medium changes on day 3 and 5. Treated cell culture plates were used as control. After 1, 3, and 7 days, cell morphology was observed using bright field microscopy (Leica DMi8).

2.10. Differentiation of PC-12 cells on NGC components

A density of $10,000 \text{ cells cm}^{-2}$ were cultured on the aforementioned materials and incubated in the growth medium. After 1 day of culture, the growth medium was exchanged with the differentiation medium (DMEM with 2% (v/v) horse serum, 1% (v/v) GlutaMAX, 1% (v/v) penicillin/streptomycin, 20 mM HEPES buffer, 100 ng ml^{-1} nerve growth factor (NGF, 2.5s Native Mouse Protein, Thermo Fisher)), which was changed on day 3 and 5 of differentiation. After 7 days of differentiation, the cells were immunostained for detecting endogenous levels of β -III tubulin, and neurite outgrowth was evaluated. The staining procedure was as follows: cells were fixed with formaldehyde (Carl Roth; 3.7% in water, 15 min, at room temperature) and made permeable with Triton x-100 (Carl Roth; 0.3% (v/v), 5 min, at room temperature). A glycine solution (Carl Roth, 300 mM, 10 min, at room temperature) was added to deactivate aldehydes. Bovine serum albumin (BSA) blocking buffer was applied (Carl Roth; 5% (w/v), 30 min, 37 °C) before adding the image enhancer (30 min, 37 °C) of the Alexa Fluor™ 488 Goat Anti-Rabbit SFX Kit (Thermo Fisher). Then, the samples were incubated in primary polyclonal antibody anti- β -III tubulin (Abcam, rabbit; 1000 x diluted in 0.1% (w/v) BSA buffer, overnight, 4 °C). On the next day, cells were stained using the secondary antibody goat-anti-rabbit with an Alexa Fluor 488 label (Sigma-Aldrich; 1000 x diluted in 0.1% (w/v) BSA buffer, 1 h, 37 °C) and Hoechst (Invitrogen; 1000 x diluted in 0.1% (w/v) BSA buffer, 1 h, 37 °C). Imaging was performed using a fluorescence microscope (Leica DMi8). For cryogels, Z stacks were taken and overlaid using the maximal projection option provided by the software (LAS X 3.6.0).

2.11. Encapsulation of cells in tubes

Tube materials were cut to rectangular shapes ($1.5 \times 0.5 \text{ cm}$ for pure chitosan, eADF4(C16)-RGD-chitosan and eADF4(C16) aligned fiber mat-chitosan tubes and $1.5 \times 1 \text{ cm}$ for chitosan tubes filled with the collagen cryogel), and the film thickness was determined to be $29.7 \pm 3.0 \mu\text{m}$ [49]. These samples were allowed to roll in PC-12 cell suspension ($10,000 \text{ cells ml}^{-1}$) to entrap the cells. In the case of the cryogel, the gel was first soaked in cell suspension and then applied on a chitosan film, which smoothly rolled around it. Collagen-coated cell culture plates were used as a positive control. After one day of culture, the medium was changed to differentiation medium. The differentiation medium was refreshed every two days. On day 7, cells were immunostained as described previously and analyzed using a wide field fluorescence microscope (Leica DMi8), and the images were processed using the software LAS X 3.6.0 by adjusting the brightness and the contrast. Z-stacks in combination with

the maximal projection mode were used to analyze all 3D samples. Importantly, cryogels were cut to slices giving a thickness of 1–3 cell layers (corresponding to 10–36 μm) and put on a glass slide covered with a coverslip to observe, whether adhered and differentiated cells could be found throughout all layers. Neurite length was determined by measuring neurites of nerve cells grown on each type of surface using ImageJ. The neurites were traced starting from their extrusion point from the cell body to the neurite's outer end, and this line was subsequently measured with the 'Measure' tool in ImageJ (collagen coating: 425 neurites, eADF4(C16)-RGD-coated tubes: 135 neurites, eADF4(C16) anisotropic non-woven mat tubes: 231 neurites, collagen cryogel in tube: 248 neurites). Then, the percentage of neurites was determined in each 10 μm length segment (0–10, 11–20, 21–30, and so on). Further, the number of cells in the images was counted using ImageJ 'Multi-point' modus to determine the neurite length per cell.

3. Results and discussion

3.1. Fabrication and characterization of NGCs

All NGC variants exhibited a tubular structure because of the used self-rolling chitosan film. The self-rolling mechanism has been recently described in Aigner and Scheibel [49] where the tubes were used as enzyme-reaction containers. The tubes could be prepared with various lengths (up to 10 cm), were stable between pH 3 and 11 and exhibited diffusion permeability with a molecular weight cutoff of 20,000 g mol⁻¹, which enables influx of nutrients, as well as gas exchange and metabolite removal. The self-rolling property of the chitosan film allowed an easy modification with other films or structured materials, the gentle and homogenous encapsulation of cells during rolling and, in principle, the

adaption of the tube size to the nerve ends or filler material.

To test the applicability of the self-rolling chitosan-based tubes for nerve regeneration, three variants of inner tube materials were tested to yield NGCs. An overview of the three NGC variants is schematically depicted in Fig. 1. Setup 1 used a hollow tube with an inner film coating made of the spider silk variant eADF4(C16)-RGD to provide a surface, where cells can efficiently adhere to; setup 2 used a hollow tube with an inner surface made of an anisotropic eADF4(C16) non-woven mat to provide a structure, where cells can adhere to and align on; setup 3 used a tube filled with a collagen cryogel with an anisotropic lamellar structure allowing cell adhesion and alignment. The first two NGCs (setups 1 and 2) possessed quasi-irreversible physical connection between the tube and the modifying materials. On the contrary, the collagen cryogel structure (setup 3) was not strongly connected to the chitosan tube, due to the processing conditions.

Upon fabrication of setups 1 and 2, rolling was induced by incubating the modified chitosan sheets with a PC-12 nerve cell suspension. For the preparation of setup 3, the cryogel was soaked in the PC-12 suspension and subsequently transferred onto the chitosan sheet, whereby immediate rolling of the sheet occurred and the encapsulation of the cryogel with cells was accomplished. The PC-12 cells were entrapped without applying mechanical stress, and they differentiated to form neurites, which has been previously shown to be crucial for peripheral nerve repair [53].

Fig. 2a,A shows the cross-section of a plain chitosan tube, and in Fig. 2a,B, the inner surface topography is presented. The chitosan tube soaked in PBS exhibited high transparency (Fig. 2a,C). Modifying the chitosan inner tube wall with an eADF4(C16)-RGD film yielded bio-functionalization, which was not visible in the cross-section because of its low thickness (Fig. 2b,A). In the particular case, the poor solubility of the

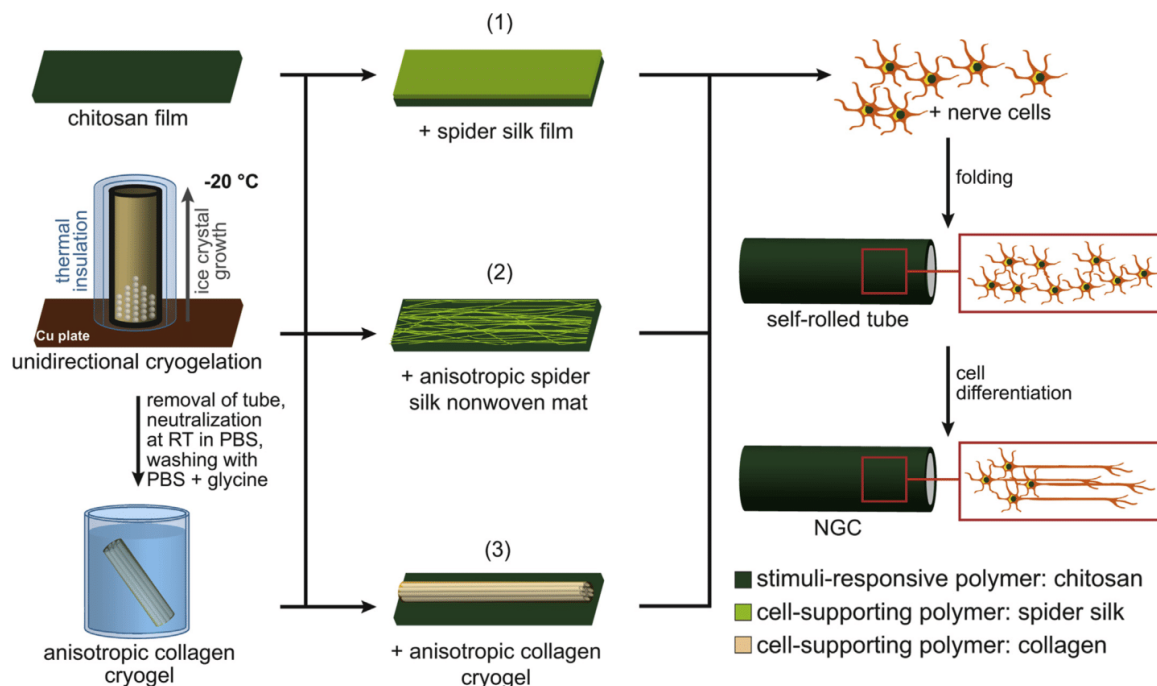


Fig. 1. Nerve guidance conduit (NGC) fabrication. Chitosan sheets were modified by either (1) a film on top of the inner wall made of the recombinant spider silk protein eADF4(C16)-RGD, (2) a layer of an anisotropic non-woven mat on top of the inner wall made of the recombinant spider silk protein eADF4(C16), or (3) an anisotropic collagen cryogel filling the inner volume of the tube. The collagen cryogel was produced using unidirectional cryogelation at -20 °C, followed by thawing, solvent neutralization, and several washing steps. The various NGC precursor constructs were placed in a PC-12 nerve cell suspension inducing self-rolling of the chitosan film used as the outer layer, and thereby encapsulated the cells, which had then the possibility to differentiate.

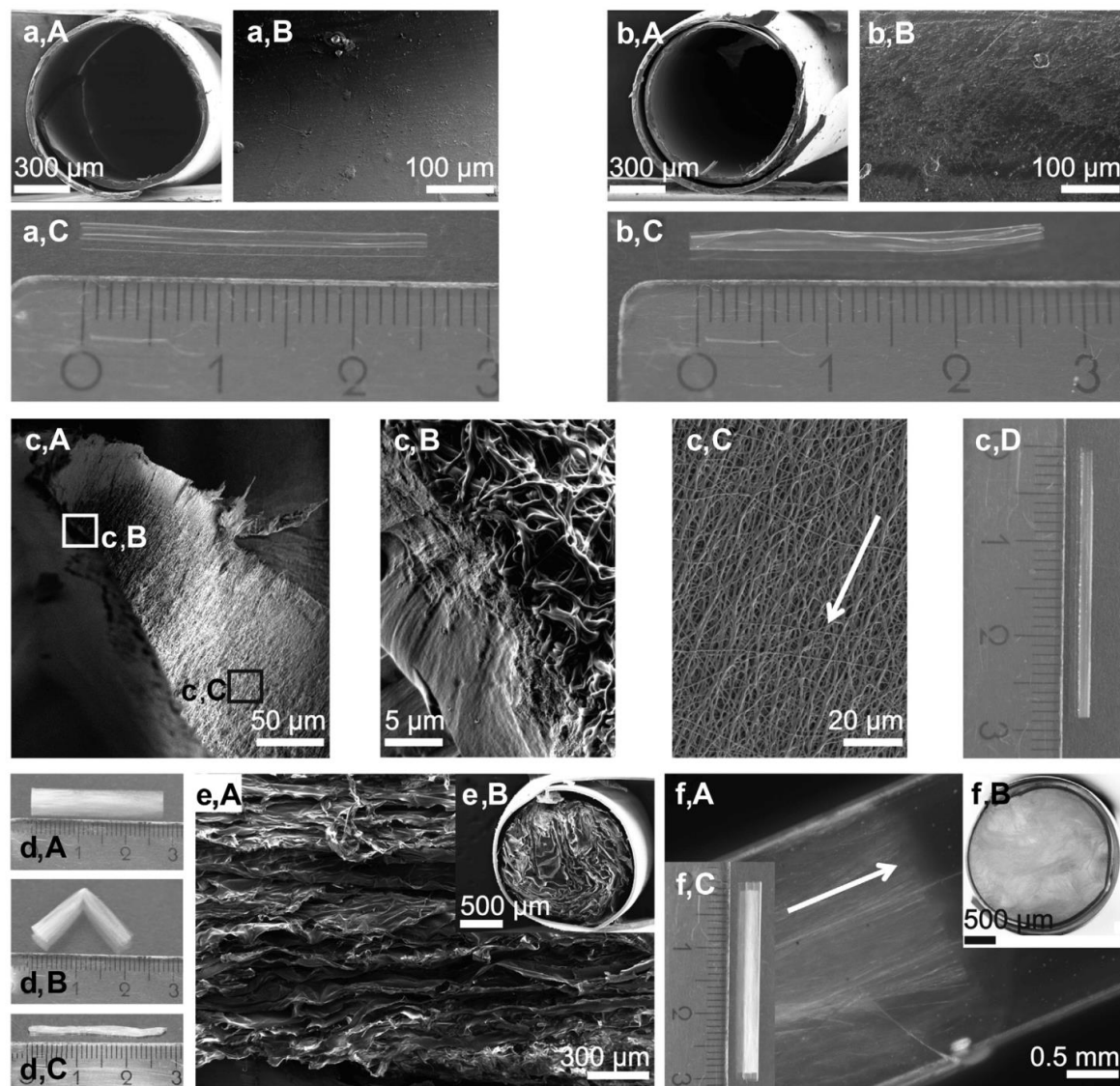


Fig. 2. Morphological characterization of NGCs. (a) (A) Scanning electron microscopy (SEM) image of the cross-section of the self-rolled chitosan tube; (B) its inner surface topography; and (C) photograph showing the whole tube after self-rolling in PBS. (b) (A) SEM image of the cross-section of the chitosan tube coated with eADF4(C16)-RGD on the inner surface (not visible here); (B) of the resulting inner surface topography; and (C) photograph showing the whole tube after self-rolling in PBS. (c) (A) SEM image of a chitosan tube comprising an inner lining with an anisotropic non-woven mat made of eADF4(C16); (B) magnified image of (c) (A) (white box): The chitosan tube and the non-woven mat are physically connected because of the processing conditions. (c) (C) Magnified image of (c) (A) (black box): The eADF4(C16) non-woven nanofibers were deposited on the chitosan inner surface in an anisotropic manner (the white arrow indicates the direction of nanofiber orientation). (c) (D) Photograph showing the whole tube after self-rolling in PBS. (d) (A) Photograph of a collagen cryogel stored in PBS; (B) Bending of the collagen cryogel in PBS resulted in a sharp bending edge indicating its anisotropic character; and (C) PBS removal from a collagen cryogel yielded a significant volume reduction. (e) (A) SEM image of a freeze-dried collagen cryogel and (B) its cross-section in the chitosan tube. (f) (A) Stereo microscopy image of the anisotropic collagen cryogel within a chitosan tube and (B) of its cross-section; (C) photograph of the chitosan tube filled with the anisotropic collagen cryogel. NGCs, nerve guidance conduits; PBS, phosphate buffered saline.

post-treated eADF4(C16)-RGD film at low pH values, compared with other biopolymers such as collagen, prevented its resolubilization when the acidic chitosan solution was cast thereon during fabrication. The eADF4(C16)-RGD layer exhibited a smooth surface topography (Fig. 2b,B). Owing to the preparation procedure of the bilayer, the

eADF4(C16)-RGD layer was physically cross-linked with the chitosan layer [49]. This bilayer tube was slightly turbid (Fig. 2b,C) compared with the plain chitosan tube.

The second NGC variant had an anisotropic non-woven mat as a cell guiding element on the inner tube wall (Fig. 2c,A). Owing to the post-

treatment during tube fabrication, the chitosan surface was molten with the non-woven mat preventing delamination (Fig. 2c,B). The silk fibers with diameters ranging from 0.5 to 1.0 μm were longitudinally oriented (Fig. 2c,C) because of the processing condition (Section 2.3) and led to slight turbidity of the tube (Fig. 2c,D). Importantly, the low thickness of both, the spider silk film and the non-woven mat, was negligible in comparison with that of the chitosan layer. Therefore, no differences in the rolling behavior and only minuscule differences in bilayer thickness were observed (data not shown).

The third NGC was fabricated slightly differently: the tubular collagen cryogels were stored in PBS buffer, transferred to the PC-12 cell suspension, and enclosed with the self-rolling chitosan film. Upon bending the tubular cryogels, sharp edges appeared indicative of having anisotropic features within this material (Fig. 2d,A and B). The bending was observed to be fully reversible. Furthermore, removing all unbound water showed the high water absorption capacity of the collagen cryogels (Fig. 2d,C). The water content of the collagen cryogels, when fully soaked in PBS, was determined to be 90.7 ± 1.4% (w/w). Accordingly, the collagen cryogels showed an 11-fold volume increase during swelling. A closer look onto the surface of freeze-dried collagen cryogels using SEM revealed longitudinally oriented structures (Fig. 2e,A), and a

lamellar structure could be observed in the cross-section (Fig. 2e,B). The anisotropic structure was well maintained after rolling (Fig. 2f,A), and the cryogel completely filled the chitosan tube lumen (Fig. 2f,B). Fig. 2f,C shows a photograph of the cryogel within the chitosan tube.

The chitosan films and the collagen cryogels were analyzed in wet/moist state using tensile testing. Because fully PBS-soaked collagen cryogels were observed to lose their unbound water during fixation, we removed the water in advance using a paper tissue, thereby ensuring a defined cross-sectional area for tensile property calculation. The tensile strength, maximum strain, and Young's modulus were determined to be 47 ± 17 MPa, 101 ± 24%, and 30 ± 13 MPa for wet chitosan films, and 0.15 ± 0.04 MPa, 70 ± 7%, and 0.22 ± 0.04 MPa for moist collagen cryogels, respectively, (values for rabbit tibial nerves are: 11.7 ± 0.7 MPa tensile strength and 38.5 ± 2% maximum strain [54]). Both the films and the cryogels showed large ramps of linear elastic deformation. In contrast to films, cryogels did not show a sharp material rupture but showed a gradual deformation after reaching the yield point (Supplementary Fig. S1). The deformation process of the cryogels continued up to 300% strain until no more force was detected. Importantly, the Young's modulus of the moist cryogels was in the range of that of peripheral nerve tissue (0.15–0.3 MPa) [55], presumably yielding a suitable environment for

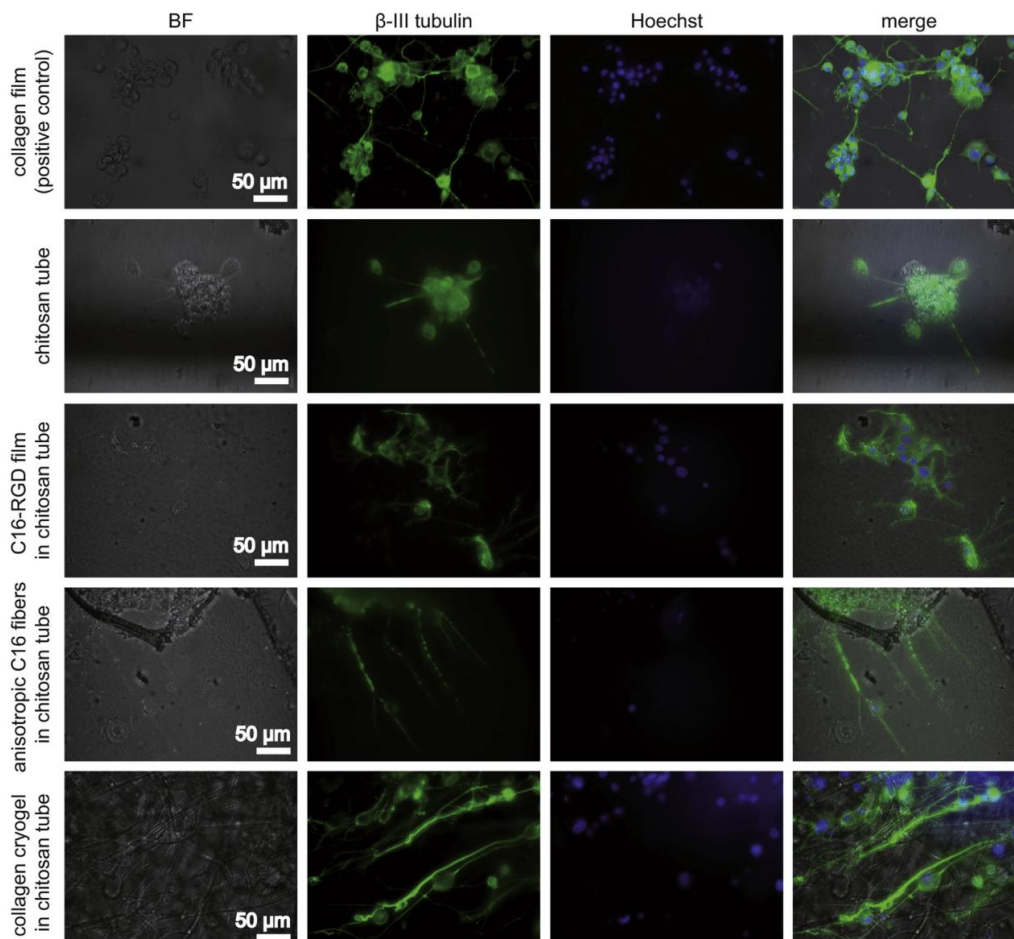


Fig. 3. Investigation of PC-12 nerve cell differentiation on all materials in tubes used in this study at day 7. A collagen film was used as a positive control for differentiation. Brightfield (BF) imaging showed the general material appearance; immunostaining against β-III tubulin (green) visualized the microtubule-forming protein present in differentiated neurons; Hoechst (blue) staining visualized cell nuclei. All images are at the same scale. C16, eADF4(C16)

nerve cells, while the chitosan film could provide stability during and after implantation, as well as structural integrity of the filler material and cells.

3.2. Differentiation of neuronal cells on individual materials

According to Orlowska et al. [56], attachment of PC-12 cells to polystyrene tissue culture flasks/plates is poor at laboratory conditions, and the cells form floating aggregates and grow in clusters [57]. Furthermore, this weak cell adhesion results in poor differentiation and insufficient levels of neurite outgrowth [57]. In agreement with Kleinman et al. [58], we therefore used collagen type I to coat the surface of our plates, yielding improved PC-12 cell attachment. Consequently, this coating was used as a positive control in our experiments. The suitability of the three different tube modifications in terms of PC-12 nerve cell adhesion was first investigated on plain materials individually. As it is shown in Supplementary Fig. S2, PC-12 cells equivalently adhered on a collagen film (positive control), an eADF4(C16)-RGD film, an eADF4(C16) spider silk non-woven mat, and on an anisotropic collagen cryogel. We did not observe any differences in terms of cell attachment or floating aggregates between these samples in comparison with the positive control within 7 days of culture.

PC-12 cells further possess the ability to differentiate upon lowering the serum content and adding NGFs [59]. This factor helps to protect neurons against camptothecin, serum deprivation, and etoposide-induced cell death. PC-12 cells offer advantages in comparison with cultured primary cortical neurons, including the ability to differentiate and show neurite formation. Studies have shown that a specific signaling pathway including the mitogen-activated protein kinase is the major mediator of PC-12 differentiation in response to NGFs. However, more signaling pathways are activated by the NGF, which is reviewed in

detail [60]. Therefore, in a second experiment, the growth medium was exchanged with differentiation medium on day 2, and cells were then monitored for seven days. Since the specific doubling time of these nerve cells is 48 h [52], they were first given time to adhere to the surface without proliferation before initiating differentiation. Cells were immunostained for β -III tubulin expression, which is a microtubule-forming protein produced in the early differentiation phase of neuronal cells [61]. On all substrates, the majority of the cells differentiated as indicated by the formation of neurites (Supplementary Fig. S3). Although cells on eADF4(C16)-RGD films showed only few and short neurites, the positive β -III tubulin staining confirmed that the cells started to differentiate. Both, the collagen film and the eADF4(C16) non-woven mat showed clear neurite outgrowth. Remarkably, nerve cells cultured and differentiated on collagen cryogels showed a high number of neurites, which were aligned with the underlying structures and they were interacting with other neurites forming bundles (Supplementary Fig. S4).

3.3. Entrapment of neuronal cells in NGCs

PC-12 cells were entrapped in the self-rolling NGCs by allowing the rolling process to occur directly in cell suspension. Thereby, the cells were distributed homogeneously throughout the tube and they were subsequently induced to differentiate for seven days (Fig. 3). Pure chitosan tubes showed poor cell adhesion, and aggregated cell clusters indicated that chitosan tubes did not promote effective cell adhesion. In contrast, chitosan tubes modified with an eADF4(C16)-RGD film coating showed good cell adhesion and isotropic neurite outgrowth similar to that on collagen films (Figs. 3 and 4A, B) because no guidance cue was provided in both cases. Chitosan tubes lined with anisotropic eADF4(C16) non-woven mats yielded adhered and differentiated PC-

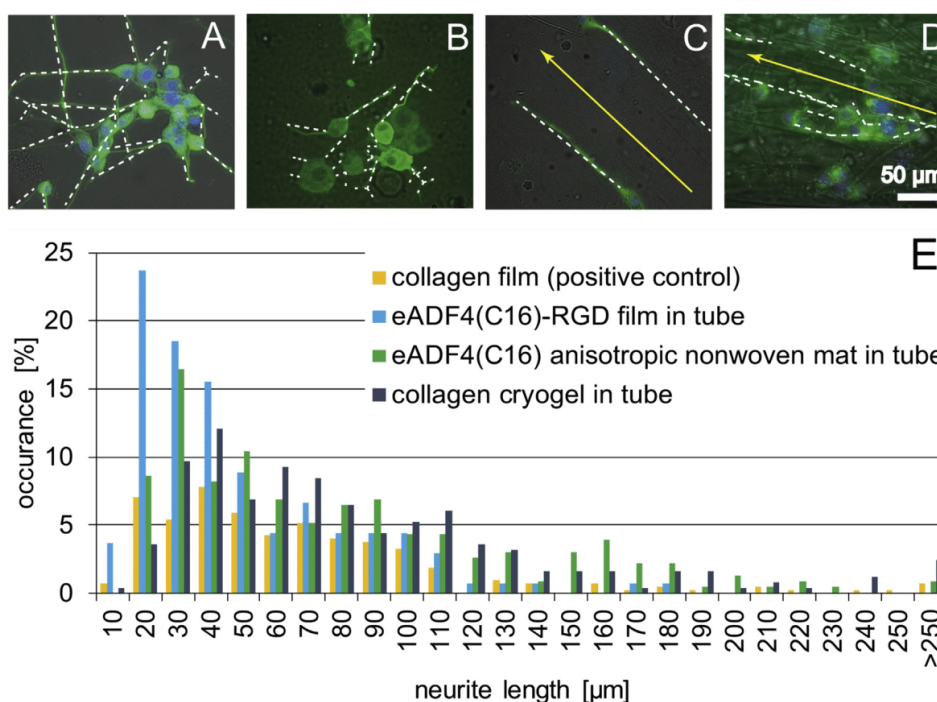


Fig. 4. Analysis of neurite lengths grown on the materials used in this study. Neurites are marked with white lines to highlight their direction of outgrowth. (A) On a collagen film (positive control) and (B) on an eADF4(C16)-RGD film, neurites grew isotropically, whereas (C) an anisotropic eADF4(C16) non-woven mat and (D) an anisotropic collagen cryogel allowed guidance of neurites into longitudinal direction. Yellow arrows indicate the orientation of anisotropic structures observed in the eADF4(C16) non-woven mat and in the collagen cryogel. (E) Neurite length distribution as detected on the materials used.

12 cells, which aligned with the nanofibers (Figs. 3 and 4C). The anisotropic collagen cryogels also allowed PC-12 cell adhesion and differentiation, and neurites followed their longitudinally oriented structure (Figs. 3 and 4D). To image the cells within the cryogels, they were cut into slices. The presence of cells within the interior of the cryogel confirmed that cells were able to migrate into the lamellar structures and that they spread their neurites longitudinally within the cryogels. Moreover, it can be assumed that sufficient perfusion of nutrients, oxygen, and waste metabolites throughout the cryogel supported the viability and differentiation of the cells. The spreading of long and parallel neurites within the lamellar structures of the cryogels is depicted in Fig. 3 and Fig. S4.

Next, neurite lengths were measured and the quantitative distribution of their lengths was determined. Therein, '10 μm ' includes all neurites with a length ranging from 0 to 10 μm , '20 μm ' includes all neurites with a length between 10 and 20 μm , and so on (Fig. 4E). NGCs comprising either an anisotropic eADF4(C16) non-woven mat or a collagen cryogel, as well as the collagen film (positive control) promoted outgrowth of neurites with lengths exceeding 250 μm . However, the longest neurites in the NGCs with an eADF4(C16)-RGD film were shown to have a length of 180 μm . Further, it could be observed that NGCs modified with an eADF4(C16)-RGD film showed the highest occurrence of neurite length in the range of 10–20 μm and, therefore, seemed to lead to the shortest neurites in this test. The chitosan tube with aligned eADF4(C16) non-woven mats peaked at 20–30 μm neurite length. The collagen film and constructs comprising the collagen cryogel exhibited most neurites at a length of 30–40 μm , hence, double the length as observed in eADF4(C16)-RGD-modified constructs. Most of the neurites longer than 250 μm were found in the collagen cryogel, which is remarkable, because the neurites in these samples could only be determined in a thin z-layer. Therefore, it can be assumed that the actual neurite length could be even longer.

To determine neurite length per cell, the number of cells in each image was counted. Cells on collagen films showed an average neurite length of 16 μm , 19 μm on eADF4(C16)-RGD films within a tube, 34 μm on eADF4(C16) anisotropic non-woven mats within a tube, and 47 μm on collagen cryogels within tube. This result further indicates the suitability of collagen cryogels encapsulated in self-rolled tubes as a promising candidate serving as an NGC.

4. Conclusions

Self-rolling tubes made of chitosan are beneficial for designing NGCs, because they enable gentle encapsulation of neuronal cells and the dedicated modification of the inner tube wall or its lumen with supporting materials, such as a bioactive recombinant spider silk film, an anisotropic recombinant spider silk non-woven mat, or an anisotropic collagen cryogel. All tube modifications were shown to be functional concerning enhancement of nerve cell attachment and differentiation. Anisotropic non-woven mats and collagen cryogels even supported guidance of neurites. This *in vitro* study opens the road toward *in vivo* studies to demonstrate the feasibility of the individual NGC or even combinations thereof and if the self-rolling properties of the NGCs will support the surgical procedure.

Author contributions

Tamara B. Aigner: Funding acquisition, Conceptualization, Methodology, Validation, Formal analysis, Investigation, Data curation, Writing - Original draft, Writing - Review and Editing, Visualization. Christian Hayn: Conceptualization, Methodology, Validation, Formal analysis, Investigation, Data curation, Writing - Original draft, Writing - Review and Editing, Visualization. Sahar Salehi: Funding acquisition, Conceptualization, Methodology, Validation, Writing - Review and Editing, Visualization. Andrea O'Connor: Funding acquisition, Writing & Editing. Thomas Scheibel: Supervision, Funding acquisition, Writing - Review & Editing.

Funding

This work was supported by the Bavarian Research Foundation (DOK-175-15, to T.B.A.). The authors would like to thank the Deutsche Forschungsgemeinschaft (DFG) project-number 326998133 - TRR 225 (project B03 to S.S. and C01 to T.S.) and Grant N. SA 3575/1-1 (to S.S.). The authors further acknowledge financial support by the German Academic Exchange service (DAAD) through its Thematic Melbourne-Bayreuth Polymer/Colloid Network sponsored from funds of the Federal Ministry of Education and Research (BMBF).

Declaration of competing interest

The authors declare that they have no known competing financial interests or personal relationships that could have appeared to influence the work reported in this paper.

Acknowledgments

The authors would like to thank Dr. Hendrik Bargel for scanning electron microscopy imaging, Carolin Grill for help with electrospinning, and Johannes Diehl for fermentation and protein purification.

Appendix A. Supplementary data

Supplementary data to this article can be found online at <https://doi.org/10.1016/j.mtbio.2020.100042>.

References

- [1] L.R. Robinson, Traumatic injury to peripheral nerves, *Muscle Nerve* 23 (6) (2000) 863–873.
- [2] W. Daly, L. Yao, D. Zeugolis, A. Windebank, A. Pandit, A biomaterials approach to peripheral nerve regeneration: bridging the peripheral nerve gap and enhancing functional recovery, *J. R. Soc. Interface* 9 (67) (2012) 202–221.
- [3] A. Magaz, A. Faroni, J.E. Gough, A.J. Reid, X. Li, J.J. Blaker, Bioactive silk-based nerve guidance conduits for augmenting peripheral nerve repair, *Adv. Healthc. Mater.* 7 (23) (2018) 1800308.
- [4] E.G. Fine, I. Decosterd, M. Papaliozios, A.D. Zurn, P. Aebischer, GDNF and NGF released by synthetic guidance channels support sciatic nerve regeneration across a long gap, *Eur. J. Neurosci.* 15 (4) (2002) 589–601.
- [5] G. Lundborg, L.B. Dahlin, N. Danielsen, R.H. Gelberman, F.M. Longo, H.C. Powell, et al., Nerve regeneration in silicone chambers: influence of gap length and of distal stump components, *Exp. Neurol.* 76 (2) (1982) 361–375.
- [6] N.P. Patel, K.A. Lyon, J.H. Huang, An update-tissue engineered nerve grafts for the repair of peripheral nerve injuries, *Neural Regen. Res.* 13 (5) (2018) 764–774.
- [7] W.Z. Ray, S.E. Mackinnon, Management of nerve gaps: autografts, allografts, nerve transfers, and end-to-side neurotaphy, *Exp. Neurol.* 223 (1) (2010) 77–85.
- [8] A. Berger, H. Millei, Nerve grafting, *Clin. Orthop. Relat. Res.* 133 (1978) 49–55.
- [9] A.M. Ghaznavi, L.E. Kokai, M.L. Lovett, D.L. Kaplan, K.G. Marra, Silk fibroin conduits: a cellular and functional assessment of peripheral nerve repair, *Ann. Plast. Surg.* 66 (3) (2011) 273–279.
- [10] S.K. Lee, S.W. Wolfe, Peripheral nerve injury and repair, *JAAOS - J. Am. Acad. Orthop. Surg.* 8 (4) (2000) 243–252.
- [11] P.A. Wieringa, A.R. Goncalves De Pinho, S. Micera, R.J.A. Van Wezel, L. Moroni, Biomimetic architectures for peripheral nerve repair: a review of biofabrication strategies, *Adv. Healthc. Mater.* 7 (8) (2018), e1701164.
- [12] W.A. Lackington, A.J. Ryan, F.J. O'Brien, Advances in nerve guidance conduit-based therapeutics for peripheral nerve repair, *ACS Biomater. Sci. Eng.* 3 (7) (2017) 1221–1235.
- [13] G.C.W. De Ruitter, M.J.A. Malessy, M.J. Yaszemski, A.J. Windebank, R.J. Spinner, Designing ideal conduits for peripheral nerve repair, *Neurosurg. Focus* 26 (2) (2009), E5–E5.
- [14] S. Kehoe, X.F. Zhang, D. Boyd, FDA approved guidance conduits and wraps for peripheral nerve injury: a review of materials and efficacy, *Injury* 43 (5) (2012) 553–572.
- [15] T.M.A. Henderson, K. Ladewig, D.N. Haylock, K.M. Mclean, A.J. O'Connor, Cryogels for biomedical applications, *J. Mater. Chem. B* 1 (21) (2013) 2682–2695.
- [16] T.M. Henderson, K. Ladewig, D.N. Haylock, K.M. Mclean, A.J. O'Connor, Formation and characterisation of a modifiable soft macro-porous hyaluronic acid cryogel platform, *J. Biomater. Sci. Polym. Ed.* 26 (13) (2015) 881–897.
- [17] D. Arslantunali, T. Dursun, D. Yucel, N. Hasirci, V. Hasirci, Peripheral nerve conduits: technology update, *Med. Devices (Auckl)* 7 (2014) 405–424.
- [18] G. Koopmans, B. Hasse, N. Sinis, The role of collagen in peripheral nerve repair, *Int. Rev. Neurobiol.* 87 (2009) 363–379.

- [19] T. Ushiki, C. Ide, Three-dimensional organization of the collagen fibrils in the rat sciatic nerve as revealed by transmission- and scanning electron microscopy, *Cell Tissue Res.* 260 (1) (1990) 175–184.
- [20] A. Sorushanova, L.M. Delgado, Z.N. Wu, N. Shologu, A. Kshirsagar, R. Raghunath, et al., The collagen suprafamily: from biosynthesis to advanced biomaterial development, *Adv. Mater.* 31 (1) (2019), 1801651.
- [21] K.L. Lin, D.W. Zhang, M.H. Macedo, W.G. Cui, B. Sarmiento, G.F. Shen, Advanced collagen-based biomaterials for regenerative biomedicine, *Adv. Funct. Mater.* 29 (3) (2019) 1804943.
- [22] R.C. Goy, S.T.B. Morais, O.B.G. Assis, Evaluation of the antimicrobial activity of chitosan and its quaternized derivative on *E. coli* and *S. aureus* growth, *Rev. Bras. de Farmacogn.* 26 (1) (2016) 122–127.
- [23] M. Rinaudo, Chitin and chitosan: properties and applications, *Prog. Polym. Sci.* 31 (7) (2006) 603–632.
- [24] D.P. Biswas, P.A. Tran, C. Tallon, A.J. O'connor, Combining mechanical foaming and thermally induced phase separation to generate chitosan scaffolds for soft tissue engineering, *J. Biomater. Sci. Polym. Ed.* 28 (2) (2017) 207–226.
- [25] M.J. Simoes, A. Gartner, Y. Shirotsaki, R.M. Gil Da Costa, P.P. Cortez, F. Gartner, et al., In vitro and in vivo chitosan membranes testing for peripheral nerve reconstruction, *Acta Med. Port.* 24 (1) (2011) 43–52.
- [26] Q. Guo, C. Liu, B. Hai, T. Ma, W. Zhang, J. Tan, et al., Chitosan conduits filled with simvastatin/Pluronic F-127 hydrogel promote peripheral nerve regeneration in rats, *J. Biomed. Mater. Res. B Appl. Biomater.* 106 (2) (2018) 787–799.
- [27] T.A. Blackledge, C.Y. Hayashi, Silken toolkits: biomechanics of silk fibers spun by the orb web spider *Argiope argentata* (Fabricius 1775), *J. Exp. Biol.* 209 (13) (2006) 2452–2461.
- [28] F. Vollrath, D. Porter, Spider silk as archetypal protein elastomer, *Soft Matter* 2 (5) (2006) 377–385.
- [29] C. Radtke, C. Allmeling, K.H. Waldmann, K. Reimers, K. Thies, H.C. Schenk, et al., Spider silk constructs enhance axonal regeneration and remyelination in long nerve defects in sheep, *PLoS One* 6 (2) (2011), e16990.
- [30] C. Allmeling, A. Jokuszies, K. Reimers, S. Kall, C.Y. Choi, G. Brandes, et al., Spider silk fibres in artificial nerve constructs promote peripheral nerve regeneration, *Cell Prolif* 41 (3) (2008) 408–420.
- [31] K. Schacht, T. Scheibel, Processing of recombinant spider silk proteins into tailor-made materials for biomaterials applications, *Curr. Opin. Biotechnol.* 29 (2014) 62–69.
- [32] M. Lewicka, O. Hermanson, A.U. Rising, Recombinant spider silk matrices for neural stem cell cultures, *Biomaterials* 33 (31) (2012) 7712–7717.
- [33] B. An, M.D. Tang-Schomer, W.W. Huang, J.Y. He, J.A. Jones, R.V. Lewis, et al., Physical and biological regulation of neuron regenerative growth and network formation on recombinant dragline silks, *Biomaterials* 48 (2015) 137–146.
- [34] K. Pawar, G. Welzel, C. Haynl, S. Schuster, T. Scheibel, Recombinant spider silk and collagen-based nerve guidance conduits support neuronal cell differentiation and functionality in vitro, *ACS Appl. Bio Mater.* 2 (11) (2019) 4872–4880.
- [35] T.B. Aigner, E. Desimone, T. Scheibel, Biomedical applications of recombinant silk-based materials, *Adv. Mater.* 30 (19) (2018), e1704636.
- [36] K. Schacht, T. Jüngst, M. Schweinlin, A. Ewald, J. Groll, T. Scheibel, Biofabrication of cell-loaded 3D spider silk constructs, *Angew. Chem. Int. Ed.* 54 (9) (2015) 2816–2820.
- [37] K. Schacht, J. Vogt, T. Scheibel, Foams made of engineered recombinant spider silk proteins as 3D scaffolds for cell growth, *ACS Biomater. Sci. Eng.* 2 (4) (2016) 517–525.
- [38] A. Leal-Egana, G. Lang, C. Mauerer, J. Wickinghoff, M. Weber, S. Geimer, et al., Interactions of fibroblasts with different morphologies made of an engineered spider silk protein, *Adv. Eng. Mater.* 14 (3) (2012) B67–B75.
- [39] C.B. Borkner, S. Wohlrab, E. Möller, G. Lang, T. Scheibel, Surface modification of polymeric biomaterials using recombinant spider silk proteins, *ACS Biomater. Sci. Eng.* 3 (5) (2017) 767–775.
- [40] C.B. Borkner, M.B. Elsner, T. Scheibel, Coatings and films made of silk proteins, *ACS Appl. Mater. Interfaces* 6 (18) (2014) 15611–15625.
- [41] E. Desimone, K. Schacht, A. Pellert, T. Scheibel, Recombinant spider silk-based bioinks, *Biofabrication* 9 (4) (2017), 044104.
- [42] D. Steiner, G. Lang, L. Fischer, S. Winkler, T. Fey, P. Greil, et al., Intrinsic vascularization of recombinant eADF4(C16) spider silk matrices in the arteriovenous loop model, *Tissue Eng. Part A* (2019) 1504–1513.
- [43] P.H. Zeplin, N.C. Maksimovikj, M.C. Jordan, J. Nickel, G. Lang, A.H. Leimer, et al., Spider silk coatings as a bioshield to reduce periprosthetic fibrous capsule formation, *Adv. Funct. Mater.* 24 (18) (2014) 2658–2666.
- [44] P.H. Zeplin, A.K. Berninger, N.C. Maksimovikj, P. Van Gelder, T. Scheibel, H. Walles, Improving the biocompatibility of silicone implants using spider silk coatings: immunohistochemical analysis of capsule formation, *Handchir. Mikrochir. Plast. Chir.* 46 (6) (2014) 336–341.
- [45] T.I. Harris, D.A. Gaztambide, B.A. Day, C.L. Brock, A.L. Ruben, J.A. Jones, et al., Sticky situation: an investigation of robust aqueous-based recombinant spider silk protein coatings and adhesives, *Biomacromolecules* 17 (11) (2016) 3761–3772.
- [46] S. Müller-Herrmann, T. Scheibel, Enzymatic degradation of films, particles, and nonwoven meshes made of a recombinant spider silk protein, *ACS Biomater. Sci. Eng.* 1 (4) (2015) 247–259.
- [47] B. Zhu, W. Li, R.V. Lewis, C.U. Segre, R. Wang, E-spun composite fibers of collagen and dragline silk protein: fiber mechanics, biocompatibility, and application in stem cell differentiation, *Biomacromolecules* (2014) 202–213.
- [48] S. Wohlrab, S. Müller, A. Schmidt, S. Neubauer, H. Kessler, A. Leal-Egana, et al., Cell adhesion and proliferation on RGD-modified recombinant spider silk proteins, *Biomaterials* 33 (28) (2012) 6650–6659.
- [49] T. Aigner, T. Scheibel, Self-rolling refillable tubular enzyme containers made of recombinant spider silk and chitosan, *ACS Appl. Mater. Interfaces* 11 (17) (2019) 15290–15297.
- [50] G. Lang, Herstellung und Charakterisierung von Fasern aus rekombinanten Spinnenseidenproteinen und deren potentielle Applikationen, 2015. Dissertation, urn:nbn:de:hbz:703-epub-2038-3. (Accessed 15 July 2019).
- [51] L. Ionov, Soft microorigami: self-folding polymer films, *Soft Matter* 7 (15) (2011) 6786–6791.
- [52] ATCC, PC-12 (ATCC® CRL-1721™), 2016. <https://www.lgcstandards-atcc.org/products/all/CRL-1721.aspx?geo.country=de#specifications>. (Accessed 6 August 2019).
- [53] M. Sarker, S. Naghieh, A.D. McInnes, D.J. Schreyer, X. Chen, Strategic design and fabrication of nerve guidance conduits for peripheral nerve regeneration, *Biotechnol. J.* 13 (7) (2018), 1700635.
- [54] M.K. Kwan, E.J. Wall, J. Massie, S.R. Garfin, Strain, stress and stretch of peripheral nerve Rabbit experiments in vitro and in vivo, *Acta Orthop. Scand.* 63 (3) (1992) 267–272.
- [55] J.B. Scott, M. Afshari, R. Kotek, J.M. Saul, The promotion of axon extension in vitro using polymer-templated fibrin scaffolds, *Biomaterials* 32 (21) (2011) 4830–4839.
- [56] A. Orłowska, P.T. Perera, M. Al Kobaisi, A. Dias, H.K.D. Nguyen, S. Ghanaati, et al., The effect of coatings and nerve growth factor on attachment and differentiation of pheochromocytoma cells, *Materials (Basel)* 11 (1) (2017) 60.
- [57] D.G. Attiah, R.A. Kopher, T.A. Desai, Characterization of PC12 cell proliferation and differentiation-stimulated by ECM adhesion proteins and neurotrophic factors, *J. Mater. Sci. Mater. Med.* 14 (11) (2003) 1005–1009.
- [58] H.K. Kleinman, L. Luckenbill-Edds, F.W. Cannon, G.C. Sephel, Use of extracellular matrix components for cell culture, *Anal. Biochem.* 166 (1) (1987) 1–13.
- [59] N. Kinarivala, K. Shah, T.J. Abbruscato, P.C. Trippier, Passage variation of PC12 cells results in inconsistent susceptibility to externally induced apoptosis, *ACS Chem. Neurosci.* 8 (1) (2017) 82–88.
- [60] E.J. Huang, L.F. Reichardt, Trk receptors: roles in neuronal signal transduction, *Annu. Rev. Biochem.* 72 (1) (2003) 609–642.
- [61] M.A. Tischfield, H.N. Baris, C. Wu, G. Rudolph, L. Van Maldergem, W. He, et al., Human TUBB3 mutations perturb microtubule dynamics, kinesin interactions, and axon guidance, *Cell* 140 (1) (2010) 74–87.

Supplementary data

Nerve guidance conduit design based on self-rolling tubes

T.B. Aigner,^{a,&} C. Haynl,^{a,&} S. Salehi,^a A. O'Connor^b and T. Scheibel^{a,c,d,e,f,*}

^aUniversity of Bayreuth, Department of Biomaterials, Prof.-Rüdiger-Bormann-Str.1, 95447 Bayreuth, Germany

^bUniversity of Melbourne, Department of Biomedical Engineering, Melbourne, Victoria 3010, Australia

^cUniversity of Bayreuth, Bayreuther Zentrum für Kolloide und Grenzflächen (BZKG), Universitätsstraße 30, 95447 Bayreuth, Germany

^dUniversity of Bayreuth, Bayreuther Zentrum für Molekulare Biowissenschaften (BZMB), Universitätsstraße 30, 95447 Bayreuth, Germany

^eUniversity of Bayreuth, Bayreuther Materialzentrum (BayMAT), Universitätsstraße 30, 95447 Bayreuth, Germany

^fUniversity of Bayreuth, Bayerisches Polymerinstitut (BPI), Universitätsstraße 30, 95447 Bayreuth, Germany

To whom correspondence should be addressed: thomas.scheibel@bm.uni-bayreuth.de

[&]contributed equally

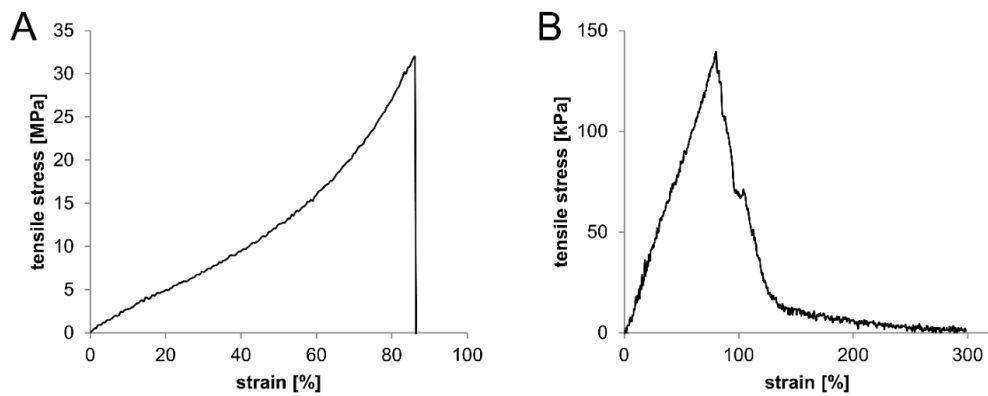


Fig. S1. Stress-strain plot of (A) a wet chitosan film used for fabricating self-rolling tubes and (B) a moist collagen cryogel.

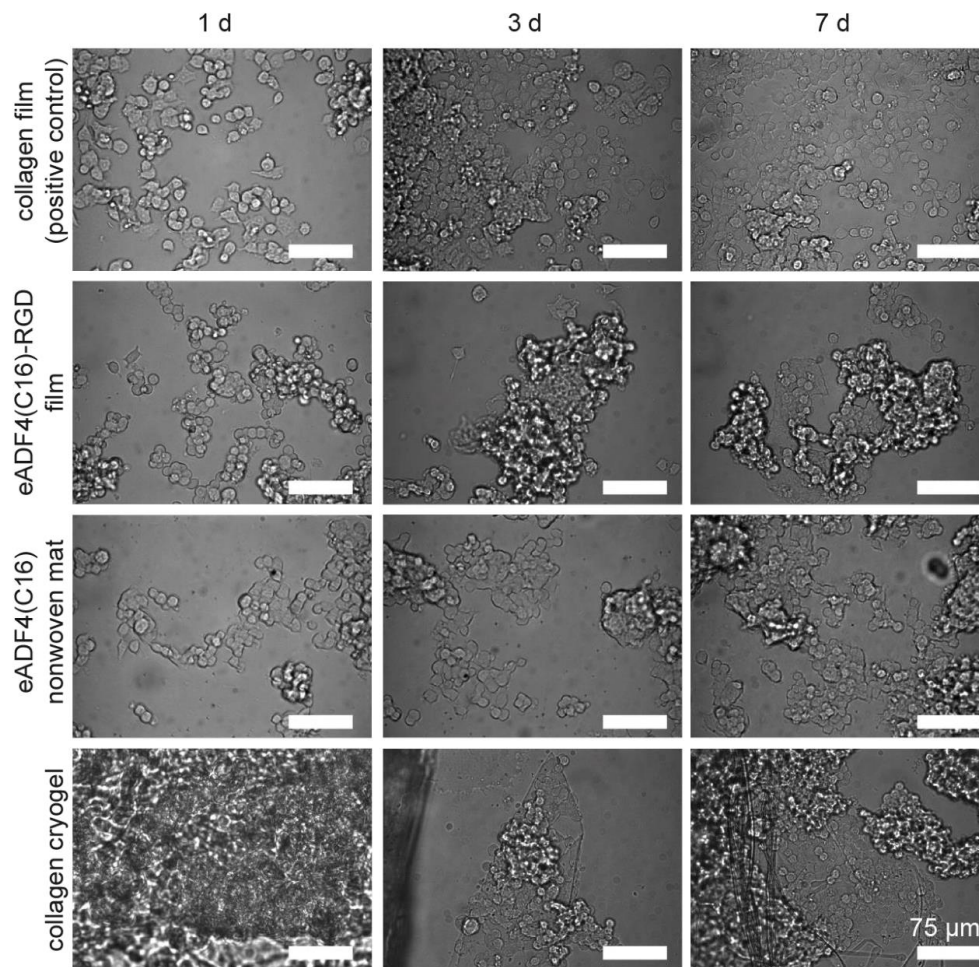


Fig. S2. Optical microscopy images showing adhesion of PC-12 cells on different substrates. Brightfield images of cells incubated in growth medium were taken after 1, 3 and 7 days to analyze cell adhesion on an eADF4(C16)-RGD film, an eADF4(C16) isotropic nonwoven mat and an anisotropic collagen cryogel in comparison to a collagen coating as the positive control. All scale bars correspond to 75 μm .

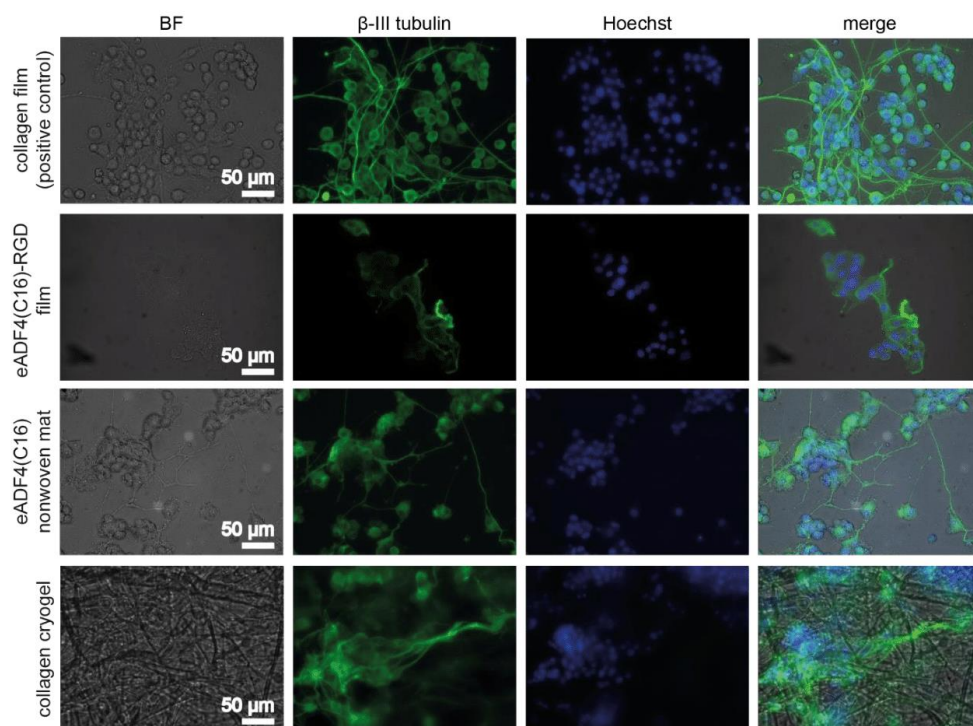


Fig. S3. PC-12 nerve cells on a collagen film (positive control), eADF4(C16)-RGD film, isotropic eADF4(C16) nonwoven mat and on an anisotropic collagen cryogel after 7 days of differentiation. Brightfield (BF) images show the surfaces of the films, nonwoven mat or the collagen cryogel. Immunostaining against β -III tubulin visualized the microtubule forming protein present in differentiated neurons, whereas Hoechst staining visualized cell nuclei.

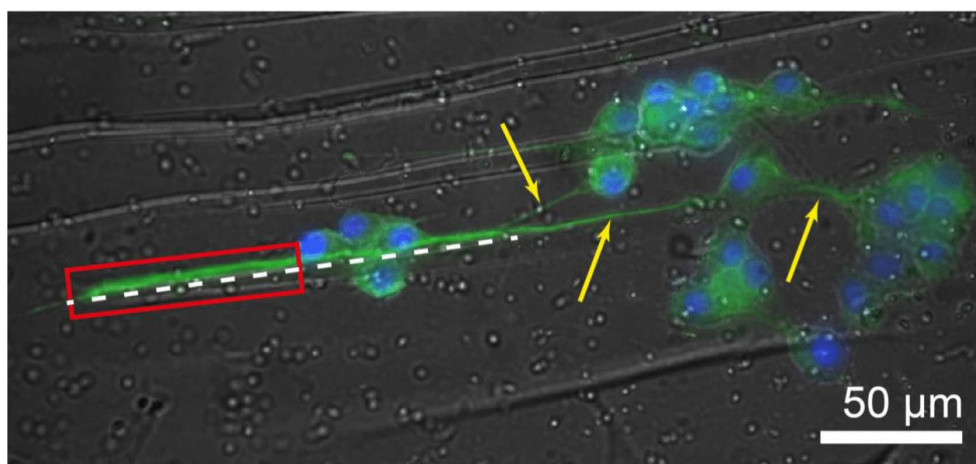


Fig. S4. PC-12 nerve cells on collagen cryogel forming bundle-like structures (red box) compared to single neurites (yellow arrows). The bundle-like structure is aligned with the collagen cryogel (dashed line).

Part 6. Self-rolling Tubular Structures made of Spider Silk and Chitosan as Enzyme Containers

Aigner, T. B.; Scheibel, T.

Published in ACS Applied Materials & Interfaces, 11, 17, 15290-15297

(2019)

Reprinted with kind permission from ACS Publications

Self-Rolling Refillable Tubular Enzyme Containers Made of Recombinant Spider Silk and Chitosan

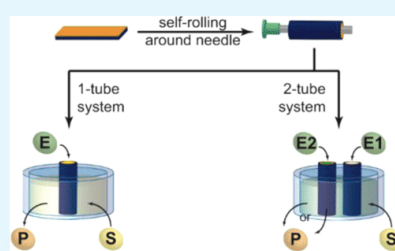
Tamara Aigner[†] and Thomas Scheibel^{*,†,‡,§,¶}

[†]Lehrstuhl Biomaterialien and [‡]Bayreuther Zentrum für Kolloide und Grenzflächen (BZKG), Bayreuther Zentrum für Bio-Makromoleküle (Bio-Mac), Bayreuther Zentrum für Molekulare Biowissenschaften (BZMB), Bayreuther Materialzentrum (BayMAT), Bayerisches Polymerinstitut (BPI), University Bayreuth, Universitätsstr. 30, 95447 Bayreuth, Germany

Supporting Information

ABSTRACT: Encapsulation of enzymes is often necessary to stabilize them against environmental conditions or to protect them from other harmful enzymes such as proteases. Here, a refillable spatial confinement system was produced using a fully degradable self-rolling biopolymer bilayer. The enzyme containers comprise spider silk and chitosan and enable one-pot reactions in the micro- to milliliter regime by trapping the enzyme inside the semipermeable tube and allow the substrate and/or product either to diffuse freely or to be entrapped. The tubes are stable toward several organic and aqueous solvents. A one-tube system with esterase-2 was used to establish the system. Further, a two-tube system was applied to mimic enzymatic cascades, where the enzymes have to be separated, because they, for example, inhibit each other. The entrapment mode was also tested in the two-tube system, which is beneficial for toxic products or for obtaining high concentrations of the desired product.

KEYWORDS: recombinant spider silk, layer-by-layer assembly, enzyme catalysis, microstructures, stimuli-responsive materials



1. INTRODUCTION

Nature is supposedly our best teacher, showing how to perform site-specific and enantiopure reactions using biocatalysts in an all-aqueous system at identical reaction conditions. In addition, all these reactions occur mainly in cells in our body, often in specific compartments thereof, in a one-pot reaction manner. The compartmentalization in cells helps to organize all reaction processes and further enhances their efficiency. Hence, it is not surprising that a lot of effort is put into the design of artificial catalyst systems mimicking or even improving the enzymatic arrangements found in nature to obtain high enantiopurity and chemical diversity, using time- and cost-effective one-pot synthesis.¹

One-pot synthesis allows to improve the efficiency and environmental sustainability of (bio)chemical reactions by circumventing the purification of intermediates and thereby minimizing waste and time.² In the context of sustainability, the use of renewable feedstock and environmentally friendly reagents and catalysts (i.e., enzymes) are inevitable components of establishing “green chemistry”.³ One-pot synthesis is especially very useful if an intermediate is unstable, toxic, or hazardous, or if there is an equilibrium between the educts and the intermediates, driving the reaction to completion by constant conversion of intermediates into products. In addition, if the side products themselves can be converted into products, or if subsequent reactions use the same reagents, one-pot synthesis is advantageous. Occurring problems are low yields, too many byproducts, and/or side products, as well as the lack of solvents allowing all reactions to take place

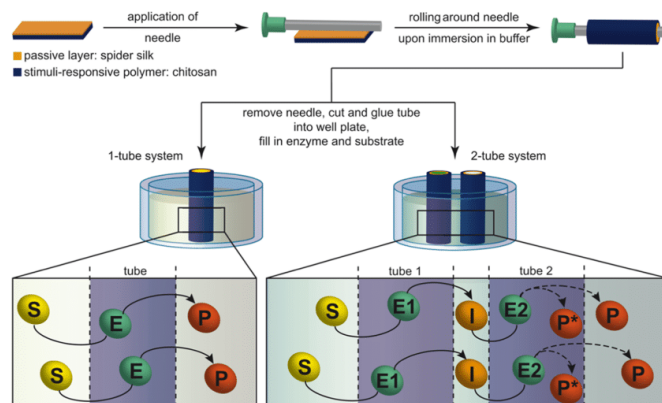
simultaneously or the removal of solvent for an exchange.² Enzymes as natural catalysts enable substrate selectivity and site specificity³ in an all-aqueous system at identical reaction conditions. These biocatalysts can lose their activity rather easily through alterations in their structure. Covalent alteration of enzymes often occurs during proteolysis or in contact with other reactive molecules, and structural changes can be induced for instance by change in temperature, solvent, pH, or mechanical forces. Therefore, several approaches, such as extraction of variants from extremophiles or biotechnological engineering of enzymes to enable protection via immobilization, enzyme PEGylation or other chemical modifications, or micro- and nanoencapsulation of the respective enzyme, have been developed to obtain stable enzymes.⁴

Volume-confined encapsulation systems comprise reverse micelles, i.e., formed by surfactants or ionic liquid emulsions,⁵ water-in-oil droplets, i.e., semipermeable capsules formed from amphiphilic molecules,^{6–9} vesicles, i.e., liposomes with biological bilayers,¹⁰ or polymersomes based on amphiphilic block copolymers,¹¹ protein cages, i.e., boundaries composed of proteins like virus capsids or prokaryotic microcompartments,¹² polymer capsules, i.e., polyelectrolytes forming a capsule using a layer-by-layer approach around a removable template,¹³ or arrays of small reaction vessels, i.e., obtained by chemical etching.¹⁴ All these systems are designed for yokto- to

Received: January 25, 2019

Accepted: March 29, 2019

Published: March 29, 2019

Scheme 1. Tube Preparation and Experimental Design^a

^aA bilayer of spider silk (passive layer) and chitosan (active layer) was prepared. A needle was applied as a template, and the bilayer rolled around it upon immersion in PBS. After drying, the needle was removed from the tube, which was cut and glued into a well plate. One tube was glued into the well to prepare a one-tube system (left) or two tubes for a two-tube system (right). The lower panel shows the possible reaction pathways: Enzymes (E, E1, and E2) are captured in the tubes, whereby the substrates (S), intermediates (I), and products (P) can diffuse freely across the membranes. Alternatively, products (P*) can be trapped inside the tube.

nanoliter volumes, and in most cases are closed and, thus, not (re-)fillable.

Here, spider silk and chitosan bilayers were used to generate tubular enzyme containers enabling easy-to-use one-pot reactions in the micro- to milliliter regime. The tubular structures were obtained by the preparation of a self-rolling bilayer. The principle behind this self-rolling mechanism is an inhomogeneous reaction of an inhomogeneous film or different layers of a film in response to an environmental stimulus.^{15,16} Commonly, the layers are termed as active and passive, where the active layer responds to the stimulus and thereby causes a change in the passive layer. In the case of a hard passive layer, wrinkles and creases are formed, whereas soft passive layers curl and roll to release the internal stress.^{15,17,18} Advantages are not only the controlled, quick, and reproducible fabrication but also the possibility to control the morphology and the chemical properties of the inner and outer surfaces of the constructs.^{16,18,19} Pioneering work in this field was done by Smela et al.²⁰ and Jager et al.,²¹ both of who utilized metal–polymer films responding to an electric signal. To transfer this principle to biomedical applications, a focus was laid on stimuli-responsive polymers responding to mild physical or chemical changes in their environment,²² like poly(*N*-isopropylacrylamide) derivatives^{16,23–30} or biodegradable polysuccinimide,¹⁹ gelatin³¹ or even silk.³²

The enzyme container system used in this work is accessible from its open top, through which, e.g., an enzyme solution can be applied and it shields the enzymes without the need of an otherwise necessary genetic modification or immobilization of the enzymes on solid carriers.³³ Although the enzyme is trapped inside the tubular container, its substrates and/or products can diffuse freely through the semipermeable engineered tube wall. With such a setup, sufficiently high local enzyme concentrations can be achieved without the need of total high amounts thereof. Further, enzyme cascades can be mimicked by either keeping the enzymes separate in different tubes, avoiding their contact, or putting them together into one tube.

2. RESULTS AND DISCUSSION

2.1. Tube Preparation.

The tubular containers are made of a self-rolling bilayer of recombinant spider silk protein and chitosan. Spider silk fibers are known for their high toughness and nontoxicity, and spider silk films have selective semipermeability.^{34–36} Chitosan is a cationic film-forming hydrating polysaccharide found to be not only nontoxic but also antimicrobial, especially against Gram-positive bacteria.^{37,38} If this polysaccharide film is subjected to an aqueous solution, it starts to swell, whereas the silk film does not significantly react at these conditions (see below). Thus, in a bilayer setup of these two components, rolling is induced. This self-rolling tubular system was prepared by a simple casting process without the need of adding cross-linkers,^{39–41} which could harm sensitive enzymes to be encapsulated.^{17–19,23–31,42} Further, due to the self-rolling process, an easy adjustment of container dimensions is possible.

Here, the bilayer from recombinant spider silk eADF4(C16) and chitosan was allowed to roll around a needle to adjust the inner diameter of the tube, whereby the silk formed the inner layer and chitosan the outer layer. The needle ensured tubes with controllable diameters after drying. Note that the needle was not required for the rolling process itself. This process takes less than 5 s. Scanning electron microscopy (SEM) images before and after rolling were taken and showed no apparent difference in surface topography (Figure S1). The bilayer possesses a thickness of $29.7 \pm 3.0 \mu\text{m}$ in dry and $56.5 \pm 4.3 \mu\text{m}$ in wet state, whereby it took up $250 \pm 20\%$ of its dry weight in water. The swelling degree of spider silk eADF4-(C16) films was determined to be $9.9 \pm 8.3\%$ by atomic force microscopy (AFM) analysis (Figure S2). Therefore, it can be concluded that the water uptake of the thin silk film can be neglected, and the determined water-induced swelling of the bilayer can be attributed to the chitosan layer. Mechanical properties of the single layers were already studied before by Wohlrab et al.,⁴³ Lintz et al.,⁴⁴ and Alekseeva et al.⁴⁵ The Young's modulus of eADF4(C16) films is 3.2 MPa ⁴⁴ and that of chitosan films is 7.06 MPa .⁴⁵ Once rolled, the tubes kept

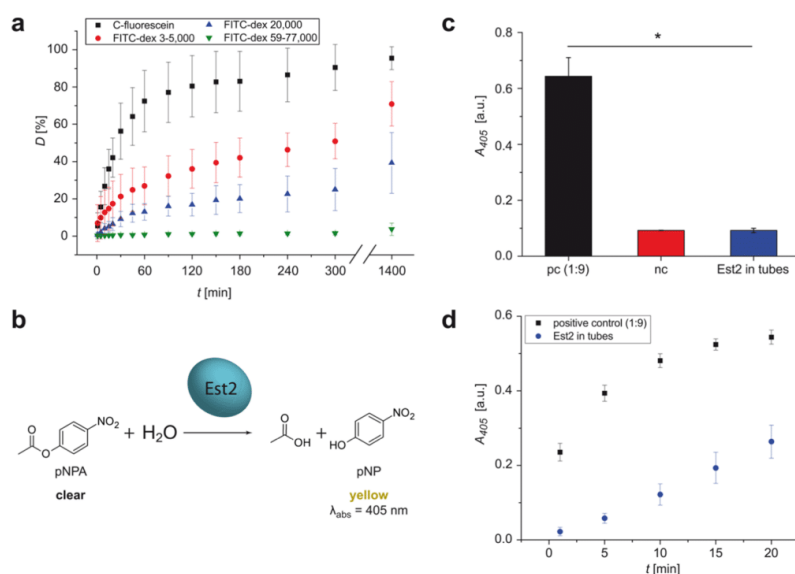


Figure 1. One-tube system. (a) Diffusion (D) test to determine the molecular weight cutoff of the tube wall using differently sized fluorescein derivatives (c-fluorescein = 5(6)-carboxyfluorescein and FITC-dex = fluorescein isothiocyanate-dextran with three different MW ranges as indicated). (b) Reaction mechanism of esterase-2 (Est2) catalyzed hydrolysis of *p*-nitrophenyl acetate (pNPA) yielding *p*-nitrophenyl (pNP) and acetate. (c) Est2 was retained inside the tubes. pc = positive control: Est2 + buffer; nc = negative control: plain buffer; Est2 in tube: Est2 in tubes + buffer in surrounding. After 15 min, the solutions were mixed with pNPA, allowed to react, and then absorbance (A) at 405 nm was measured; pc was diluted 1:9 to get $A < 1$ (statistics: t -test: $p < 0.05$). (d) pNP production observed via absorbance measurements. Positive control: Est2 in buffer + pNPA (diluted 1:9); Est2 in tubes: Est2 in tubes and buffer + pNPA in surrounding; negative control: buffer + pNPA (plain or 1:9) was subtracted from positive control and sample. The reaction rate depended on the diffusion rate.

their tubular shape, and no delamination of the bilayer was observed (Figure S1). This was achieved by two factors: (i) The used spider silk protein is negatively charged and chitosan is positively charged, allowing electrostatic interactions between the two layers. (ii) Since the chitosan film was cast on top of the silk film from an acidic solution, it presumably slightly roughened the silk surface by partial dissolution, enabling a tight connection.

Next, the stability of the tubes was analyzed in several organic and aqueous solvents at different pH values gravimetrically and by SEM (Figure S3). Both layers showed no apparent response to dimethylformamide (DMF), ethanol, and glycerol treatment. Dimethylsulfoxide (DMSO) caused wrinkling on the silk layer, and 5% hydrogen peroxide caused little disintegration on the chitosan layer. Silk was stable in all aqueous solutions, whereas chitosan showed little bubbles on the surface at pH 3 and slight disintegration at pH 11. Chitosan dissolves in acidic solutions; therefore, the described bubbles presumably derive from partially dissolved material. Next, gravimetric analysis showed a reduction in weight of about 10% in all cases except at pH 3 and 5, presumably due to the removal of the remaining phosphate-buffered saline (PBS) (self-rolling buffer) during the washing steps (Figure S4). In case of pH 3 and 5, the solvent stability test showed an increase in weight of about 10%. The reason for this could be the interaction of chitosan (positively charged) with the used citrate buffer (negatively charged). Nevertheless, none of the solvents caused a complete destruction of both layers within at least 3 h of incubation at room temperature, and the tubular structure was maintained in all solvents, confirming the

usability of the system for different enzymatic reaction solutions.

2.2. One-Tube System. The hollow tubes were removed from the needle after drying and cut into the desired length before they were glued into tissue culture well plates, yielding reaction containers with one open end on the top for loading and semipermeable side walls (Scheme 1 and Figure S5). Note that the bottom end of the tubes was tightly closed by gluing, and the level of the surrounding medium was always lower than the height of the tube, yielding diffusion only through the tube walls. The molecular weight cutoff (MWCO) of the biodegradable reaction containers was determined using differently sized fluorescein derivatives placed inside the tubes. Then, their diffusion into the surrounding media was measured over time (Figures 1a and S6a). The MWCO was determined to be above $20\,000\text{ g mol}^{-1}$.

In the next step, the tube (one-tube system) was filled with esterase-2 (Est2). Est2 possesses a typical α/β -hydrolase fold showing the highest activity at $70\text{ }^\circ\text{C}$.^{46,47} Its long-term stability and activity at wide ranges of temperature and pH predestines it as a model for biosensor development.^{48–51} The catalytic activity of Est2 is described in Figure 1b. With a molecular weight of 34.2 kDa, it was above the MWCO (Figures 1c and S6b). *p*-Nitrophenyl acetate (pNPA) was added as a substrate to the surrounding, and the reaction (hydrolysis yielding *p*-nitrophenol (pNP, yellow) and acetate^{46,49}) was monitored. The substrate was able to enter and the product to leave the tube after the reaction. The overall reaction time was slowed down due to the diffusion limitation (Figure 1d). The specific activity of the entrapped

C

DOI: 10.1021/acsami.9b01654
ACS Appl. Mater. Interfaces XXXX, XXX, XXX–XXX

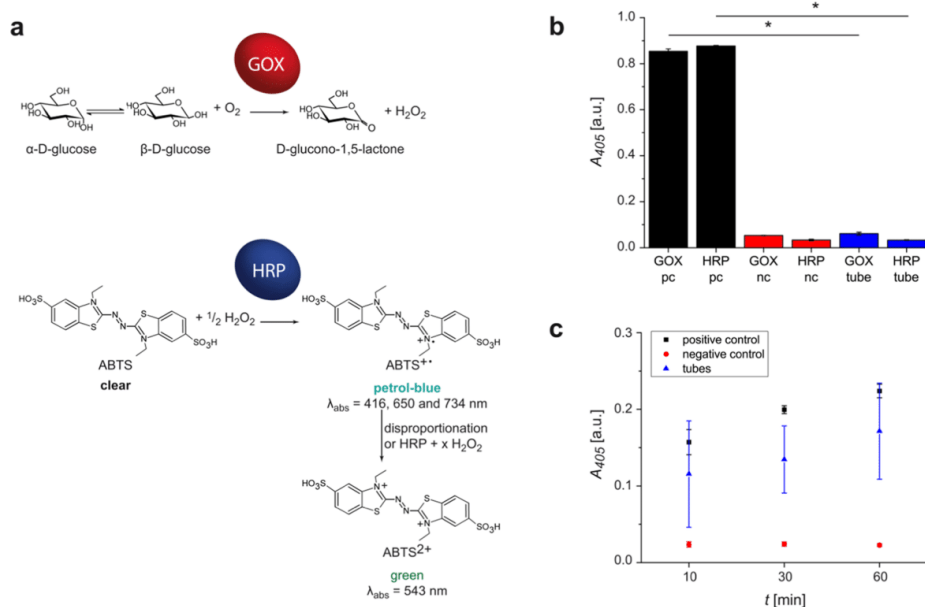


Figure 2. “Product trapping” two-tube system. (a) Reaction mechanism of H₂O₂ production from glucose catalyzed by glucose oxidase (GOX) as well as 2,2′-azino-bis(3-ethylbenzothiazoline-6-sulfonic acid) (ABTS) oxidation catalyzed by horseradish peroxidase (HRP). (b) GOX and HRP were retained inside the tubes. pc = positive control: GOX or HRP + buffer; nc = negative control: buffer; tubes: GOX or HRP in tubes + buffer in surrounding. After 15 min, the solutions were mixed with the respective substrates, and absorbance (*A*) was measured (statistics: *t*-test: *p* < 0.05). (c) Production of ABTS^{•+}. Positive control: GOX + HRP + substrates in buffer (diluted 1:9); negative control: substrates in buffer; tubes: GOX and HRP in tubes + substrates in buffer in the surrounding.

enzyme was 12 770 U μmol⁻¹, which corresponds to 30% of the activity of the nonencapsulated soluble enzyme as determined by Humenik et al.⁵² The reduction in specific activity can be attributed to the double diffusion of the substrate (into the tube and out of the tube).

2.3. Two-Tube System. To test an enzymatic cascade in one-reaction setup, an exemplary two-tube system containing glucose oxidase (GOX) and horseradish peroxidase (HRP) was investigated next. GOX is a glycoprotein consisting of two 80 kDa subunits possessing two FADs as co-enzyme, which act as electron carrier during the catalytic reaction. GOX catalyzes the oxidation reaction of D-glucose to D-gluconolactone, and H₂O₂ is produced as a byproduct.⁵³ This byproduct is used as a substrate by HRP to enable the oxidation reactions, e.g., of 2,2′-azino-bis(3-ethylbenzothiazoline-6-sulfonic acid) (ABTS) (Figure 2a) and 5(6)-carboxyfluorescein (Figure 3a). HRP is a heme-bearing glycoprotein with two calcium atoms, which are essential for functional and structural integrity of the enzyme. The 44.2 kDa enzyme comprises two domains and four disulfide bridges connecting the mainly α-helical parts. Several substrates ranging from aromatic phenols to indoles, phenolic acids, sulfonates, and amines can be oxidized.⁵⁴ The diffusion test showed that both enzymes retained inside their tubes (Figures 2b and S6c). Then, wells with two tubes, one for each enzyme, were prepared in the same reaction mixture but without direct contact. Such a system is especially of interest when the enzymes or products inhibit each other and close contact should be avoided to achieve a full function. ABTS is a nontoxic substrate for peroxidase reaction with H₂O₂, which was here created by GOX (Figure 2b,c). The petrol-blue

product of the reaction with HRP and H₂O₂ is a metastable radical cation. This radical cation disproportionates only slowly, giving azodication, and thus, the reaction could be observed for an hour without facing a problem.^{55,56} Here, the desired petrol-blue product was formed in the samples as well as in the positive control. Importantly, the product was not able to diffuse out of the tubular structures and retained inside (Figure S6d). A reason therefore could be that the product, as a radical cation, is prone to stick to or react with various surfaces.⁵⁷ ABTS^{•+} was harvested by pipetting it out of the tube. The yield of the two-tube system was lower than that of the positive control, as some product was presumably captured in the tube walls. However, such a system will be very useful in case such species should be removed from a solution or toxic products are gained.

To show a second two-tube system, where the goal was to release the intermediate/product to the surroundings, carboxyfluorescein was used as a substrate and its degradation was analyzed over time (Figure 3b,c). In the presence of HRP and H₂O₂, first radical species are formed, which could further react by radical polymerization or degradation as proposed in Figure 3a. Due to the presence of different radical and anionic species in the reaction mixture, also further reactions and degradation routes are possible.⁵⁸ It was shown that degradation occurs in the two-tube system as well as in the positive control, where the enzymes were floating freely in the reaction mixture. In case of the positive control, a very fast drop in fluorescein concentration could be detected, whereas the encapsulated enzymes showed a slower and steadier decrease in fluorescein concentration. It was shown that in case

D

DOI: 10.1021/acsami.9b01654
ACS Appl. Mater. Interfaces XXXX, XXX, XXX–XXX

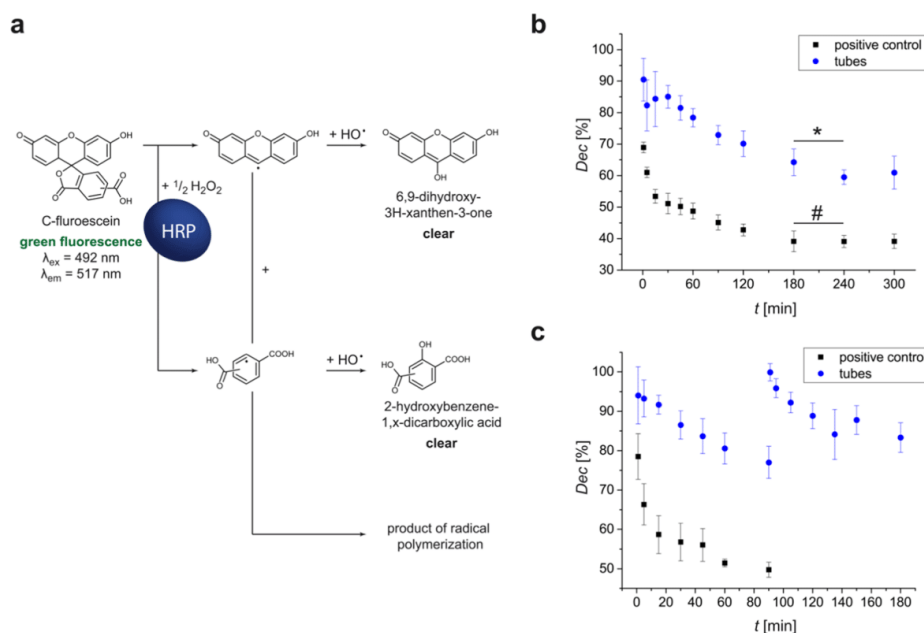


Figure 3. “Free product” two-tube system. (a) Possible routes for 5(6)-carboxyfluorescein (c-fluorescein) degradation reactions catalyzed by horseradish peroxidase (HRP). (b) Degradation of c-fluorescein (Dec = decrease compared to that of the negative control). Positive control: GOX + HRP + substrates in buffer; tubes: GOX and HRP in tubes + substrate in buffer in the surroundings (statistics: t -test: $p < 0.05$; * = significant difference; # = no significant difference). (c) as (b) but surrounding media of tubes was removed after 90 min, and fresh substrate solution was added after washing, followed by determining the degradation.

of the positive control, the reaction stopped after 180 min, whereas in the case of the two-tube system, it prolonged to 240 min. Nevertheless, the overall degree of degradation was higher in the free-floating system (Figure 3b). Importantly, the tube container allowed the exchange of the surrounding media, thus fresh substrate could be added as shown in Figure 3. The media were exchanged after 90 min, and it was confirmed that the fluorescein continuously degraded; thus, the enzymes were still active. In addition, the one-tube system was applied as a negative control in this experimental setup by pipetting both enzymes into one tube to show putative inhibitory effects. Therein, a carboxyfluorescein degradation of only $16 \pm 1\%$ was detected (results not shown). Presumably, the high H_2O_2 concentration decreased the respective enzyme activity.

3. CONCLUSIONS

Tubular reaction container for enzymes were established by self-rolling spider silk and chitosan bilayers. Two modes of action were shown: either the product of the enzymatic reaction can diffuse out of the tube, thus allowing harvesting the product, which is thereby separated from the enzyme. Alternatively, the product can be retained inside the tubes, which is of high interest, if the product is toxic or high concentrations are desired. The advantage is that the system allows exchanging the surrounding reaction medium without the need to exchange costly enzymes. In addition, a multienzyme cascade combined with constant substrate flow, as, for instance, in a microfluidic device, could be employed. Since the enzymes can be kept separately encapsulated, enzymes can be studied, which would otherwise inhibit each

other. Another application is the use of the system as the biological recognition element of a biosensor, in which the sample can be added to the surrounding, and an enzyme in the tube catalyzes the production of a detectable signal in response to the presence of a distinct biomolecule. Further, one could imagine encapsulating cells (bacterial or eukaryotic) inside the tube and analyze their metabolism in response to environmental changes. Additionally, the encapsulated cells could be modified to produce a desired product, which can be continuously harvested from the surrounding.

4. MATERIALS AND METHODS

4.1. Tube Formation. **4.1.1. Bilayer Preparation.** Bilayers were prepared by subsequent casting of spider silk and chitosan solutions. Therefore, lyophilized eADF4(C16) powder (AMSilk, $M_w = 47\,698 \text{ g mol}^{-1}$)⁵⁹ was dissolved overnight in 1,1,1,3,3,3-hexafluoro-2-propanol (8.33 mg mL^{-1}), and this solution was cast in Petri dishes (Sterilin, diameter: 90 mm) to obtain 0.08 mg cm^{-2} . Afterward, the film was allowed to air-dry for 4 h before it was post-treated for 2 h using 70% ethanol to induce β -sheet formation to render it water-insoluble.⁶⁰ A 1% chitosan solution was prepared by dissolving the chitosan powder ($190\text{--}310\,000 \text{ g mol}^{-1}$, Sigma-Aldrich) in 2% formic acid for 6 h and by subsequent filtering through polyester cloth to remove insoluble parts. This solution was cast on top of the silk film and air-dried overnight to obtain 2.36 mg cm^{-2} . The chitosan layer was post-treated with NaOH (0.2 M) for 5 min to render the film water-insoluble and then washed with H_2O .

4.1.2. Self-Rolled Tube Preparation. The dried bilayer was cut into rectangles ($1.5 \times 0.5 \text{ cm}^2$). A needle ($0.80 \times 22 \text{ mm}^2$, B. Braun) was applied onto the silk layer, and the bilayer was allowed to self-roll in phosphate-buffered saline (PBS, pH 7.4). The tubes were dried on the needle and then cut into 7 mm length. These tubes were glued into

48-well tissue culture plates (Thermo Scientific) with clear nail polish (OPI).

4.2. Characterization. **4.2.1. Scanning Electron Microscopy (SEM).** For the bilayer analysis, the bilayer and the wet tubes were frozen in N_2 liq and then broken. For the solvent stability tests, the tubes were immersed in organic solvents (dimethylformamide (DMF), ethanol (EtOH), glycerol, dimethylsulfoxide (DMSO), and hydrogen peroxide (H_2O_2 ; 5–7%)) in aqueous buffers at different pH (pH 3 and 5: citrate buffer, pH 7.4: 4-(2-hydroxyethyl)-1-piperazineethanesulfonic acid, pH 9: tris(hydroxymethyl)aminomethane/HCl (Tris/HCl), pH 11: $Na_2CO_3/NaHCO_3$ buffer) and in H_2O as a control for 3 h. Then, the samples were washed twice with H_2O to remove residual salts, dried, and cut. All samples were prepared by mounting them onto studs with an adhesive sticker for SEM. The samples were sputter coated with platinum (2.0 nm) and images were taken by an SEM 1540EsB Cross Beam (Zeiss). The device was operated at 2 kV with a collector bias of 300 V. Images were detected with an SE2 lens, and a 30 μm aperture and a line-averaging method were used to reduce noise.

4.2.2. Gravimetric Solvent Stability Test. The tubes were weighed before and after immersion into different organic and aqueous solvents (as mentioned in section “Scanning Electron Microscopy (SEM)”) using an analytical balance (Sartorius Lab Instruments GmbH & Co. KG). For each condition, five samples were analyzed ($n = 5$).

4.2.3. Light Microscopy. Dry and wet (freshly rolled) tubes were placed upright on a glass plate and analyzed using a light microscope (Leica, DMI3000B).

4.2.4. AFM. Silk films were prepared on a silica wafer using the same method as described above. Then, the films were scratched with tweezers to allow for thickness measurements. The films were measured dry and after incubation in PBS for 10 min. AFM scanning was performed using a Dimension Icon (Bruker) in a tapping mode with 0.01–0.02 Ω cm Si-cantilevers (OTESPA-R3, Bruker, spring constant of 26 $N\ m^{-1}$, resonance frequency of 300 kHz). AFM scans were processed using NanoScope Analysis software Version 1.9 (Bruker, Santa Barbara, CA). AFM analysis was done using NanoScope Analysis software Version 1.5 (Bruker, Santa Barbara, CA). For the determination of the film thickness, the tool section and the depth were used on 6 different spots on 3 different scratches and pictures ($n = 3 \times 6$).

4.2.5. Water Uptake. The dry and wet weights of the bilayer were measured using an analytical balance (Sartorius Lab Instruments GmbH & Co. KG) to determine the amount of bound water. The test was performed with 46 samples ($n = 46$).

4.2.6. Thickness Measurements. The thicknesses of the dry and wet bilayers were determined using a micrometer screw (Hohlex).

4.2.7. Diffusion Measurements. The fluorescein derivatives 5(6)-carboxyfluorescein ($M_w = 376.32\ g\ mol^{-1}$, Sigma-Aldrich), fluorescein isothiocyanate (FITC)–dextran 3–5000 ($M_w = 3–5000\ g\ mol^{-1}$, Sigma-Aldrich), FITC–dextran 20 000 ($M_w = 20\ 000\ g\ mol^{-1}$, Sigma-Aldrich), and FITC–dextran 59–77 000 ($M_w = 59–77\ 000\ g\ mol^{-1}$, Sigma-Aldrich) were used for analysis. Stock solutions of these fluorescein derivatives were prepared in DMSO (10 mM in case of 5(6)-carboxyfluorescein, FITC–dextran 3–5000 and 20000 and 2 mM in case of FITC–dextran 59–77 000). The stock solutions were diluted with PBS (to 2 and 0.5 mM) just before usage, and 2 μL were injected into each tube. Then, PBS (700 μL) was transferred to the surrounding and the measurement was started. At each time point (1, 5, 10, 15, 20, 30, 45, 60, 90, 120, 150, 180, 240, 300, and 1440 min), 100 μL of the surrounding solution were transferred to a 96 black bottom well plate (Nunc), and the fluorescence (ex: 485 nm, em: 535 nm) was measured using a plate reader (LB940, Mithras). Further, a calibration curve was measured to calculate the diffusion. Each test was done in triplicates with a sample number of 6 ($n = 3 \times 6$) per experimental group.

4.3. Enzyme Tests. **4.3.1. Diffusion Test of Est2.** For the diffusion of esterase-2 (Est2, $M_w = 34\ 303\ g\ mol^{-1}$), the solution (3 μL , 0.25 $mg\ mL^{-1}$ in 0.1 M potassium phosphate buffer, pH 7 (KPi)) was pipetted into the tubes, and KPi (300 μL , 0.1 M) was added to the

surrounding and incubated for 15 min. Then, the surrounding solution was transferred to a fresh well, *p*-nitrophenyl acetate (pNPA, predissolved in acetonitrile, 5 mM final concentration, Sigma-Aldrich) was added and allowed to react for 5 min. The reaction mixture was analyzed using a plate reader (abs: 405 nm). Plain KPi buffer with pNPA was used as a negative control, and Est2 in KPi with pNPA diluted 10 times was used as a positive control. The sample number was 6 ($n = 6$), and *t*-test was used for statistical analysis.

4.3.2. pNPA Reaction Test. The reaction test was performed as before, except that pNPA was added directly to the surrounding mixture. At each time point (1, 5, 10, 15, and 20 min), absorbance was measured using a plate reader (abs: 405 nm). Est2 in KPi with pNPA diluted 10 times was used as a positive control. KPi buffer with pNPA (plain or diluted 10 times) was used as negative control and subtracted from the results of the tube test and the positive control. The experiment was performed twice with a sample number of 6 ($n = 2 \times 6$). The specific activity was calculated according to Humenik et al.⁵² Linear least-squares analysis of the absorption measurements was used to determine the enzyme activity (*U*), which was defined as the amount of esterase-2 catalyzing the reaction of 1 μM of pNP ($\epsilon = 14\ 000\ M\ cm^{-1}$) per minute.

4.3.3. Diffusion Test of GOX/HRP. For the diffusion of glucose oxidase (GOX, EC 1.1.3.4., from *Aspergillus niger*, $M_w = 160\ 000\ g\ mol^{-1}$, Sigma-Aldrich) and horseradish peroxidase (HRP, EC 1.1.1.7, $M_w = 44\ 200\ g\ mol^{-1}$, Sigma-Aldrich) each solution (3 μL , 0.25 $mg\ mL^{-1}$ in 0.1 M KPi) was pipetted into a tube, and KPi (250 μL) was added to the surrounding and left for 15 min. Then, the surrounding solution was transferred to a fresh well. Glucose solution (129 mM final concentration, Sigma-Aldrich), 2,2'-azino-bis(3-ethylbenzothiazoline-6-sulfonic acid) (ABTS, 2.74 mM final concentration, Sigma-Aldrich) were added, and the reaction mixture was allowed to react for 5 min. The reaction mixture without enzymes was used as a negative control and that with both enzymes was used as a positive control. All mixtures were diluted 1:3 and analyzed using a plate reader (abs: 405 nm). The sample number was 6 ($n = 6$), and *t*-test was used for statistical analysis.

4.3.4. ABTS Reaction Test. For the reaction test, two tubes were glued into one well, and one tube was filled with GOX and the other with HRP solution (3 μL , 0.25 $mg\ mL^{-1}$). The reaction mixture was the same as stated in “Diffusion Test GOX/HRP”. At distinct time points (10, 30, and 60 min), the product was removed from the tubes, diluted with KPi, and measured using a plate reader (abs: 405 nm). As negative control, the plain reaction mixture was used, and GOX and HRP solution (3 μL , 0.25 $mg\ mL^{-1}$ in 0.1 M KPi) were added as a positive control. The controls were diluted 1:9 before measurement to obtain a dilution factor comparable to that of the samples. For each time point, three experiments were performed ($n = 3 \times 6$) with 6 samples each.

4.3.5. Fluorescein Degradation Test. The setup was prepared as in “ABTS Reaction Test”, except higher enzyme concentrations were used (1.5 $mg\ mL^{-1}$). The reaction mixture was the same as stated in Diffusion Test of GOX/HRP, except 5(6)-carboxyfluorescein (5 μM final concentration) was used as a reagent instead of ABTS. At each time point (1, 5, 15, 30, 45, 60, 90, 120, 180, 240, and 300 min) the emission was measured using a plate reader (ex: 485 nm, em: 535 nm). The reaction mixture without enzymes was used as a negative control, and the reaction mixture with both enzymes was used as a positive control. The experiment was performed three times with a sample number of 6 ($n = 3 \times 6$).

■ ASSOCIATED CONTENT

● Supporting Information

The Supporting Information is available free of charge on the ACS Publications website at DOI: 10.1021/acsami.9b01654.

SEM images of bilayers before and after rolling in PBS; AFM analysis of silk film thickness; gravimetric solvent stability test (PDF)

F

DOI: 10.1021/acsami.9b01654
ACS Appl. Mater. Interfaces XXXX, XXX, XXX–XXX

AUTHOR INFORMATION

Corresponding Author

*E-mail: thomas.scheibel@bm.uni-bayreuth.de.

ORCID

Thomas Scheibel: 0000-0002-0457-2423

Author Contributions

The manuscript was written through contributions of all authors. All authors have given approval to the final version of the manuscript.

Funding

The authors would like to thank the Bavarian Research Foundation for financial support (DOK-175-15, T.A.)

Notes

The authors declare the following competing financial interest(s): Thomas Scheibel is co-founder and shareholder of the biotech company AMSilk GmbH in Germany.

ACKNOWLEDGMENTS

The authors would like to thank Sarah Lentz for conducting the AFM experiments, Martin Humenik for providing Esterase-2, Andreas Kumschier, and Philipp Neßbach for experimental help, Claudia Stemmann for SEM imaging, and Prof. Leonid Ionov and Prof. Hans-Werner Schmidt for fruitful discussions.

REFERENCES

- (1) Denard, C. A.; Hartwig, J. F.; Zhao, H. M. Multistep One-Pot Reactions Combining Biocatalysts and Chemical Catalysts for Asymmetric Synthesis. *ACS Catal.* **2013**, *3*, 2856–2864.
- (2) Hayashi, Y. Pot Economy and One-Pot Synthesis. *Chem. Sci.* **2016**, *7*, 866–880.
- (3) Climent, M. J.; Corma, A.; Iborra, S. Heterogeneous Catalysts for the One-Pot Synthesis of Chemicals and Fine Chemicals. *Chem. Rev.* **2011**, *111*, 1072–1133.
- (4) Silva, C.; Martins, M.; Jing, S.; Fu, J.; Cavaco-Paulo, A. Practical Insights on Enzyme Stabilization. *Crit. Rev. Biotechnol.* **2018**, *38*, 335–350.
- (5) Sintra, T. E.; Ventura, S. P. M.; Coutinho, J. A. P. Superactivity Induced by Micellar Systems as the Key for Boosting the Yield of Enzymatic Reactions. *J. Mol. Catal. B: Enzym.* **2014**, *107*, 140–151.
- (6) Theberge, A. B.; Courtois, F.; Schaerli, Y.; Fischlechner, M.; Abell, C.; Hollfelder, F.; Huck, W. T. S. Microdroplets in Microfluidics: An Evolving Platform for Discoveries in Chemistry and Biology. *Angew. Chem., Int. Ed.* **2010**, *49*, 5846–5868.
- (7) Blüm, C.; Nichtl, A.; Scheibel, T. Spider Silk Capsules as Protective Reaction Containers for Enzymes. *Adv. Funct. Mater.* **2014**, *24*, 763–768.
- (8) Hermanson, K. D.; Huemmerich, D.; Scheibel, T.; Bausch, A. R. Engineered Microcapsules Fabricated from Reconstituted Spider Silk. *Adv. Mater.* **2007**, *19*, 1810–1815.
- (9) Hermanson, K. D.; Harasim, M. B.; Scheibel, T.; Bausch, A. R. Permeability of Silk Microcapsules Made by the Interfacial Adsorption of Protein. *Phys. Chem. Chem. Phys.* **2007**, *9*, 6442–6446.
- (10) Walde, P.; Ichikawa, S. Enzymes Inside Lipid Vesicles: Preparation, Reactivity and Applications. *Biomol. Eng.* **2001**, *18*, 143–177.
- (11) Vriezema, D. M.; Garcia, P. M. L.; Oltra, N. S.; Hatzakis, N. S.; Kuiper, S. M.; Nolte, R. J. M.; Rowan, A. E.; van Hest, J. C. M. Positional Assembly of Enzymes in Polymersome Nanoreactors for Cascade Reactions. *Angew. Chem., Int. Ed.* **2007**, *46*, 7378–7382.
- (12) Lee, H.; DeLoache, W. C.; Dueber, J. E. Spatial Organization of Enzymes for Metabolic Engineering. *Metab. Eng.* **2012**, *14*, 242–251.
- (13) Sakr, O. S.; Borchard, G. Encapsulation of Enzymes in Layer-by-Layer (LbL) Structures: Latest Advances and Applications. *Biomacromolecules* **2013**, *14*, 2117–2135.
- (14) Liebherr, R. B.; Gorris, H. H. Enzyme Molecules in Solitary Confinement. *Molecules* **2014**, *19*, 14417–14445.
- (15) Ionov, L. Biomimetic 3D Self-Assembling Biomicroconstructs by Spontaneous Deformation of Thin Polymer Films. *J. Mater. Chem.* **2012**, *22*, 19366–19375.
- (16) Ionov, L. Soft Microorigami: Self-Folding Polymer Films. *Soft Matter* **2011**, *7*, 6786–6791.
- (17) Luchnikov, V.; Ionov, L.; Stamm, M. Self-Rolled Polymer Tubes: Novel Tools for Microfluidics/Microbiology, and Drug-Delivery Systems. *Macromol. Rapid Commun.* **2011**, *32*, 1943–1952.
- (18) Stoychev, G.; Zakharchenko, S.; Turcaud, S.; Dunlop, J. W. C.; Ionov, L. Shape-Programmed Folding of Stimuli-Responsive Polymer Bilayers. *ACS Nano* **2012**, *6*, 3925–3934.
- (19) Zakharchenko, S.; Sperling, E.; Ionov, L. Fully Biodegradable Self-Rolled Polymer Tubes: A Candidate for Tissue Engineering Scaffolds. *Biomacromolecules* **2011**, *12*, 2211–2215.
- (20) Smela, E.; Inganas, O.; Lundstrom, I. Controlled Folding of Micrometer-Size Structures. *Science* **1995**, *268*, 1735–1738.
- (21) Jager, E. W. H.; Inganas, O.; Lundstrom, I. Microbots for Micrometer-Size Objects in Aqueous Media: Potential Tools for Single-Cell Manipulation. *Science* **2000**, *288*, 2335–2338.
- (22) Ju, X. J.; Xie, R.; Yang, L.; Chu, L. Y. Biodegradable 'Intelligent' Materials in Response to Physical Stimuli for Biomedical Applications. *Expert Opin. Ther. Pat.* **2009**, *19*, 493–507.
- (23) Bassik, N.; Abebe, B. T.; Laflin, K. E.; Gracias, D. H. Photolithographically Patterned Smart Hydrogel Based Bilayer Actuators. *Polymer* **2010**, *51*, 6093–6098.
- (24) Zakharchenko, S.; Puretskiy, N.; Stoychev, G.; Stamm, M.; Ionov, L. Temperature Controlled Encapsulation and Release using Partially Biodegradable Thermo-Magneto-Sensitive Self-Rolling Tubes. *Soft Matter* **2010**, *6*, 2633–2636.
- (25) Stoychev, G.; Turcaud, S.; Dunlop, J. W. C.; Ionov, L. Hierarchical Multi-Step Folding of Polymer Bilayers. *Adv. Funct. Mater.* **2013**, *23*, 2295–2300.
- (26) Stoychev, G.; Puretskiy, N.; Ionov, L. Self-Folding All-Polymer Thermoresponsive Microcapsules. *Soft Matter* **2011**, *7*, 3277–3279.
- (27) Zakharchenko, S.; Puretskiy, N.; Stoychev, G.; Waurisch, C.; Hickey, S. G.; Eychmuller, A.; Sommer, J. U.; Ionov, L. Stimuli-Responsive Hierarchically Self-Assembled 3D Porous Polymer-Based Structures with Aligned Pores. *J. Mater. Chem. B* **2013**, *1*, 1786–1793.
- (28) Apsite, I.; Stoychev, G.; Zhang, W. Z.; Jehnichen, D.; Xie, J.; Ionov, L. Porous Stimuli-Responsive Self-Folding Electrospun Mats for 4D Biofabrication. *Biomacromolecules* **2017**, *18*, 3178–3184.
- (29) Liu, L.; Jiang, S. H.; Sun, Y.; Agarwal, S. Giving Direction to Motion and Surface with Ultra-Fast Speed Using Oriented Hydrogel Fibers. *Adv. Funct. Mater.* **2016**, *26*, 1021–1027.
- (30) Chen, T. T.; Bakhshi, H.; Liu, L.; Ji, J.; Agarwal, S. Combining 3D Printing with Electrospinning for Rapid Response and Enhanced Designability of Hydrogel Actuators. *Adv. Funct. Mater.* **2018**, *28*, No. 1800514.
- (31) Stroganov, V.; Zakharchenko, S.; Sperling, E.; Meyer, A. K.; Schmidt, O. G.; Ionov, L. Biodegradable Self-Folding Polymer Films with Controlled Thermo-Triggered Folding. *Adv. Funct. Mater.* **2014**, *24*, 4357–4363.
- (32) Ye, C. H.; Nikolov, S. V.; Calabrese, R.; Dindar, A.; Alexeev, A.; Kippelen, B.; Kaplan, D. L.; Tsukruk, V. V. Self-(Un) rolling Biopolymer Microstructures: Rings, Tubules, and Helical Tubules from the Same Material. *Angew. Chem., Int. Ed.* **2015**, *54*, 8490–8493.
- (33) Corroero, M. R.; Moridi, N.; Schützinger, H.; Sykora, S.; Ammann, E. M.; Peters, E. H.; Dudal, Y.; Corvini, F. X.; Shahgaldian, P. Enzyme Shielding in an Enzyme-thin and Soft Organosilica Layer. *Angew. Chem., Int. Ed.* **2016**, *55*, 6285–6289.
- (34) Leal-Egaña, A.; Scheibel, T. Silk-Based Materials for Biomedical Applications. *Biotechnol. Appl. Biochem.* **2010**, *55*, 155–167.
- (35) Heidebrecht, A.; Eisoldt, L.; Diehl, J.; Schmidt, A.; Geffers, M.; Lang, G.; Scheibel, T. Biomimetic Fibers Made of Recombinant Spidroins with the Same Toughness as Natural Spider Silk. *Adv. Mater.* **2015**, *27*, 2189–2194.

G

DOI: 10.1021/acsami.9b01654
ACS Appl. Mater. Interfaces XXXX, XXX, XXX–XXX

- (36) Doblhofer, E.; Schmidt, J.; Riess, M.; Daab, M.; Suntinger, M.; Habel, C.; Bargel, H.; Hugenschmidt, C.; Rosenfeld, S.; Breu, J.; Scheibel, T. Structural Insights into Water-Based Spider Silk Protein-Nanoclay Composites with Excellent Gas and Water Vapor Barrier Properties. *ACS Appl. Mater. Interfaces* **2016**, *8*, 25535–25543.
- (37) Goy, R. C.; Morais, S. T. B.; Assis, O. B. G. Evaluation of the Antimicrobial Activity of Chitosan and its Quaternized Derivative on *E. coli* and *S. aureus* Growth. *Rev. Bras. Farmacogn.* **2016**, *26*, 122–127.
- (38) Rinaudo, M. Chitin and Chitosan: Properties and Applications. *Prog. Polym. Sci.* **2006**, *31*, 603–632.
- (39) Rath, A.; Mathesan, S.; Ghosh, P. Folding Behavior and Molecular Mechanism of Cross-linked Biopolymer Film in Response to Water. *Soft Matter* **2016**, *12*, 9210–9222.
- (40) Saito, Y.; Luchnikov, V.; Inaba, A.; Tamura, K. Self-Scrolling Ability of Differentially Acetylated Chitosan Film. *Carbohydr. Polym.* **2014**, *109*, 44–48.
- (41) Duan, J. J.; Liang, X. C.; Guo, J. H.; Zhu, K. K.; Zhang, L. N. Ultra-Stretchable and Force-Sensitive Hydrogels Reinforced with Chitosan Microspheres Embedded in Polymer Networks. *Adv. Mater.* **2016**, *28*, 8037–8044.
- (42) Guan, J. J.; He, H. Y.; Lee, L. J.; Hansford, D. J. Fabrication of Particulate Reservoir-Containing, Capsulelike, and Self-Folding Polymer Microstructures for Drug Delivery. *Small* **2007**, *3*, 412–418.
- (43) Wohlrab, S.; Spiess, K.; Scheibel, T. Varying surface hydrophobicities of coatings made of recombinant spider silk proteins. *J. Mater. Chem.* **2012**, *22*, 22050–22054.
- (44) Lintz, E. S.; Neinhuis, C.; Scheibel, T. Altering Silk Film Surface Properties through Lotus-Like Mechanisms. *Macromol. Mater. Eng.* **2018**, *303*, 1700637–1700645.
- (45) Alekseeva, M.; Fedoseeva, E.; Frolov, V.; Nistratov, V.; Smirnova, L. The strength of chitosan films. The role of molecular weight, the degree of order, the nature of counter-ion. *Prog. Chem. Appl. Chitin Its Deriv.* **2009**, *14*, 65–74.
- (46) Manco, G.; Adinolfi, E.; Pisani, F. M.; Ottolina, G.; Carrea, G.; Rossi, M. Overexpression and Properties of a new Thermophilic and Thermostable Esterase from *Bacillus Acidocaldarius* with Sequence Similarity to Hormone-Sensitive Lipase Subfamily. *Biochem. J.* **1998**, *332*, 203–212.
- (47) De Simone, G.; Galdiero, S.; Manco, G.; Lang, D.; Rossi, M.; Pedone, C. A Snapshot of a Transition State Analogue of a Novel Thermophilic Esterase Belonging to the Subfamily of Mammalian Hormone-Sensitive Lipase. *J. Mol. Biol.* **2000**, *303*, 761–771.
- (48) Febbraio, F.; Merone, L.; Cetrangolo, G. P.; Rossi, M.; Nucci, R.; Manco, G. Thermostable Esterase 2 from *Alicyclobacillus Acidocaldarius* as Biosensor for the Detection of Organophosphate Pesticides. *Anal. Chem.* **2011**, *83*, 1530–1536.
- (49) Pöhlmann, C.; Wang, Y. R.; Humenik, M.; Heidenreich, B.; Gareis, M.; Sprinzl, M. Rapid, Specific and Sensitive Electrochemical Detection of Foodborne Bacteria. *Biosens. Bioelectron.* **2009**, *24*, 2766–2771.
- (50) Humenik, M.; Mohrand, M.; Scheibel, T. Self-Assembly of Spider Silk-Fusion Proteins Comprising Enzymatic and Fluorescence Activity. *Bioconjugate Chem.* **2018**, *29*, 898–904.
- (51) Humenik, M.; Pöhlmann, C.; Wang, Y. R.; Sprinzl, M. Enhancement of Electrochemical Signal on Gold Electrodes by Polyvalent Esterase-Dendrimer Clusters. *Bioconjugate Chem.* **2008**, *19*, 2456–2461.
- (52) Humenik, M.; Mohrand, M.; Scheibel, T. Self-Assembly of Spider Silk-Fusion Proteins Comprising Enzymatic and Fluorescence Activity. *Bioconjugate Chem.* **2018**, *29*, 898–904.
- (53) Wong, C. M.; Wong, K. H.; Chen, X. D. Glucose Oxidase: Natural Occurrence, Function, Properties and Industrial Applications. *Appl. Microbiol. Biotechnol.* **2008**, *78*, 927–938.
- (54) Veitch, N. C. Horseradish Peroxidase: A Modern View of a Classic Enzyme. *Phytochemistry* **2004**, *65*, 249–259.
- (55) Childs, R. E.; Bardsley, W. G. Steady-State Kinetics of Peroxidase with 2,2'-Azino-Di-(3-Ethylbenzthiazoline-6-Sulphonic Acid) as Chromogen. *Biochem. J.* **1975**, *145*, 93–103.
- (56) Kadnikova, E. N.; Kostic, N. M. Oxidation of ABTS by Hydrogen Peroxide Catalyzed by Horseradish Peroxidase Encapsulated into Sol-Gel Glass. Effects of Glass Matrix on Reactivity. *J. Mol. Catal. B: Enzym.* **2002**, *18*, 39–48.
- (57) Aliaga, C.; Lissi, E. A. Reactions of the Radical Cation Derived from 2,2'-Azinobis(3-Ethylbenzthiazoline-6-Sulfonic Acid) (ABTS(.+)) with Amino Acids. Kinetics and Mechanism. *Can. J. Chem.* **2000**, *78*, 1052–1059.
- (58) Pirillo, S.; Einschlag, F. S. G.; Ferreira, M. L.; Rueda, E. H. Eriochrome Blue Black R and Fluorescein Degradation by Hydrogen Peroxide Oxidation with Horseradish Peroxidase and Hematin as Biocatalysts. *J. Mol. Catal. B: Enzym.* **2010**, *66*, 63–71.
- (59) Huemmerich, D.; Helsen, C. W.; Quedzuweit, S.; Oschmann, J.; Rudolph, R.; Scheibel, T. Primary Structure Elements of Spider Dragline Silks and their Contribution to Protein Solubility. *Biochemistry* **2004**, *43*, 13604–13612.
- (60) Spiess, K.; Ene, R.; Keenan, C. D.; Senker, J.; Kremer, F.; Scheibel, T. Impact of Initial Solvent on Thermal Stability and Mechanical Properties of Recombinant Spider Silk Films. *J. Mater. Chem.* **2011**, *21*, 13594–13604.

Supporting Information

Self-Rolling Refillable Tubular Enzyme Containers

Made of Recombinant Spider Silk and Chitosan

Tamara B. Aigner¹, Thomas Scheibel^{1,2}*

¹ University Bayreuth, Lehrstuhl Biomaterialien, Universitätsstr. 30, 95447 Bayreuth, Germany

² University Bayreuth, Bayreuther Zentrum für Kolloide und Grenzflächen (BZKG), Bayreuther Zentrum für Bio-Makromoleküle (bio-mac), Bayreuther Zentrum für Molekulare Biowissenschaften (BZMB), Bayreuther Materialzentrum (BayMAT), Bayerisches Polymerinstitut (BPI), Universitätsstr. 30, 95447 Bayreuth, Germany

* corresponding author: thomas.scheibel@bm.uni-bayreuth.de

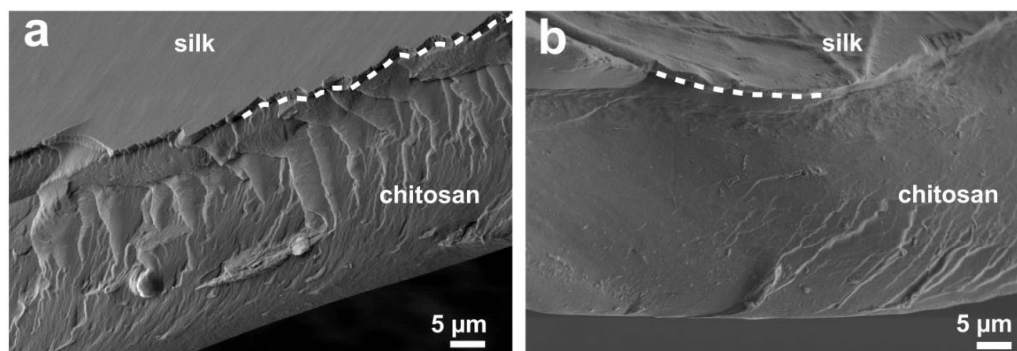


Figure S1. SEM images of bilayers before (a) and after (b) rolling in PBS. Both layers can clearly be identified, and no delamination was observed in both samples. There is apparently no difference in the layers before and after rolling.

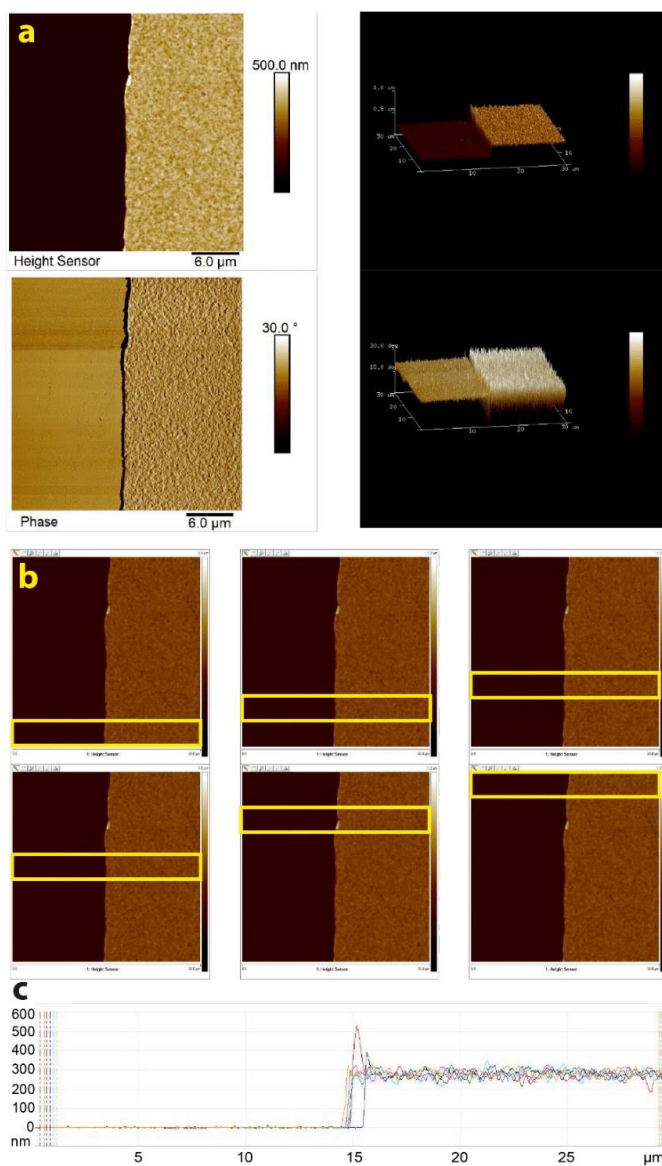


Figure S2. AFM analysis of silk film thickness. (a) Height sensor and phase image of the scratch in 2D (left) and 3D (right), (b) yellow frames mark the analyzed areas of the scratch. (c) Height profile.

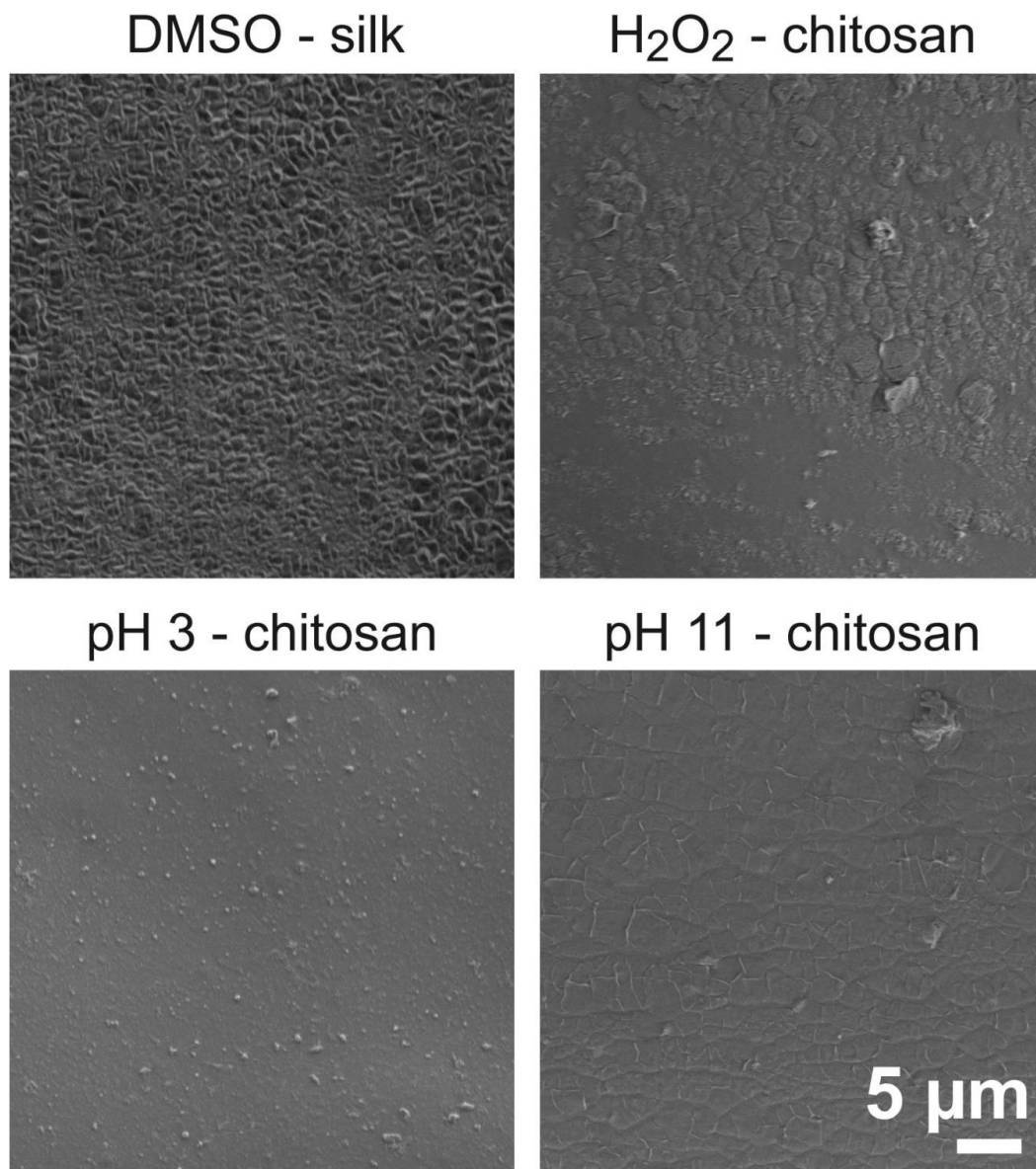


Figure S3. Stability test of tubes within organic and aqueous solvents. Samples were subjected to corresponding solvents for 3 h and subsequently washed, dried and cut. Here, the samples are shown, where the surface was affected by the solvent treatment. In all other cases a plain flat unchanged surface could be detected.

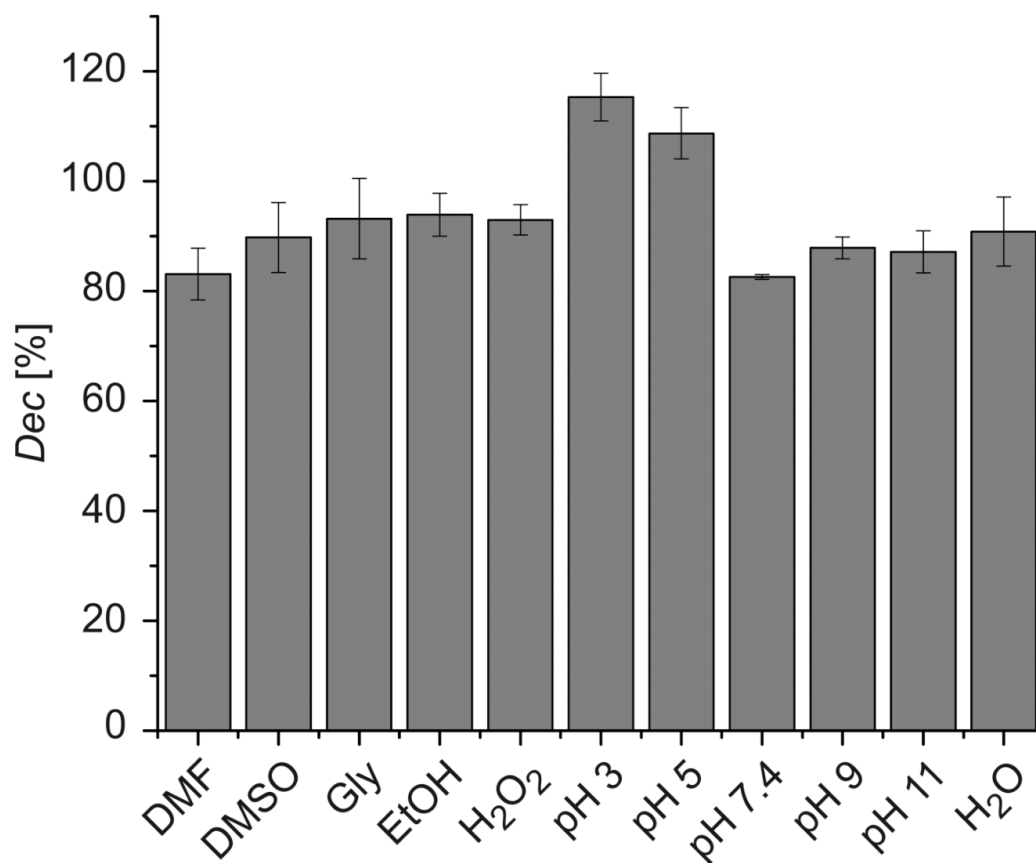


Figure S4. Gravimetric solvent stability test. The graph shows the decrease (*Dec*) of weight due to immersion in different solvents in percent. Around 10 % decrease was observed in all samples except at pH 3 and 5, presumably due to removal of PBS from the self-rolling buffer during the washing steps. In case of pH 3 and 5 citrate buffer was used, which could interact with chitosan explaining the increase in weight.

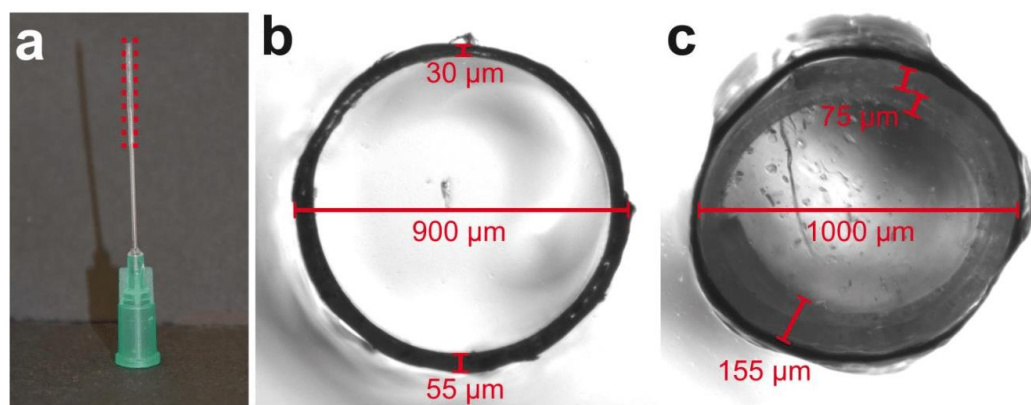


Figure S5. Tubular structures: (a) Photo of tube on needle (dashed red lines indicate the tube); (b) and (c) light microscopy images of dry (b) and wet (c) tubes, respectively, diameter and wall thicknesses are shown as determined by light microscopy.

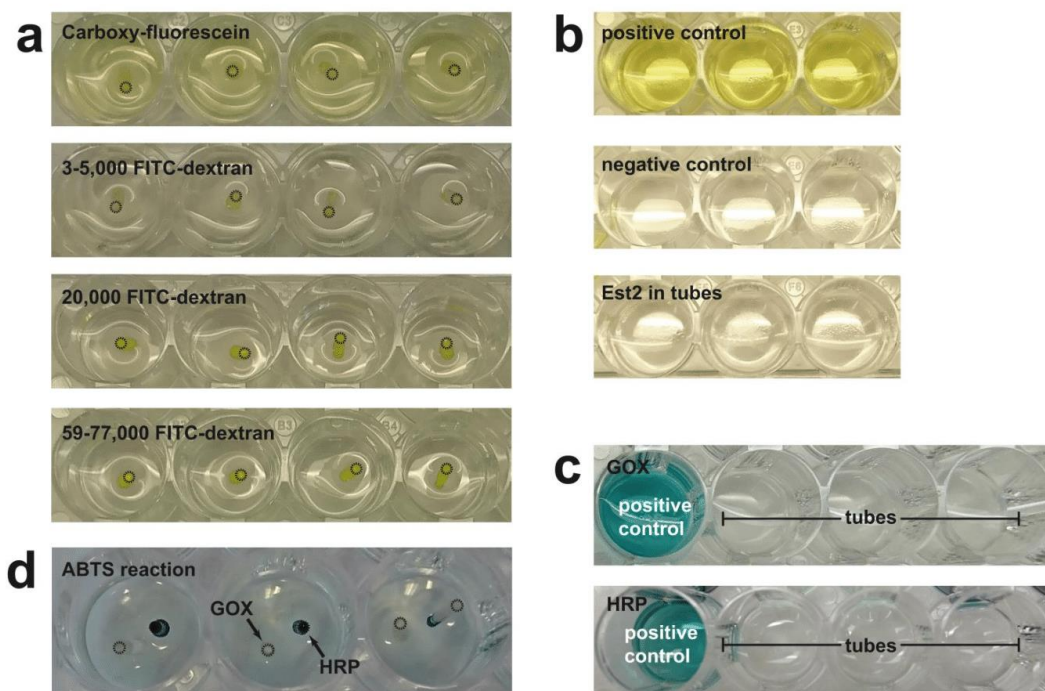


Figure S6. Photo of (a) diffusion of different fluorescein derivatives (tube openings marked with dashed circles). (b) Diffusion tests with Est2 from Figure 1c. Positive control: Est2 + buffer; negative control: plain buffer; Est2 in tube: Est2 in tubes + buffer in surrounding. After 15 min the solutions were mixed with pNPA, allowed to react, and then pictures were taken. (c) Diffusion test with glucose oxidase (GOX) and horseradish peroxidase (HRP). Positive control: GOX + HRP + buffer; tubes: GOX and HRP in tubes + buffer in the surrounding. After 15 min the solutions were mixed with substrates, allowed to react, and then pictures were taken. (d) Reaction of ABTS with GOX (left tube) and HRP (right tube) providing substrates in the surrounding.

Acknowledgement

First, I would like to direct my thanks to Prof. Dr. Thomas Scheibel for his guidance and teaching me to think outside of the box. Further, I would like to thank Prof. Dr. Leonid Ionov and Prof. Dr. Hans-Werner Schmidt for fruitful discussions and Prof. Dr. Brüggemann for supervision. Further I would like to thank the Bavarian Research Foundation for generous funding.

My cooperation projects allowed me to get a deeper insight into different fields and thereby, helped me to broaden my horizon. Therefore, big thanks go to the Cardio-Team around Prof. Dr. Felix Engel – especially to Jana Petzold for her unfaltering motivation and friendship. In addition, I would like to thank the group from Prof. Andrea O’Connor – especially Tao Huang and I thank the group of Prof. Dr. Andreas Taubert.

Then I thank my whole BioMat-family for making this PhD-journey such a wonderful experience – I will never forget all the awesome celebrations, the fun during coffee breaks and of course our productive time in lab. Gratitude is owed to the lab technicians Alex, Eva, Claudia, Anderl and Johannes and the secretary keeping the lab up and running. Big thanks go to Martin for hours of discussing my problems, complaints and crazy ideas with just the right portion of criticism. Very special thanks go to Elise for being my bridge over troubled water from the very first moment we met. I would also like to thank her for proof reading the work. Big thanks go to my master students Andreas and Philipp. Thank you Caro, Christian B., Christian H., Heike, Indra, Kim, Sarah and Sahar for valuable time and tips – I don’t know, how I would have survived without you.

Moreover, I want to thank my friends here in Bayreuth, whereby I especially have to mention my flatmates Luisa, Juliane and Nadine for their open ears and uncountable delightful moments. Then I want to direct my dearest thanks to my friends at home in Austria, it’s amazing that even several hundred kilometers cannot separate us. Without you guys my life would not have been half as enjoyable!

Last, but not least, I would like to thank my whole family. Especially, my parents Christine and Gerhard for their unconditional love, understanding and constant support in all situations of life. My brother Benjamin for always keeping me down to earth and thereby, helping me to see my goals and making me fight for them a bit harder every time.

Eidesstattliche Versicherungen und Erklärungen

(§ 9 Satz 2 Nr. 3 PromO BayNAT)

Hiermit versichere ich eidesstattlich, dass ich die Arbeit selbstständig verfasst und keine anderen als die von mir angegebenen Quellen und Hilfsmittel benutzt habe (vgl. Art. 64 Abs. 1 Satz 6 BayHSchG).

(§ 9 Satz 2 Nr. 3 PromO BayNAT)

Hiermit erkläre ich, dass ich die Dissertation nicht bereits zur Erlangung eines akademischen Grades eingereicht habe und dass ich nicht bereits diese oder eine gleichartige Doktorprüfung endgültig nicht bestanden habe.

(§ 9 Satz 2 Nr. 4 PromO BayNAT)

Hiermit erkläre ich, dass ich Hilfe von gewerblichen Promotionsberatern bzw. -vermittlern oder ähnlichen Dienstleistern weder bisher in Anspruch genommen habe noch künftig in Anspruch nehmen werde.

(§ 9 Satz 2 Nr. 7 PromO BayNAT)

Hiermit erkläre ich mein Einverständnis, dass die elektronische Fassung meiner Dissertation unter Wahrung meiner Urheberrechte und des Datenschutzes einer gesonderten Überprüfung unterzogen werden kann.

(§ 9 Satz 2 Nr. 8 PromO BayNAT)

Hiermit erkläre ich mein Einverständnis, dass bei Verdacht wissenschaftlichen Fehlverhaltens Ermittlungen durch universitätsinterne Organe der wissenschaftlichen Selbstkontrolle stattfinden können.

Bayreuth, 04.04.2020,